Effect of different plastic films as soil mulches and in low tunnels on crop microclimate

and production

by

Hughie Jones

B.Sc., The University of Alberta, 2012
M.Sc., The University of British Columbia, 2014

A THESIS SUBMITTED IN PARTIAL FULFILLMENT OF

THE REQUIREMENTS FOR THE DEGREE OF

DOCTOR OF PHILOSOPHY

in

THE FACULTY OF GRADUATE AND POSTDOCTORAL STUDIES

(Soil Science)

THE UNIVERSITY OF BRITISH COLUMBIA

(Vancouver)

December 2019

The following individuals certify that they have read, and recommend to the Faculty of Graduate and Postdoctoral Studies for acceptance, the dissertation entitled:

Effect of different plastic films as soil mulches and in low tunnels on crop microclimate and production

submitted by __Hughie Jones__ in partial fulfillment of the requirements for

the degree of __Doctor of Philosophy__

in __Soil Science__

Examining Committee:

Dr. Thomas Andrew Black, Land and Food Systems
Supervisor

Dr. Mark Johnson, Institute for Resources, Environment and Sustainability, Department of Earth, Ocean and Atmospheric Sciences
Supervisory Committee Member

Dr. Sean Smukler, Land and Food Systems
Supervisory Committee Member

Dr. Michael Novak, Land and Food Systems
University Examiner

Dr. Nicholas Coops, Geography
University Examiner

Additional Supervisory Committee Members:

Dr. Andreas Christen, Geography
Supervisory Committee Member

Abstract

Plastic film soil mulches (i.e., protective soil covers) and plastic covered low tunnels (i.e., enclosure) have the potential to alter crop microclimate, lengthen the growing-season, and increase plant productivity. A plastic film's ability to alter microclimate is related to its shortwave (S) and longwave (L) radiative properties (reflectivity (ρ), transmissivity (τ) and absorptivity (α)). This thesis examines the effect of plastic films with different radiative properties on 1) surface energy balance, 2) crop microclimate, and 3) crop productivity.

A study of nine plastic film mulches with various radiative properties (Chapter 2) showed that all films increased daily soil heat flux density, including a high ρ_s value film (0.45), due to its insulating effect at night. A comparison of three black plastic films with high shortwave absorptivity ($\alpha_s \approx 0.95$) but different α_L values showed that low and high α_L value films achieved the highest and lowest daytime soil temperatures, respectively.

A study of vegetation-free plastic film low tunnels with similar τ_s but different α_L values (Chapter 3) showed that a high α_L value cover (i.e., glass-like) increased net longwave radiation inside the low tunnel compared to a low α_L value cover, and increased inside air temperature (T_{ain}) by 5 and 2°C during the daytime and nighttime, respectively. A model to predict daytime and nighttime T_{ain} is presented and validated.

A study of Padrón peppers (*Capsicum annuum*) grown inside and outside low tunnels (Chapter 4) showed that low tunnels increase pepper growth, productivity (10%) and growing-season length (~2 weeks), but CO_2 depletion and high water vapour density occurs when leaf area index is high. A study of summer squash (*Cucurbita pepo*) grown within black plastic

mulch showed that the addition of a perforated low tunnel increased yield 27%. A study of broccoli (*Brassica oleracea*) showed that low tunnels increased yield due to wind protection in spring, which conserved soil moisture and increased T_{ain} during low temperatures. This thesis shows that plastic film covered low tunnels and soil mulches are an effective tool for altering crop microclimate and increasing yield, but trade-offs regarding microclimate exist that crop producers should consider.

Lay Summary

Plastic film mulches (protective soil cover) and low tunnels (small greenhouse) are used worldwide in agriculture to increase crop productivity and have the potential to protect crops from weather variability and climate change, by altering crop microclimate. Therefore, it is important to study their impact on surface radiation balance, crop microclimate and productivity. The goal of this thesis was to measure the radiative properties of commercially available plastic films and perform field experiments to understand how plastic film radiative properties impact 1) soil microclimate, 2) crop microclimate and 3) crop productivity. Plastic film mulches increase or decrease daytime soil temperature depending on their radiative properties but tend to increase soil temperature at nighttime. I validated a model that accurately predicts air temperature inside a low tunnel. Finally, low tunnels can increase growing season length and crop productivity, but trade-offs exist when using low tunnels (low CO_2 and high water vapour).

Preface

Chapter 1 comprises a review of soil mulch and enclosure (e.g., glasshouses, high tunnels and low tunnels) history, use in agriculture, microclimatic benefits and drawbacks, theoretical advancements and current challenges. The author was responsible for the literature review, interpretation and writing for Chapter 1.

Chapter 2 comprises work conducted in the Biometeorology and Soil Physics Laboratory – Land and Food Systems – UBC, and at UBC Farm and Totem Field, UBC. The author designed a protocol for measuring the shortwave spectral radiative properties of plastic films using a shortwave spectroradiometer (supplied by the Integrated Remote Sensing Studio, led by Nicholas Coops) indoors. The shortwave property measurements were performed in the Biometeorology and Soil Physics Laboratory. The author designed a protocol (outdoors) for measuring the longwave radiative properties of plastic films using 1) thermocouples, 2) a pyrgeometer and 3) a sheet of glass. The longwave property measurements were performed at Totem Field, UBC. Drs. Andrew Black and Paul Jassal helped measure the longwave properties at Totem Field, UBC. The radiative measurements provided the foundation for interpreting the radiative impacts of plastic films on soil heating in the field experiment that followed. The author led the design, construction and conduction of a field experiment in 2015 that measured the impact of various plastic film mulches on soil heat flux density and soil temperature at UBC Farm. Dr. Andrew Black, Thea Rodgers (Undergraduate Research Assistant), Ernest Wu (Undergraduate Research Assistant) and Dr. Paul Jassal helped in the setup and monitoring for the study. The author led and supervised all aspects of this research and then analyzed the data and wrote a draft paper,

with the guidance and contributions of Drs. Andrew Black, Paul Jassal, Mark Johnson, Sean Smukler. Zoran Nesic provided technical support throughout the research. The author was the primary supervisor of Thea and Ernest.

Chapter 3 comprises work conducted in the Biometeorology and Soil Physics Laboratory – Land and Food Systems – UBC, and at UBC Farm and Totem Field, UBC. The required shortwave and longwave radiative properties were measured using the same shortwave spectroradiometer and longwave radiative property methods used in Chapter 2 (with the help of Drs. Andrew Black and Paul Jassal), respectively, which provided the foundation for interpreting the field experiment that followed. The author led the design, construction and conduction of a field experiment in 2016 that measured the impact of vegetation-free plastic film low tunnels, with different longwave properties, on daytime and nighttime internal and external surface energy balance, air temperature, soil heat flux density and soil temperature. Dr. Andrew Black, Nicolette Lax (Undergraduate Research Assistant), Dr. Paul Jassal and Zoran Nesic helped in the setup and monitoring for the study. The author led and supervised all aspects of this research and then analyzed the data and wrote a draft paper, with the guidance and contributions of Drs. Andrew Black, Paul Jassal, Mark Johnson and Sean Smukler. Zoran Nesic provided technical support throughout the research. The author was the primary supervisor of Nicolette Lax.

Chapter 4 comprised work conducted at the UBC Horticultural Centre, Biometeorology and Soil Physics Laboratory – Land and Food Systems – UBC, UBC Farm and Totem Field, UBC.

The required shortwave and longwave radiative properties were measured using the shortwave spectroradiometer and longwave radiative property methods used for Chapter 2 (with the help of Drs. Andrew and Paul Jassal), respectively, which provided the foundation for interpreting the field experiment that followed. The author led the design, construction and conduction of a field experiment in 2017 that measured the impact of plastic film low tunnels, with different longwave properties, on Padrón pepper growth, productivity and microclimate. Mike Wagner (UBC Farm Manager) seeded the pepper used in this experiment, after which they were grown under the supervision of Melina Biron (UBC Horticultural Centre Manager), Brian Wang (Undergraduate Research Assistant) and the author until they were transplanted into soil at UBC Farm. Mike Wagner, Brian Wang and the author were responsible for all site visits regarding irrigation, data collection and system troubleshooting. The author led and supervised all aspects of this research and then analyzed the data and wrote a draft paper, with the guidance and contributions of Drs. Andrew Black, Paul Jassal, Mark Johnson and Sean Smukler. Zoran Nesic provided technical support throughout the research. The author was the primary supervisor of Brian Wang.

Chapter 5 comprises the conclusions drawn from the dissertation work. These were written by the author.

Appendix A comprises photographs and supplementary data for Chapter 2.

Appendix B comprises photographs and supplementary data for Chapter 3.

Appendix C comprises photographs and supplementary data for Chapter 4.

Appendix D comprised work performed at Mackin Creek Farm, Soda Creek, BC. The author and Ernest Wu installed soil and climate monitoring equipment to assess the impact of low tunnels on lettuce-spinach mix in 2016 and broccoli in 2016 and 2017. Unfortunately, the lettuce-spinach crop failed in 2016. Rob Borsato and Catherine Allen collected data regarding the yield of broccoli in 2016 and 2017 and provided the author with the data. Jilmarie Stephens helped to install the low tunnels used in the experiments.

Appendix E comprised work performed at Cropthorne Organic Farm, Westham Island, BC. Nicolette Lax and the author conducted a field experiment in 2016 that measured the impact of plastic film low tunnels on summer squash growth and productivity. Nicolette was responsible for all the data collection and sample processing. The author, Nicolette and Dr. Andrew Black were responsible for the initial design and construction of the experiment. Lydia Ryall (Cropthorne Organic Farm owner and operator) was responsible for the soil preparation, seeding and transplanting of the summer squash plants used in the experiment. Nicolette analyzed the data and wrote a preliminary draft paper, with the guidance of Drs Andrew Black and Paul Jassal, and the author.

An important component of this research involved outreach and the presentation of relevant results at farmer organizations and scientific conferences. The presentations and posters produced during this study are listed below.

Project presentations

Hughie Jones, Andrew Black, Rachhpal Jassal, Zoran Nesic, Mark Stephen Johnson and Sean Smukler. *The Microclimate of Plastic Mulches and Low Tunnels*. Certified Organic Associations of BC Conference 2019, Vernon BC, Canada. February 2019 (Invited)

Hughie Jones, Andrew Black, Rachhpal Jassal and Zoran Nesic. *Using plastic film mulches and low tunnels for crop protection and season extension in the Cariboo Region of BC*. Cariboo Agricultural Research Alliance: Launch and Applied Research Workshop, Williams Lake BC, Canada. February 2018 (Invited)

Hughie Jones, Andrew Black, Rachhpal Jassal and Zoran Nesic. *Using plastic film mulches and low tunnels for crop protection and season extension*. Horticulture Growers Short Course, Abbotsford BC, Canada. January 2018 (Invited)

Hughie Jones, Andrew Black, Rachhpal Jassal and Zoran Nesic. *Plastic films and their use as soil mulches and in low tunnels to modify crop microclimate and productivity*. BC Agricultural Climate Adaptation Research Workshop, Abbotsford BC, Canada. December 2017 (Invited)

Hughie Jones. *Soil moisture for farmers*. Tsawwassen Farm School, Tsawwassen BC, Canada. September 2017 (Invited)

Hughie Jones, Andrew Black, Rachhpal Jassal and Zoran Nesic. *Radiative properties of plastic films and their use as soil mulches and in low tunnels to modify crop microclimate*. CGU and CSAFM Joint Annual Scientific Meeting, Vancouver BC, Canada. May 2017

Hughie Jones, Andrew Black, Rachhpal Jassal and Zoran Nesic. *Radiation and heat transfer from plastic films used as soil mulches and low tunnels*. Society Promoting Environmental Conservation Workshop, Vancouver BC, Canada. January 2017 (Invited)

Hughie Jones, Andrew Black, Rachhpal Jassal, Zoran Nesic, Sean Smukler and Veronik Campbell. *Radiative properties of plastic films and their use as soil mulches and low tunnels to modify crop microclimate*. UBC Farm staff meeting, Vancouver BC, Canada. June 2016 (Invited)

Hughie Jones, Andrew Black, Rachhpal Jassal, Zoran Nesic, Sean Smukler and Veronik Campbell. *Radiative properties of plastic films and their use as soil mulches and low tunnels to modify crop microclimate*. CSSS/PRSSS Annual Meeting, Kamloops BC, Canada. May 2016

Andrew Black, **Hughie Jones**, Rachhpal Jassal, Zoran Nesic, Sean Smukler and Veronik Campbell. *Plastic film mulches and low tunnels to help BC farmers adapt to climate change*. FAIP Workshop Forum, Kelowna BC, Canada. December 2015

Hughie Jones, Andrew Black, Rachhpal Jassal and Zoran Nesic. *Effect of plastic mulches on surface albedo and soil temperature*. Faculty of Land and Food Systems, UBC Farm Joy of Feeding, Vancouver BC, Canada. September 2015 (Invited)

Table of Contents

List of Tables

List of Figures

List of Symbols

Symbol	Units	Description
ρ		Reflectivity
τ		Transmissivity
α		Absorptivity
ρ_s		Shortwave reflectivity
τ_s		Shortwave transmissivity
α_s		Shortwave absorptivity
ρ_L		Longwave reflectivity
τ_L		Longwave transmissivity
α_L		Longwave absorptivity
σ	$W\,m^{-2}\,K^{-4}$	Stefan-Boltzmann constant
ρ_{Lfilm}		L film reflectivity
α_{Lfilm}		L film absorptivity
τ_{Lfilm}		L film transmissivity
α_{Lm}		L mulch absorptivity
α_{Ls}		L soil absorptivity
α_{Lw}		L cover or wall absorptivity
τ_{PARw}		PAR cover or wall transmissivity
ΔS_a	$W\,m^{-2}$	Rate of change in air heat storage between the measurement of G and R_n
ΔS_s	$W\,m^{-2}$	Rate of change in soil heat storage in soil above the heat flux plate
ρ_{ss}		S soil reflectivity
ρ_{sm}		S mulch reflectivity
τ_{sm}		S mulch transmissivity
α_{sm}		S mulch absorptivity
ρ_{sw}		S cover reflectivity

Symbol	Units	Description
τ_{sw}		S cover transmissivity
α_{sw}		S cover absorptivity
$\alpha_{s\lambda}$		Spectral absorptivity
$\rho_{s\lambda raw}$		Raw reflectivity
$\rho_{s\lambda ref0}$		Reference zero-reflectivity panel
$\rho_{s\lambda ref100}$		Reference 100-reflectivity panel
a		Slope coefficient
A_m	m^2	Area of mulch
A_w	m^2	Area of cover
b		y-intercept
d	m	Thickness
D	$g\ cm^{-3}$	Water vapour density
E	mm	Evapotranspiration
E_c	mm	Canopy transpiration
E_s	mm	Soil evaporation
$E_{s\lambda}$	$W\ m^{-2}\ nm^{-1}$	Spectral irradiance
G	$W\ m^{-2}$	Soil surface heat flux density $(G = G_{3cm} + \Delta S_s)$
G_{3cm}	$W\ m^{-2}$	3-cm soil heat flux density
g_c	$mmol\ m^{-2}\ s^{-1}$	Stomatal conductance
G_{in}	$W\ m^{-2}$	Internal low tunnel soil surface heat flux density
h	time	hour
H	$W\ m^{-2}$	Sensible heat flux density
h	$W\ m^{-2}\ k^{-1}$	Heat transfer coefficient
H_m	$W\ m^{-2}$	Mulch to internal air H
h_m	$W\ m^{-2}\ k^{-1}$	Mulch to internal air h
H_v	$W\ m^{-2}$	Ventilation H
h_v	$W\ m^{-2}\ k^{-1}$	Ventilation h

Symbol	Units	Description
H_{win}	W m^{-2}	Wall to outside air H
h_{win}	W m^{-2} k^{-1}	Internal air to wall h
H_{wou}	W m^{-2}	Internal air to wall H
h_{wou}	W m^{-2} k^{-1}	Wall to external air h
L	W m^{-2}	Longwave radiation
L_d	W m^{-2}	Downwelling L
L_{dgl}	W m^{-2}	Downwelling L (glass)
L_{din}	W m^{-2}	Internal downwelling L
$L_{dincalc}$	W m^{-2}	Internal downwelling L (calculated)
L_{dou}	W m^{-2}	External downwelling L
L_{dsky}	W m^{-2}	Downwelling L (sky)
$L_{dskyfilm}$	W m^{-2}	Downwelling L (sky and film)
$L_{dskyfilmgl}$	W m^{-2}	Downwelling L (sky, film and glass)
L_{dskygl}	W m^{-2}	Downwelling L (sky and glass)
LE	W m^{-2}	Surface latent heat flux density
LE_c	W m^{-2}	Canopy LE
LE_s	W m^{-2}	Soil LE
l_l	cm	Leaf length
L_{nin}	W m^{-2}	Internal net L
L_u	W m^{-2}	Upwelling L
L_{uin}	W m^{-2}	Internal upwelling L
$L_{uincalc}$	W m^{-2}	Internal upwelling L (calculated)
L_{uou}	W m^{-2}	External upwelling L
$L_{uoucalc}$	W m^{-2}	External upwelling L (calculated)
l_w	cm	Leaf width
n		Sample size
^{o}		Degree
P	mm	Precipitation
p		Probability values

Symbol	Units	Description
P_{cum}	mm	Cumulative precipitation
P_N	μmol CO_2 m^{-2} s^{-1}	Net photosynthesis
Q	W m^{-2}	Photosynthetic flux density
Q_d	W m^{-2}	Downwelling Q
Q_{dbelow}	W m^{-2}	Below canopy downwelling Q
Q_{dou}	W m^{-2}	External downwelling Q
Q_u	W m^{-2}	Upwelling Q
Q_u	W m^{-2}	Upwelling Q
Q_{uin}	W m^{-2}	Internal upwelling Q
Q_{uou}	W m^{-2}	External upwelling Q
R^2		Coefficient of determination
R_a	W m^{-2}	Available energy ($R_n - G$)
r_a	s m^{-1}	Aerodynamic resistance
r_{ct}	s m^{-1}	Contact resistance
r_m	s m^{-1}	Mulch water vapour resistance
R_n	W m^{-2}	Net radiation
R_{nin}	W m^{-2}	Internal net radiation (inside low tunnel)
R_{nou}	W m^{-2}	External net radiation (outside low tunnel)
$R_{s\lambda}$		Spectral reflectivity
S	W m^{-2}	Shortwave radiation
S_d	W m^{-2}	Downwelling S
S_{din}	W m^{-2}	Internal downwelling S
$S_{dincalc}$	W m^{-2}	Internal downwelling S (calculated)
S_{dou}	W m^{-2}	External downwelling S
S_n	W m^{-2}	Net S
S_{nin}	W m^{-2}	Internal net S
S_{nou}	W m^{-2}	External net S

Symbol	Units	Description
S_u	W m^{-2}	Upwelling S
S_{uin}	W m^{-2}	Internal upwelling S
$S_{uincalc}$	W m^{-2}	Internal upwelling S (calculated)
S_{uou}	W m^{-2}	External upwelling S
$S_{uoucalc}$	W m^{-2}	External upwelling S (calculated)
T	ºC	Temperature
T_0	ºC	Surface temperature
T_{0film}	ºC	Film surface temperature
T_{0gl}	ºC	Glass surface temperature
T_{0s}	ºC	Soil surface temperature
T_a	ºC	Air temperature
T_{a2m}	ºC	2-m air temperature
T_{ain}	ºC	Internal air temperature
T_{ainmod}	ºC	Internal air temperature (calculated)
T_{aou}	ºC	External air temperature
T_m	ºC	Mulch surface temperature
T_s	ºC	Soil temperature
$T_{s\lambda}$		Spectral transmissivity
T_w	ºC	Wall or cover surface temperature
u	m s^{-1}	Horizontal wind velocity
u_{2m}	m s^{-1}	2-m external horizontal wind velocity
u_{in}	m s^{-1}	Internal horizontal wind velocity
v_{in}	m s^{-1}	Internal cross wind velocity
w_{in}	m s^{-1}	Internal vertical wind velocity
z	m	Height
B		Bowen ratio
ε		Emissivity
ε_{Lfilm}		Emissivity of film
ε_{Lgl}		Emissivity of glass

Symbol	Units	Description
ε_{Lsky}		Emissivity of sky
θ_s	$m^{-3}\,m^{-3}$	Soil volumetric water content
λ	nm	Wavelength
μ		Mean

List of Abbreviations

Acronym	Units	Description
ACCFHES		Aquifer coupled cavity flow heat exchanger system
AI		Apogee Instruments Inc.
BC		British Columbia
BE2		Black embossed #2
BEP		Black embossed PABPNARB
BSD		Basal stem diameter
BW		Black on white
C		Control
CA		Canada
CH_4		Methane
CO_2		Carbon dioxide
CSI		Campbell Scientific Inc.
DOY		Day of year
E		East
EAHE		earth-to-air heat exchanger
EMP		Empty
EVA		Ethylenvinylacetate
FAIP		Farm Adaptation Innovator Program
GHG		Greenhouse gas
GN		Green
H_2O		Water vapour
HDPE		High density polyethylene
IRGA		Infrared gas analyzer

Acronym	Units	Description
IRT100		Infrared transmitting
LA	m^{-2}	Leaf area
LAI	$m^{-2} m^{-2}$	Leaf area index
LDPE		Low density polyethylene
N		North
N_2O		Nitrous oxide
NIR		Near infrared radiation (700 – 1400 nm)
PAR		Photosynthetically active radiation
PC		Polycarbonate
PE		Polyethylene
PI		Protection index
POLY		Polyethylene (6 mil)
$POLY_P$		Perforated polyethylene (4 mil)
PP		Padrón pepper
PPFD	$\mu mol\ m^{-2}\ s^{-1}$	Photosynthetic photon flux density
PST		Pacific Standard Time
PVC		Polyvinylchloride
Q		Quadrant
RD		Red
ref		Reference
RMSE		Root mean square error
S		South
S4		©Super 4
SD		Standard deviation
SWIR		Shortwave infrared radiation (1400 – 2500 nm)

Acronym	Units	Description
TMX		©Thermax
UBC		The University of British Columbia
USA		United States of America
VPD	kPa	Vapour pressure deficit
W		West
WB		White on black
WUE	g of carbon (kg of $H_2O)^{-1}$	Water use efficiency

Acknowledgements

I would like to thank the Alexis Nakota Sioux Nation and Yellowhead Tribal College for supporting me throughout my PhD, your support lifted a lot of stress out of my life which allowed me to focus on my work. Thank you to the University of British Columbia (UBC) for awarding me an Aboriginal Graduate Fellowship, allowed me to attend UBC well supported and happy. The research in this thesis was supported financially by the Farm Adaptation Innovator Program in collaboration with Cropthorne Farm (Lydia Ryall), Mackin Creek Farm (Rob Borsato and Catherine Allen), the UBC Research Farm (Tim Carter and Mike Wagner), the UBC Horticulture Centre glasshouse (Melina Biron), Integrated Remote Sensing Studio (Dr. Nicholas Coops, Curtis Chance and Paul Hacker), The Centre for Sustainable Food Systems, Totem Field Science Field Station (Glen Healy), Dubois Agrinovation Inc. and AT Films Inc.. I am so grateful for the support of the people and organizations listed above.

I am further indebted to Dr. Thomas Andrew Black (Andy). Andy has been a great mentor and friend, who has changed my life forever. Andy challenged me to learn constantly and improve my skill-level, which required a tremendous amount of effort and dedication. Effort and dedication well spent. Perhaps the great lesson he has taught me is; success requires hard work, and despite your inherent gifts and talents you must push yourself to grow and transform. Thank you, Andy.

Zoran Nesic, despite my inability to understand all his analogies and metaphors when describing a concept or course of action, has been a great mentor and friend. Zoran pushed me to improve and emphasized that I would be responsible for doing so. Zoran helped me set

boundaries and trust people when leading. Zoran always made time to help me, even when it was clear I could not reciprocate soon. Thank you, Zoran.

Nicholas Grant (Nick) has been a great mentor and friend. Nick always pushed me to broaden my view of science and consider people and societal issues, more than I had, in an environment where it's easy to get drawn into the details. Nick has made me a better researcher and has been a true pleasure to chat with over the years (often while we have a cold beer after work). Thank you, Nick.

Dr. Paul Jassal has been a great mentor and friend. Paul has always been a great support and taught me to not waste time and proceed with my work immediately. I have not met many people who procrastinate so little as Paul, and I admire him for that. Thank you, Paul.

Dr. Iain Hawthorne has been a great friend and mentored me like a big brother. Iain congratulated me often, but he also held me to a high standard and kept me honest. He is truly passionate and always had time to discuss difficulties during my time at UBC. Thank you, Iain.

I would like to thank Drs. Mark Stephen Johnson and Sean Smukler for their incredible support and time. Mark and Sean have always supported my work and shown a lot of faith in me. Thanks to Drs. Michael Novak and Nicholas Coops for their time and valuable input regarding my thesis and thesis defense, and Dr. Roland Stull for taking time to chair my PhD oral examination.

Thank you to Dr. Bruce McGee for all of words of support and acts of kindness. You inspire me and I really appreciate your friendship.

A very special thank you to Thea Rodgers, Ernest Wu, Nicolette Lax and Brian Wang for all the hard work and dedication you put into my PhD work, and for your ability to be patient with me through tough times. I benefited so much from your help. I have a special place for you

in my heart. Thank you to all past and present Biometeorology and Soil Physics Group members (a few: Jilmarie, Gesa, Trevor, Pat, Chitra, Eugenie, Rick, Peng, Maggie, Carmen).

Thank you to mom and dad, along with my entire family (Jones, Potts, Clash, McInerney) for giving me a great start in life and showing so much pride in my accomplishments. My family always taught me to take nothing for granted and finish what you start. Finally, thank you to Emma P. Holmes who believes in me and supports me every day with incredible compassion, love and class. You are a star in my life Emma, and I am so grateful for you and our beautiful family (Andrew (Rew) Basil George Jones… so far).

To this point in time, I have spent the last 8 years at the University of British Columbia, and I am humbled by the great people, experiences, challenges and the hard times I've endured. It seems so little time has passed, which reveals the limitation of people's time. I have received time so generously from so many beautiful people, that is a blessing. The goal of my life is to serve a cause that improves myself, those close to me and those far away. Time is my greatest gift and I want to give it meaningfully. Looking back, my journey to receive my PhD has been incredibly meaningful and fulfilling.

Dedication

To my grandmother, Helen Elvira McInerney

To my grandmother, Annie Potts

To my mother, Georgeann Jones

To my sister, Margaret Kateri Ida Jones

To my niece, Mia Maria Jones-Ferrara

Chapter 1: Introduction

1.1   Pre-plasticulture

Long before modern plastic-covered structures became widely used by crop growers, glasshouses existed in Europe in the 13th century under Roman rule (Rasmussen 2012) and structures covered with transparent paper existed in 14th century China, during the Ming dynasty, to alter microclimate for flower and vegetable production (Jiang et al., 2004). Kew Royal Botanical Garden in London, UK, founded in 1759, is one of the most famous glasshouse gardens in the world and signifies the early beginnings of modern horticulture and Victorian glasshouses. The Victorian Age, which began during and soon after the Napoleonic Wars (1803-1815) was marked by significant advancements in botany, horticulture and glasshouse structures. John C. Loudon (1783-1843), a naturalist and influential writer of his time, became an avid collector of exotic plants from foreign countries which he grew throughout Britain. This was possible with the microclimatic benefits of glasshouses (Valen 2016). During this time engineers and architects recognized the potential of glasshouse technologies and began incorporating them into a variety of structures, leading to scientific advances in water circulation, ventilation and the invention of the first hot water radiator by Angier Perkins (1799-1881) in 1832 (Valen 2016). The Great Exhibition (later known as The Crystal Palace when it was dismantled and moved to Sydenham, UK) was constructed for the first World's Fair in 1851 located in Hyde Park, London, UK, not only exhibited technological achievements from around the world but also the impacts of using glasshouses on humans and plants. In order to make the microclimate in The Great Exhibition comfortable for visitors, Joseph Paxton (1803-1865), horticulturalist and architect of The Great Exhibition, incorporated various techniques to control the microclimate

1

within the structure (e.g., ventilation, cooling/warming and shading). In order to measure the effectiveness of microclimate control, up to forty thermometers placed inside and outside the structure were checked manually at 2-hour intervals from 9 am to 5 pm. The experimental findings and innovative techniques used for The Great Exhibition were incorporated into large estates like the Dangstein estate in Sussex, which had numerous and purposefully designed glasshouses (hot-houses), where a large variety of domestic and exotic plants were grown: orange, peach, nectarine, plum and cherry trees, strawberries, orchids, ferns, insectivorous plants, heaths, and various aquatic plants (Trotter 1988).

1.2 Plasticulture

1.2.1 Background

Plastic became commercially available in the 1940's to early 1950's, giving rise to the Plastic Age. Dr. Emery Myer Emmert at the University of Kentucky, "the father of plastic greenhouses", began studying polyethylene greenhouses as an affordable alternative to glass-covered greenhouses, and later studied plastic mulches for their use in early vegetable production systems (Emmert 1954; Emmert 1955; Emmert 1956). Since that time, global annual production of plastic increased from 1.3 to 322 Mt yr^{-1} in 2016, and global annual consumption of plastics in agriculture reached 6.5 Mt yr^{-1} (PlasticEurope 2016; Scarascia-Mugnozza et al. 2011). As of 2016, the largest producer of plastic materials is China, accounting for 27.8% of global production, followed by Europe, North America and South Asia, who account for 18.5, 18.5 and 16.7% of global production, respectively. The incorporation of plastic materials into agricultural production systems (i.e., plasticulture) involves many products with various applications: films (greenhouse, low tunnels, mulches, silage covers); conduits (irrigation and drainage); containers

(pesticide cans, fertilizer bags, pots, packaging, collection containers, and liquid storage containers); nets (orchard and vineyard covers, fruit collection, woven and non-woven floating covers) (Espi et al., 2006; Scarascia-Mugnozza et al., 2011). Plastic films account for approximately 35% of plastic consumed in European agriculture and have been very prominent in plasticulture, not only due to their general affordability, versatility, low weight and mechanical strength but also due to their unique radiative properties (reflectivity, transmissivity and absorptivity), and potential to alter soil and atmospheric microclimate.

1.2.2   Use in agriculture and composition

The most common thermoplastic polymers used to produce plastic films in agriculture include polyethylene (PE) (i.e., linear low-density polyethylene, low-density polyethylene (LDPE), high-density polyethylene), polycarbonate, ethylenvinylacetate, and, to a lesser extent, polyvinylchloride (PVC) (Scarascia-Mugnozza et al., 2011). China is the largest producer of plastic films used in agriculture, producing 700,000-1,000,000 tons year^{-1} which can cover 50 million ha year^{-1} (Li et al., 2013). In 2002 walk-in high tunnels, low tunnels and mulches covered approximately 1,200,000, 700,000 and 10,000,000 ha, respectively, in China alone, whereas only 19,000, 70,000 and 420,000 ha, respectively, were covered in Europe, the second largest consumer of plastic films globally (Epsi et al., 2006). Increased abundance of plastic film products has corresponded to diversification of plastic film properties, resulting in the emergence of 'designer' plastic films, which contain numerous additives. Additives give plastic films unique chemical, physical and radiative properties, enabling consumers to choose the film most suitable for their specific growing applications. The additives used in plastic film manufacturing include ultraviolet (UV) stabilizers, longwave radiation absorbers and reflectors, photo-selective

additives, fluorescent additives, photo-luminescent additives, anti-drip and anti-fog surfactants, pro-degradant additives (i.e., increased degradation in-situ) and ultra-thermic additives (Epsi et al., 2006; Markarian 2006; Markarian 2009; Scarascia-Mugnozza et al., 2011). Despite the technological advances in plastic film manufacturing and the benefits to consumers, plastic films also have the potential to cause adverse negative impacts to the local, regional and global environment.

1.2.3 Pollution

As the consumption and distribution of plastic increases worldwide so do concerns regarding the rate and fate of plastic pollution, e.g., whether it accumulates in landfills, is recycled and reused or discharged into waterways (Astrup et al., 2009; Barnes et al., 2009; Eriksen et al., 2014; Steinmetz et al., 2016). In agriculture, the installation and removal of plastic films is labor-intensive (6 and 82 hours (h) ha^{-1} when mechanized and hand-applied, respectively, and 7 h ha^{-1} to remove) and often results in plastic film debris accumulating in the soil (McCraw and Motes 1991; Schonbeck 1995). In the USA, approximately 6% of municipal solid waste is recovered for recycling and reuse (Barnes et al., 2009) and as of 2014 it is estimated that ~260,000 tons of plastics are in the world's oceans listed as follows in order from highest to lowest total mass of plastics: the North Pacific, India Ocean, North Atlantic, Mediterranean Sea, South Pacific and South Atlantic (Eriksen et al., 2014). Plastic waste typically accumulates in specific locations within the ocean, known as zones of accumulation: near large urban centers; convergence zones; trade routes. It is estimated that 3-14% of plastic debris in the ocean resides on the ocean surface, of which 99% of the particle size distribution is dominated by microplastic ($\leq$ 5 mm) (Cózar et al., 2015).

Given that marine mammals, birds, reptiles and fish all ingest plastics of various sizes (micro-, meso- and macro) plastics are of concern in aquatic ecosystems. Microplastics are the most abundant size class in the world's oceans (91%), yet they account for only 13% of total plastic mass in the world's oceans (Cozar et al., 2013). Microplastics enter the aquatic food chains more easily than macroplastics and are of concern because they are mistaken as food by zooplanktivorous fish (Cozar et al., 2014). Although studies regarding plastic size distribution and total mass have been performed, little is known about the vertical distribution of plastic in the ocean water column and on the ocean floor, indicating that the full magnitude of plastic pollution in aquatic ecosystems and food chains remains relatively unknown. Given that the longevity of plastic ranges from hundreds to thousands of years (Barnes et al., 2009; Cozar et al., 2014) the continued use of plastic in agriculture requires strategies to ensure it is recycled or reused to avoid pollution of terrestrial and aquatic ecosystems.

1.3   Radiation balance

1.3.1   Shortwave radiation

When plastic films are applied to the soil surface as a mulch or on an enclosure (e.g., low tunnel, high tunnel), the shortwave (S; subscript s refers to shortwave radiation) (all symbols are defined in the List of Symbols section) properties of the plastic film strongly control the soil and enclosure microclimate, particularly during the daytime. In general, if a producer intends to cool or warm the soil surface, they will choose a plastic film that has a high shortwave reflectivity (ρ_s) or high shortwave transmissivity (τ_s) or absorptivity (α_s) value, respectively. Ham et al. (1993) found that a plastic film mulches with a high ρ_s value (0.48) was able to reduce the maximum mean daily soil temperature (T_s: subscript s refers to soil) by only ~0.5 ^{o}C compared to the

5

control (bare soil), whereas soil covered with plastic film mulches with high τ_s (0.84) and α_s (0.96) values experienced increases of 1 and 3 °C, respectively. Often plastic films with high τ_s values are favored over films with high α_L values to achieve very high T_s values in order to kill soil-borne pathogens (solarization, Culman et al., 2006), but there is controversy in the literature whether plastic films with high τ_s or α_s values are most effective at soil heating. Some workers have pointed out that the degree of contact between the plastic film mulch and the soil surface controls whether plastic films with high τ_s or α_s values are most effective at soil heating (Ham et al., 1993; Ham and Kluitenberg, 1994). It is also important to consider the role of plastic film longwave properties in their ability to alter soil T_s, during both the daytime and nighttime.

Plastic films on low tunnels that have high τ_s values are often desired in order to achieve the highest internal air temperature (T_{ain}), particularly in temperate regions, but τ_s can fluctuate depending on plastic film age, soiling, condensation and time of day. Geoola et al. (1998) found that for dry polycarbonate τ_s decreased ~6%, 7% and 14% after 9 months with dirt accumulation (i.e., no cleaning), 18 months with cleaning and 18 months with dirt accumulation, respectively. Condensation can impact plastic film τ_s values and Pieters et al. (1997) showed that glass and polyethylene τ_s were ~90% and 85% (0° angle of incidence) without and ~80% and 65% with droplet condensation, respectively, a relatively large reduction in τ_s, particularly for polyethylene. Studies have shown that anti-drip polyethylene (maintains a smooth film of water) τ_s decreases 12% less than that for conventional polyethylene when wet, which is significant when calculating the annual energy balance (Geoola et al., 1998). In terms of plastic film aging, Ngouajio et al. (2005) found that τ_s decreased ~3% for a white plastic mulch but increased ~2%, 6% and 3% for grey, IRT (Infrared transmitting) green and IRT mulch after one growing season

of use. Studies of high transparency polyethylene show τ_s decreases and α_s increases with age (Youssef et al., 2008; Graefe and Sandmann 2015). On an hourly basis, τ_s changes depending on the angle of incidence and is typically highest at 0° and $50 - 60^{o}$ angle of incidence for dry and wet polyethylene, respectively (Pieters et al., 1997).

1.3.2   Longwave radiation

The emission of longwave (L) radiation from a plastic film covered soil is controlled by 1) spectral properties and 2) surface temperature (T_0) ($L = \varepsilon \sigma T_0{}^4$, where σ is the Stefan-Boltzmann constant and ε is the surface emissivity or α_L) of the soil surface (T_{0s}) and plastic film mulch. Typically, plastics film mulches and naturally occurring soils have very low ρ_L values (<0.05) and τ_L and α_L control L. Unlike soil, plastic films can have τ_L values greater than zero and the relative proportions of τ_L and α_L of a plastic film controls the proportions of upwelling (i.e., outgoing) longwave emission (L_u) originating at the film and soil surfaces ($L = \alpha_{Lfilm}\sigma T_{0film}{}^4 + \tau_L \alpha_{Ls}\sigma T_{0s}{}^4$, where T_{0s} is soil surface temperature). Although studies on the impact of mulch longwave spectral properties on T_s exist (Tarara 2000), studies that focus on the impact of mulch shortwave spectral properties on T_s are more prominent. On the other hand, when it comes to enclosures, like glasshouses and low tunnels, there have been more studies that focus on the impact of longwave spectral properties on T_{ain}.

Just over 100 years ago, the microclimate of transparent enclosures was misunderstood and there was debate as to whether 1) longwave emission from an enclosure's cover or 2) wind protection caused T_{ain} to exceed the external air temperature (T_{aou}), or both (Wood 1909; Van Gulik 1910). Both Wood and Van Gulik performed temperature experiments indoors and observed no difference in T_{ain} within enclosures covered with materials that had high or low α_L

values. Later, Businger (1963) pointed out that both experiments were not representative of outdoor conditions and that only covers with high α_L values would increase T_{ain} on cloud-free days, when net longwave radiation (L_n) is largely negative. According to Businger (1963), approximately 25% of the difference between T_{ain} within a glasshouse ($\alpha_L = 1$) and T_{aou} (T_{ain} - T_{aou}) is a result of longwave radiation being absorbed and re-emitted back to the glasshouse floor from the glass cover, and the remaining 75% is a result of wind protection. The effectiveness of any greenhouse cladding material for trapping radiant heat depends on the α_L of the material. High α_L value materials, like glass, have the greatest potential for re-emitting longwave back to the floor of a greenhouse-like structure and are preferred for decreasing longwave losses from a greenhouse and increasing L_n (i.e., less negative during daytime and nighttime). In Japan, Al-Mahdouri et al. (2014) found that noon T_a (in January) was approximately 8.3 and 9.5 $^{\circ}$C greater in greenhouses covered in silica glass (1 mm thick) and PVC (50 μm thick), respectively, compared to a greenhouse covered with LDPE (50 μm thick), which was attributed to the high α_L of silica glass and PVC. Although glass is one of the most effective single-layer longwave absorbers, the use of double layer plastic covers provides additional thermal benefits. Zhang et al. (1996) showed that a double-layer greenhouse comprising PE and anti-fog thermal PE with a 0.25-cm thick air gap had 107% of the average energy consumption of that for silica glass; and if a 50% aluminized thermal screen was used, in addition, the average energy consumption was 76% of that for silica glass, which equates to substantial energy-cost savings in temperate climates. Interestingly, Zhang et al. (1996) found that the greenhouse with covers with the highest heat loss rates (i.e., 1-year anti-fog polyethylene) experienced the greatest heat loss reduction when they added a thermal screen, and that the differences in heat loss rates decreases

under cloudy conditions. The findings of Zhang et al. (1996) explain the lack of T_{ain} difference

observed by Wood (1909) and Van Gulik (1910) when they compared rocksalt and glass covered

enclosures indoors (i.e., like a cloudy sky). Zhang et al. (1996) were able to demonstrate a 24%

reduction in longwave loss using thermal screens, which agrees well with analytical solutions,

which estimate that the maximum reduction in longwave emission loss using a single layer glass

cover is approximately 25% (Businger 1963; Lee 1976).

1.4   Energy balance

1.4.1   Latent and sensible heat fluxes

Use of mineral and organic mulches (corn residue; barley straw; dolerite) for reducing E_s

has been studied by many workers (Groenevelt et al., 1989; Tanner and Shen, 1990; Hares and

Novak, 1992; Novak et al., 2000; Fuchs and Hadas, 2011; Dlamini et al., 2016). Both the water

vapour resistance of the mulch layer (r_m) and vapour density gradient between the soil surface

and free-air above the mulch control E_s (Tanner and Shen, 1990). Fuchs and Hadas (2011)

showed that both increased organic mulch (they used straw) thickness and decreased wind

velocity (u) above the mulch which resulted in an exponential increase in r_m. Over a 40-day

period, Groenevelt et al. (1989) showed the average cumulative E_s for three mulches (10-mm-

thick layer) (black volcanic scoria, white zeolite and black sand) was 15.5 mm compared to 95.5

mm for bare soil. Modaihsh et al. (1985) found average values of cumulative E_s from soil

covered with 20 mm coarse and fine sand layers, and 60 mm coarse and fine sand layers were

46.2, 37.6, 15.5 and 15.0 mm, respectively, compared to 67.9 mm from control (bare soil).

Unlike mineral, organic mulches and permeable fabric (e.g., polypropylene row covers), which

are permeable to water (liquid and vapour), plastic film mulches are impermeable to water (i.e.,

infinite r_m) even with low thickness (~0.025 mm) (Hopfenberg 1974), meaning their

effectiveness for reducing E_s should exceed that of mineral and organic mulches. Dlamini et al.

(2016) found that 120-day cumulative E_s from bare (control), dolerite-covered and plastic-film

covered soil was 184, 124 and 118 mm, respectively, revealing the large reduction in E_s that can

be achieved when using plastic or mineral mulches. Nevertheless, despite their effectiveness in

reducing E_s, mineral mulches are difficult to transport, apply, remove and are often supply

limited due to large distances to sources.

Organic mulches are often favorable to mineral mulches due to their low weight, on-site

availability, transportability and effectiveness (i.e., reduction in E_s) (Li et al., 2013). Farzi et al.,

(2017) found in Iran that pistachio shell mulch (10 mm thick) was more effective at reducing E_s

than gravel mulch (25 mm thick), whereas Mellouli et al. (2000) found that straw mulch applied

at a rate 450 g m^{-2} (5 cm thick) caused a small reduction in E_s (4.5 % over 46 days; soil water

content was near field capacity on day 1) compared to bare soil (Mellouli et al., 2000 performed

their experiment in laboratory conditions with no wind). Despite this low value it is generally

accepted that organic mulches reduce E_s by 30 – 60 % compared to bare soil E_s and are an

effective means of conserving soil moisture (Unger and Parker 1968; Bristow et al., 1986). A

common goal when using mulches (mineral, organic and/or plastic film) is to reduce E_s in order

to reduce evapotranspiration (E), increase gross primary productivity (GPP) (i.e., photosynthesis)

by making more soil water available for crop uptake, and increase water use efficiency (WUE =

GPP/E) of crop production systems.

During pre-leaf-emergence when leaf area index (LAI) and the soil volumetric water

content (θ_s) near the soil surface are low, sensible heat flux (H) and the Bowen ratio ($\beta = H/LE$,

where LE is the latent heat flux density) are typically large (Jones et al., 2017), but when the soil is wet β decreases (Fuchs et al., 1997). Often in the pre-leaf-emergence period, soil heat flux density (G) is large and T_s increases which can hasten seed germination. As mentioned in Section 1.3.1, the use of plastic film mulches with high τ_s or α_s values (the latter is preferred when the soil surface and plastic film are in close contact), can increase both G and T_s, which is beneficial to producers attempting to warm the soil early in the growing season.

As discussed before (Businger 1963; Lee 1976), an enclosure with a high τ_s cover elevates T_{ain} by 1) altering heat transfer by providing a physical barrier to convective heat transfer (i.e., increased r_a), and 2) altering R_n by decreasing L_n losses (day and night), when a cover with a high α_L value is used. Fuchs et al. (1997) found that the internal sensible heat flux resistance (r_{in}) (between the soil surface and enclosed air) and the heat exchange resistance (r_{ou}) (between the enclosed air and outside air) values were 157 and 245 s m^{-1}, respectively, in an unventilated 7.5-m-wide and 23-m-long greenhouse, which are much greater than r_a values reported for sparse crops (~20 – 40 s m^{-1}, Ham and Heilman 1991). Given, enclosed structures greatly increase aerodynamic resistance, H, which would have otherwise escaped to the free atmosphere in absence of the enclosure, is trapped within the enclosure causing T_{ain} to rise. Therefore, sensible heat must be conducted through the enclosure's cover, diffuse through air gaps in the enclosure cover, and/or be ventilated purposely. Increased T_{ain} of an enclosure can be beneficial for crop production but it is crucial to consider how vapour pressure deficit (VPD), E_s, canopy transpiration (E_c) and productivity inside the enclosure are impacted.

To predict the sensible heat transfer of an enclosure, heat transfer coefficients (h; W m^{-2} K^{-1}) must first be calculated using experimental data, and then modelled. The heat transfer

processes and h for the external cover (h_{wou}) are primarily a function of wind velocity (i.e., forced convection), and, to some degree, by the temperature gradient between the enclosure cover and the outside air (i.e., free convection). On the other hand, heat transfer processes and h for the enclosure floor (h_m) are primarily a function of the temperature difference between the floor and the internal air (i.e., free convection), and, to a lesser degree, the external wind velocity (i.e., forced convection).

E_s can be reduced substantially and E_c can remain unaffected when plastic film mulches are used alone. On the other hand, high τ_{sw} enclosures (i.e., low tunnels) can alter E_c by altering stomatal conductance (g_s), aerodynamic conductance, water vapour concentrations, and T_a in the crop canopy. Yang et al. (1990) found that daytime and nighttime g_s for cucumber (with no supplementary light), grown in optimal water supply conditions, were approximately 20 mm s^{-1} and 8 mm s^{-1}, respectively. Bakker (1991) found that values of maximum nighttime g_s were 1.76, 3.93, 2.08 and 4.4 mm s^{-1} for eggplant, cucumber, pepper and tomato, respectively, which declined exponentially with increasing VPD. Zhang and Lemeur (1992) found aerodynamic conductance in a high τ_{sw} enclosure, with vegetation, to be a function of both free and forced convection with values of the Reynolds and Grashof numbers of approximately 6.8 x 10^2 and 6.3 x 10^4, respectively,(i.e., mixed convection) and average air velocity of 0.02 m s^{-1} when the canopy-to-air temperature difference was 2 $^{\circ}$C. In an analysis of three studies (Fujii et al., 1973; Kreith, 1965; Stanghellini, 1987), Zhang and Lemeur (1992) found that the aerodynamic conductance, typically overestimated using the existing models, resulted in overestimation of H and LE. Examination of the inverted Penman-Monteith equation to calculate g_s (i.e., LE is measured) indicates that if VPD is large inside the enclosure, error in the estimation of

12

aerodynamic conductance will produce large errors in the calculation of g_s (Monteith and Unsworth 2008). Although increasing T_{ain} may benefit plant growth and fruit production, particularly in cold and temperate regions, T_a may reach the critical maximum temperature for a crop. Hermida-Carrera et al. (2016) found that average ribulose 1,5-bisphosphate CO_2 assimilation rate for 18 C3 plant species and 2 C4 species was 10, 23 and 42 μmol m^{-2} s^{-1} and 35, 49 and 60 μmol m^{-2} s^{-1} at 15, 25 and 30 ^{o}C, respectively. Yield-temperature-response models analyzed by Makowski et al. (2015) estimate that in hotter climates, temperature increases would cause a decline in yield while in cool climates increased temperatures will increase yield, which emphasizes the need for regional strategies to maximize the effectiveness of enclosures with high τ_s values for increased crop productivity. Although many enclosures with high τ_s values (i.e., greenhouses, low tunnels, and glasshouses) ventilate passively, cooling and heating technologies are crucial to properly controlling the microclimate within them.

1.4.2   Water use efficiency

Zegada-Lizarazu and Berliner (2011) found corn (*Zea mays* L.) inter-row mulched with polyethylene film exhibited a reduction in E and a significant increase in dry biomass production along with increases in leaf-level WUE, transpiration, and photosynthesis, implying reductions in E_s exceeded increases in transpiration. In peach production on a loess plateau in China, Wang et al. (2015) found annual E was 445, 396 and 363 mm, E_c was 172, 201 and 191 mm, and fruit yield WUE (WUE$_f$, fruit yield/E (kg ha^{-1} mm^{-1})) was 57, 81 and 90 kg m^{-3} for bare soil, plastic film mulch and straw mulch, respectively. Singh et al. (2011) found grain and biomass yield increased for winter wheat grown with plastic mulch, and measured a reduction in E_s of 35 and 40 mm and an increase in E_c of 30 and 37 mm, in 2006 and 2007, respectively, resulting in nearly

no change in annual E, grain transpiration efficiency (TE$_g$, TE$_g$ = grain yield/E_c (kg ha^{-1} mm^{-1}))

or biomass transpiration efficiency (TE$_b$, TE$_b$ = dry biomass/E_c (kg ha^{-1} mm^{-1})). Similar results

were reported by Liu et al. (2014) who found plastic mulch did not significantly change annual

E, but did increase grain yield WUE (WUE$_g$, WUE$_g$ = grain yield/E^{-1} (kg ha^{-1} mm^{-1})). In contrast

Huang et al. (2005) found that wheat field E declined 15-20 % as a result of mulching which

caused WUE$_g$ and biomass WUE (WUE$_b$, WUE$_b$ = biomass yield/E^{-1} (kg ha^{-1} mm^{-1})) to increase

from 5.58 to 7.32 and 19.26 to 24.10 kg ha^{-1} mm^{-1} for non-mulched and mulched wheat,

respectively. These research findings show that: 1) mineral, organic and plastic film mulches are

an effective tool for reducing E_s, 2) reductions in E_s caused by mulches are sometimes associated

with equal increases in E_c causing E to remain unchanged, 3) mineral, organic and plastic film

mulches increase WUE when E decreases and GPP increases, and 4) WUE$_b$, WUE$_g$ and WUE$_f$

all have the potential to increase through increased TE$_b$ and TE$_g$.

1.4.3   Cooling strategies

Crop producers in arid or tropical climates often experience excessively high T_{ain} and

VPD, and high values of direct S_d during the summer, which can cause unwanted plant heat

stress. In that case, several strategies are available to reduce internal downwelling shortwave S_{din}

and T_{ain}, which include evaporative cooling (i.e., misting) to reduce T_{ain} and VPD (Katsoulas et

al., 2001; Fuchs et al., 2006; Kumar et al., 2009), cover whitening or shading to decrease τ_s

(Baille et al., 2001; Kumar et al., 2009; Mashonjowa et al., 2010), natural (or free) and forced

ventilation (Boulard et al., 1997; Fuchs et al., 1997; Teitel and Tanny 1999; Critten and Bailey

2002; Boulard et al., 2000 Kumar et al., 2009), and geothermal cooling and heating (Sethi and

Sharma 2007). Baille et al. (2001) found that reducing τ_{sw} by ~25% using calcium oxide (CaO)

reduced greenhouse VPD, the difference between T_{ain} and T_{aou}, the difference between canopy temperature and T_{ain}, and increased λE_c by 1 kPa, 5 °C, 6 °C and 50 Wm^{-2}, respectively, at midday. Similarly, Mashonjowa et al. (2010) found maximum greenhouse T_{ain}, VPD and the difference between T_{ain} and canopy temperature declined after the application of CaO, but unlike Baille et al. (2001) E_c declined and g_s remained unchanged.

Evaporative cooling is an effective strategy for reducing plant heat stress because it changes the partitioning of available energy (R_a), typically reducing the sensible heat flux (H) and Bowen ratio (H/LE). Katsoulas et al. (2001) found that T_{ain} and VPD declined after misting (maximum evaporative cooling potential = 245 Wm^{-2}, i.e., latent heat of 100% mist evaporation), but E_c and g_s were not significantly changed. Using a fan-pad-system (i.e., evaporative cooling with forced ventilation), Fuchs et al. 2006 showed that it is possible to lower T_{ain} (7.5 m wide, 23 m long and 5 m height) below T_{aou} given the outside relative humidity is below 50%. Typically, evaporative cooling strategies are used in extremely hot climates, whereas ventilation and shading are used in temperate climates, but a combination of many cooling strategies can be advantageous depending on the outcomes desired by the producer (Kittas et al., 2003). For example, Ghosal et al. 2003 found that wetted shade-cloth and non-wetted shade-cloth reduced greenhouse T_a by 6 and 2 °C, respectively, emphasizing the importance of multiple cooling strategies when required.

Additional greenhouse cooling strategies include earth-to-air heat exchanger (EAHE) and aquifer-coupled-cavity-flow heat exchanger systems, which are capable of lowering T_{ain} by 5 - 7 °C (Sethi and Sharma 2007), but these exchanger systems can be costly. In hot climates EAHE's are typically used to moderate excessive temperatures in the hottest period of the growing season

and consist of pipes buried 1-4 m below the soil surface, in which hot greenhouse air is circulated and cooled as heat fluxes into the surrounding soil. In Delhi, India Ghosal et al. (2004) found greenhouse temperature was reduced 3 - 4 °C on a clear summer day, and latter Ghosal and Tiwari (2006) showed that lower airflow rates, increased pipe length, increased pipe depth and decreased pipe diameter all caused greater reductions in T_{ain}, causing a maximum reduction of 6 - 7 °C during a typically clear summer day. An aquifer coupled cavity flow heat exchanger system's (ACCFHES) is another cooling strategy for greenhouses, similar to a EAHE, in which air is blown or drawn through a pipe containing water below the soil surface causing negative sensible heat flux and evaporative cooling for the air circulating through the pipe. Sethi and Sharma 2007 found that an ACCFHES used in a 6 x 4 m greenhouse caused T_{ain} to remain 6 - 7 °C below the T_{aou}.

1.4.4   Heating strategies

In contrast to crop producers in hot climates, crop producers in temperate and cold climates experience low annual air temperatures, low and high VPD, depending on seasonality, and low values of direct S_d during the summer which result in short growing seasons. As a result, cheap and effective, preferably passive, heating strategies are invaluable to crop producers in cold regions because it allows them the opportunity to produce crops on the shoulders of the growing season typical of their region, and in the winter months in some cases. Mariani et al. (2016) estimated heating requirements for Europe and found that December – February heating requirements range from 1056 MJ m^{-2} in Finland to 45 MJ m^{-2} in Sous-Massa, Morocco. Sethi and Sharma (2007) measured the heating potential of an ACCFHES in India during winter

months (November - February) and found that T_{ain} can be increased by 7 - 8 °C and showed that the ACCFHES will allow substantial increases in revenue for the producer.

1.5 Crop productivity

1.5.1 Effects of mulches

Taber et al. (1993) found that clear polyethylene and wavelength selective (IRT 76) polyethylene film used as mulch increased early muskmelon yield by 300% and muskmelon survivability from 64% to 86% and 98% when plastic mulch and row covers (i.e., like low tunnels) were used, respectively. Brandenberger and Wiedenfeld 1997 found use of any plastic mulch increased average T_s, total yield and fruit size, with an average yield increase of 42% and 27% for muskmelon in the first and second year of growth, respectively. Differences in soil temperature were largest early in the growing season and small during the full-leaf period, likely due to the low LAI during that period (Brandenberger and Wiedenfeld 1997). Ibarra et al. 2001 found that early muskmelon plant biomass, total leaf area and total marketable yield (10 to 32 days after seeding) were 0.59 g, 27.7 cm^2 and 13 t ha^{-1} for bare soil and 1.77 g, 195 cm^2 and 48 t ha^{-1} for black plastic mulch, respectively. Interestingly, Egel et al. (2008) found that although cumulative watermelon yields were 19,655 and 35,373 kg ha^{-1} for bare soil and black plastic mulch, respectively, tap-root length was significantly lower for watermelons grown using black plastic, which was attributed to drought-like conditions experienced by the watermelon grown in bare soil. In Syria, Yaghi et al. (2013) found that the yield of cucumbers grown in bare soil with drip irrigation was 44.1 t ha^{-1} and was 57.9 and 63.9 t ha^{-1} for cucumbers grown in black and transparent mulches, respectively. In China, Wang et al. 2016 showed that black plastic mulch increased maize yield and aboveground biomass more in dry regions, 93% and 59%,

respectively, and less in wet regions, 30% and 37%, respectively, compared to bare soil. In Eastern Canada, Kwabiah et al. (2004) found black plastic mulch increased corn cob weight, compared to corn grown in bare soil, by 18-26%, 19-24% and 9-13% for corn planted on May 1, May 15 and May 29, respectively. In BC Canada, Baumann et al. (1997) found that total strawberry yield increased from 2.8 t ha^{-1} in bare soil (i.e., control) to 3.2 and 3.5 t ha^{-1} when strawberries were grown in green and black plastic mulches, respectively, but no direct measurements of crop microclimate were used to explain the difference in yield. Regarding peppers, Liang et al. (2011) found that straw mulch, black plastic mulch and black plastic mulch combined with straw increased hot pepper yield in a greenhouse by 82%, 65% and 112%, respectively, compared to the no mulch treatment (i.e., control), but all treatment effects diminished in the following years. Ćosić et al. (2017) found that sweet pepper yield increased from 5.2 Mg ha^{-1} in non-mulched with full irrigation (100% of potential evaporation) plots to 9.7 Mg ha^{-1} in black plastic mulched plots with deficit irrigation (70% of potential evaporation). As discussed in previous sections, increases in T_s and decreases in E_s are the two most cited explanations for the productivity increases associated with plastic mulches. In contrast to many studies that found increased yield associated with plastic mulch, Wang et al. (2009) and Li et al. (1999) found reductions in yield of potato and spring wheat when black and transparent mulches were used for too long. Li et al. 1999 found if transparent plastic mulch was used for more than 40 days after sowing (DAS), photosynthesis was suppressed, which decreased yield. Wang et al. 2009 found that use of plastic mulch decreased potato yield in all cases, unless it was removed earlier than 60 DAS.

1.5.2 Effects of enclosures

Like plastic film mulches, enclosures covered with high transparency materials (e.g., low tunnels, high tunnels and glasshouses) can improve crop microclimate and alter crop productivity. Often high tunnels are most effective in the early or late growing season. Enclosures with medium to high τ_{sw} values are not only effective during the early and late growing season (Hunter et al., 2012; Retamal-Salgado et al., 2014) but are also effective during peak growing season to cool crops which would otherwise experience heat stress (Singh et al., 2012). Planting density inside high τ_s enclosures can also play an important role in determining water use and total yield. Qiu et al. 2013 compared various planting densities of greenhouse grown tomatoes (average 3.1, 3.7, 4.4, 5.0 and 5.6 plants m^{-2}) and found average single fruit weight yield per plant decreased with increased planting density. Although enclosures with high τ_{sw} values have great potential to increase yield and crop productivity, climate, soil and water management are very important for the ultimate success of the crop grown in the enclosure.

1.6 Thesis focus and outline

Crop producers worldwide are facing challenges and opportunities associated with climate change and variability (e.g., Lee et al. 2011; Olesen et al. 2011; Traore et al. 2013; Mereu et al. 2015). In Canada, increased temperatures may provide opportunities for new types of crops, increased growing-season length, and increased crop productivity due to low mean annual temperatures, but water deficits may offset potential crop productivity gains in some regions (Smith et al. 2011). In British Columbia (BC), increased annual temperature may enable establishment of fruit in regions where it was not possible previously (Rayne and Forest 2016). In BC, temperatures have increased on average by 1.4 ℃ from 1900 to 2013 (BC Ministry of

Environment 2016), and it is predicted that in southwestern BC temperatures will increase by 0.8 to 2.6 ºC and 1.4 to 3.6 ºC in the wintertime and summertime, respectively, by the 2050's (Zwiers et al., 2011). Annual precipitation has increased across BC, yet it is expected that more wintertime precipitation will fall as rain, which will limit snowpack and glacier accumulation essential for summer streamflow, important for irrigated lands in BC (Kang et al. 2016; Schiefer et al. 2007; Werner et al. 2013). This thesis is the result of research conducted within the umbrella of the BC Farm Adaptation Innovator Program (FAIP). The objectives of the project were to 1) evaluate state-of-the-art commercially available plastic films for their ability to enable crop producers to adapt to regional climate variability and change, 2) communicate predicted climate change impacts on growing conditions to increase grower awareness and knowledge regarding the role and efficacy of soil mulches and low tunnels. The field research for this project took place at three certified organic farms: UBC Farm (Vancouver, BC), Mackin Creek Farm (Near Soda Creek, BC) and Cropthorne Farm (Westham Island, BC). Work performed at UBC Farm and in the Biometeorology and Soil Physics Group (BIOMET) laboratory focused on instrument-intensive experiments related to radiation, energy and gas exchange in various soil mulch and low-tunnel treatments, which required continuous on-site measurements during the growing season. Work performed at Mackin Creek Farm and Cropthorne Farm focused on quantifying the effects of treatments on crop productivity.

The goal of this dissertation is to characterize the radiative properties of various plastic films and determine their effect on soil and atmospheric microclimate when used as mulches or on low tunnels. More specifically:

1. Chapter 2 presents the study of shortwave and longwave radiative characteristics of 9 state-of-the-art commercially available plastic films and reports the results of a field experiment to quantify their effect as mulches on T_s and the radiation balance of the soil surface.

2. Chapter 3 presents a study of radiation balance, energy balance and microclimate of unvegetated low-tunnels covered with plastic films with different longwave radiation transmissivities.

3. Chapter 3 also presents a study of sensible heat transfer coefficients of plastic films as mulches and in low tunnels and validates a model to calculate low-tunnel air temperature.

4. Chapter 4 presents a study of changes in air temperature, water vapour and CO_2 concentrations as a result of using low tunnels with and without vegetation.

5. Chapter 4 also presents a study on the effect of low tunnels on Padrón pepper yield.

6. Chapter 5 presents an overview of the findings from this dissertation and discusses knowledge gaps that should be studied in the future.

7. Appendices A, B and C provide further information on Chapters 2, 3 and 4, respectively, including supplementary graphs and photographs of experiments in the field and laboratory.

8. Appendix D provides a brief overview of a multi-year study on the effect of low tunnels on broccoli production.

9. Appendix E presents the preliminary results from a study on the effect of perforated low tunnels on summer squash production.

Chapter 2: The effect of spectral radiative properties of plastic film mulches on surface energy balance and soil temperature

2.1 Summary

Plastic film mulches are widely used in agriculture to control soil microclimate, yet their impact on daytime and nighttime soil heating and the energy balance is not fully understood. We measured the shortwave (S) and longwave (L) spectral radiative properties (reflectivity (ρ), transmissivity (τ) and absorptivity (α)) of nine plastic film mulches, and quantified their effect on soil heat flux density (G), net radiation (R_n, above the films) and soil temperature (T_{s2cm}, 2-cm depth; T_{s10cm}, 10-cm depth) in comparison to a control (bare soil). During the daytime, all plastic film treatments increased G when compared to the control to a maximum of ~45%, except for a plastic film that had a high shortwave ρ (ρ_s) value (0.45). Total daily G increased for all plastic films, even for the plastic film with the high ρ_s value due to the insulating effect of the plastic films during the nighttime, which is attributed to the low longwave τ (τ_{Lm}) values of the plastic films and the still air layer between the films and the soil surface which decreases sensible heat loss. The plastic films with the highest α_{sm} and ρ_{sm} values had the highest and lowest daytime R_n, respectively. As a rule, plastic films with high τ_s and α_L values caused the greatest increases in T_{s2cm} and T_{s10cm}, followed closely by plastic films with low τ_{sm} values and ρ_{sm} values, with low α_{Lm} values. Total daily G increased for all plastic films in proportion to daily net shortwave radiation (S_n) and the lowest total daily downwelling shortwave radiation (S_d) required for total daily G to become positive was 9.4 MJ m^{-2} compared to 17.6 MJ m^{-2} for the control, which highlights the potential of plastic films to promote soil warming and extend the growing season.

2.2 Introduction

Mulches are protective covers placed on the soil surface. Like mineral and organic mulches, plastic films have the potential to suppress weeds (Brault et al., 2002; Ngouajio and Ernest 2004), decrease erosion (Zhang et al., 2013), conserve volumetric water content (θ_s) by reducing soil evaporation (E_s) (Dlamini et al. 2016; Yin et al. 2016), alter the surface energy balance (Hanson 1963; Tanner 1974), and modify soil (T_s) and air temperature (T_a) (Baille et al., 2001; Tarara 2000; Singh et al., 2012). Although the exact motivation for the historical use of mulches is debated, mineral mulches have been used for thousands of years in North and South America, Europe, Africa, Asia, and Australia (Lightfoot and Eddy, 1995; Lightfoot, 1996). Unlike mineral (e.g., sand, gravel and stones) and organic (e.g., crop residue, sawdust, wood chips, and bark,) mulches, which generally slow soil warming (unless mineral mulch is applied to high organic matter soils), plastic film mulches can permit faster or slower soil warming depending on their radiative properties.

The characteristic that makes plastic films unique when compared with mineral and organic mulches is their radiative properties. For mineral or organic mulches to effectively reduce E_s they must have a critical thickness, but it is well known that as mineral or organic mulch thickness increases, mulch shortwave transmissivity (τ_{sm}) declines (Hares and Novak, 1992), which results in lower net radiation (R_n) and soil heat flux (G) at the soil surface. As a result, attempts to reduce E_s using mineral (Diaz et al., 2005) or organic mulches may have secondary effects on soil radiative and heat exchange that may be undesirable. In contrast, plastic film mulches are thin which allows them to possess unique shortwave (S) and longwave (L) radiative properties (e.g., high τ_{sm} and low τ_{Lm}).

Net solar radiation (S_n) is the difference between downwelling shortwave radiation (S_d) and upwelling shortwave radiation (S_u), where $S_n = S_d - S_u$. During the daytime, S_d is the largest radiative component of the surface radiation balance. Since S_u is the product of S_d and the shortwave ρ (ρ_s or albedo) of the surface ($S_u = S_d\rho_s$), alteration of ρ_s strongly controls the surface radiation balance of a plastic film mulch and can vary from ~ 0.03 to 0.5 (Ham et al., 1993). High ρ_s plastic films decrease S_n at the film surface and thereby decrease S_n of the soil they cover, which results in decreased G and T_s near the soil surface (Ham et al., 1993). A potential benefit of high ρ_s plastic films (as a mulch on the soil surface) is their ability to increase photosynthetic flux density in the lower part of the crop canopy by reflecting photosynthetically active radiation (PAR) that has passed through the canopy, which has been shown to increase plant survival and root biomass in Echinacea (*Echinacea angustifolia*) (Burrows and Reese, 2007), strawberry production (Meyer et al., 2012; Shiukhy et al., 2015) and apple fruit quality (Overbeck et al., 2013).

Plastic film mulches that have high solar α (α_s) also have the highest film surface temperatures and can reach values of 90 °C in Manhattan, Kansas (Ham et al., 1993). Although high α_s or ρ_s implies less S_d is directly transmitted to and absorbed by the soil surface, which is essential for weed suppression (Brault et al., 2002; Ngouajio and Ernest, 2004), radiative and sensible heat flux through the air between the soil surface and the warm plastic mulch can be large via longwave emission and conductive heat transfer, respectively. If the plastic film were in contact with the soil surface, the absorbed radiation would transfer by conduction to the soil. Generally, plastic films mulches with very high α_s values (>0.75) (i.e., black plastic films) increase T_s near the soil surface by almost 5 °C compared to bare soil and are often desired to

24

warm the soil during cold periods (Ham et al., 1993; Ham and Kluitenberg, 1994). In combination with the soil, plastic film mulches exchange energy with the atmosphere through sensible heat flux (H, i.e., convection), shortwave reflection and longwave emission. The relative dominance of G and H (i.e., heat gain by the soil vs. heat gain by the atmosphere) is known as 'heat sharing' and is expressed as the ratio, H/G. It is related to: 1) the degree of contact between the plastic film and the soil surface (i.e., contact resistance (r_{ct})) (Ham and Kluitenberg, 1994) and 2) the aerodynamic resistance (r_a) between the plastic film and the surface atmospheric layer (Tarara and Ham, 1999).

High τ_s plastic films are often used as mulches to achieve the maximum T_s (i.e., solarization) (Katan, 2015) in order to sterilize the soil against pests and pathogens (Mahrer et al., 1987), alter soil microbial populations (Culman et al., 2006; Murase et al., 2015; Yokoe et al., 2015), alter soil nutrient balance and availability (Komariah et al., 2011; Ihara et al., 2014; Oz et al., 2017), alter greenhouse gas emissions (Cuello et al., 2015), decrease invasive seed abundance (Cohen et al., 2008), and increase crop productivity (Feng-Min Li et al., 2009). Although solarization typically involves the use of high τ_s plastic films to achieve maximum T_s, there are disagreements within the literature as to whether high α_{sm} or high τ_{sm} causes the largest increases in soil temperature (Liakatas et al., 1986; Ham 1993; Ham and Kluitenberg, 1994). The controlling factor seems to be directly related to the degree of contact between the soil and the plastic film mulch (i.e., r_{ct}), but will not be the focus of this study.

The objectives of this study were to (i) measure the radiative properties of various commercially available plastic film mulches, (ii) measure the soil warming and cooling potential

of plastic film mulches in a field experiment, and (iii) determine the radiative controls on soil

warming or cooling potential of plastic film mulches to assist farmers in decision-making.

2.3   Methods

2.3.1   Site description

The study was conducted at the University of British Columbia (UBC) Research Farm

(UBC Farm) located on the UBC Vancouver Campus, Vancouver, BC (49°14'59.3"N,

123°14'15.4"W, 72 m.a.s.l). UBC Farm has a mild oceanic climate with humid, mild winters and

dry summers with 25-year (1991-2016) mean (μ) $\pm$ standard deviation (SD) annual T_a and

precipitation (P) values of 10.6 $\pm$ 0.7 ºC and 1054 $\pm$ 238 mm, respectively (UBC Climatology

Station, Totem Field, 1 km NW of the study site). UBC Farm often experiences a sea breeze and

land breeze during the daytime and nighttime, respectively, due to its proximity to the Salish Sea.

In July of 2015, 10 treatments (9 plastic film mulches, 1 control (C) i.e., bare soil with no plastic)

were installed in 1 m x 1 m plots on a gravelly sandy loam Ferro-Humic Podzolic soil in a

randomized complete block design ($n = 3$) with a 0.75 m buffer between each treatment (Figure

2.1). The plastic mulch treatments comprised three black mulches: black embossed #2 (BE2);

black embossed PABPNARB (BEP); and black on white (BW), two clear: ©Thermax (TMX);

and ©Super 4 (S4), infrared transmitting (IRT100), green (GN), red (RD), and white on black

(WB) (Table 2.2) (BW and WB are the same plastic films but are oriented differently). The

blocks were laid out parallel to one another and to the slope contours to remove any effect of

elevation on soil or microclimate. The site was prepared by installing an irrigation dripline at

0.05 m depth (near the center of all three blocks) and leveling the soil surface parallel to the

predominant slope at the site (1º grade, southerly aspect). The irrigation dripline was only used

26

before the calibration period to increase the volumetric water content to similar values for all treatments before the sensors were installed. A 0.15-m-wide and 0.15-m-deep perimeter trench was dug around each 1 m x 1 m treatment area to bury the edges of the plastic film, after which stones (> 2 cm) on the soil surface were removed by hand and the treatment area was levelled again with a ruler (Figure A.5). 1.2 m x 1.2 m sheets were cut from each plastic film roll and installed by: 1) securing one edge of the plastic film by replacing soil removed during trenching, and 2) minimizing the air gap between the soil surface and the plastic film by pulling the remaining 3 edges of the plastic tight while replacing soil removed during trenching (Figure A.6). Although each plastic film was installed to minimize air gap between the soil surface and the plastic film, a $0.01 - 0.02$ m air gap remained after installation overall. Soil samples taken after site preparation showed the soil bulk density near the soil surface (0.05 m) was 0.92 Mg m^{-3} (Table 2.1).

Table 2.1 Climatic, geographic and soil characteristics at the UBC Research Farm study site.

Calibration period start and end dates	Jul 14 – Jul 15 (DOY 194 – 196), 2015
Treatment period start and end dates	Jul 16 – Sep 30 (DOY 197 – 273), 2015
Location	49°14'59.3"N, 123°14'15.4"W
Elevation (m, above mean sea level)	72
25-year $\mu \pm$ SD annual temperature (^{o}C)	10.6 ± 0.7
25-year $\mu \pm$ SD annual precipitation (mm)	1054 ± 238
Soil order (Canadian System of Soil Classification[a])	Ferro-Humic Podzol
Soil texture	Gravelly sandy loam
Bulk density depth (m)	
0.05	0.92 Mg m^{-3}

[a] Soil Classification Working Group (1998).

Table 2.2 List of names, abbreviations and symbols for the 9 plastic film mulch treatments and the control in this study.

Plastic mulch name	Plastic mulch abbreviation
Black embossed #2	BE2[1]
Black embossed PABPNARB	BEP[1]
Black on white	BW[1]
Green	GN[1]
Infrared transmitting	IRT100[1]
Red	RD[1]
©Super 4	S4[2]
©Thermax	TMX[2]
White on black	WB[1]
Control (bare soil)	C

[1] sourced from Dubois Agrinovation Inc. (http://www.duboisag.com/)

[2] sourced from AT Films Inc. (http://www.atfilmsinc.com/)
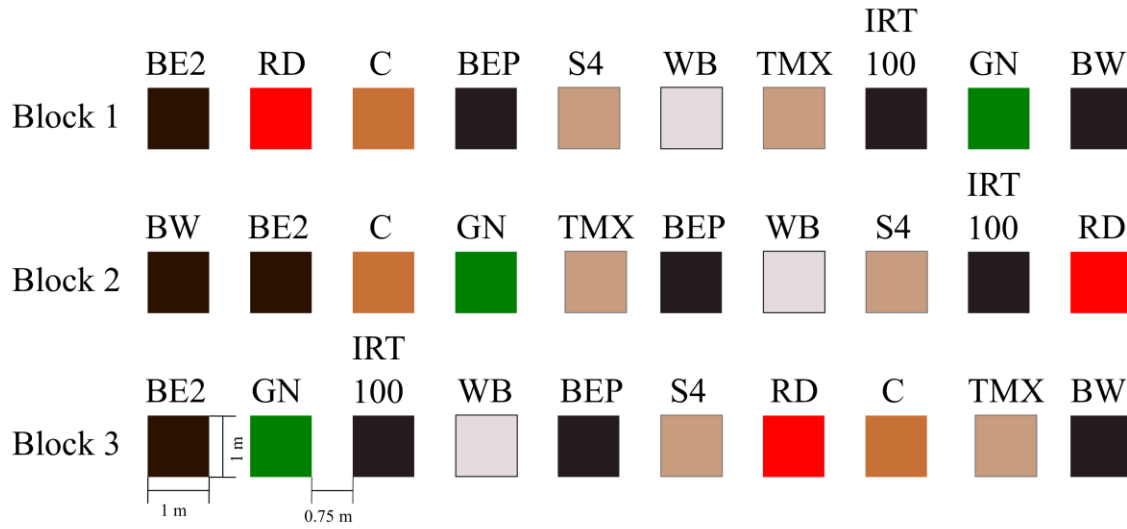
Figure 2.1 Experimental layout of the randomized complete block design for comparing plastic film mulches at UBC Farm (49°14'59.3"N, 123°14'15.4"W). See text for further explanation (Figure A.7 and Figure A.8).

2.3.2 Climate and soil measurements

A weather transmitter (WXT520, Vaisala Oy, Helsinki, Finland) mounted 2 m above the soil surface measured half-hourly mean T_{a2m}, P, wind velocity (u_{2m}) and direction, and relative humidity (VPD_{2m}). In addition to P from the weather transmitter, half-hourly P measurements were made using a tipping-bucket (0.1 mm) rain gauge (model TR525 M, Texas Electronics Inc., Dallas, TX, USA). Two T_s and θ_s sensors (5TM, Decagon Devices Inc., Pullman, WA, USA) were installed, in each of the 10 plots in Block 1 only, at the 2-cm (T_{s2cm} and θ_{s2cm}) and 10-cm (T_{s10cm} and θ_{s10cm}) depths, 12 cm uphill of the dripline, previous to installing the plastic films.

2.3.3 Radiative properties

2.3.3.1 Shortwave radiation properties

Shortwave reflectivity ($\rho_{s\lambda}$) and transmissivity ($\tau_{s\lambda}$) spectra were measured for all nine plastic films using 1) a shortwave spectroradiometer (350 nm – 2500 nm) which accounts for ~98% of the energy in the solar spectrum (Fieldspec 3, ASD Inc., Longmount CO, USA), 2) a 0.15 m x 0.15 m reflectance panel (nominal reflectance value = 99%) (model SRT-99-050, Labsphere Inc., North Sutton, NH, USA), 3) a low shortwave reflectivity and transmissivity panel made of a 0.1 m x 0.12 m x 0.05 m (width x length x height) cardboard box wrapped tightly with four layers of BE2 film (Table 2.2), and 4) a light fixture (Pro Lamp, ASD Inc.) with a halogen lamp (Model JC14.5V-50WC, Ushio Inc., Cypress, CA, USA) (Figure A.1). Transmissivity (for 5-nm wavelength increments) was measured by 1) positioning the spectroradiometer fiberoptic sensor at the level of the plastic film being measured and below and facing the light source mounted above to measure its spectral irradiance ($E_{s\lambda}$), and 2) positioning each plastic film 1 mm above the spectroradiometer fiberoptic sensor to measure the spectrum of the transmitted shortwave radiation (i.e., $\tau_{s\lambda}$) (Figure A.2). Values of $\tau_{s\lambda}$ were calculated as $\tau_{s\lambda}/E_{s\lambda}$. Reflectivity was measured by 1) measuring the reflectivity of the reflectance panel ($\rho_{s\lambda ref100}$), 2) measuring the reflectivity of the low reflectance panel ($\rho_{s\lambda ref0}$) (placed beneath the film being measured), 3) tightly wrapping the plastic film over the low reflectivity panel and measuring the raw reflectivity ($\rho_{s\lambda raw}$), and 4) calculating the reflectivity of each plastic film using $R_{s\lambda}/E_{s\lambda}$ where $R_{s\lambda}$ is the spectrum of the reflected shortwave radiation, and correcting for reflection from the low reflectance panel ($\rho_{s\lambda} = \rho_{s\lambda raw} - \tau_{s\lambda}^2 \rho_{s\lambda ref0}$). The correction term ($\tau_{s\lambda}^2 \rho_{s\lambda ref0}$)

was always less than 5% of $\rho_{s\lambda raw}$. Shortwave spectral absorptivity ($\alpha_{s\lambda}$) was calculated as a residual of the sum of $\rho_{s\lambda}$ and $\tau_{s\lambda}$ ($\alpha_{s\lambda} = 1 - (\rho_{s\lambda} + \tau_{s\lambda})$). ρ_s and τ_s were calculated as:

$$\rho_s = \frac{\int\limits_{350}^{2500} \rho_\lambda E_\lambda d\lambda}{\int\limits_{350}^{2500} E_\lambda d\lambda} = \frac{\int\limits_{350}^{2500} R_{s\lambda} d\lambda}{\int\limits_{350}^{2500} E_{s\lambda} d\lambda} \tag{1}$$

$$\tau_s = \frac{\int\limits_{350}^{2500} \tau_{s\lambda} E_{s\lambda} d\lambda}{\int\limits_{350}^{2500} E_{s\lambda} d\lambda} = \frac{\int\limits_{350}^{2500} T_{s\lambda} d\lambda}{\int\limits_{350}^{2500} E_{s\lambda} d\lambda} \tag{2}$$

where $E_{s\lambda}$, $\rho_{s\lambda}$, $\tau_{s\lambda}$ and $\alpha_{s\lambda}$ are the shortwave spectral irradiance (Diffey et al., 2015), reflectivity, transmissivity and absorptivity, respectively.

2.3.3.2 Longwave radiation properties

Longwave transmissivity ($\tau_{L\lambda}$) was measured for all nine plastic films (Table 2.2) using the pyrgeometer of a 4-component net radiometer (model SN-500-SS, Apogee Instruments Inc., Logan, UT), three chromel-constantan thermocouples, and a 0.44 m x 0.82 m x 0.042 m (width x length x thickness) glass sheet. The experiment was performed on a sunny day between 13:00 and 15:00 PST at Totem Field, UBC in an open field location with a large sky view-factor, and all experimental components were mounted facing south on a 2.5-m-tall tripod. The net radiometer was mounted and levelled 1.5 m above the soil surface. Sheets of each plastic film (0.25 m x 0.25 m) were fastened tightly onto a Styrofoam cut-out sheet (square 0.2 m x 0.2 m, inner diameter 0.15 m x 0.15 m) which was mounted 1.55 m above the soil surface using a steel-

rod mount that extended from the tripod. Two 1.6-m-tall flat-top tripods were positioned and levelled on each side of the net radiometer to support the glass sheet. Thermocouples were positioned: 1) 2.5 m above the soil surface at the top of the tripod to measure air temperature (T_a), 2) on the surface of the glass sheet to measure glass surface temperature (T_{0gl}), and 3) on the surface of the plastic film to measure plastic film surface temperature (e.g., BE2, T_{0BE2}).The latter two were attached using 1 cm^2 of clear packing tape. All variables were measured and stored every 2 s on a datalogger (model CR1000, Campbell Scientific Inc. (CSI), Logan, UT, USA). The measurement procedure took 2 minutes for each plastic film and required the following 4 sequential steps (Figure 2.2), each taking 30 s: 1) downwelling longwave radiation from the sky was measured using the up-facing Apogee SN-500-SS pyrgeometer in the absence of the plastic film or sheet of glass (L_{dsky}), 2) downwelling longwave radiation was measured after placing the plastic film sheet above the pyrgeometer ($L_{dskyfilm}$), 3) downwelling longwave radiation was measured after placing the sheet of glass above the plastic film sheet ($L_{dskyfilmgl}$), and 4) downwelling longwave radiation was measured beneath the glass sheet after removing the plastic film sheet (L_{dskygl}) (Figure A.3). The procedure was repeated for each plastic film shown in Table 2.2 (Figure A.4).

Downwelling longwave radiation measured in the presence of the plastic film ($L_{dskyfilm}$) is the sum of the longwave radiation from the sky (L_{dsky}) that is transmitted through the film and longwave radiation emitted by the film, written as:

$$L_{dskyfilm} = L_{dsky}\tau_{Lfilm} + \varepsilon_{Lfilm}\sigma T_{0film}{}^4 \qquad (3)$$

where σ is the Stefan-Boltzmann constant, and τ_{Lfilm} and ε_{Lfilm} are the film longwave

transmissivity and emissivity, respectively. Since glass is opaque to longwave radiation ($\tau_L = 0$,

Wang and Deltour, 1999), the downwelling longwave radiation in the presence of the film and

the glass ($L_{dskyfilmgl}$) placed above it is the sum of the longwave emission from the glass (L_{dgl}) that

is transmitted through the film and longwave radiation emitted by the film, written as:

$$L_{dskyfilmgl} = L_{dgl}\tau_{Lfilm} + \varepsilon_{Lfilm}\sigma T_{0film}^{4} \tag{4}$$

Our measurements showed that T_{0film} remained unchanged after placing the glass above the

plastic film (see Figure 2.2); therefore, τ_{Lfilm} can be obtained by subtracting Eq. (4) from (3) and

after rearrangement, written as:

$$\tau_{Lfilm} = \frac{\left(L_{dskyfilm} - L_{dskyfilmgl}\right)}{\left(L_{dsky} - L_{dgl}\right)} \tag{5}$$

Then ε_{Lfilm} (or α_{Lfilm} by Kirchhoff's Law) can be obtained by substituting Eq (5) for τ_{Lfilm} into Eq

(3) and rearranging to give:

$$\varepsilon_{Lfilm} = \frac{L_{dsky}L_{dskyfilmgl} - L_{dgl}L_{dskyfilm}}{(L_{dsky} - L_{dgl})\sigma T_{0film}^{4}} \tag{6}$$

Finally, ρ_{Lfilm} is calculated as $\rho_{Lfilm} = 1 - (\alpha_{Lfilm} + \tau_{Lfilm})$.

1) sky

4- way
Net radiometer

2) sky + plastic fil film

Plastic film

3) sky + plastic fillm + glass

Glass

Plastic film

4) sky + glass

Glass
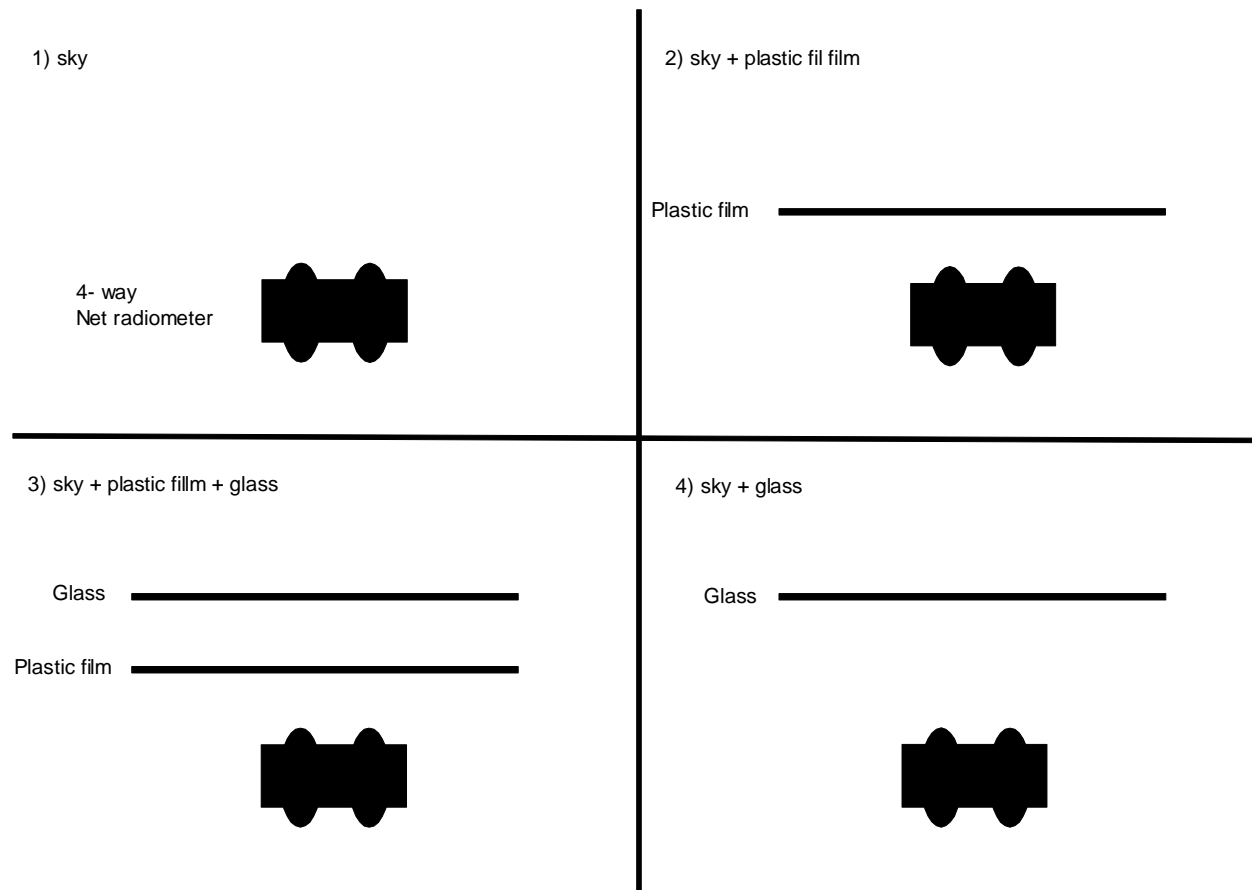
Figure 2.2 Cross-sectional diagram showing the 4 steps required to measure the plastic film longwave radiative coefficients using an upward-facing pyrgeometer (Apogee SN-500-SS) to measure downwelling longwave radiation as explained above. The order of the steps involved in the procedure above is not crucial to the validity of the results. We chose the procedure sequence above because it only required the sheet of glass to be moved quickly once (step 2 to 3) which made the procedure easy, logistically.

2.3.4   Energy balance measurements

The land surface energy balance can be written as $R_n = H + LE + G + \Delta S_a$ where R_n is the net radiation, H is sensible heat flux, LE is the latent heat flux, G is the soil heat flux density (at the soil surface) and ΔS_a is the rate of change in energy storage between the soil surface and the

height of the net radiation sensor. The available energy flux was calculated as $R_a = R_n - G - \Delta S_a$

$= H + LE$. Given that the plastic film mulches used in this study are impermeable to water vapour

(Hopfenberg, 1974), LE is equal to zero, which allowed H to be calculated for each plastic film

treatment ($R_a = R_n - G - \Delta S_a = H$), but not the control. For the control, only R_a was calculated,

given that LE was not measured or estimated in this study. R_n was measured using 2 four-

component net radiometers (model CNR1, Kipp and Zonen, The Netherlands) consisting of

upward- and downward-facing pyranometers and pyrgeometers: 1) A fixed-position-net-

radiometer that was mounted 1.5 m above the experimental layout for the entire study period and

2) a roving-position net radiometer was mounted 0.15 m above the control and plastic film

treatments (Blocks 1, 2 and 3, Figure 2.1) on four separate sunny days (DOY 224, 225, 272 and

273) at midday (12:00 – 14:00 h (Pacific Standard Time (PST)). R_n was calculated as the sum of

downwelling shortwave (S_d) and longwave (L_d) radiation minus the sum of the upwelling

shortwave (S_u) and longwave (L_u) radiation (i.e., $R_n = S_d - S_u + L_d - L_u$). Downwelling shortwave

and longwave radiation values were the same for all treatments in this study, therefore the

challenge was to calculate upwelling shortwave and longwave radiation for each plastic film

treatment and the control. For the control, daytime half-hourly S_u was calculated by multiplying

S_d by the mean ρ_s value calculated using the midday ρ_s values measured using the roving-net-

radiometer on four separate sunny days ($S_u = \rho_{ss} S_d$, ρ_{ss} is the bare soil shortwave reflectivity

beneath each plastic film treatment and was set equal to ρ_{sC}). For the plastic film treatments,

daytime half-hourly S_u values were calculated by multiplying respective ρ_s values measured

using spectral analysis (see Section 2.2.1) by S_d measured using the fixed-net-radiometer, plus a

term to account for multiple reflections from the two surfaces which comprise the soil surface

and the plastic film ($S_u = S_d\rho_{ss} + S_d\rho_{ss}\tau_{sBE2}^2$, with BE2 mulch). Given that the value of τ_{sBE2} is equal to zero, the multiple reflection term is equal to zero.

Upwelling longwave radiation for the control was set equal to L_u measured using the fixed-net-radiometer, given that most of its downward-facing view factor was occupied by a surface similar to the control (i.e., bare soil). For the plastic mulches, upwelling longwave radiation was only calculated for daytime. For the daytime, regression analysis showed there was a strong linear relationship between L_u and S_d measured above each plastic film using the roving-net-radiometer (all plastic film linear regressions: $R^2 = 0.56 \pm 0.16$, RMSE $= 29 \pm 11$ W m^{-2}, $n = 12$), yet the range of S_d values over which L_u was measured was limited (400 – 900 W m^{-2}). In the following year (2016) a study very similar to this one was performed, also at UBC Farm, but only involved BE2 (Table 2.1), in which half-hourly L_u was measured continuously. Regression analysis using the 2016 data showed a strong linear relationship between L_u and S_d (for BE2: $R^2 = 0.89$, RMSE $= 31$ W m^{-2}; $n = 5890$) across the full scale of S_d (0 – 1000 W m^{-2}), which gave us confidence to gap fill daytime L_u using the regression equations developed for each plastic film treatment from 2015 data.

For each treatment and the control, before installing the plastic films, one soil heat flux plate (Peltier Cooler) was installed to measure G at the 3-cm depth (G_{3cm}) and 12 cm uphill of the dripline, only for the 10 plots in Block 1. All soil heat flux plates were calibrated over a period of 4 days at Totem Field UBC prior to being installed at the study site by 1) filling a 0.75 x 0.75 x 0.2 m (long x wide x tall) wooden box with sand, 2) making a 0.5 m diameter and 0.05 m deep circular hole within the sand, 3) positioning and leveling the standard soil heat flux sensor (model HFP01, Hukseflux Inc., Delft, The Netherlands) and 10 Peltier coolers at the

center and near the edge of the circular hole, respectively, and 4) carefully burying all the sensors with a sand layer of uniform thickness (0.03 m). The agreement between HFP01 and all 10 Peltier Coolers was very good (all soil heat flux sensors regressions: $R^2 = 0.99 \pm 0.0045$, RMSE $= 6.6 \pm 0.29$ W m^{-2}, $n = 148$). G was calculated by adding the measured heat flux density to the rate of change in heat storage in the 3-cm layer of soil above the heat flux plate (ΔS_s, $G = G_{3cm} + \Delta S_s$). The rate of change in heat storage was calculated using values of T_{s2cm} and θ_{s2cm} within each treatment. The heat storage within the air gap between the soil surface and the plastic film was not included in the storage calculation and was assumed to be small. Soil temperature and volumetric water content values measured at the 2-cm depth (T_{s2cm} and θ_{s2cm}, respectively) were used to calculate the soil heat capacity.

All climate, soil and radiation variables were measured every 5 s using a solid-state multiplexer (model AM25T, CSI) and a datalogger (model CR5000, CSI), after which half-hourly averages were calculated and collected weekly. Half-hourly S_u, S_d, L_d, L_u, P, u, T_a and VPD were retrieved from the UBC Climate Station located at Totem Field, 500 m away, for gap-filling purposes and to calculate 25-year-mean P and T_a. All data cleaning, calculations and analysis were performed in MATLAB® (Version 7.5.0, The Math Works Inc., Natick, USA).

2.4   Results

2.4.1   Radiative properties

2.4.1.1   Shortwave radiative properties

2.4.1.1.1   Solar spectral irradiance

The solar spectral irradiance (350-2500 nm), for noon on a typical sunny July day in Vancouver, BC, was used to calculate total shortwave radiation (S, 350- 2500 nm), photosynthetically active radiation (PAR, 400 – 700 nm), near-infrared radiation (NIR, 700 – 1400 nm) and shortwave infrared (SWIR, 1400 – 2500 nm) reflectivity (ρ_s), transmissivity (τ_s) and absorptivity (α_s) using Eqs. (1), (2) and 1 - ($\tau_s + \rho_s$), respectively (Figure 2.3 and Table 2.3). Of the total shortwave (i.e., solar) irradiance (S_d) equal to 938 W m^{-2} (Figure 2.3), total downwelling PAR (Q_d), NIR and SWIR account for 44% (414 W m^{-2}), 41% (391 W m^{-2}) and 11% (99 W m^{-2}) of S_d, respectively. Given that the majority of S_d comprises PAR and NIR, the spectral properties of each plastic film within those spectral regions strongly controls the changes in surface radiation balance caused by each plastic film.
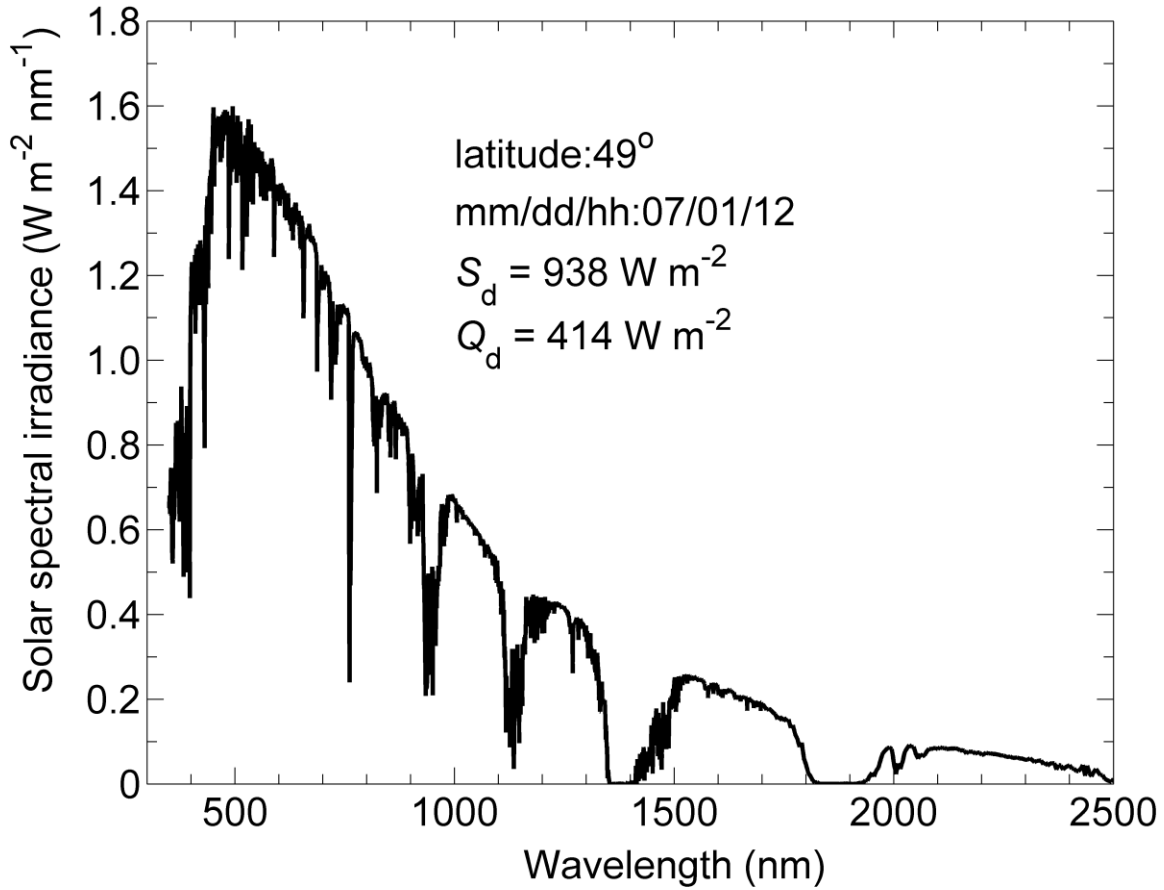
Figure 2.3 Solar spectral irradiance data (350 – 2500 nm, 1 nm resolution) taken from Diffey (2015). Latitude (similar to Vancouver BC), time of year and day, and values of S_d (W m^{-2}) and Q_d (W m^{-2}) are shown.

2.4.1.1.2   Reflectivity

Of the nine plastic films used in this study six have ρ_s values less than 0.1, they comprise BEP, BE2, BW, TMX, GN, and S4, which have ρ_s values equal to 0.03, 0.04, 0.05, 0.05, 0.08, and 0.09, respectively (Figure 2.4 and Table 2.3). Interestingly, S4 has a higher ρ_{PAR} value than GN, but it has a lower ρ_{NIR} value than GN. WB and RD have the largest ρ_s values of 0.45 and 0.22, respectively, but have quite different ρ_{PAR} and ρ_{NIR} values (Figure 2.4 and Table 2.3). In the

PAR region, WB has more than three times the reflectivity of RD, while in the NIR and SWIR

regions RD and WB reflectivity is very similar (Table 2.3).
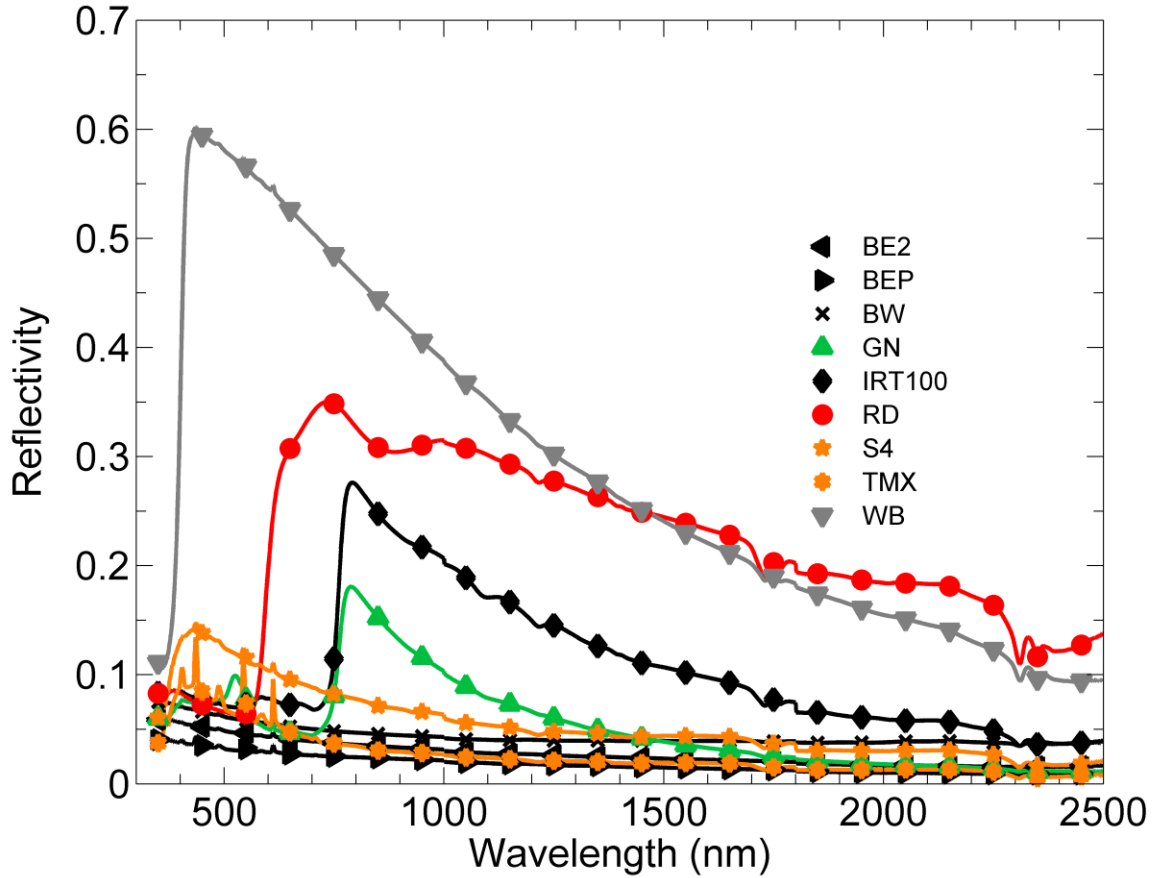
Figure 2.4 Shortwave spectral reflectivity (350 – 2500 nm) of all plastic films listed in Table 2.2.

2.4.1.1.3   Transmissivity

TMX and S4 both have high transmissivity (0.75 - 0.85) in the PAR and NIR spectral

regions, with τ_{PAR} values of 0.80 and 0.75 and τ_{NIR} values of 0.86 and 0.85, respectively (Figure

2.5 and Table 2.3). τ_{SWIR} is also high, equal to 0.82 and 0.84 for TMX and S4, respectively, but

declines abruptly in two regions of the SWIR region to minimum values of ~0.70 and ~0.40 -

0.50 for wavelengths 1700 to 1850 nm and 2200 to 2500 nm, respectively (Figure 2.5 and Table

2.3). Given that, SWIR represents only 11% of S_d, the low transmissivity values have little

impact on τ_s. GN and IRT100 have much lower τ_s (0.36 and 0.34, respectively) than TMX and S4

primarily due to them having low τ_{PAR} values of 0.16 and 0.13, respectively (Table 2.3). RD has

a very distinct spectral shortwave transmissivity, with constant values of ~0.03 in the PAR

region after which the spectral transmissivity gradually increases, with a near constant slope, to

0.3 in the SWIR region. All the remaining plastic films (WB, BW, BE2 and BEP) have

extremely low τ_s. Aside from BEP and BE2, which has a transmissivity of about 0 for all

shortwave wavelengths, WB and BW have τ values of ~0 near 350 nm, which gradually

increases to a maximum of 0.1 at 2500 nm (Figure 2.5).
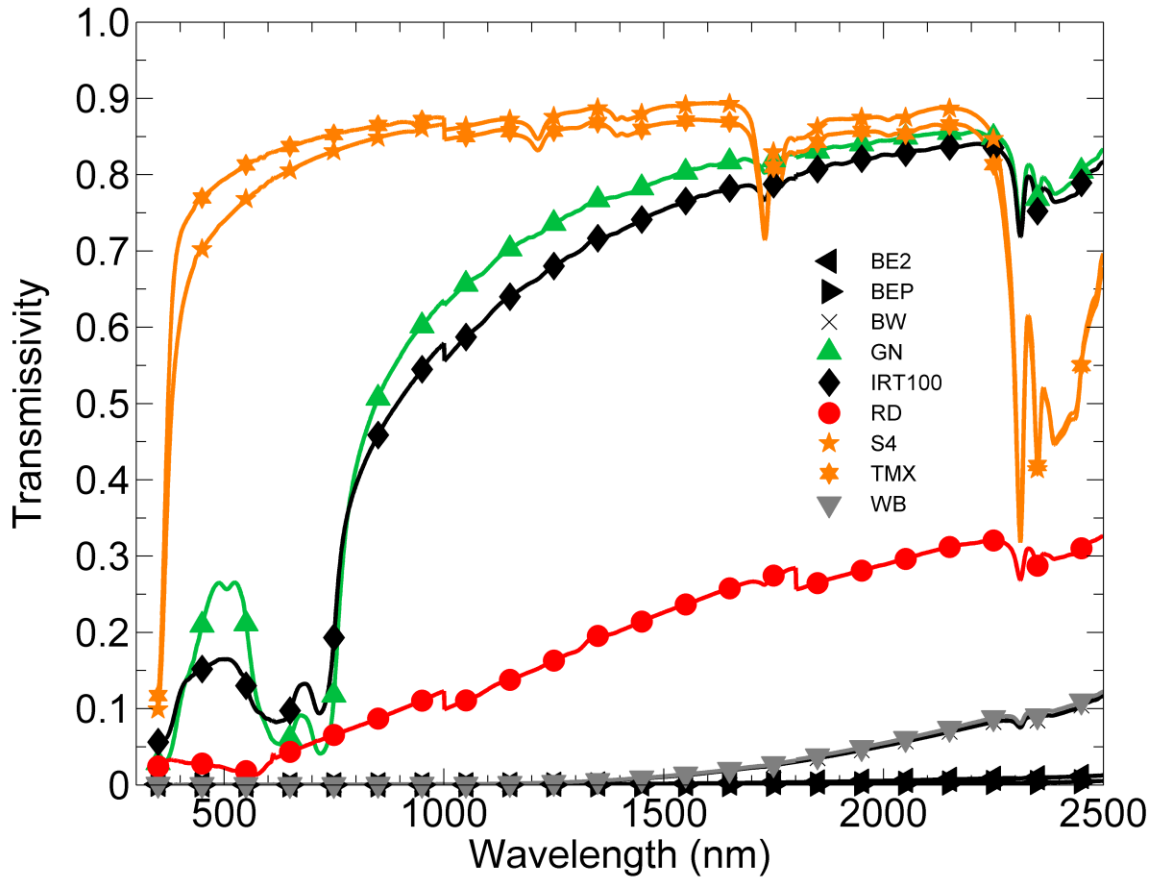
Figure 2.5 Shortwave spectral transmissivity (350 – 2500 nm) of all plastic films listed in Table 2.2.

2.4.1.1.4   Absorptivity

BE2, BEP and BW are highly absorptive with α_s values of 0.96, 0.97 and 0.94, respectively, and have very low reflectivity and transmissivity for all shortwave spectral regions (Figure 2.6 and Table 2.3). RD is the 4th most absorptive plastic film in this study with an α_s value of 0.70, followed by GN, WB and RD, which all have similar α_s values equal to 0.56, 0.55 and 0.54, respectively. In the PAR region, GN and RD are more absorptive than WB, by ~0.4, but in the NIR region, GN absorptivity declines abruptly to 0.40 while WB and RD absorptivity

remains high with α_{NIR} value of 0.59 and 0.58, respectively (Figure 2.6 and Table 2.3). TMX and S4 have the lowest absorptivity with α_s values equal to 0.14 and 0.12, respectively, with each achieving α_{PAR} values of 0.13 and 0.13 and α_{NIR} values of 0.11 and 0.08, respectively (Table 2.3).
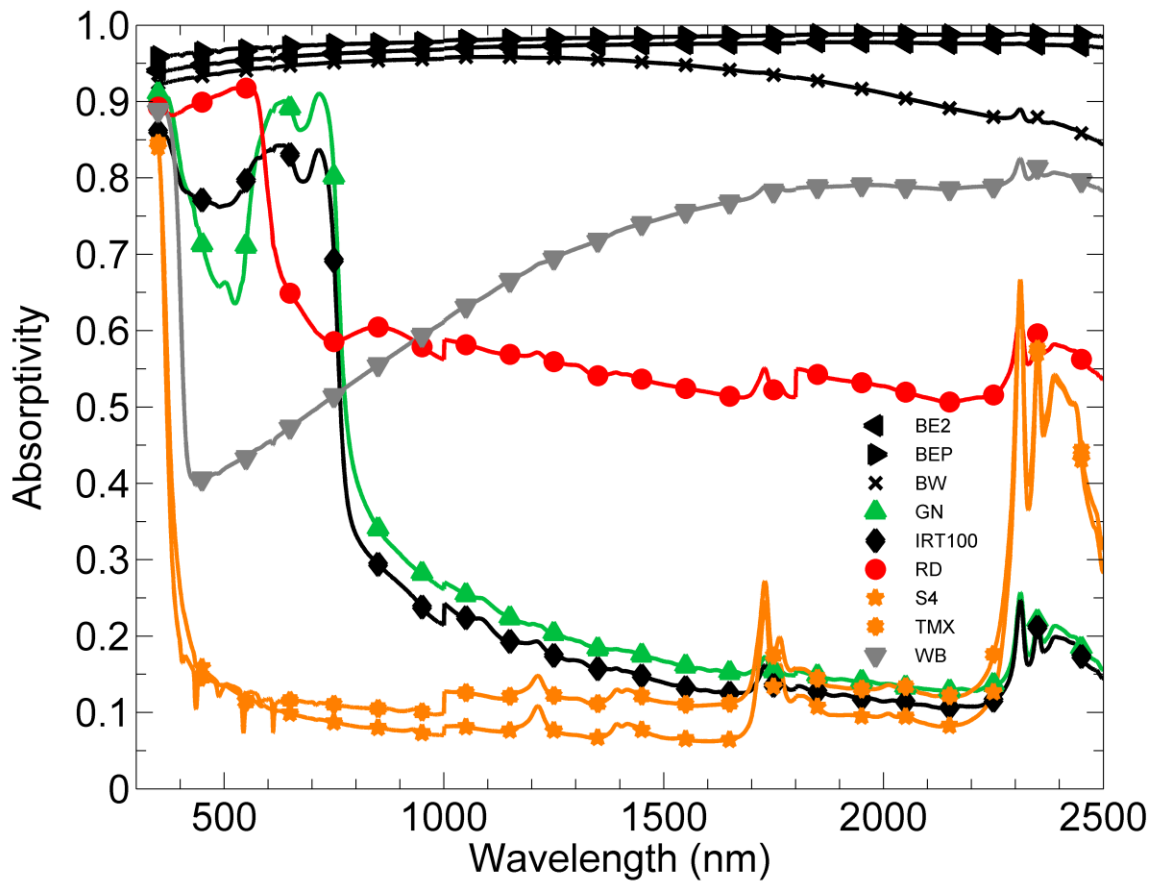
Figure 2.6 Shortwave spectral absorptivity (350 – 2500 nm) of all plastic films listed in Table 2.2.

2.4.1.2 Longwave radiative properties

In this study, the longwave radiative characteristics of the plastic films varied considerably, except for the longwave reflectivity (ρ_L) which was equal to or less than 0.05 for all plastic films (Table 2.3). The lowest and highest longwave transmissivity (τ_L) values were 0.06 and 0.81 for BE2 and GN, respectively. Except for BE2 and BEP, all the plastic films had τ_L values greater than 0.35 with a mean (μ) ± standard deviation (SD) for all plastic films of 0.50 ± 0.26. As expected, given that ρ_L values were very low, the plastic films with high and low τ_L values had low and high longwave absorptivity (α_L) values, respectively, resulting in the μ ± SD α_L for all plastic films being similar to that of the τ_L of 0.49 ± 0.25. Overall, the fact that our measurements of τ_L agreed well with manufacturer reported τ_L values for S4 and TMX, provides confidence in our longwave radiation measurements. Also, it is important to note that BW and WB are the same plastic film but with different orientation and their longwave properties were very similar ($\tau_{L_{BW}} = 0.37$ and $\tau_{L_{WB}} = 0.40$). The longwave radiative properties for all plastic films used in this study are shown in Table 2.3.

Table 2.3 Shortwave and longwave radiative coefficients (ρ, τ, and α) for all plastic films and the control (C) in this study.

Plastic mulch abbreviation	Shortwave												Longwave		
	S (350 – 2500 nm)			PAR (400 – 700 nm)			NIR (700 – 1400 nm)			SWIR (1400 – 2500 nm)			L (2500 – 100000 nm)		
	ρ_S	τ_S	α_S	ρ_{PAR}	τ_{PAR}	α_{PAR}	ρ_{NIR}	τ_{NIR}	α_{NIR}	ρ_{SWIR}	τ_{SWIR}	α_{SWIR}	ρ_L	τ_L	α_L
BE2	0.04	0.00	0.96	0.05	0.00	0.95	0.03	0.00	0.97	0.02	0.00	0.98	0.00	0.06	0.94
BEP	0.03	0.00	0.97	0.03	0.00	0.97	0.02	0.00	0.98	0.01	0.00	0.99	0.05	0.18	0.77
BW	0.05	0.00	0.94	0.06	0.00	0.94	0.04	0.00	0.95	0.04	0.03	0.93	0.02	0.37	0.61
GN	0.08	0.36	0.56	0.07	0.16	0.78	0.10	0.50	0.40	0.03	0.82	0.16	0.00	0.81	0.19
IRT100	0.12	0.34	0.54	0.08	0.13	0.80	0.19	0.47	0.35	0.08	0.79	0.13	0.00	0.77	0.23
RD	0.22	0.08	0.70	0.15	0.03	0.83	0.31	0.10	0.58	0.21	0.27	0.53	0.01	0.66	0.33
S4	0.09	0.79	0.12	0.12	0.75	0.13	0.07	0.85	0.08	0.04	0.84	0.12	0.01	0.60	0.39[3]
TMX	0.05	0.82	0.14	0.07	0.80	0.13	0.03	0.86	0.11	0.02	0.82	0.16	0.01	0.36	0.63[3]
WB	0.45	0.00	0.55	0.56	0.00	0.44	0.41	0.00	0.59	0.19	0.04	0.77	0.02	0.40	0.58
C	0.07[1]	0	0.93[2]	-	-	-	-	-	-	-	-	-	-	-	-

[1] ρ_{sC} was measured using a 4-component net radiometer at midday (12:00 – 14:00 h PST) on four separate sunny days.

[2] α_{sC} was calculated as a residual 1-ρ_{sC}, assuming τ_{sC} to be equal to 0.

[3] AT Films Inc. reported values of 0.60 and 0.40 for TMX and S4, respectively.

2.4.2   Soil and near-surface microclimate

The study period (Jul 14 – Sept 30, 2015) was dominated by sunny days with several periods of cloud and precipitation (P), with mean, maximum and minimum daily downwelling shortwave irradiance (S_d) of 14.1 ± 8.0 (mean $\pm$ standard deviation), 28.4 and 0.4 MJ m^2 day^{-1}, respectively. During sunny periods, downwelling longwave radiation (L_d) was relatively constant with a value of ~350 W m^{-2}, which increased to ~400 W m^{-2} on cloudy days (e.g., DOY 240 – 245 Figure 2.7a). Mean daytime T_{a2cm} and control T_{s2cm} (i.e., 0.02-m depth in bare soil) were 17.5 $\pm$ 3.4 and 24.2 $\pm$ 7.1 ^{o}C, respectively, while for nighttime the respective values were 14.6 $\pm$ 2.8 and 16.8 $\pm$ 3.7 ^{o}C. 2-cm soil volumetric water content (θ_{s2cm}) for the control (θ_{s2cmC}) increased due to P events (DOY 205, 207, 240 – 245, 263 and 265) but θ_{s2cm} below the plastic film treatments did not. For the majority of the study period, θ_{s2cm} remained between 0.10 and 0.30 for the control, while θ_{s2cm} below the plastic-covered treatments remained remarkably constant (θ = 0.20) throughout the study period (Figure 2.7d). The cumulative precipitation during the study period was 121 mm, all of which came as rainfall.
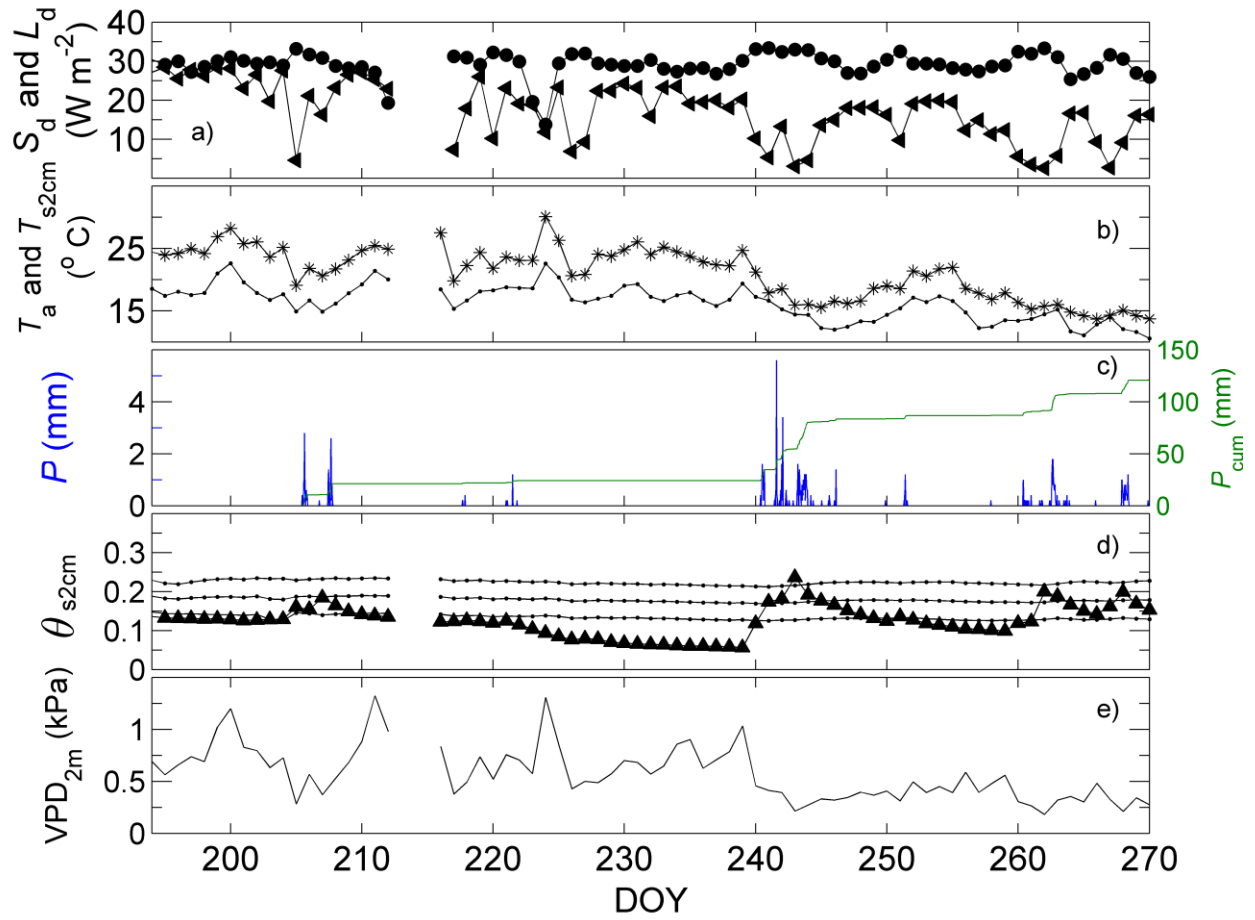
Figure 2.7 Climate and soil variables at UBC Farm from the beginning of the calibration period

on July 14 to the end of the treatment period on Sep 30, 2015. Panel a) shows total daily

downwelling shortwave (S_d, filled left-facing triangles with line) and longwave radiation (L_d,

filled circles with line), panel b) shows mean daily air (T_{a2m}, dotted line) and control soil

temperature (T_{s2cm}, asterisks line), panel c) shows half-hourly precipitation (P, left axis) and

cumulative precipitation (P_{cum}), panel d) shows mean daily volumetric water content (θ_{s2cm}) for

the control (i.e., bare soil, filled upward-facing triangles with line) and the (μ) ± standard

deviation (SD) of all treatments (i.e., plastic covered, dotted lines) and panel e) shows mean

daily vapour pressure deficit (VPD$_{2m}$).

2.4.3   Energy balance

During the calibration period the agreement for the regression of treatment G (e.g., G_{TMX}) and control G (G_C) was good, with slopes equal to 1.00 and y intercept (b) values < 5 W m^{-2} for all treatments, except for TMX which had a b value of ~12 W m^{-2} (data not shown). During the treatment period, the regression slopes and b values increased for all treatments, except for WB (Figure 2.8). After the installation of plastic film mulches, G_{BEP} and G_{BW} experienced slope increases of ~0.35 compared to the calibration period but the slope of G_{BE2} only experienced a slope increase of ~0.15, which was unexpected given the similarity in shortwave spectral properties between the three black plastic films. On the other hand, BEP, BW and BE2 differ in their longwave spectral properties, with BE2 and BW having low and relatively high longwave transmissivity, respectively. The regression scatter for G_C vs. $G_{BEP,}$ G_{BE2} and G_{BW} was low with RMSE values of 18.23, 15.23 and 13.69 W m^{-2}, which is 7% to 10% of their full-range during the daytime (Figure 2.8).

Interestingly G_{RD}, G_{TMX} and G_{S4} vs. G_C have slopes and RMSE's similar to G_{BEP} and G_{BW} vs. G_C with the exception of G_{S4} vs. G_C which has the lowest R^2 (0.92) and highest RMSE (25.35 W m^{-2}) of all treatments. Of all treatments, G_{TMX} vs. G_C and G_{WB} vs G_C experienced the largest slope increase and decrease of 0.45 and -0.18, respectively. For all treatments, the b values from the regression analysis were positive and ranged in value from $5 - 15$ W m^{-2} except for G_{WB} vs. G_C which has a $b < 1$ W m^{-2}. In general, the plastic film mulches with the highest τ_s values (i.e., TMX, S4, GN and RD) had among the highest RMSE values, perhaps due to their susceptibility to changes in τ_s caused by condensation.
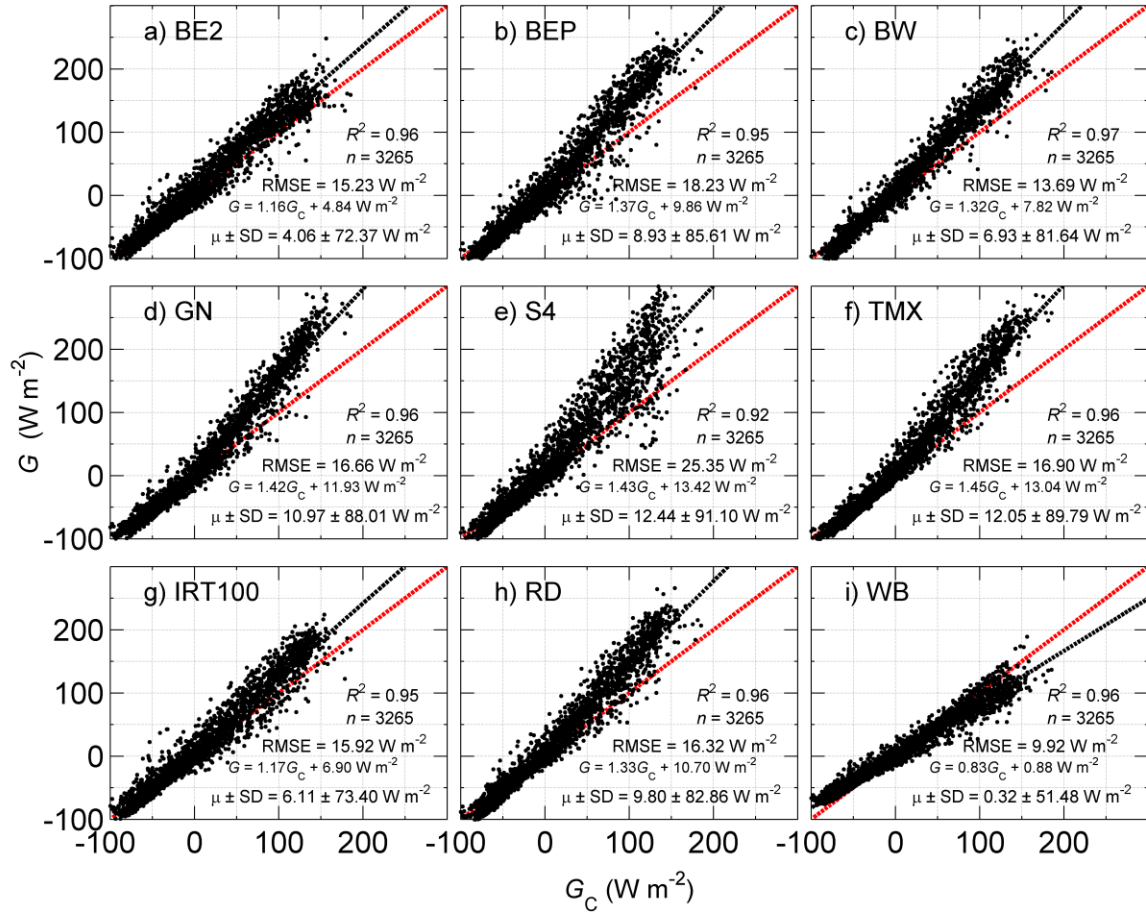
Figure 2.8 Panels a), b), c), d), e), f), g), h), and i) show linear regressions for half-hourly measurements of surface soil heat flux density (G) for G_{BE2}, G_{BEP}, G_{BW}, G_{GN}, G_{S4}, G_{TMX}, G_{IRT100}, G_{RD} and G_{WB}, respectively, vs G_C for data collected between July 16, 2015 and September 30, 2015 (post plastic film installation). For each regression, the coefficient of determination (R^2), sample size (n), root mean square error (RMSE), mean (μ) $\pm$ standard deviation (SD) (for half-hourly daytime and nighttime values) and the linear regression equation are shown. Pre-treatment data is shown in Figure A.9.

During the daytime, on a typical sunny day (July 23, 2015, Day 1 of Figure 2.9), G in all plastic film treatments and the control increased proportionally to S_d and quickly shifted from

being negative to positive after sunrise. As S_d approaches its daily maximum (i.e., solar noon), all G values are highly coupled to S_d, including G_{WB}. For example, on July 23, 2015, S_d declined at 10:00 and 13:00 h PST due to cloud cover which caused a decrease in all treatments G values. Unexpectedly, from 10:00 – 13:00 h PST, G_{S4} declined abruptly due to droplet formation (i.e., condensation) which occurred daily, whereas TMX did not because it has a surfactant coating on its downward-facing side which prevents droplet formation. Interestingly, G_{GN} was higher than G_{TMX} at noon but G_{IRT100} was less than G_{TMX}, even though G_{GN} and G_{IRT100} have similar shortwave and longwave properties. All treatment G values, except G_C and G_{WB}, remained highly coupled to S_d until sunset. Interestingly, G_{WB} values were greater than G_C values near 11:00 h PST, but G_{WB} was less than G_C from 12:00 – 15:00 h PST, potentially due to increased ρ_s at solar noon.

During the daytime, on a cloudy day (July 24, 2015), treatment and control values increased in proportion to S_d, but the order of highest to lowest G was different than on sunny days (Figure 2.9). Although, some of the treatments with the highest midday G values on cloudy days were the same as those on sunny days (i.e., G_{TMX}, G_{S4} and G_{IRT100}), other treatments which had high G values on sunny days (i.e., G_{BE2}, G_{BEP} and G_{GN}) were less than G_{WB} (Figure 2.9). Unlike sunny days, G_C had the highest values during much of the daytime on cloudy days, particularly before 16:00 h PST, and G_{GN} consistently had the lowest daytime values, not G_{WB} as on sunny days (Figure 2.9). Overall, on July 24, 2015, G remained negative (-25 W m^{-2}) for most of the daytime, for almost all treatments. In general, on cloudy days, the plastic film treatments with the highest τ_s and α_L (i.e., TMX and S4) consistently achieved the highest G values when compared to the other plastic film treatments.

During cloud-free nighttime conditions, treatment and control G were controlled by downwelling longwave radiation. Before sunset on July 23, 2015 (i.e., sunny day, Figure 2.9) G shifted from being positive to negative at ~0.33 of the value of S_d at solar noon for all treatments, which corresponds to ~18:00 h PST on July 23, 2015. After shifting from positive to negative values, G becomes increasingly negative at a constant rate until sunset, to a minimum value of -100 W m^{-2}, after which G began to increase to a value of -70 W m^{-2} just before midnight. At 01:00 h PST on July 24, 2015, L_d increased from a value of 350 to 400 W m^{-2} as cloud cover increased. At that time, control and treatment G increased abruptly from -70 to -50 W m^{-2}, which shows the strong control L_d has on nighttime G. Interestingly, G_{WB} was the least negative of all the mulch treatments during both cloud-free and cloudy nights.
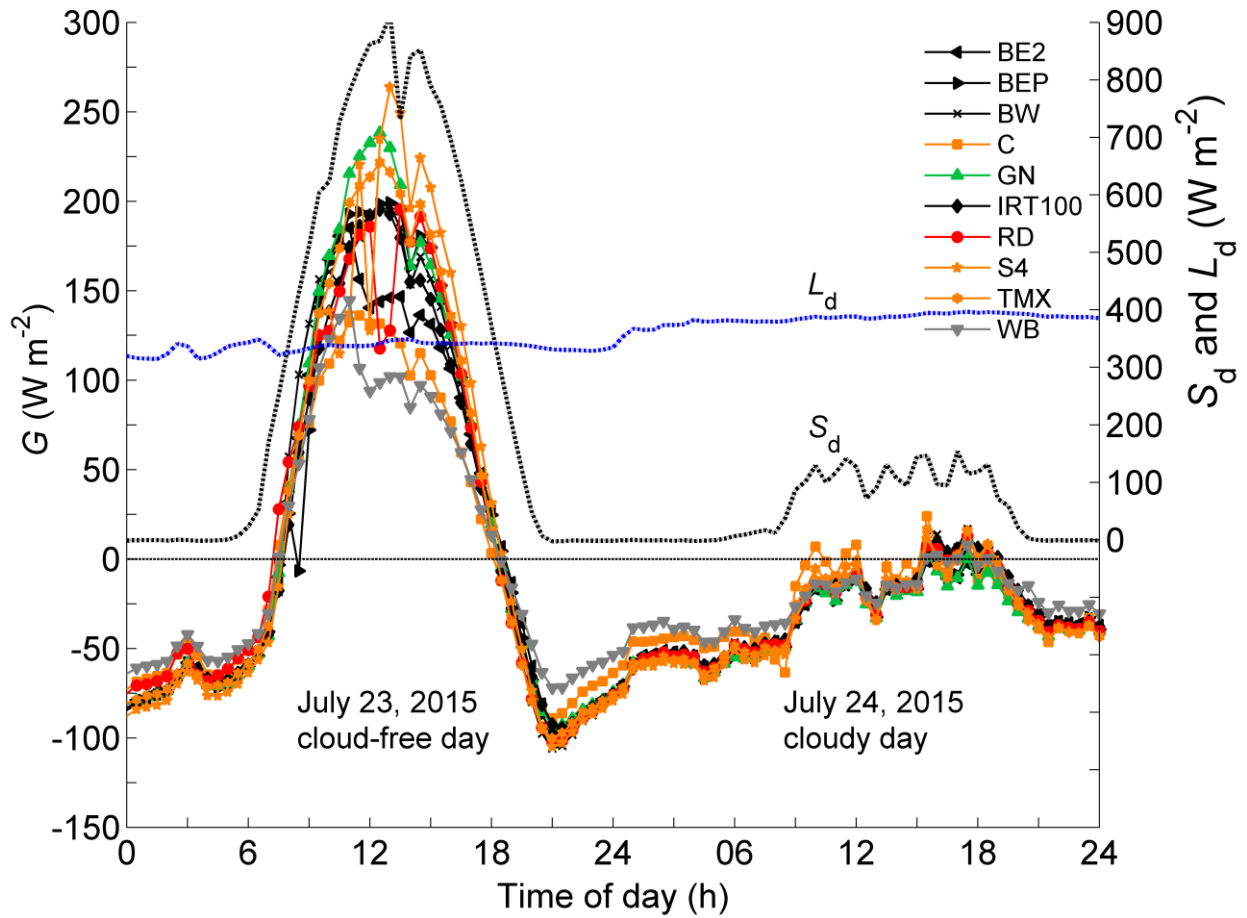
Figure 2.9 Shortwave (blue dotted-dashed line) and longwave downwelling radiation (green dotted-dashed lines) (S_d and L_d, scale on right y-axis, W m^{-2}) and soil heat flux density (G, scale on left y-axis) for BE2 (left-facing triangles), BEP (right-facing triangles), BW (crosses), C (squares), GN (upward-facing triangles), IRT100 (diamonds), RD (circles), S4 (stars), TMX (pentagrams) and WB (downward-facing triangles) for two consecutive days (July 23 and 24, 2015).

The daytime energy balance varied for each plastic film treatment depending on the magnitude of incoming radiation (i.e., shortwave and longwave) and the plastic film radiative properties. On a clear sunny day (July 23, 2015 Figure 2.10) total daytime net radiation for WB

(R_{nWB}) of 6.07 MJ m^{-2} was approximately half of the total daytime net radiation for the control (R_{nC}) of 13.82 MJ m^{-2}, yet the total daytime G_{WB} and G_c were similar 2.52 and 2.68 MJ m^{-2}, respectively. The large difference between R_{nWB} and R_{nC} is due to the high shortwave reflectivity of WB (0.45, Table 2.3). Since *LE* from C was not measured, *H* and therefore the heat sharing ratio (*G/H*) for C cannot be calculated or compared to *G/H* for the plastic film treatments, but G_C/R_{aC} can be determined. Comparison of *G/H* for WB and G/R_a for C shows that a greater proportion of R_a is converted to *G* at midday for WB than C, which is the case for all plastic film treatments when compared to C. For example, on July 23, 2015, both RD and C had very similar total daytime R_n values of ~13.82 and 13.1 MJ m^{-2}, respectively, yet G_{RD} and G_C are 4.01 and 2.58 MJ m^{-2}, respectively. On July 23, 2015 TMX and BW have the highest midday R_n values in Figure 2.10 with total daytime R_n of 13.10 and 14.77 MJ m^{-2}, respectively, with TMX having a higher value of total daytime *G/H* (0.50) than BW (0.42). Daytime total *G/H*, or G/R_a for C, was 0.71, 0.24 and 0.48 for WB, C and RD, respectively, on July 23, 2015. Overall, on clear sunny days, the maximum half-hourly *G/H* value occurred within 1 h of sunrise (~06:00 h PST on July 23, 2015) (Figure 2.10). On a particular cloudy day (July 24, 2018), total daytime R_{nWB}, R_{nC}, R_{nRD}, R_{nTMX} and R_{nBW} were 1.56, 3.32, 1.73, 0.45 and 0.70 MJ m^{-2}, respectively, while the total daytime G_{WB}, G_C, G_{RD}, G_{TMX} and G_{BW} were -0.85, -0.76, -0.97, -0.76 and -0.99 MJ m^{-2}, respectively. As a result *G/H*, or G/R_a for C, were all negative with values of -0.35, -0.19, -0.36, -0.63 and -0.59 for WB, C, RD, TMX and BW, respectively. Over the whole study period, the mean (μ) ± standard deviation (SD) total daytime ($S_d > 5$ W m^{-2}) *G/H* ranged from 0.19 ± 0.10 for C to 0.80 ± 0.47 for S4 (Table 2.5).
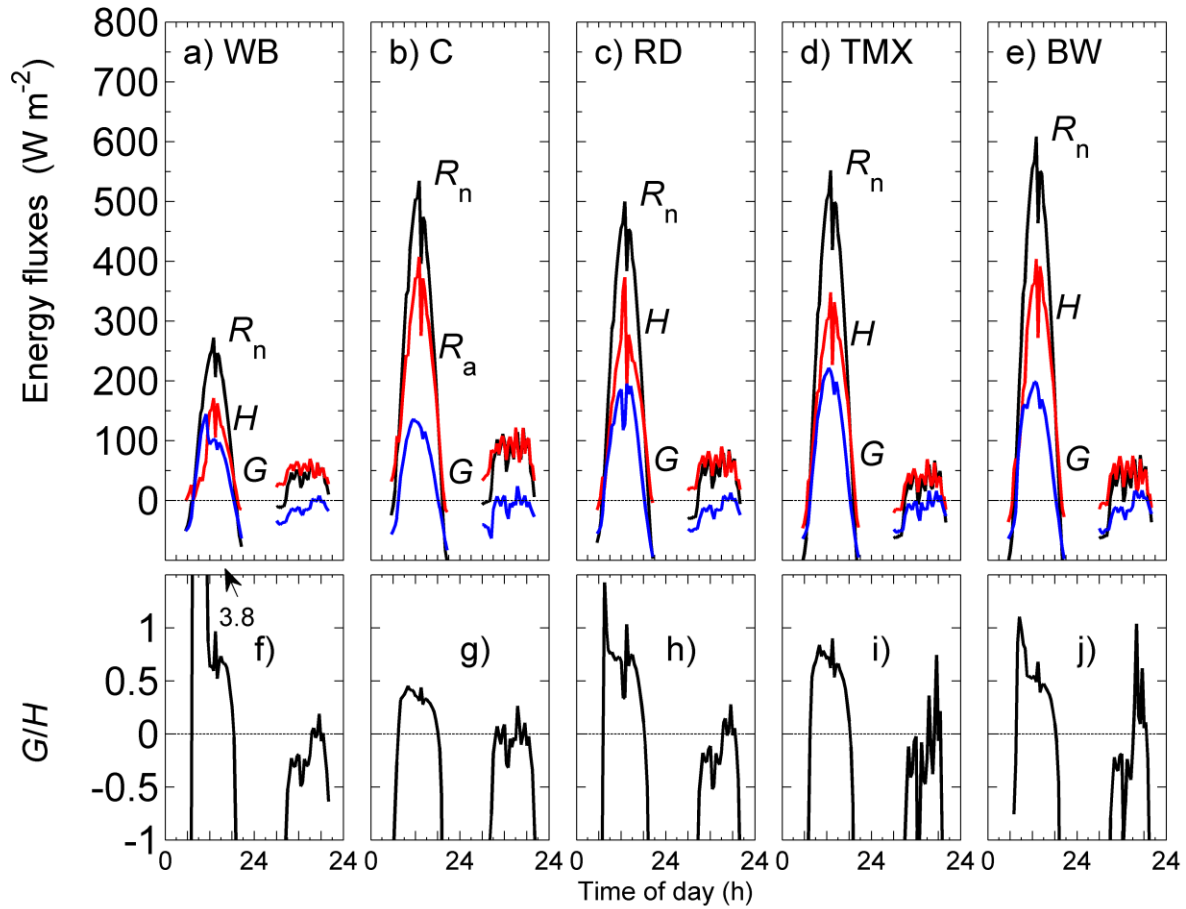
Figure 2.10 Panels a), b), c), d), and e) show half-hourly net radiation (R_n), available energy flux (R_a) or sensible heat (H) and soil heat flux (G) for the four zero-τ_s films and the control and panels f), g), h), i) and j) show the corresponding half-hourly heat-sharing-ratios (G/H, G/R_a for panel g) for two consecutive days (July 23 and 24, 2015).

      For all treatments and the control, total G has a positive linear correlation with total S_d on a daily basis, with slope coefficients ranging from 0.08 to 0.17 (Table 2.4). Except for G_C, G_{WB} and G_{BW} vs. S_d, the regressions for the plastic film treatments have R^2 values greater than 0.70 and RMSE values ranging from 0.46 to 0.67 MJ m^{-2} day^{-1}. The low R^2 values for G_C and G_{WB} vs. S_d are likely due to evaporation (E) and high reflectivity which fluctuated throughout the day,

respectively. Based on our analysis, the daily total S_d required for daily total $G \geq 0$ ranges from 9.4 W m^{-2} day^{-1} for G_{TMX} to 17.6 W m^{-2} day^{-1} for the G_C (i.e., bare soil). Even though WB is the most reflective of all the plastic films, and G_{WB} is less than G_C at midday, ~ 1 W m^{-2} day^{-1} less total S_d is required for G_{WB} to become positive than G_C, likely due to WB's insulation properties at night (Figure 2.8 and Table 2.4). There is a stronger linear correlation for G vs. S_n than for G vs. S_d and unlike the slope coefficients for G vs. S_d, which vary for each plastic (0.08 − 0.17), the slope coefficients for G vs. S_n are very similar (~0.15). This is expected, given that S_n accounts for the bulk surface reflectivity ($S_n = S_d (1 - \rho_s - S_d\rho_{ss} \tau_{sm\lambda}^2)$) and represents the net solar load on the plastic covered soil. Additional variance, unaccounted for by G vs. S_n, could be due to exclusion of the net longwave radiation (L_n) from the analysis (i.e., excluded due to discontinuous surface temperature measurements). Overall, the slope for G_C vs. S_n was less than those for the plastic film treatments, with a value of 0.09, likely due to a greater sensitivity of the surface temperature to wind (i.e., lower and more variable aerodynamic resistance compared to the plastic film treatments) (Figure 2.8 and Table 2.4). The difference between the slope of G_C vs. S_n and those for the plastic films is a direct measurement of the increased resistance to heat transfer caused by the still air gap between the plastic film and the soil surface, which is the mechanism for most of the plastic film heating.
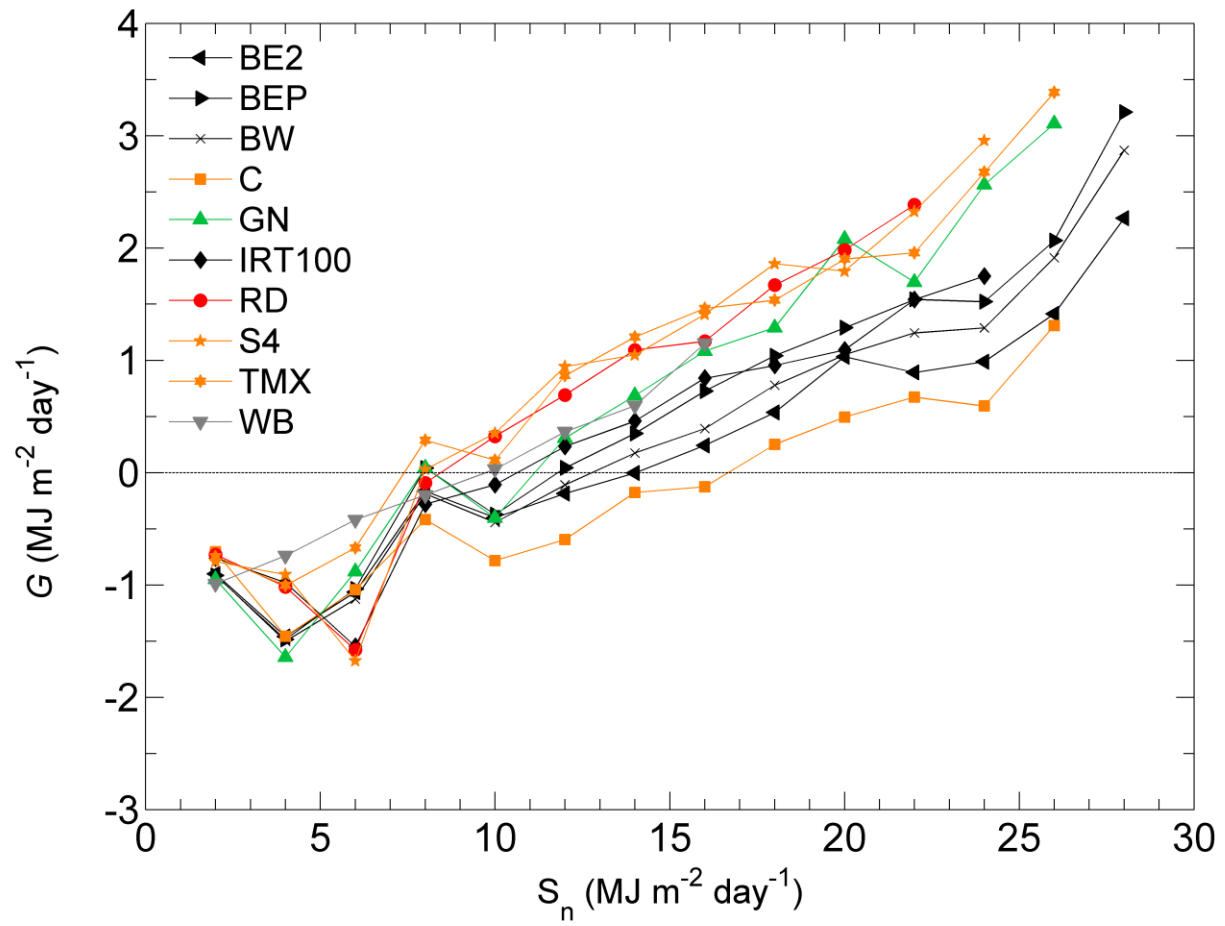
Figure 2.11 Binned daily net shortwave radiation (S_n) vs. daily soil heat flux density (G) for the control and plastic film mulch treatments (0.2 MJ m^{-2} day^{-1} bins). Linear regression statistics for the daily values are in Table 2.4.

Table 2.4 Values of linear regression coefficients, slope (a) and intercept (b) for the relationships between G and S_d ($G = aS_d + b$), coefficient of determination (R^2), and root mean square error (RMSE), and for the relationships between daily total G and S_n ($G = aS_n + b$) shown in Figure 2.11. The daily S_d and S_n values at which $G = 0$ for all treatments are also listed.

		# of days ($n = 96$)			
Plastic mulch abbreviation	a	b	R^2	RMSE (MJ m^{-2} day^{-1})	Daily total S_n and S_d ($G = 0$) (MJ m^{-2} day^{-1})
BE2	0.12[a] (0.11[b])	-1.59 (-1.60)	0.74[c]	0.50	13.8 (13.9)
BEP	0.15 (0.15)	-1.74 (-1.75)	0.77	0.61	11.5 (11.8)
BW	0.14 (0.14)	-1.79 (-1.79)	0.75	0.59	12.5 (12.9)
GN	0.18 (0.17)	-1.90 (-1.90)	0.82	0.58	10.3 (11.4)
IRT100	0.13 (0.12)	-1.42 (-1.42)	0.76	0.47	10.7 (12.3)
RD	0.17 (0.14)	-1.49 (-1.50)	0.78	0.54	8.5 (10.9)
S4	0.18 (0.15)	-1.48 (-1.50)	0.77	0.61	8.3 (9.8)
TMX	0.17 (0.15)	-1.42 (-1.42)	0.80	0.56	8.3 (9.4)
WB	0.14 (0.08)	-1.26 (-1.27)	0.68	0.38	9.3 (16.6)
C	0.09 (0.08)	-1.48 (-1.48)	0.66	0.45	15.8 (17.6)

[a] values outside the parentheses are for S_n vs. G.

[b] values inside the parentheses are for S_d vs. G.

[c] columns without parentheses represent values for both regressions.

Table 2.5 Mean (μ) ± standard deviation (SD) daytime heat sharing ratio (G/H) for the whole

study period (DOY 197 – 273).

Plastic mulch abbreviation	G/H
BE2	0.26 ± 0.13
BEP	0.54 ± 0.38
BW	0.47 ± 0.37
C	0.19 ± 0.10
GN	0.45 ± 0.22
IRT100	0.40 ± 0.20
RD	0.66 ± 0.37
S4	0.80 ± 0.47
TMX	0.68 ± 0.49
WB	0.68 ± 0.45

2.4.4 Soil temperature

During the calibration period, the agreement between 2-cm soil temperature of the

treatments (e.g., T_{s2cmWB} for WB) and the control plot (T_{s2cmC}) was generally good, with slopes, b

values, R^2 and RMSE values of > 0.90, < 2.5 $^{\circ}$C, ≥ 0.97 and ≤ 1 $^{\circ}$C, respectively (data not

shown). The agreement of $T_{s2cmBE2}$, $T_{s2cmBEP}$ and $T_{s2cmIRT100}$ vs. T_{s2cmC} was less good with

positive $b < 2$ $^{\circ}$C and slopes of ~0.9. Following the installation of plastic film mulches, slopes of

treatment vs. control T_{scmC} increased for all treatments, except for WB, with increases of 0.39,

0.36, 0.30, 0.25, 0.24, 0.24, 0.18 and 0.16 for TMX, BEP, S4, GN, BW, RD, IRT100 and BE2, respectively (Figure 2.12). T_{s2cmWB} vs. T_{s2cmC} experienced a decrease in slope of 0.12 from the calibration to treatment period, but the b value for the regression increased by 3.67 ^{o}C. For all the plastic film treatments the R^2 values decreased from the calibration to treatment period, but not below 0.94, and RMSE values increased from ~0.5 to 1.5 - 2 ^{o}C (Figure 2.12).
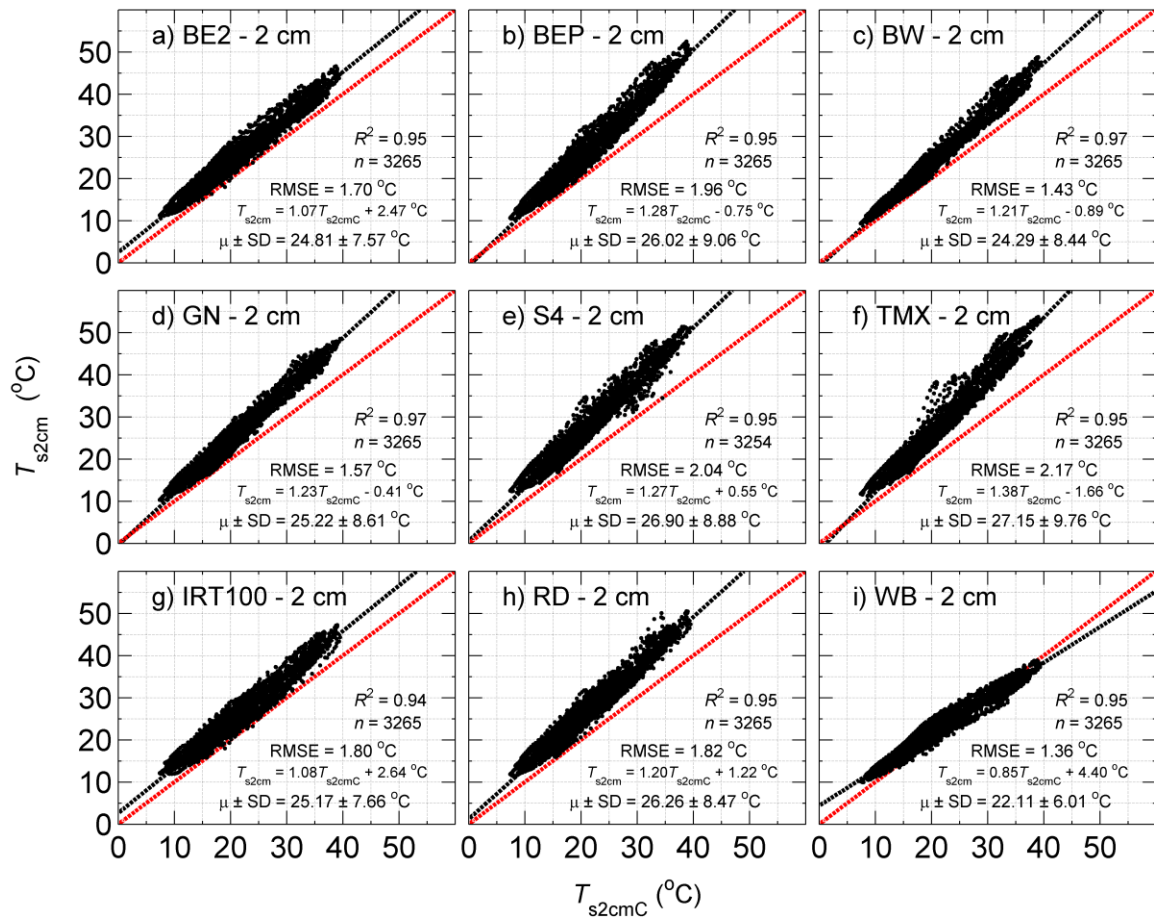
Figure 2.12 Panels a), b), c), d), e), f), g), h), and i) show linear regressions for half-hourly measurements of 2-cm soil temperature (T_{s2cm}) for $T_{s2cmBE2}$, $T_{s2cmBEP}$, T_{s2cmBW}, T_{s2cmGN}, T_{s2cmS4}, $T_{s2cmTMX}$, $T_{s2cmIRT100}$, T_{s2cmRD}, and T_{s2cmWB}, respectively, vs. T_{s2cmC} for data collected between July 16, 2015 and September 30, 2015 (post plastic film installation). For each regression, the

coefficient of determination (R^2), sample size (n), root mean square error (RMSE), mean (μ) $\pm$ standard deviation (SD) (for half-hourly daytime and nighttime values) and the linear regression equation are shown. Pre-treatment data is shown in Figure A.10.

As for G and T_{s2cm}, the agreement of the regressions between 10-cm soil temperature for the treatments (e.g., $T_{s10cmWB}$ for WB) and control soil temperature (T_{s10cmC}) was good with R^2 and RMSE values were greater than 0.96 and less than 0.35 °C (data not shown), respectively, with the exception of $T_{s10cmBEP}$ vs. T_{s10cmC} which has a slope and intercept of 0.88 and 2.59 °C, respectively. The regressions of $T_{s10cmBEP}$, $T_{s10cmS4}$, $T_{s10cmWB}$, $T_{s10cmTMX}$, and $T_{s10cmIRT100}$ vs. T_{s10cmC} had b values >1 °C but had slopes within 12% of the 1:1 line. For all treatments, the 10-cm T_s slopes increased from the calibration to treatment period, except for $T_{s10cmWB}$, and the b values from the regressions decreased. From the calibration to the treatment period the slope changes at the 10-cm depth were 0.29, 0.32, 0.27, 0.24, 0.27, 0.24, 0.25, 0.23 and -0.01 for TMX, BEP, S4, GN, BW, RD, IRT100, BE2 and WB (Figure 2.13).

T_{s10cm} (°C)

T_{s10cmC} (°C)

a) BE2 - 10 cm
$R^2 = 0.96$
$n = 3265$
RMSE = 0.95 °C
$T_{s10cm} = 1.20T_{s10cmC} - 1.10$ °C
$\mu \pm SD = 23.93 \pm 4.76$ °C

b) BEP - 10 cm
$R^2 = 0.96$
$n = 3265$
RMSE = 0.96 °C
$T_{s10cm} = 1.20T_{s10cmC} - 0.79$ °C
$\mu \pm SD = 24.22 \pm 4.75$ °C

c) BW - 10 cm
$R^2 = 0.97$
$n = 3265$
RMSE = 0.91 °C
$T_{s10cm} = 1.25T_{s10cmC} - 2.50$ °C
$\mu \pm SD = 23.47 \pm 4.92$ °C

d) GN - 10 cm
$R^2 = 0.96$
$n = 3265$
RMSE = 1.02 °C
$T_{s10cm} = 1.27T_{s10cmC} - 2.34$ °C
$\mu \pm SD = 24.12 \pm 5.03$ °C

e) S4 - 10 cm
$R^2 = 0.94$
$n = 3265$
RMSE = 1.18 °C
$T_{s10cm} = 1.20T_{s10cmC} + 0.12$ °C
$\mu \pm SD = 25.00 \pm 4.78$ °C

f) TMX - 10 cm
$R^2 = 0.95$
$n = 3265$
RMSE = 1.12 °C
$T_{s10cm} = 1.24T_{s10cmC} - 1.12$ °C
$\mu \pm SD = 24.64 \pm 4.93$ °C

g) IRT100 - 10 cm
$R^2 = 0.96$
$n = 3265$
RMSE = 0.89 °C
$T_{s10cm} = 1.20T_{s10cmC} - 0.61$ °C
$\mu \pm SD = 24.31 \pm 4.72$ °C

h) RD - 10 cm
$R^2 = 0.96$
$n = 3265$
RMSE = 0.99 °C
$T_{s10cm} = 1.23T_{s10cmC} - 0.61$ °C
$\mu \pm SD = 24.94 \pm 4.86$ °C

i) WB - 10 cm
$R^2 = 0.96$
$n = 3265$
RMSE = 0.77 °C
$T_{s10cm} = 0.92T_{s10cmC} + 2.46$ °C
$\mu \pm SD = 21.52 \pm 3.63$ °C

Figure 2.13 Panels a), b), c), d), e), f), g), h), and i) show linear regressions for half-hourly measurements of 10-cm soil temperatures (T_{s10cm}) for $T_{s10cmBE2}$, $T_{s10cmBEP}$, $T_{s10cmBW}$, $T_{s10cmGN}$, $T_{s10cmS4}$, $T_{s10cmTMX}$, $T_{s10cmIRT100}$, $T_{s10cmRD}$ and $T_{s10cmWB}$, vs. T_{s10cmC}, respectively, for data collected between July 16, 2015 and September 30, 2015 (post plastic films installation). For each regression, the coefficient of determination (R^2), sample size (n), root mean square error (RMSE), mean (μ) ± standard deviation (SD) (for half-hourly daytime and nighttime values) and the linear regression equation are shown. Pre-treatment data is shown in Figure A.11.

During the night on a cloud-free day (July 23, 2015), 2-cm T_s for all treatments was greater than T_{s2C}, ranging from 1 to 6 °C for T_{s2cmRD} and $T_{s2cmIRT100}$, respectively, and the

difference remained relatively constant until sunrise (06:00 h PST, July 23) (Figure 2.14). On the morning of July 23, 2015, T_{s2cm} began to increase approximately 1 h after sunrise, at which time the order of lowest to highest T_{s2cm} changed. For example, near 08:00 to 9:00 h PST, $T_{s2cmTMX}$, T_{s2cmRD}, T_{s2cmS4}, T_{s2cmGN}, and T_{s2cmBW} began to exceed $T_{s2cmIRT100}$, which had the highest value before sunrise. At the same time T_{s2cmWB}, which was greater in value than T_{s2cmC} during the nighttime, is similar in value to T_{s2cmC} and remained so until 12:00 h PST, after which it fell below T_{s2cmC} (i.e., similar to G in Figure 2.9). From 12:00 to 15:00 h PST, T_{s2cmWB} continued to have the lowest values after which it began to exceed T_{s2cmC} (Figure 2.14). As it was for G at the 2-cm depth, the highest T_{s2cm} values occurred under the plastic mulches with high τ_s followed closely by high α_s plastic mulches. On July 23, the high τ_s and α_s plastic film mulches reached maximum daytime T_{s2cm} at 16:00 h PST (i.e., 4 h after solar noon), whereas T_{s2cmC} reached its maximum near 15:00 h PST.

During cloudy nighttime conditions, 2-cm T_{s2cm} for all treatments is consistently greater than T_{s2cmC}, like cloud-free nights, but the differences are slightly smaller than those for cloud-free nights with values of 1.5 and 4.5 ^{o}C for T_{s2cmWB} and $T_{s2cmIRT100}$, respectively (Figure 2.14). After sunrise on July 24, 2015, 2-cm T_{s2cm} increased in response to increased S_d but only by a maximum of 2 – 3 ^{o}C. Between 06:00 h (i.e., sunrise) and 08:00 h PST on July 24, S_d remained below 50 W m^{-2} and T_s continued to decline as if it were a cloudy night, after which S_d increased above 100 W m^{-2} and T_{s2cm} increased for all treatments and T_{s2cmC} (Figures 2.9 and 2.14). Unlike on cloud-free days, T_{s2cmWB} and T_{s2cmC} had similar values, within 0.5 ^{o}C, for the whole day. Overall, daytime and nighttime T_{s2cm} were quite similar during cloudy periods (Figures 2.9 and 2.14).

On July 23, all treatment T_{s10cm} values (e.g., $T_{s10cmWB}$ for WB) reached their minimum ~1 h after sunset and were greater than T_{s10cmC} by 1.75 and 5 $^{\circ}$C for $T_{s10cmBW}$ and $T_{s10cmTMX}$, respectively. Throughout the nighttime, all treatment T_{s10cm} values decreased more quickly than T_{s10cmC}, except for $T_{s10cmBW}$, which resulted in a smaller difference between the treatment T_{s10cm} and T_{s10cmC} just before sunrise, than at sunset of the previous day. In the morning of July 23, T_{s10cm} under the high τ_s plastic film mulches (i.e., TMX, S4 and GN) increased slightly faster than T_{s10cm} under the high α_s plastic film mulches (i.e., BW, WB, BE2 and BEP) and the control (Figure 2.14). As expected, $T_{s10cmWB}$ and T_{s10cmC} had the lowest daytime T_{s10cm} values, reaching their maximum values near 18:00 h and 19:00 h PST, respectively. From 14:00 h to 16:00 h PST, $T_{s10cmWB}$ was nearly equal to T_{s10cmC}, reaching a maximum daytime difference of ~1 $^{\circ}$C near 19:00 h PST. All other treatments reached their maximum T_{s10cm} value near 18:00 h or 19:00 h PST.

Before dawn on July 24, all treatment and control T_{s10cm} were decreasing and ~1 h after sunrise the values continued to decrease but generally remained close to their pre-dawn values. T_{s10cm} for the treatments and the control increase very little during the daytime on July 24 compared to their pre-dawn values. Throughout the daytime, all treatments were warmer than T_{s10cmC}, with a minimum and maximum T_{s10cm} difference of 1.5 and 4.5 $^{\circ}$C for $T_{s10cmWB}$ and $T_{s10cmTMX}$, respectively. After sunset, all treatment temperatures began to decrease as solar irradiance (i.e., S_d) reached 0 in value. Overall, all the plastic film treatments increased T_{s10cm} and kept T_{s10cm} consistently greater under the plastic film than T_{s10cmC}, except during clear daytime conditions when WB's high ρ_s value caused $T_{s10cmWB}$ to equal T_{s10cmC}.
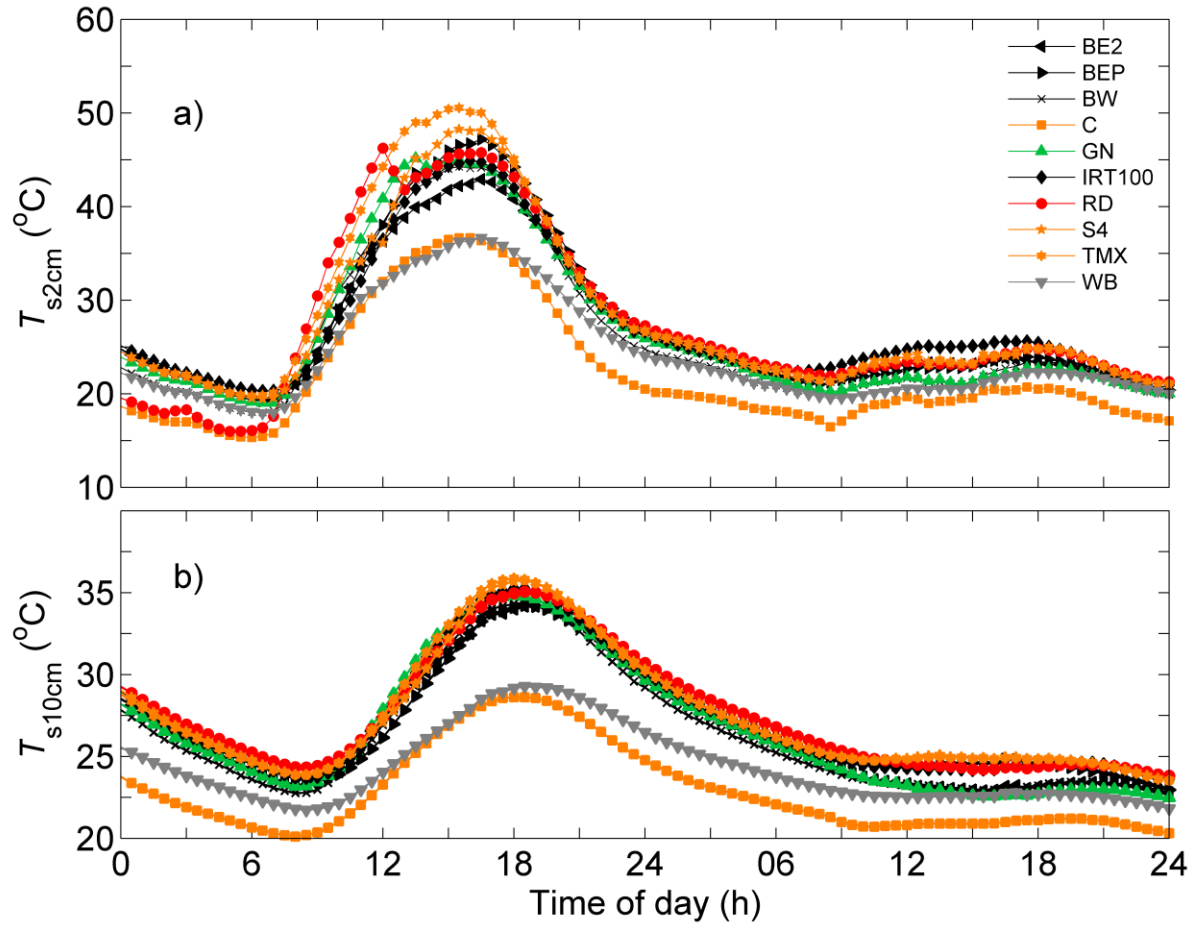
Figure 2.14 Panels a) and b) show diurnal courses of soil temperature at the 2-cm (T_{s2cm}) and 10-cm (T_{s10cm}) depths, respectively, for BE2 (left-facing triangles), BEP (right-facing triangles), BW (crosses), C (squares), GN (upward-facing triangles), IRT100 (diamonds), RD (circles), S4 (stars), TMX (pentagrams) and WB (downward-facing triangles) on two consecutive days (July 23 and 24, 2015).

2.5 Discussion

2.5.1 Plastic film radiative properties

2.5.1.1 Shortwave radiation properties

We studied the effect of nine plastic mulches, with various shortwave and longwave radiative properties, on surface energy balance and 2-cm and 10-cm soil temperature (T_{s2cm} and T_{s10cm}) and found that soil heat flux density (G), T_{s2cm} and T_{s10cm} were highly correlated with net solar radiation (S_n) of the bulk surface (i.e., the combined shortwave absorptivity ($1 - \rho_s$) of the plastic film and the soil surface). The surface with the lowest bulk shortwave absorptivity of 0.55 (i.e., WB covered soil) has the greatest potential for soil cooling, particularly at midday (i.e., within 2 h of solar noon), but its low longwave transmissivity ($\tau_{LWB} = 0.4$) and relatively high longwave absorptivity caused it to remain warmer than the control (C, bare soil) during the nighttime. Cover-whitening is typically performed on the covers of high transmissivity enclosures (e.g., low tunnels, high tunnels, glasshouses) to increase surface reflectivity (i.e., decrease surface absorptivity) and decrease S_n. Whitening subsequently decreases enclosure air temperature, vapour pressure deficit (D), canopy transpiration and canopy conductance (Baille et al., 2001; Kumar et al., 2009; Mashonjowa et al., 2010). The radiative properties and soil heating effect of highly reflective plastic films have been studied by other workers (Liakatas et al., 1986; Decoteau et al., 1988; Ham et al., 1993; Ham and Kluitenberg, 1994; Baille et al., 2001; Fan et al., 2015). Like our study, Ham et al. (1993) found that mulches with high reflectivity (i.e., white (WHIT, $\rho_s = 0.48$) and silver (SILV, $\rho_s = 0.39$)) caused soil cooling at midday but kept the soil warmer than bare soil during the nighttime, due to their high longwave absorptivity (i.e., low transmissivity). The popularity of high shortwave reflectivity plastic films has increased, in part,

66

due to their ability to increase photosynthesis in the lower part of the plant canopy by reflecting

it from the ground, which has the potential to increase plant biomass (Burrows and Reese, 2007)

and fruit production (Meyer et al., 2012). Although, it is important to note that other workers

(e.g., Baumann et al., 1997) have reported limited yield and photosynthesis (Privé et al., 2008)

increases when using reflective ground mulches. In south-eastern Spain, large areas are covered

with highly reflective materials, and an analysis by Campra et al. (2008) found that resultant

increased shortwave reflectivity (i.e., albedo) is the single largest driver of climate change in the

region, which has a significant role in offsetting radiative warming due to CO_2 emissions

(Muñoz et al., 2010). As the total area covered by highly reflective plastic films increases, so too

will their impact on surface radiation balance at local, and perhaps regional, scales.

In our study, even though RD has the second highest shortwave reflectivity, a value of

0.22, it had a soil warming effect like that of the black and clear plastic films which had very low

shortwave reflectivity values ranging from 0.04 to 0.1. Meyer et al. (2012) found that a red

plastic film with a similar shortwave reflectivity to RD in this study caused a higher soil

temperature when compared to bare gravel, indicating that a larger shortwave reflectivity value,

perhaps equal to or greater than 0.3 or 0.4, is required to lower S_n enough to cause systematic soil

cooling (i.e., to offset the increased resistance to heat loss from the ground caused by the

physical presence of the plastic film maintaining a still layer of air between the ground and

plastic film). Like highly reflective plastic film mulches (e.g., WB in this study), moderately

reflective plastic films (e.g., RD in this study) have the potential to increase PAR lower in the

plant canopy and increase plant growth and fruit production (Meyer et al., 2012; Shiukhy et al.,

2015). Shiukhy et al. (2015) found that strawberries grown with white, black and red plastic film

mulches experienced better fruit quality, increased the number of large pieces of fruits and resulted in 36%, 26% and 42% more total-growing-season yield when compared to the control (i.e., bare soil). These findings indicate that strawberries may benefit from various plastic film mulches, not only for their soil warming properties but also from increased PAR lower in their canopy. Other workers have shown that alteration of the ratio of far-red (700 – 800 nm) to red (600 – 700 nm) using light emitting diodes (LED) (Craig and Runkle, 2013; Darko et al., 2014) or plastic films mulches (Decoteau et al., 1988; Shiukhy et al., 2015; Miao et al., 2016) cause subtle changes in the light regime deep in the plant canopy, which can cause significant changes in plant physiology (e.g., flowering, stem elongation, fruit production) and chemical composition.

High transmissivity (i.e., S4 and TMX in this study) and high absorptivity (i.e., BE2, BEP and BW in this study) mulches are the most studied characteristics in the plasticulture literature (Liakatas et al., 1986; Ham et al., 1993; Ham and Kluitenberg, 1994; Li et al., 1999; Tarara and Ham, 1999; Tarara, 2000; Ibarra et al., 2001; Brault et al., 2002; Lamont, 2005; Culman et al., 2006; Cohen et al., 2008; Al Khatib et al., 2008; Komariah et al., 2011; Bonachela et al., 2012; Yokoe et al., 2015; Katan 2014; Murase et al., 2015; Li et al., 2016; Oz et al., 2017). Regarding spectral properties and weed growth suppression, black plastics are superior to high transmissivity plastic films because they absorb nearly all PAR (> 90%) necessary for photosynthesis. Although high transmissivity plastic films can "solarize" and supress weed growth up to 15 cm depth in the soil (Stapleton, 2000; Cohen et al., 2008), they can also increase weed growth during spring because their microclimate is similar to a low volume greenhouse with bare soil which is optimal for plant growth. With regards to soil thermal change, both high

transmissivity and high absorptivity plastic films are used to achieve similar goals (e.g., maximum heating and reduced soil *LE*), yet the mechanism is quite different. For high transmissivity plastic films, like TMX and S4 in this study, the surface they cover absorbs the majority of the incoming shortwave radiation and given that most vegetated and non-vegetated surfaces have shortwave reflectivity coefficients less than 0.25 (Monteith and Unsworth, 2008), the bulk shortwave reflectivity of a natural surface covered with high transmissivity plastic film is typically low. Therefore, the plastic film longwave properties and the still air-gap created by the physical presence of the plastic film, both of which trap radiant and heat energy, respectively, are fundamental to the heating potential of a given plastic film.

2.5.1.2   Longwave radiation properties

The longwave radiative characteristics of the plastic films are important to the plastic film radiation and energy balances. In this study, the plastic film with the highest τ_L values (e.g., GN, BW, IRT100, and RD) experienced the highest negative nighttime heat flux density near the surface of the soil (resulting from high longwave loss). Both of the high shortwave transmissivity plastic films in this study, TMX and S4, have glass-like properties (i.e., $\tau_L \sim = 0$) in that they have low longwave transmissivity of 0.36 and 0.6, respectively. This fact distinguishes them from standard low-density polyethylene (LDPE) films which has high longwave transmissivity and enabled them to increase daytime and nighttime net radiation at the soil surface they by reducing longwave loss. As a result, "designer polyethylene films" like TMX and S4 provide an opportunity to provide additional heating due to their radiative properties (i.e., high τ_s and low τ_L values), which may be desirable in soil mulches. Unfortunately, we did not use a standard LDPE in our study to provide a comparison, and we suggest this is done by future workers. The

presence of condensation and water droplets typically causes a reduction in both shortwave (Pieters et al., 1997, 20% reduction; Pollet and Pieters, 2002) and longwave transmissivity (Nijskens et al., 1984). In this study, S4 experienced condensation daily on its downward-facing side which increased S_n and L_n (via increased α_s and α_L, respectively) at the plastic film surface, respectively, causing its radiative properties to be similar to highly absorptive (shortwave and longwave) plastic films. Unlike S4, TMX is coated with a surfactant on its downward-facing side which prevents droplet formation, keeping TMX's shortwave transmissivity high in the presence of condensation. For high absorptivity plastic films, like BE2, BEP and BW in this study ($1 - \rho_s$ > 0.95), nearly all shortwave radiation is absorbed at the plastic film surface and the shortwave transmissivity is equal to 0, which means that differences in their longwave spectral properties distinguish them in terms of radiation balance and soil heating. Despite having similar shortwave properties, BE2, BEP and BW have different longwave properties and diurnal soil heat flux density (G). For example, BE2, which has the lowest τ_L value, experienced the least negative G on clear nights whereas BW, which has the highest τ_L value, experienced the most negative G on clear nights. Interestingly, during the daytime, BE2 had the lowest G values when compared to BEP and BW, which may be due to BE2's high emissivity (i.e., high longwave absorptivity by Kirchhoff's Law) and increased loss of longwave radiation loss during the daytime when compared to BW and BEP. When discussing the microclimatic impact of soil mulches, it is important to consider their impact on the full energy balance (i.e., partitioning of R_a into H and LE particularly when used inside an enclosure (i.e., low tunnel, high tunnel or glasshouse) or over large areas.

2.5.2   Surface energy balance

BW, BEP and BE2 had the 1st, 2nd, and 3rd highest daytime net radiation (R_n), respectively, when compared to all plastic films used in this study, and the control typically had the 4th highest R_n. We found G had a strong linear correlation with R_n which has also been documented by others (Tarara and Ham, 1999). Given that daytime G_{BE2}, G_{BW} and G_{BEP} increased more than daytime R_{nBE2}, R_{nBW} and R_{nBEP}, the available energy ($R_a = R_n - G$) decreased when compared to C. Fan et al. (2017) found that black plastic mulch caused a reduction of R_a due to reduced R_n and increased G compared to bare soil, whereas we estimate that black plastic mulches increase R_n. On the other hand, daytime total R_{nTMX} and R_{nS4} were both smaller in value than R_{nC} by ~ 1 – 2 MJ m^{-2} and had larger G values, which resulted in R_{aTMX} and R_{aS4} being much smaller than R_{aC}. Therefore, if an enclosure (e.g., low tunnel, high tunnel or glasshouse) was floored with unperforated plastic film mulch such as BE2 or TMX (i.e., $LE = 0$ and $R_a = H$), our analysis indicates that air temperature (T_a) would be highest in the enclosure floored with BE2, since $R_{aBE2} > R_{aTMX}$. Interestingly, Bonachela et al. (2012) compared sensible heat exchange within two greenhouses floored with transparent and black mulch and found the T_a inside the greenhouse with black mulch was higher than the greenhouse floored with transparent mulch, which is consistent with our findings. In theory, the sensible heat flux will always be higher for unperforated plastic films mulches than for the bare soil since $E > 0$, despite the fact that R_a is smaller for the plastic films than the bare soil. In practice plastic film mulches are perforated to allow for planting and stem growth, and as a result their ability to alter the Bowen ratio, through reductions in E, will ultimately control their heating potential when used inside or outside enclosures.

The relative amount of heat energy that enters the soil (G) vs. that which enters the atmosphere (H) is described using the heat sharing ratio (G/H) which is proportional to the ratio of the thermal admittance of the soil to that of the atmosphere (Tanner, 1974). In this study all plastic films had a higher mean daytime G/H than C (i.e., bare soil), which is because of the increased aerodynamic resistance (r_a) caused by the still-air gap between the plastic film mulch and soil surface, which ultimately prevents turbulent mixing and transport of heat energy from the soil surface into the atmosphere (Tanner, 1974; Ham and Kluitenberg, 1994). Interestingly, G_{WB} exceeded H_{WB} particularly in the morning (06:00 – 10:00 h PST) which has been documented by other workers (Tarara and Ham, 1999), reaching a maximum value near 15:00 h. Since daytime G_{WB} was only slightly smaller than G_C, and daytime total R_{aWB} was less than half of R_{aC}, the use of WB as a soil mulch may be an effective method to reduce atmospheric heating, particularly when used to cover the soil surface of a clear plastic low tunnel (Ham et al., 1993; Campra et al., 2008; Muñoz et al., 2010).

2.5.3   Soil temperature effects

We found that WB, the plastic film mulch with a high ρ_s value (~0.45), kept the soil slightly cooler than bare soil during midday but kept the soil ~2 °C warmer than bare soil on clear nights like all other plastic film mulches in this study. We found that the treatments that achieved the 1st and 2nd highest maximum 2 cm soil temperature (T_{s2}) during the daytime were TMX and S4, respectively, both of which have high shortwave transmissivity (τ_s) and low longwave transmissivity (TMX, $\tau_L = 0.36$; S4, $\tau_L = 0.60$). The next highest daytime maximum T_{s2cm} occurred in soil covered with high shortwave absorptivity plastic films that comprise BE2, BEP, BW, GN and RD. Somewhat similar to our study, Liakatas et al. (1986) found that a clear

polyethylene ($\tau_s \sim= 0.93, \tau_L \sim= 0.78$) and a black polyethylene film ($\tau_s \sim= 0.02, \tau_L \sim= 0.14$) increased T_{s2cm} by ~7 °C and 2 °C at midday, respectively, compared to bare soil, and Ham et al. (1993) found that a clear polyethylene ($\tau_s \sim= 0.84, \tau_L \sim= 0.78$) and a black polyethylene film ($\tau_s \sim= 0.01, \tau_L \sim= 0.67$) increased T_{s10cm} by ~2 °C and 5 °C at midday, respectively. Our results show that black films with a low τ_L value (BE2) had a smaller daytime soil temperature increase than the black plastic films with higher τ_L values (BW and BEP), which is consistent with findings by Liakatas et al. (1986) and Ham et al. (1993). Although it was expected that T_{s2cmBW} would exceed $T_{s2cmBEP}$, due to BW having a higher τ_L, the fact that $T_{s2cmBEP}$ exceeded T_{s2cmBW} is likely due to the fact that BEP had a slightly higher α_s than BW. For high shortwave absorptivity plastic films, like BE2, BEP and BW in this study, nearly all shortwave radiation is absorbed at the plastic film surface and fluxes toward the soil surface by 1) conduction when the plastic film and soil are in contact, 2) longwave radiation emission, and 3) convection when a still-air gap exists (i.e., plastic film and soil do not touch). Ham and Kluitenberg (1994) showed how the existence or lack of a still-air-gap between the plastic film and the soil will alter the soil heating effect of high absorptivity and high transmissivity plastic film mulches, where lack of a still-air-gap will maximize soil heating for high absorptivity plastics and the existence of a gap will maximize soil heating for high transmissivity plastic film mulches. In practise, when plastic film mulches are used by producers, the plastic film mulch touches both the soil and "floats" above the soil depending on tilling practices, soil texture and site preparation. Another important consideration is the impact of plastic mulch's longwave transmissivity on T_s both during the daytime and nighttime. During the nighttime, all plastic films used in this study remained warmer than bare soil, particularly on clear nights, due to the increased downwelling longwave

radiation emitted from the plastic films to the soil below. Similar results have been reported in previous studies (Liakatas et al., 1986; Ham et al., 1993). IRT100 and GN films, with very similar shortwave and longwave spectral properties with low τ_s and α_L values, had similarly high 2-cm soil temperatures during the midday on cloud-free days. Similarly, RD had low τ_s and α_L values and T_{s2cmRD} achieved the highest values of all plastics in the morning, after which T_{s2cmRD} declined abruptly likely due to condensation that was observed on the lower side of the film which altered its spectral properties. Based on data in this study plastic films with high τ_s values, and low α_s and ρ_s values, achieve the highest T_{s2cm} values when they have a high α_L value, i.e., radiative characteristics like those of glass. In contrast, plastic films that have low τ_s and ρ_s values, and high α_s values, achieve the highest T_{s2cm} values when they have a low α_L value. A theoretical analysis (i.e., a model) that examines the linkages between plastic film mulch shortwave and longwave spectral properties and near-surface temperature will be crucial to better understand the impacts of plastic film mulches on soil microclimate and surface energy balance.

2.6   Conclusions

1. During the daytime on cloud-free days, plastic films with high shortwave transmissivity (τ_s) and highest longwave absorptivity (α_L) caused the greatest increase in soil heat flux density (G), and films with high α_s and low α_L caused the next highest increases in G.

2. Like G, the highest daytime 2-cm and 10-cm soil temperatures (T_{s2cm} and T_{s10cm}, respectively) measured on cloud-free days occurred beneath plastic films with high τ_S and α_L values, followed by films with high α_s and low α_L values.

3. The only plastic film that decreased G, T_{s2cm} and T_{s10cm}, when compared to the control (i.e., bare soil), had a shortwave reflectivity (ρ_s) value of 0.45 (WB). However, decreased values of G, T_{s2cm} and T_{s10cm} only occurred at midday on cloud-free days and never during the nighttime or daytime on cloudy days.

4. Total daily (daytime and nighttime) G had a strong linear correlation with total daily downwelling solar radiation (S_d), and all plastic films showed a more positive correlation coefficient than the control (i.e., bare soil).Overall, the minimum and maximum total daily S_d required to make total daily G positive was 9.4 MJ m^{-2} and 16.6 MJ m^{-2} for TMX and WB, respectively, whereas the control (i.e., bare soil) required 17.6 MJ m^{-2}.

5. The soil surfaces covered by plastic films with high τ_s or shortwave absorptivity (α_s) values had the highest total daytime net radiation (R_n). The films generally increased soil thermal admittance relative to that of the atmosphere resulting in high ratios of G to H with daytime total values of G/H ranging from 0.26 (BE2) to 0.80 (S4).

Chapter 3: The radiation and energy balances of vegetation-free low tunnels with black plastic film mulch and various polyethylene covers

3.1 Summary

Low tunnels are low-cost and versatile structures with plastic film coverings that have the potential to improve crop microclimate and productivity. Despite wide usage, their impact on the surface energy balance and air temperature is not well understood and is difficult to measure or calculate. Three vegetation-free low tunnels were constructed with black plastic film mulch floors and plastic film covers with varying shortwave (S) and longwave (L) spectral radiative properties (reflectivity (ρ), transmissivity (τ) and absorptivity (α)). Net radiation (R_n), soil heat flux density (G), mulch surface temperature, internal air temperature (T_{ain}) and airflow inside the low tunnels were compared to a control treatment (i.e., no low tunnel with black plastic film mulch). During the daytime downwelling shortwave radiation inside the tunnels was always lower than downwelling shortwave radiation outside the tunnels. We found that the low tunnels covered with high longwave absorptivity (α_L) plastic film increased downwelling longwave radiation inside the low tunnels compared to that measured above the tunnels. This caused R_n in those tunnels to exceed R_n measured above the control and inside low tunnels covered with plastic film that had low α_L values, by as much as 35% daily. The presence of a low tunnel in addition to plastic film mulch only caused a small (~3%) increase in daytime G. The plastic film mulch sensible heat flux density (H_m) was higher inside low tunnels covered with films that had high α_L values. The increased H_m resulted in T_{ain} being 5 and 2 °C higher for low tunnels covered with high α_L values during the daytime and nighttime, respectively. We show that, the increase in T_{ain} inside the low tunnels resulted from 1) using a high τ_s cover, 2) protection of the mulch

surface from external wind and 3) increased R_n by choosing covers with high α_L values and 4) mulches with low ρ_s.

3.2   Introduction

Before polyethylene became commercially available in the early 1950's glass-covered greenhouses were the most popular structures used to modify crop microclimate. Glass and polyethylene have similar shortwave transmissivity (τ_s) values ranging from $0.7 - 0.9$ (Pieters et al., 1997; Wang and Deltour 1999), yet they are very different with regards to their longwave transmissivity (τ_L) (i.e., glass and polyethylene have low and high τ_L values, respectively). In the early 20th century, few experiments had been performed to quantify or, more importantly, understand the fundamental processes that cause glasshouses to alter microclimate. This point is exemplified by Wood (1909), who wrote in the *Philosophical Magazine and Journal of Science*, the following:

> There appears to be a widespread belief that the comparatively high temperature produced within a closed space covered with glass, and exposed to solar radiation, results from transformation of wave-length, that is, that the heat waves from the sun, which are able to penetrate the glass, fall upon the walls of the enclosure and raise its temperature: the heat energy is re-emitted by the walls in the form of longer waves, which are unable to penetrate the glass, the greenhouse acting as a radiation trap.

> I have always felt some doubt as to whether this action played any very large part in the elevation of temperature. It appeared much more probable that the part played by the glass was the prevention of the escape of warm air heated by the ground within the enclosure.

Despite the fact that polyethylene was not available in the early 20th century, comparisons of enclosures covered with halite (i.e., rock salt), which has similar shortwave and longwave radiative characteristics to polyethylene (i.e., high τ_s and τ_L), and glass showed that there was little, or no, difference in temperature rise between rock salt and glass covered enclosures (Wood 1909; Van Gulik 1910), which caused Wood to point out that:

> Is it therefore necessary to pay much attention to trapped radiation in deducing the
>
> temperature of a planet as affected by its atmosphere?

Nearly half a century later, Businger (1963) pointed to the fact that both Wood and Van Gulik (1910) performed their experiments indoors which eliminated net longwave radiation (L_n) losses to the sky, resulting in invalid conclusions for the outdoor radiation balance. Analytically, Businger (1963) estimated that there are two processes by which glasshouses increase air temperature: 1) enclosures increase the aerodynamic resistance of the air they enclose by protecting the surface from forced convection (i.e., wind) and this accounts for ~75% of the observed heating and 2) enclosures covered with materials possessing low τ_L values decrease the loss of longwave radiation to the sky (which has low emissivity, ~0.75) above the enclosure and this accounts for ~25% of the observed heating. Given that downwelling shortwave radiation (S_d) is the largest term in the radiative balance during the daytime, the shortwave transmissivity of the plastic film used to cover a low tunnel is of critical importance and strongly controls the heating of the air and the floor inside the enclosure. Particularly in temperate climates, and during the shoulder seasons of tropical and arid climates, producers aim to increase the enclosure internal air temperature (T_{ain}) and, as a result, seek covers with the highest τ_s values. Equally important to

the radiation balance of a low tunnel, particularly at night, is the longwave spectral properties of the cover material.

The ability of any greenhouse cover material to absorb and emit radiant heat depends on the α_L value of the cover material. Cover materials with high α_L values, like glass, have the greatest potential to emit longwave radiation downward to the floor of an enclosure. Because longwave emission (L) is related to the surface temperature (T_0) and emissivity (ε) of an object ($L = \varepsilon\sigma T_0{}^4$, where σ is the Boltzmann constant), covers with high longwave absorptivity (α_L) values are preferred for decreasing longwave losses from an enclosure, because they increase downwelling longwave radiation (L_d) and net longwave radiation (L_n) (i.e., less negative during daytime and nighttime). Like glass, other materials such as PVC or polycarbonate increase L_n when compared to single layer polyethylene (A-Mahdouri et al., 2014). In addition, crop producers use double layers comprising polyethylene and aluminized thermal screens or fabric screens (Zhang et al., 1996). Double layers have two advantages regarding enclosure heating: 1) one of the two layers may have a high α_L value which increases L_n and enclosure heating and 2) the air-gap between the two layers decreases the thermal conductivity of the cover (i.e., or heat loss). Our analysis is restricted to single-layer covers since low tunnels are preferably low-cost, non-permanent and low-maintenance structures, enabling the producer to quickly alter surface energy balance and crop microclimate.

To predict the sensible heat transfer of an enclosure (H) the heat transfer coefficients (h; W m^{-2} K^{-1}) must first be calculated using experimental data, and then modelled. Heat transfer coefficient between the cover and the outside air (h_{wou}) is primarily a function of wind velocity (i.e., forced convection), and, to some degree, by the temperature gradient between the enclosure

cover and the inside and outside air. On the other hand, heat transfer coefficients inside the enclosure between the floor and air (h_m) and cover and air (h_{win}) are primarily a function of the temperature gradient between the floor and the internal air (i.e., free convection), and to a lesser degree the external wind velocity. Many workers have calculated empirical relationships for predicting h_{wou} using wind velocity outside enclosures: $h_{wou} = 8.3 + 3.8u$ (ASHRAE)$;$ $h_{wou} = 5.62 + 3.91u$, $0 < u < 5$ m s^{-1} and $h_{wou} = 7.17u^{0.78}$, $5 < u < 20$ m s^{-1} (McAdams 1954); $h_{wou} = 7.2 + 3.8u$ (Garzoli and Blackwell 1981); $h_{wou} = 17.9u^{0.576}$, $u < 20$ m s^{-1} (Iqbal and Khatry 1977); $h_{wou} = 0.95 + 6.76u^{0.49}$, $u \leq 6.3$ m s^{-1} (Papadakis et al., 1992); $h_{wou} = 3u$ Businger (1954) (All equations are shown in Figure B.11). This paper aims to quantify the effect of both the 'wind effect' and 'greenhouse effect' for low tunnels covered with commercially available plastic films. More specifically, this study was designed to i) determine the impact of shortwave and longwave transmissivity on daytime and nighttime low tunnel R_n, ii) determine the low tunnel heat transfer coefficients, and iii) predict the air temperature inside low tunnels. Overall, the results from this study aim to assist crop producers in making informed decisions regarding season extension and crop protection using low tunnels, and enclosures in general. This is an essential step to better understand the microclimate of vegetated low tunnels.

3.3 Methods

3.3.1 Site description

The research was conducted at the University of British Columbia (UBC) Research Farm (UBC Farm) located on the UBC Vancouver Campus, Vancouver, BC (49°14'56.4"N 123°14'14.0"W, 68 m.a.s.l) from June 2016 to Sept 2016 and comprised two time periods: 1) a calibration period (May 14 – June 21, 2016) and 2) a treatment period (June 22 – Sept 30, 2016).

UBC Research Farm experiences a mild oceanic climate with humid, mild winters and dry summers with a 25-year (1991-2016) 2-m mean annual temperature (T_{a2m}) and precipitation (P) of 10.6 ℃ and 1054 mm at Totem Field (~500 m from the site) (Table 3.1). The UBC Research Farm experiences a sea and land breeze during the daytime and nighttime, respectively, due to its close proximity to the Salish Sea located to the west of UBC Farm. The experiment consisted of 4 treatments (3 low-tunnels floored with black embossed #2 plastic film mulch (BE2) topped by differing plastic covers, and a control treatment floored with BE2 mulch without a low tunnel). These were installed on a gravelly sandy loam Ferro-Humic Podzolic soil. The low tunnel treatments were covered with 3 polyethylene plastic films: polyethylene (POLY, thickness (d) = 0.15 mm), Thermax (TMX, d = 0.15 mm) and perforated polyethylene (POLY$_P$, d = 0.1 mm) (Table 3.2). The soil was prepared by disk cultivation at 0.3 m depth and by installing an irrigation dripline at the 0.05 m depth near the center of each treatment. Afterwards the soil surface was leveled, and a 0.15-m x 0.15-m-deep perimeter trench was dug around each 12-m x 1-m treatment area to bury the edges of the BE2 plastic film, after which stones (> 0.02 m) on the soil surface were removed by hand and the treatment area was levelled again using a ruler (Figure B.1). The 12-m x 1-m BE2 plastic film mulch sheets were installed by 1) securing one edge of the plastic film replacing soil removed during trenching, 2) minimizing the air gap between the soil surface and the plastic film by pulling the remaining 3 edges of the plastic tight while replacing soil removed during trenching (Figure B.2). Although each plastic film was installed to minimize air gap between the soil surface and the plastic film a distribution of air gaps was present after installation, with a maximum air gap of ~0.01 m. The three low tunnels (10-m-long x 0.8-m-wide x 0.7 m height) were then installed and comprised gable roof shaped steel rod hoops (0.008 m rod diameter, 0.8 m low tunnel base width, 2.1 m low-tunnel arch

perimeter length) Dubois Agrinovation Inc.installed at 1.5-m spacing (7 hoops low-tunnel^{-1}).

Low-tunnel covers were cut to size ($A_w = 21$ m^2) and secured at the ends using a 0.6-m-long steel

rod stake and cable ties (Figure B.3 and Figure B.4). Even though a 12-m x 1-m plastic film

mulch was installed, only 10-m x 1-m was covered by the low tunnel and the mulch surface area

($A_m = 10$ m^2). Finally, the low tunnel cover was secured to each hoop using 1.2-m-long bungee

cords tied to the tunnel base. The low tunnel edges, along the sides of the low tunnels, were held

within 0.01 m of the ground by the bungee cord system but were not made to be airtight. The

perforations on POLY$_P$ comprised 8 offset rows (running along the length of low tunnel) (with

holes about 5 cm apart in each row and offset by 2.5 cm in every other row) on each side of the

low tunnel, within an area from 0.15 m to 0.40 m above the base of the low tunnel. There are 320

holes m^{-1} of low tunnel (160 holes m^{-1} on each side) and each perforation has a surface area equal

to 0.79 cm^2 (diameter 1.0 cm). Therefore, the density of the perforations is 0.025 m^2 m^{-1} of low

tunnel, which represents 1.19 % of A_w (since width of plastic film is 2.1 m).

Table 3.1 Climatic, geographic and soil characteristics for UBC Research Farm.

Calibration period start and end dates	May 14 – Jun 21 (DOY 135 – 173), 2016
Treatment period start and end dates	Jun 21 – Sep 30 (DOY 175 – 274), 2016
Location	49°14'56.4"N 123°14'14.0"W
Elevation (m, above mean sea level)	68
25-year mean annual temperature (^{o}C)	10.6 ± 0.7
25-year mean annual precipitation (mm)	1054 ± 238
Soil order (Canadian System of Soil Classification[a])	Ferro-Humic Podzol
Soil texture	Gravelly sandy loam
Bulk density (kg m^{-3}) depth (m)	
0.05	0.92

[a]Soil Classification Working Group 1998

Table 3.2 List of names and abbreviations for the three plastic low tunnel polyethylene covers and single plastic film mulch used (used in all treatments) in this study.

Low tunnel cover name	Low tunnel cover abbreviation	Supply Company	Plastic film mulch name and abbreviation
Polyethylene	POLY	The Home Depot	Black embossed #2 (BE2)
Perforated polyethylene	$POLY_P$	Dubois Agrinovation Inc.	BE2
©Thermax	TMX	AT Films Inc.	BE2

3.3.2 General climate measurements

A weather transmitter (WXT520, Vaisala Oy, Helsinki, Finland) mounted 2 m above the soil surface measured half-hourly mean air temperature (T_{a2m}), precipitation (P), wind velocity (u_{2m}) and direction and relative humidity (VPD_{2m}). In addition to P from the weather transmitter, half-hourly P measurements were made using a tipping-bucket (0.1 mm) rain gauge (model TR525 M, Texas Electronics Inc., Dallas, TX, USA). All climate, soil and radiation variables (see following sections) were measured every 5 s using a solid-state multiplexer (model AM25T, Campbell Scientific Inc. (CSI)) and a datalogger (model CR5000, CSI), after which half-hourly averages were calculated and collected weekly. Half-hourly downwelling shortwave (outside the tunnels) (S_{dou}) and longwave (L_{dou}), P, u_{2m}, T_{a2m} and VPD_{2m} were retrieved from the UBC

Climatology Station located at Totem Field, 500 m away, for gap filling purposes and to calculate 25-year-mean P and T_{a2m}.

3.3.3 Low tunnel, mulch and soil microclimate measurements

For each low-tunnel treatment and the control, two soil temperature (T_s) and volumetric water content (θ_s) sensors (5TM, Decagon Devices Inc., Pullman, WA, USA) were installed at the 1-cm (T_{s1cm} and θ_{s1cm}) (Pre-treatment data is shown in Figure B.8 and) and 10-cm (T_{s10cm} and θ_{s10cm}) depths, 12 cm away from the dripline, prior to installing the plastic films. Mulch surface temperature (T_m) was measured, for each treatment and the control, using two methods which comprised 1) a chromel-constantan thermocouple (0.5 mm, Thermocouple Type-E, Omega Engineering Inc., Norwalk, CT, USA) woven 6 times into and adhered onto the upward facing side of the plastic film mulch using a high thermal conductivity adhesive (Omegabond® 101, Omega Engineering Inc., Norwalk, CT, USA) and 2) a infra-red thermometer (model IRTS, Campbell Scientific Inc. (CSI), Edmonton, AB, CA) positioned 0.3 m above and facing the plastic film mulch (Figure B.6). Air temperature inside (T_{ain}) and outside (T_{aou}) was measured with a fine wire (75 μm) chromel-constantan thermocouple positioned 0.60 m above the plastic film mulch inside each low tunnel and above the control, respectively. Cover, or wall, surface temperature (T_w) was measured with a chromel-constantan thermocouple using the same technique used to measure T_m and the thermocouple was adhered to the outside of the enclosure wall (Figure B.6). A 3-axis sonic anemometer (model 81000, R.M. Young Company, Traverse City, MI, USA) was positioned inside the TMX low tunnel to measure horizontal, vertical and cross-wind speed (u_{in}, v_{in} and w_{in}, respectively) inside the low tunnel, with the center of the array at a height of 0.6 m above the plastic film mulch film floor, from Sept 1 to Sept 30, 2016.

3.3.4 Radiation measurements and gap-filling

3.3.4.1 Net radiation and soil heat flux density

The energy balance of a vegetation-free low tunnel with plastic film mulch floor (impermeable to water vapour, $LE = 0$) can be written as $R_n = H + G + \Delta S_a$ where R_n is the net radiation, H is sensible heat flux density, G is the soil heat flux density and ΔS_a is the rate of change in energy storage between the soil surface and the height of the net radiation sensor. G was measured in two locations 0.12 m away from the dripline using two soil heat flux plates (model HP-127-1.0-1.3-71, TE Technology Inc., Traverse City, MI, USA) at the 3-cm depth and corrected for heat storage change between the plates and the soil surface (ΔS_s, $G = G_{1cm} + \Delta S_s$), in each treatment and the control (pre-calibration data is shown in Figure B.7). R_n was measured above the plastic film mulch (R_{nin}) and the low tunnel covers (R_{nou}) for each treatment (R_{nou} was not measured for the control) using two four-way net radiometers (model CNR1, Kipp and Zonen, The Netherlands). A CNR1 was mounted 0.15 m above the plastic film mulch and a second CNR1 was mounted 0.15 m above the top of the low tunnel cover, respectively (Figure B.1.5). The mounting height of 0.15 m was chosen to ensure that the maximum proportion of the net radiometer view-factor was occupied by the low-tunnel cover and plastic film mulch, respectively. Downwelling shortwave (S_d) and longwave (L_d), upwelling shortwave (S_u) and longwave (L_u) and R_n were measured above the plastic film mulch and cover of POLY, POLY$_P$ and TMX low tunnel for ~10 days, July 25 to August 3 (DOY 207 – 216), August 3 to 14 (DOY 216 – 227) and August 14 to 26 (DOY 227 – 239), respectively, after which the net radiometer mounted outside the low tunnels was mounted 0.15 m above the control (i.e., BE2 with no tunnel) for the remainder of the study period to measure net radiation (R_{ninC}). Net shortwave (i.e.,

solar) radiation (S_n) was calculated as S_d - S_u, and net longwave radiation (L_n) was calculated as L_d - L_u, respectively. Net radiation was calculated as the sum of net shortwave and longwave radiation ($R_n = S_n + L_n$). During the periods when measurements were not available, R_{nin} and R_{nou} were calculated using the spectral properties of the cover (e.g., TMX), plastic film mulch and the soil in combination with S_{dou}, L_{dou} and surface temperature measurements.

3.3.4.2   Shortwave radiation

Gap-filling was necessary for shortwave radiation inside and above the low tunnels during periods when measurements were not performed. During those periods downwelling shortwave radiation above the low tunnels (S_{dou}) was set equal to S_{dou} measured at Totem Field. Downwelling shortwave inside the low tunnels was calculated ($S_{dincalc}$) by multiplying S_{dou} by the shortwave transmissivity of each plastic film cover (wall) (τ_{sw}) and a multiple reflection term, $S_{dincalc} = S_{dou}\,\tau_{sw}\left(1 - \rho_{sm}(1 - \rho_{sw})\right)$, where ρ_{sm} and ρ_{sw} are the shortwave reflectivity's of the mulch and wall, respectively. There was strong agreement between S_{din} (measured downwelling shortwave radiation inside the tunnels) and $S_{dincalc}$ for TMX, POLY and POLY$_P$, with R^2 values of 0.99, 0.95 and 0.98 and RMSE values of 25.03, 51.59 and 27.96 Wm^{-2}. Nevertheless, S_{din} was systematically greater than $S_{dincalc}$ and the slope of the regression of $S_{dincalc}$ vs. S_{din} was 1.15, 1.09 and 1.13 for TMX, POLY and POLY$_P$, respectively. Therefore, $S_{dincalc}$ was corrected using the slopes listed above before it was used to gap-fill S_{din}. I suspect that S_{din} exceeded $S_{dincalc}$ due to multiple reflections and scatter from the low tunnel cover wall which were not accounted for in the multiple refection term above. Interestingly, aside from TMX, the increase in the slope beyond 1 was nearly equal to the ρ_s values for POLY and POLY$_P$. The low

tunnel hoops, which supported the low tunnel cover, caused abrupt decreases in S_{din} and were not included in the calculation of $S_{dincalc}$ given that they covered a small proportion of A_m.

Calculated upwelling shortwave radiation above the low tunnels, $S_{uoucalc} = S_{dou}\left(\rho_{sw} + \tau_{sw}{}^2\left(\rho_{sm}(1 - \rho_{sw})\right)\right)$, agreed well with measured upwelling shortwave above the low tunnels (S_{uou}) for POLY and POLY$_P$ with slope coefficients equal to 1.18 and 1.08 and RMSE values equal to 12.4 and 11.5 W m^{-2}, respectively. For TMX, $S_{uoucalc}$ was systematically smaller in value than S_{uou} by three times, which may be due to placement of the net radiometer near folds in the cover which caused the cover to have a larger ρ value than was measured in the laboratory, using the spectroradiometer (Table 3.3). Calculated upwelling shortwave radiation inside the low tunnels ($S_{uincalc} = S_{dincalc}\rho_{sm}$) generally agreed well with upwelling shortwave radiation measured inside the low tunnels (S_{uin}), particularly during the morning and evening. During the late morning and afternoon S_{uin} consistently exceeded $S_{uincalc}$ for all low tunnel treatments, with the measured ρ_{sm} value equalling approximately 0.1. This is unexpected given that the net radiometer shadow occupied the net radiometer pyranometer view-factor which would only cause the measured ρ_{sm} value to be less than the ρ_{sm} value derived from the spectroradiometer measurements. The spectroradiometer-measured shortwave reflectivity value of 0.05 for BE2 is very low and is susceptible to change due to soiling (Table 3.3). As was the case for downwelling shortwave, upwelling shortwave radiation fluctuated abruptly due to the low tunnel hoops, but no attempt to account for these in the calculation of the radiation balance was made.

3.3.4.3 Longwave radiation

Gap-filling was necessary for longwave radiation inside and above the low tunnels during periods when measurements were not performed. During periods when it was not measured, downwelling longwave radiation above the low tunnels (L_{dou}) was set equal to L_{dou} measured at Totem Field. Downwelling longwave radiation inside the low tunnels was calculated by adding the downwelling longwave radiation from the sky above the cover (L_{dou}) and from the cover itself (L_{dw}), which took into account the longwave transmissivity (τ_{Lw}) of the plastic film cover ($L_{dincalc} = L_{dou}\tau_{Lw} + \alpha_{Lw}\sigma T_w^4 + \rho_{Lw}\alpha_{Lm}\sigma T_m^4$, where σ is the Boltzmann constant). The reflection of upwelling longwave radiation from the mulch floor was not included because the longwave reflectivity of the cover was very small. The agreement for the regression of L_{din} vs $L_{dincalc}$ was strongest for POLY$_P$, which had the highest τ_L value, with slope, R^2 and RMSE values of 0.99, 0.96 and 5.3 W m^{-2}, respectively. Although the R^2 and RMSE values were strong for POLY and TMX, the measured values systematically exceeded the measured values, causing the slopes of L_{din} vs $L_{dincalc}$ to be less than a value of 1. It is important to note that the $L_{dincalc}$ is highly sensitive to changes in τ_L, therefore errors associated with the measurement of τ_L cause large errors in the calculation of $L_{dincalc}$. For POLY, $L_{dincalc}$ consistently exceeds L_{din} by 20 and 5 W m^{-2} during the daytime and nighttime, respectively. Regarding L_{din}, given that evaporation (E) was equal to zero inside the low tunnel's condensation was not observed. Also, significant soiling on the low-tunnel covers was not observed during the study.

Upwelling longwave radiation outside (above) the low tunnels was calculated ($L_{uoucalc}$) as the sum of the longwave emission from the cover and the transmitted upwelling emission inside the low tunnels ($L_{uoucalc} = \alpha_{Lw}\sigma T_w^4 + L_{uin}\tau_{Lw}$). Generally, the agreement between L_{uou} (measured)

89

and L_{uoucalc} was good but during the midday and nighttime L_{uoucalc} was greater and less than L_{uou}, respectively, which is likely due to the fact that the view-factor for the downward-facing pyrgeometer was occupied by surfaces adjacent to the low tunnel, which were not representative of the cover and mulch spectral properties and surface temperatures (i.e., evaporating soil and vegetation adjacent to the low tunnels and control). Upwelling longwave radiation inside the low tunnels (L_{uin}) was calculated using mulch (T_{mBE2}) and soil surface temperatures (T_{0s}) in combination with the longwave absorptivity (i.e., emissivity) of BE2 (α_{LBE2}) and the emissivity of the soil surface (ε_s) ($L_{\text{uincalc}} = \alpha_{\text{LBE2}}\sigma T_{\text{mBE2}}^4 + \tau_{\text{LBE2}}\varepsilon_s\sigma T_{0s}^4$). The agreement for the regression of L_{uin} vs. L_{uincalc} was strong for all low tunnel treatments during the daytime and nighttime. As a result, L_{uin} was replaced by L_{uincalc} for the entire study period. During the period for which R_n was measured the agreement for the linear regression of measured vs calculated R_n was good, with slopes of 1.07, 1.26 and 1.09, R^2 values of 0.97, 0.89 and 0.93 and RMSE values 26, 70, and 45 Wm^{-2}, for TMX, POLY and POLY$_P$, respectively. The good agreement gave us confidence in using the calculated R_n for gap filling purposes.

The net radiation of the control (C, BE2 plastic film mulch without a low tunnel) was determined using the shortwave and longwave spectral properties of the soil and the plastic film mulch, as was done for inside the low tunnel, and is written as $R_{\text{ninC}} = S_{\text{dou}}(1 - \rho_{s\text{BE2}}) + (L_{\text{dou}} - (\alpha_{\text{LBE2}}\sigma T_{\text{mBE2}}^4 + \tau_{\text{LBE2}}\alpha_{ss}\sigma T_{0s}^4))$. Overall, the agreement between measured and calculated upwelling shortwave and longwave inside the low tunnel was also observed for the control.

3.3.5   Low tunnel temperature model

Because the plastic film mulch (BE2) in this study was unperforated and impermeable to water vapour (Hopfenberg 1974) the surface latent heat flux (LE) was zero for all of the low

90

tunnels (POLY, POLY$_P$, TMX) and the control. Therefore, the energy balance above the plastic film mulch, inside all the low tunnels and above the control, can be written as $R_{nin} = H_m + G + \Delta S_a$, where R_{nin} and H_m are the net radiation and sensible heat flux on the upward-facing side of plastic film mulch, G is the soil heat flux at the depth of the plates and ΔS_a is the rate of change in energy storage between the soil surface and the height of the net radiation sensor. Finally, the available energy flux above the plastic film mulch (R_{ain}) inside the low tunnels and above the control (i.e., $R_{ain} = R_{nin} - (G + \Delta S_a)$) is equal to H_m at the plastic film mulch surface (i.e., $H_m = R_{nin} - (G + \Delta S_a)$).

The low tunnel temperature model used in this study uses an approach modified from Businger (1963). The radiation balances of the control treatment (C) and the plastic film mulch inside the low tunnels can be related to the radiation balance of the low tunnel cover wall, by accounting for the area of the plastic mulch (A_m) (i.e., the ground area of the tunnel) and the cover wall (A_w), written as:

$$(R_{nou} - R_{nin})\frac{A_m}{A_w} = H_{win} + H_{wou} \tag{1}$$

where H_{win} is the sensible heat transfer from the low tunnel wall to the air inside the tunnel, and H_{wou} is the sensible heat transfer from the low tunnel wall to the air outside the low tunnel. In this analysis, we assume that the sensible heat transfer due to ventilation is negligible for the TMX and POLY covered low tunnels (i.e., the cover wall is completely closed, no perforations exist, and no mechanical device actively ventilates), but this is not assumed for the POLY$_P$ covered low tunnel, therefore sensible heat transfer due to ventilation (H_v) must be accounted

91

for. An expression for the fact that, at steady state, the sensible heat released at the plastic mulch surface (H_m) must be transferred through the low-tunnel wall (other than H_v) is written as:

$$H_m = \frac{A_w}{A_m}(H_v - H_{win})$$ (2)

where a negative value of H_{win} means sensible heat is transferred from the low tunnel air to the downward facing side of the low tunnel cover.

The heat transfer coefficient for the plastic film mulch and the air inside the low tunnel (h_m) is the ratio of H_m to the temperature difference between the plastic film mulch (T_m) and T_{ain}, written as:

$$h_m = \frac{H_m}{T_m - T_{ain}}$$ (3)

A similar expression can be written for the heat transfer coefficient for the plastic film wall and the air inside the low tunnel (h_{win}):

$$h_{win} = \frac{-H_{win}}{T_{ain} - T_w}$$ (4)

where T_w is the wall temperature. The coefficient of heat transfer for the low tunnel wall and the outside air (h_{wou}) is written as:

$$h_{wou} = \frac{H_{wou}}{T_w - T_{aou}}$$ (5)

where H_{wou} is the sensible heat transfer between the wall of the low tunnel and the air outside the low tunnel and T_{aou} is the air temperature outside the low tunnel. The heat transfer coefficient for ventilation (h_v) can be written as:

$$h_v = \frac{H_v}{T_{ain} - T_{aou}} \qquad (6)$$

In general, the heat transfer coefficients mentioned above will be functions of wind velocity (i.e., forced convection) and temperature difference of surfaces-to-air interfaces (i.e., free convection). Under conditions in which the low tunnel is completely closed, mixing within the low tunnel is controlled mainly by free-convection and is similar for the plastic film mulch and the low-tunnel-cover wall. Therefore, the heat transfer coefficients within the low tunnel are approximately equal and we assume that $h_m = h_{win}$. Finally, we use an expression derived by Businger (1963), by combining $R_{nin} = H_m + G_{in}$ (energy balance of the mulch-covered tunnel floor) with Eqs. (1), (2), (3), (4), (5) and (6) as follows:

$$(T_{ain} - T_{aou}) = \frac{1}{B}\frac{A_m}{A_w}\left[h_{wou}R_{nin} + h_{win}R_{nou} - \left(h_{win} + h_{wou} \right)G_{in} \right] \qquad (7)$$

where G_{in} is the soil heat flux at 3-cm depth corrected for the rate of change in soil heat storage between the soil surface and heat flux plate, and $B = h_{win}\,h_{wou} + h_{win}\,h_v + h_{wou}\,h_v$. Analysis related to changes in heat transfer coefficients based on wind direction was not performed.

3.4   Results

3.4.1   Radiative properties of mulch and low-tunnel covers

Of the three low-tunnel covers, $POLY_P$ and POLY have the highest and lowest shortwave transmissivity (τ_s), 0.86 and 0.77, respectively, and $POLY_P$ has the highest transmissivity in the photosynthetically active (PAR, 400 – 700 nm), near infrared (NIR, 700 – 1400 nm), and shortwave infrared radiation (SWIR, 1400 – 2500 nm) regions (Table 3.3). $POLY_P$ also has the highest shortwave reflectivity (ρ_s) of all the low-tunnel covers, with an ρ_s value of 0.12, compared to values of 0.04 and 0.10 for TMX and POLY, respectively. The plastic mulch floor, BE2, has an τ_s value of 0.00 and an ρ_s value of 0.04, and therefore has a very high shortwave absorptivity (α_s) value of 0.96 (Table 3.3).

Regarding longwave radiative properties, all low-tunnel covers and the mulch have very small longwave reflectivity (ρ_L) values (< 0.02), and as a result their τ_L and α_L values determine their impact on the surface radiation balance. The mulch, BE2, has a very low longwave transmissivity (τ_L) and high longwave absorptivity (α_L) of 0.06 and 0.94, respectively (Table 3.3). For the low-tunnel covers, $POLY_P$ and TMX have the highest and lowest τ_L values, 0.83 and 0.36, respectively, and POLY has a τ_L value of 0.50. The shortwave properties of the three films are quite similar which allowed us to examine the impact of their longwave properties on the low tunnel radiation balance and microclimate.

Table 3.3 Shortwave and longwave radiative coefficients (ρ, τ, and α) for all plastic films and the control in this study.

Plastic films abbreviation	Shortwave												Longwave		
	S (350 – 2500 nm)			PAR (400 – 700 nm)			NIR (700 – 1400 nm)			SWIR (1400 – 2500 nm)			L (2500 – 10000 nm)		
	ρ_s	τ_s	α_s	ρ_{PAR}	τ_{PAR}	α_{PAR}	ρ_{NIR}	τ_{NIR}	α_{NIR}	ρ_{SWIR}	τ_{SWIR}	α_{SWIR}	ρ_L	τ_L	α_L
BE2 (Mulch)	0.04	0.00	0.96	0.05	0.00	0.95	0.03	0.00	0.97	0.02	0.00	0.98	0.00	0.06	0.94
POLY	0.10	0.77	0.13	0.13	0.74	0.13	0.07	0.82	0.11	0.04	0.81	0.15	0.01	0.50	0.49
POLY$_P$	0.12	0.86	0.02	0.17	0.84	0.00	0.09	0.88	0.04	0.05	0.89	0.07	0.00	0.83	0.17
TMX	0.04	0.82	0.14	0.07	0.80	0.13	0.03	0.86	0.11	0.02	0.82	0.16	0.01	0.36	0.63
C (bare soil)	0.07	0	0.93	-	-	-	-	-	-	-	-	-	-	-	-

[1] ρ_{sC} was measured using a 4-component net radiometer at midday (12:00 – 14:00 h PST) on four separate sunny days (see section 2.3.3).

[2] α_{sC} was calculated as a residual 1-ρ_{sC}, assuming τ_{sC} to be 0. All other shortwave (S) spectral values were measured in lab using a spectroradiometer.

3.4.2 Soil and near-surface microclimate

The study period comprised three distinct periods with different weather conditions covering two wet periods and one dry period. The first period (DOY 175 - 197) was dominated by cloudy days and precipitation (P), with average daily downwelling shortwave radiation (S_d) and longwave radiation (L_d) of 20.9 ± 7.0 and 30.6 ± 1.4 MJ $m^{-2} d^{-1}$, respectively (mean (μ) ± standard deviation (SD), Figure 3.1). The second period (DOY 198 – 243) was dominated by sunny days with very little precipitation and average daily S_{dou} and L_{dou} of 20.2 ± 5.3 and 30.4 ± 1.5 MJ $m^{-2} d^{-1}$, respectively (Figure 3.1). Similar to the first period, the third period was dominated by cloudy days, with average daily S_{dou} and L_{dou} of 13.7 ± 5.3 and 32.1 ± 2.6 MJ m^{-2} d^{-1}, respectively (Figure 3.1). Average daily S_{dou} in the third period was much lower than in the third period because the sun zenith angle was lower. For the whole study period, the average daily S_{dou} and L_{dou} was 18.4 ± 6.5 and 31.0 ± 2.0 MJ $m^{-2} d^{-1}$ and the average half-hourly daytime and nighttime L_{dou} was 364 ± 32 and 348 ± 27 W m^{-2}, respectively.

Overall, mean daily air temperature at the 2-m height (T_{a2m}) remained relatively constant for the whole study period with a value of 16.8 ± 3.1 °C. Cumulative precipitation (P_{cum}) values for the first, second and third periods were 57.2, 5.2 and 54.0 mm, respectively, with a P_{cum} value of 116.8 mm for the whole period. The soil volumetric water content (θ_{s1cm}) below the control responded similarly to the low tunnel treatments. θ_{s1cm} increased in response to P events, but never by more than 3% for any single P event and remained nearly constant throughout the study with a value of 0.091 ± 0.005 for all treatments and the control (i.e., BE2 without a low tunnel) (Figure 3.1). Daily mean vapour pressure deficit at the 2-m height (VPD_{2m}) ranged from 0.15 to

0.80 kPa. Overall, except for the precipitation events, the climate near the surface remained

relatively constant throughout the study period.
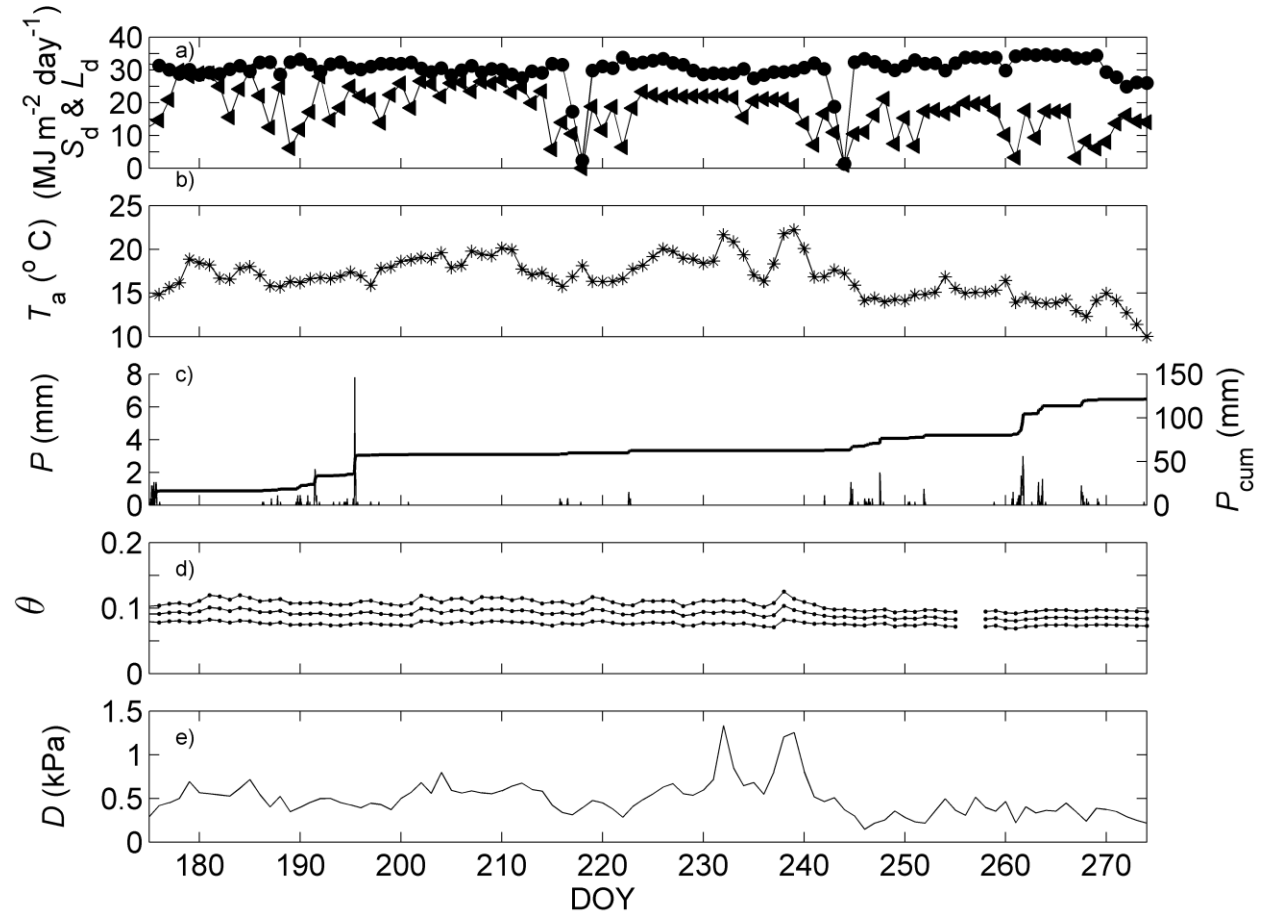
Figure 3.1 Panel a) shows daily (24-h) downwelling shortwave (S_{dou}, filled left-facing triangles

with line) and longwave radiation (L_{dou}, filled circles with line), panel b) shows mean daily air

(T_{a2m}, dotted line) and control soil temperature (T_{s1cm}, stars with line), panel c) shows half-hourly

precipitation (P, left axis) and cumulative precipitation (P_{cum}), panel d) shows mean daily 1-cm

soil volumetric water content (θ_{s1cm}) $\mu \pm$ SD for all treatments and the control and panel e) shows

mean daily vapour pressure deficit (VPD_{2m}). Only data for the treatment period is shown (June

22 – Sept 30, 2016).

3.4.3   Radiation balance

Overall, there was strong agreement between the daily shortwave transmissivity (τ_s) and reflectivity (ρ_s) values measured at UBC Farm (see Section 3.3.4.2) and the values measured in the biomet laboratory using the spectroradiometer. The daily total measured τ_s values (

$\tau_S = \sum_{i=1}^{48} S_{\text{din}i} / \sum_{i=1}^{48} S_{\text{dou}i}$) at UBC farm for the TMX, POLY, POLY$_P$ low tunnels were 0.82, 0.78 and

0.88, which are remarkably similar to the values of 0.82, 0.77 and 0.86 (Table 3.3) measured in the laboratory (Figure 3.2). On a half-hourly basis, τ_s values fluctuated in response to angle of incidence, with the lowest values occurring ~1 h after sunrise and before sunset, and during midday τ_s values decreased slightly in response to the low tunnel hoops. Overall the $\mu \pm$ SD half-hourly daytime τ_s values were 0.78 ± 0.11, 0.70 ± 0.21 and 0.86 ± 0.11 for TMX, POLY, POLY$_P$, respectively.

The daily total shortwave reflectivity values measured for BE2 ($\rho_S = \sum_{i=1}^{48} S_{\text{uin}i} / \sum_{i=1}^{48} S_{\text{din}i}$,

where S_{dou} and S_{din} are internal downwelling and upwelling shortwave radiation) at UBC Farm inside the TMX, POLY and POLY$_P$ low tunnels and above the control (no cover) (C) were 0.05, 0.08, 0.07 and 0.08, respectively, which are similar to the value of 0.05 measured using the spectroradiometer in the laboratory (Table 3.3). Regarding the radiation balance, all of the low tunnel covers absorbed and reflected ($\alpha_s + \rho_s$) a relatively large proportion of S_{dou}, with values of 0.18, 0.23 and 0.14 for TMX, POLY and POLY$_P$, respectively, whereas C did not show any reduction in S_{dou} due to the absence of a cover. As a result, on any given day the daily total net shortwave radiation (S_{nin}) must have been greatest for the control compared to treatments with covered tunnels. In Figure 3.2, which shows four separate days, S_{nin} is less for C than the low

98

tunnel treatments due to the fact that the data shown for C is later in the year than the other treatments when the suns zenith angle was low. On a half-hourly basis, in the morning all of the low tunnels have slightly larger values of S_{nin} than C, between 08:00 and 09:00 h PST (Figure 3.2), perhaps due to shortwave radiation reflection from the cover walls which increased S_{din} when the angle of incidence was large.

Since, in this study, the mulch surface temperature (T_m) and correspondingly the longwave upwelling radiation inside the low tunnels and from C (L_{uin}) were very similar day to day, the ability of the plastic covers to alter downwelling longwave radiation (L_{din}) had a great impact on net longwave radiation (L_{nin}). Ultimately, the effects of the plastic film cover's on L_{nin} at the plastic film mulch surface are of particular interest in this study. Both POLY$_P$ and C had large negative L_{nin} values which reached a minimum half-hourly value of ~-250 W m^{-2} at 15:00 h PST (Pacific Standard Time). This is expected since POLY$_P$ has a large longwave transmissivity (τ_L) (0.83, Table 3.2), which caused downwelling longwave radiation outside the POLY$_P$ low tunnel (L_{dou}) to largely determine downwelling L_{din} for POLY$_P$ with longwave emission from the plastic cover being much smaller than for TMX and POLY. Interestingly, for POLY$_P$, daily total L_{din} was less than daily total L_{dou} with values of 31.25 and 32.78 MJ m^{-2}, respectively, on August 8, 2016 (Figure 3.2).

Unlike POLY$_P$, both TMX and POLY increased downwelling longwave radiation inside the low tunnel above the measured L_{dou} values, as a result L_{nin} at the plastic film mulch surface was less negative than it was for POLY$_P$ and C, on a typical cloud-free day (Figure 3.2). Since the α_L values for TMX and POLY are 0.63 and 0.49 τ_L values are 0.36 and 0.50, respectively (Table 3.3), respectively, the relative impacts of L_{dou} and longwave emission from the plastic

film cover on L_{din} are quite similar ($L_{dincalc} = L_{dou}\tau_{Lw} + \alpha_{Lw}\sigma T_w^4$, where T_w is the wall surface

temperature). As a result, the minimum half-hourly L_{nin} value measured in a low tunnel covered

with TMX or POLY, on a typical cloud-free day (Figure 3.2), was approximately -160 W m^{-2}

compared to -250 W m^{-2} for POLY$_P$. Overall, in both TMX and POLY low tunnels, daily total

L_{din} was greater than daily total L_{dou} with increases in downwelling longwave (i.e., L_{din} - L_{dou}) of

5.6 and 4.4 MJ m^{-2}, respectively, on the two separate days shown in Figure 3.2. The greater

increase in downwelling longwave caused by TMX, when compared to POLY, is consistent with

the former's larger longwave emissivity (i.e., α_L).

a)

MJ m^{-2} day^{-1}

	S_{dou}	S_{din}	S_{nin}
POLY	24.84	19.42	18.47
TMX	21.99	18.06	16.69
POLY$_P$	22.35	19.74	18.27
C	19.01	19.01	17.56

TMX (08/17)
POLY (07/30)
POLY$_P$ (08/12)
C (08/26)

b)

	L_{dou}	L_{din}	L_{nin}
POLY	27.47	31.86	-8.20
TMX	28.60	34.18	-7.69
POLY$_P$	32.78	31.25	-11.02
C	29.74	29.74	-11.01

c)

	R_{nou}	R_{nin}
POLY	10.50	10.27 (0.20)
TMX	7.78	9.00 (0.18)
POLY$_P$	12.91	7.25 (0.13)
C		6.54 (0.13)

Time of day (h)
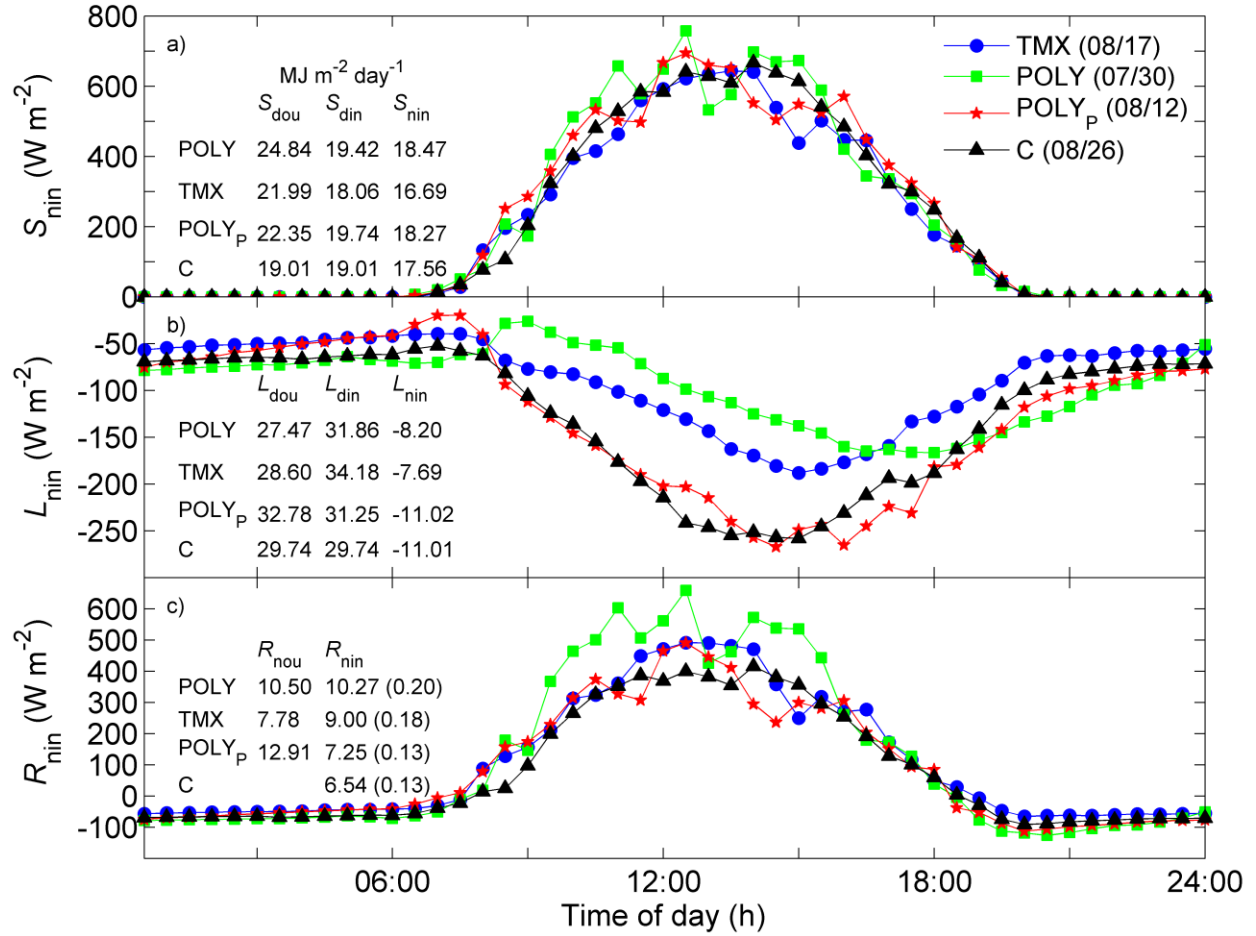
Figure 3.2 Panels a), b) and c) show half-hourly net shortwave (S_{nin}), longwave (L_{nin}) and all-wave radiation (R_{nin}), respectively, at the plastic film mulch surface inside the TMX, POLY, and POLY$_P$ low tunnels and for the control (C) and, on four separate days in 2016 (dates are show within parentheses (mm/yy) in the legend). In panels a) and b) total daily values (MJ m^{-2} day^{-1}) of downwelling shortwave (S_{dou}) and longwave (L_{dou}) outside and downwelling shortwave (S_{din}) and longwave (L_{din}) inside the low tunnels are listed for the TMX, POLY, and POLY$_P$ low tunnels and for C, as well as total daily values of S_{nin} and L_{nin}, respectively. In panel c) daily total values of net R_{nin} and R_{nou} measured directly above the tunnels are listed for the TMX, POLY, and POLY$_P$ low tunnels and C, as well as the ratios of total daily $R_{nin}/(S_{dou} + L_{dou})$ in parentheses.

101

Regarding net radiation, POLY and TMX were more efficient for capturing $S_{dou} + L_{dou}$ (Figure 3.2 and Figure 3.3) than $POLY_P$, despite the high τ_s value of $POLY_P$. This is due to TMX and POLY's large α_L values and consequent ability to increase L_{nin} (Figure 3.2 and Table 3.3). Overall, TMX and POLY have similar radiation balances, which is somewhat unexpected given that TMX's α_L and τ_s values are 14% and 5% larger than POLY's, respectively, on separate days. The root mean square error (RMSE) values for the regression of R_{nin} vs. $(S_{dou} + L_{dou})$ were 29, 44, 54 and 83 W m^{-2} for C, TMX, $POLY_P$ and POLY, respectively (Figure 3.3). The fact that C has the lowest RMSE is expected since S_{din} and L_{din} are unaffected by the presence of a cover which, for TMX, POLY and $POLY_P$, can result in increased variablility of R_{nin} due to abrupt changes in S_{din} and changes in T_w throughout the day.

In Figure 3.3, all of the low tunnels have slope values less than C (0.66) due to the fact that all of the tunnel covers reflect and absorb ~15 – 20 % of S_{dou}, which reduces S_{din}. The slope for $POLY_P$ (0.57) is the smallest because the low α_L value of $POLY_P$ is unable to compensate for loss of S_{dou} caused by covers shortwave absorbtion and reflection. Like $POLY_P$, S_{din} is less than S_{dou} for both TMX and POLY due to shortwave absorbtion and reflection by the cover, but their relatively high α_L values compensate for the loss of S_{dou}, which causes their slopes to increase to values of 0.64 and 0.63, respectively.

$R_{ninTMX} = 0.63(S_{dou} + L_{dou}) - 273 \text{ W m}^{-2}$

$R_{ninPOLY} = 0.64(S_{dou} + L_{dou}) - 288 \text{ W m}^{-2}$

$R_{ninPOLY_P} = 0.57(S_{dou} + L_{dou}) - 266 \text{ W m}^{-2}$

$R_{ninC} = 0.66(S_{dou} + L_{dou}) - 267 \text{ W m}^{-2}$

TMX
POLY
POLY$_P$
C

	n	RMSE (W m^{-2})	R^2
TMX	475	44	0.94
POLY	420	83	0.84
POLY$_P$	518	54	0.90
C	910	29	0.96

y-axis: R_{nin} (W m^{-2}), range -200 to 700

x-axis: $S_{dou} + L_{dou}$ (W m^{-2}), range 200 to 1400
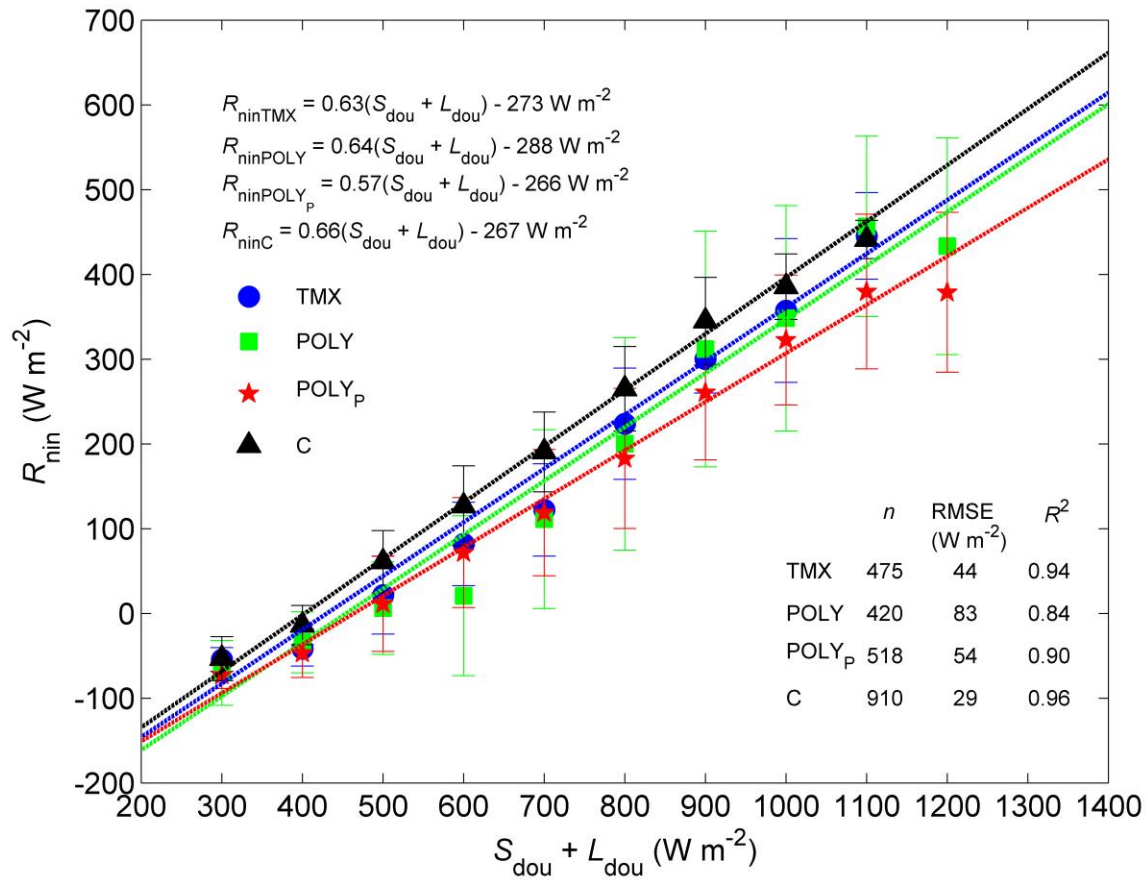
Figure 3.3 Linear regression of half-hourly net radiation at the plastic film mulch (BE2) surface (R_{nin}) vs the sum of downwelling shortwave and longwave radiation outside the low tunnels ($S_{dou} + L_{dou}$), for TMX (blue open circles), POLY (green open squares), POLY$_P$ (red stars) and the control no tunnel (C) (black triangles). For each treatment and the control, the regression equation ($R_{nin} = ax + b$), sample number (n), root mean square error (RMSE) and coefficient of determination (R^2) are listed. The vertical bars represent the standard deviation for each bin interval. The data shown for POLY, POLY$_P$ and TMX low tunnel are from July 25 to August 3 (DOY 207 – 216), August 3 to 14 (DOY 216 – 227) and August 14 to 26 (DOY 227 – 239), respectively.

Net radiation outside (R_{nou}) and inside (R_{nin}) the low tunnels are crucial environmental variables required to calculate low tunnel air temperature, using the tunnel air temperature model represented by Eq. (8). The difference between R_{nou} and R_{nin} is a direct measure of the radiation balance of the low tunnel cover and can be either negative or positive. For $POLY_P$, R_{nou} - R_{nin} typically remained positive during the nighttime and daytime (Figure 3.4a), with mean nighttime and daytime R_{nou} - R_{nin} of 33.5 $\pm$ 10.9 and 40.0 $\pm$ 79.5 W m^{-2}, respectively. For POLY and TMX, nighttime R_{nou} - R_{nin} was far less than for $POLY_P$ with values of 5.19 $\pm$ 40.2 and -1.21 $\pm$ 12.9, respectively. The negative value for TMX, and for POLY intermittently, indicate that unlike $POLY_P$, which typically remained positive, R_{nou} - R_{nin} were negative during part of the daytime for POLY and TMX (Figure 3.4a), with mean daytime (6:00 to 20:00 h PST) R_{nou} - R_{nin} values of 47.2 $\pm$ 88.4 and 24.4 $\pm$ 27.8 W m^{-2}. Overall, high longwave absorptivity covers can cause R_{nin} to exceed R_{nou} whereas low absorptivity covers $POLY_P$ cannot. The large changes in R_{nou} - R_{nin} are a result of fluctuations in R_{nin} that result from changes in S_{din}, caused by the presence of the tunnel

hoop support structures.
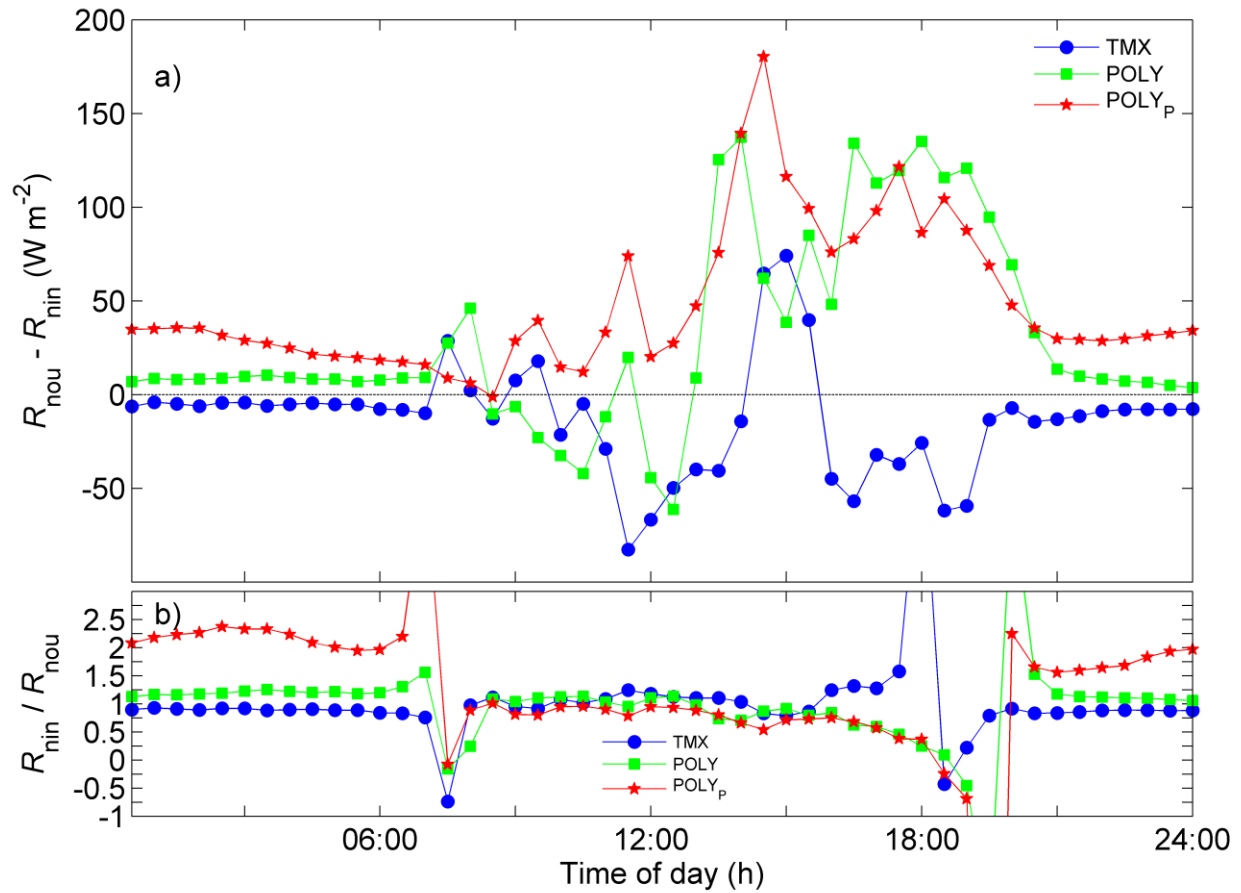
Figure 3.4 Panel a) shows the difference between half-hourly ensemble mean net radiation outside (R_{nou}) and inside (R_{nin}) TMX, POLY and POLY$_P$ low tunnels, respectively (R_{nou} - R_{nin}, W m^{-2}) from July 25 to August 3 (DOY 207 – 216), August 3 to 14 (DOY 216 – 227) and August 14 to 26 (DOY 227 – 239), respectively. Panel b) shows mean ensemble R_{nin} / R_{nou} for the same time period.

3.4.4   Energy balance

For a sequence of cloud-free days in late July (Figure 3.5), available energy flux (R_{ain}) shifted from values of approximately -50 W m^{-2} before sunrise to values greater than 50 W m^{-2}

105

within two hours of sunrise (Figure 3.5). On cloudy days, R_{ain} typically remained positive in value during the daytime and had small negative values (-5 to -10 W m^{-2}) during the nighttime (data not shown). On both cloud-free and cloudy days R_{ain} reached its most negative values ~1 h after sunset, reaching values ranging from -75 to -100 W m^{-2} and -25 to -50 W m^{-2}, respectively and gradually increased during the nighttime ($S_{dou} < 5$ W m^{-2}) until sunrise of the following day. Daytime, nighttime and daily values of G were similar for the TMX, POLY, POLY$_P$ and C. For a sequence of cloud-free days (Figure 3.5), during the nighttime, mean G_{POLYP} and G_C were less than G_{POLY} and G_{TMX} but only by an average value of ~3 W m^{-2}. The cloud-free daytime mean G_{POLYP} and G_C were slightly less than G_{POLY} and G_{TMX} by a value ranging from 5 - 7 W m^{-2}.

On the 6 cloud-free days shown in Figure 3.5 half-hourly mean midday (11:00 – 13:00 pm PST) heat-sharing ratios (G/R_{ain} i.e., G/H) were only slightly larger for the low tunnels than for C, with $\mu \pm$ SD values of 0.46 ± 0.09, 0.50 ± 0.19, 0.46 ± 0.10 and 0.42 ± 0.08 for TMX, POLY, POLY$_P$ and C, respectively, which indicates that the addition of a low tunnel to a soil with plastic film mulch causes little change in the ratio of soil thermal admittance to atmospheric thermal admittance. On cloud-free days, G/R_{ain} typically became positive 2 - 3 h after sunrise, when G switched from negative to positive values and slowly rose to ~50% of the daily maximum by mid-morning (10:00 h PST). The linear regressions of half-hourly G vs R_{nin} were very similar for all of the low tunnels and C, with similar y-intercepts ranging from -9 to -13 W m^{-2} and slopes of 0.34, 0.30, 0.30 and 0.30 for TMX, POLY, POLY$_P$ and C (Figure 3.6). Interestingly, the regression for C had the lowest RMSE value which was 17 W m^{-2} and the highest coefficient of determination ($R^2 = 0.88$) (Figure 3.6).
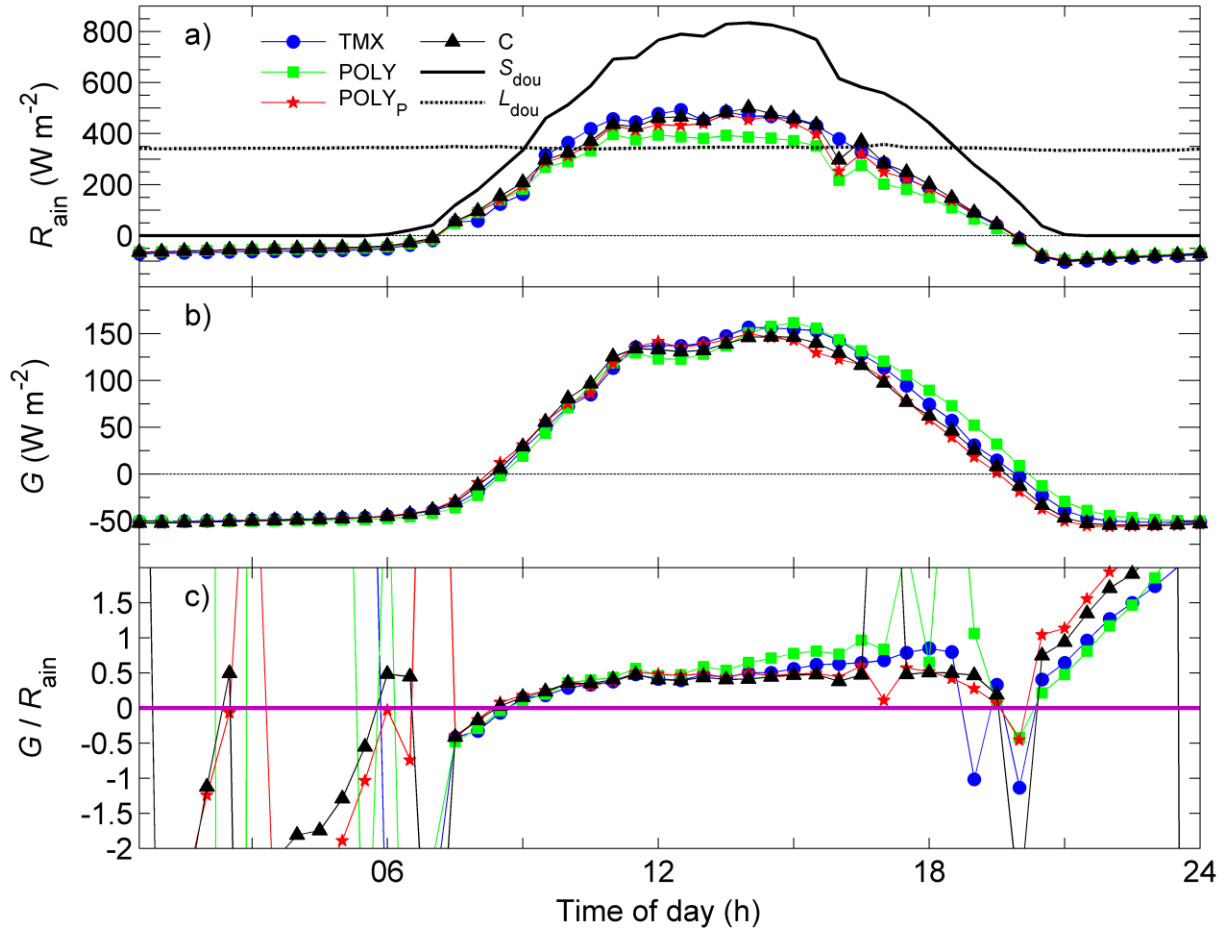
Figure 3.5 Panels a) shows half-hourly ensemble mean downwelling shortwave (S_{dou}) and longwave radiation (L_{dou}) above the low tunnels, and available energy flux ($R_{ain} = R_{nin} - G = H$) for the control (C) and inside the TMX, POLY, and POLY$_P$ low tunnels. Panels b) and c) show the soil heat flux density (G) and the heat-sharing ratio (G/R_{ain}) (i.e., G/H), respectively, for C and inside the TMX, POLY, and POLY$_P$ low tunnels. Ensemble mean values are for 6 sequential sunny days on July 26 – July 31 (DOY 206 – 213).
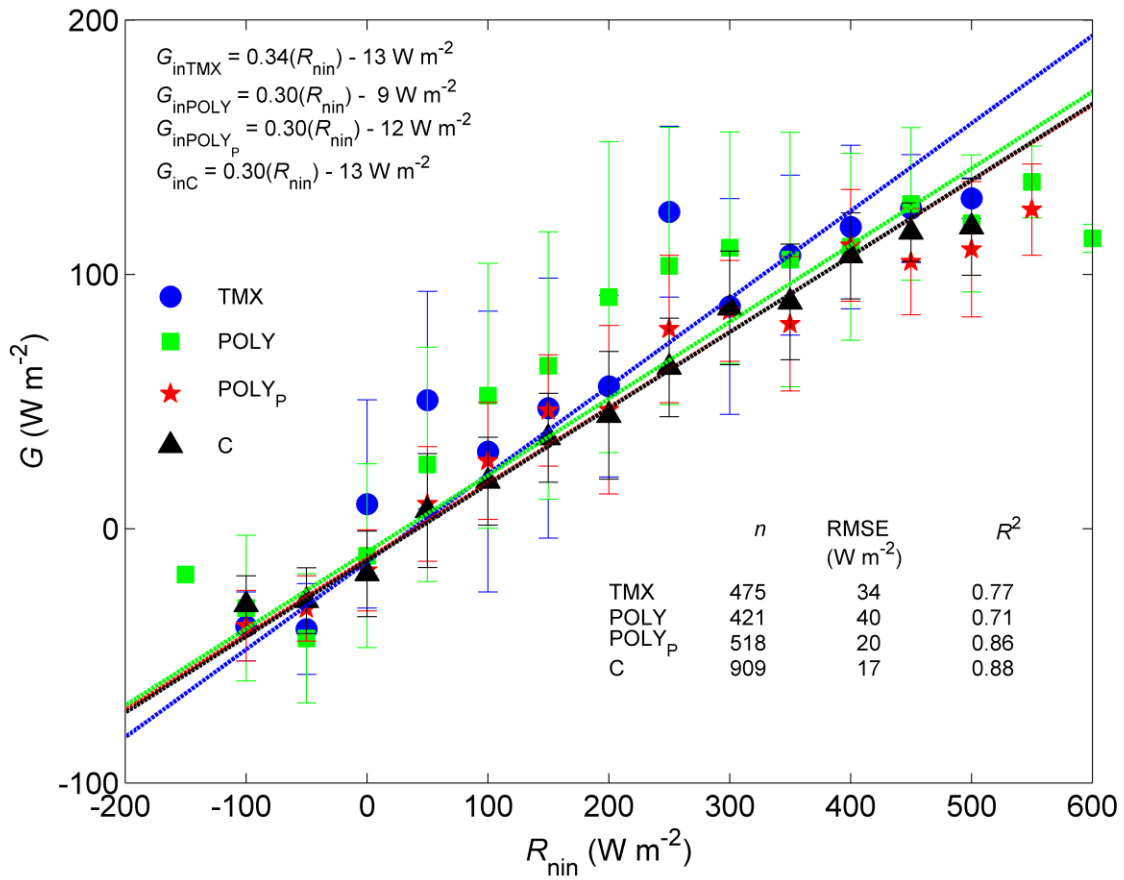
Figure 3.6 Linear regression of half-hourly soil heat flux density (G) vs the net radiation (R_{aincalc}), for TMX (blue circles), POLY (green squares), POLY$_P$ (red stars) and C (black triangles). For each treatment and the control the regression equation ($G = aR_{\text{nin}} + b$), sample number (n), root mean square error (RMSE) and coefficient of determination (R^2) are listed. The bars represent the standard deviation for each bin interval. The data shown for POLY, POLY$_P$, TMX and C low tunnels are from July 25 to August 3 (DOY 207 – 216), August 3 to 14 (DOY 216 – 227) and August 14 to 26 (DOY 227 – 239) and August 26 to September 30 (DOY 239 – 274), respectively.

3.4.5   Low tunnel cover, air and mulch temperature

Pre-treatment BE2 mulch surface temperatures for TMX (T_{mTMX}), POLY (T_{mPOLY}) and

POLY$_P$ (T_{mPOLYP}) plots agreed well with BE2 mulch surface temperature for the control (T_{mC})

with a half-hourly $\mu \pm$ SD daily T_{mC}, T_{mTMX}, T_{mPOLY} and T_{mPOLYP} of 23.6 ± 14.7, 23.5 ± 14.4, 23.3

± 15.1 and 23.0 ± 15.3 ^{o}C, respectively, and regression slopes very close to unity (Figure 3.18).

From the pre-treatment to the treatment period, the slope of T_{mTMX}, T_{mPOLY} and T_{mPOLYP} vs. T_{mC}

regression changed very little but the y-intercept values increased 4.23, 3.01 and 1.64 ^{o}C, and

mean daily T_{mTMX}, T_{mPOLY} and T_{mPOLYP} were 3.8, 2.3 and 0.8 ^{o}C greater than T_{mC}, respectively

(Figure 3.7 and 3.18). During the nighttime, on a typical cloud-free day the highest to lowest

mulch surface temperatures were T_{mTMX}, T_{mPOLY}, T_{mPOLYP} then T_{mC} (Figure 3.9). Between sunrise

and solar noon T_{mTMX}, T_{mPOLY}, T_{mPOLYP} and T_{mC} were very similar in value, after which the

previously mentioned order of highest to lowest values is re-established in the afternoon and

evening.

Aside from the control air temperature (T_{aouC}), cover surface temperatures (T_w) were

lower than mulch and tunnel air temperatures during the daytime (Figure 3.9). On a typical

cloud-free night T_{wTMX} T_{wPOLY} and T_{wPOLYP} were all less than T_{aouC} by $1 - 2$ ^{o}C. After sunrise

T_{wTMX}, T_{wPOLY} and T_{wPOLYP} quickly increase in value and were greater than T_{aouC} by $8 - 10$ ^{o}C in

the afternoon (15:00 h PST, Figure 3.9). In the afternoon and early evening, both T_{wTMX} and

T_{wPOLY} were greater than T_{wPOLYP}, which is likely due to TMX's and POLY's relatively large

shortwave absorptivity (α_s) of 0.14 and 0.13 and longwave absorptivity (α_L) of 0.63 and 0.49,

respectively, compared to values of 0.02 and 0.17 for POLY$_P$. In general, plastic films with

higher α_s and α_L values had higher T_w during the daytime. On a typical cloudy night T_{wTMX},

T_{WPOLY} and T_{wPOLYP} were less than T_{aouC}, like cloud-free nights, but only by ~0.5 ºC, rather than 1

– 2 ºC. On a typical cloudy day during the daytime, T_w exceeded T_{aouC} depending on S_{dou} (Figure

3.10). Overall, the difference between T_w for any treatment and T_{aouC} was greatest under cloud-

free conditions, day and night, and smallest under cloudy conditions. (Figures 3.9 and 3.10).
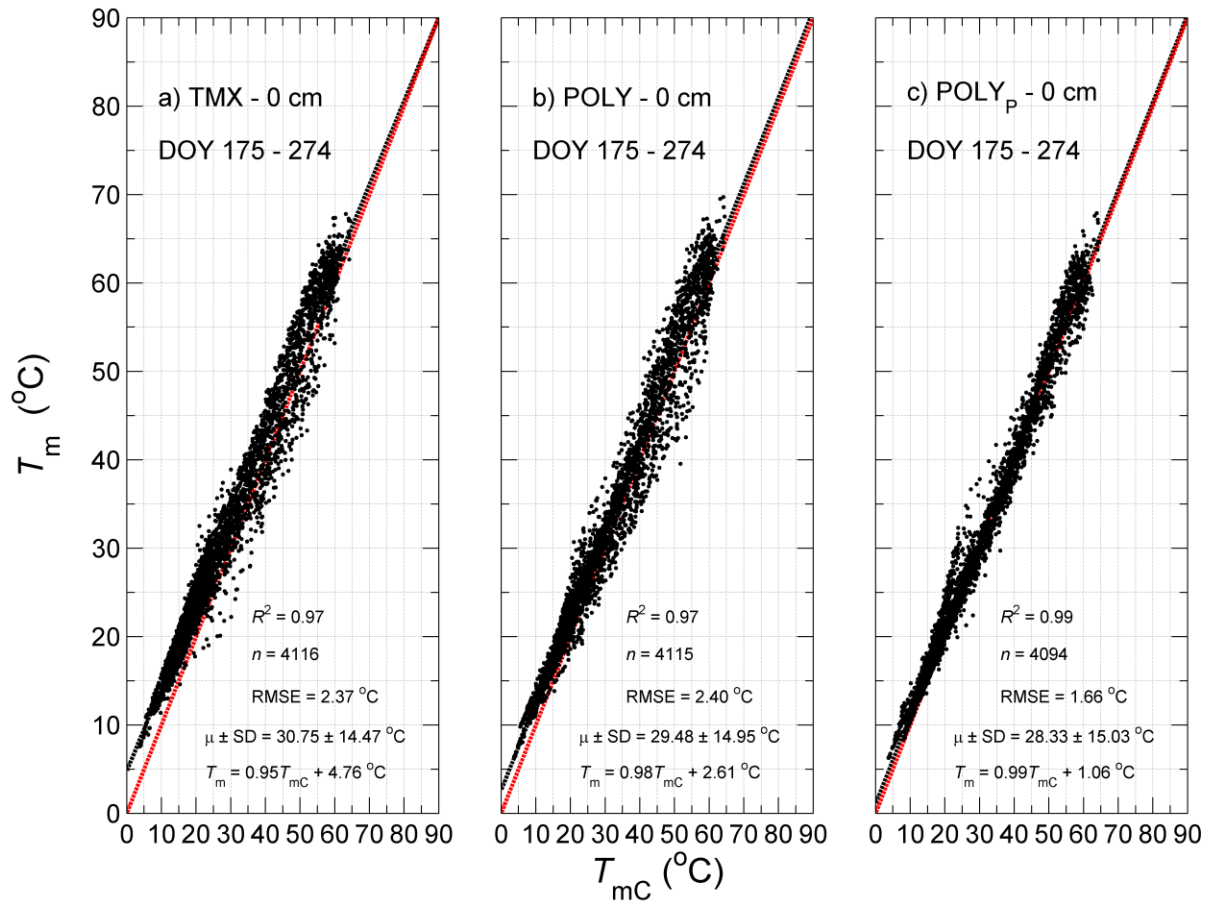
Figure 3.7 Panels a), b) and c) show linear regressions for low tunnel mulch surface temperatures T_{mTMX}, T_{mPOLY} and T_{mPOLYP} vs T_{mC}, respectively, from June 21 (DOY 175) – September 30 (DOY 274). The regression equation ($T_m = aT_{mC} + b$) (black dashed lines), mean (μ) ± standard deviation (SD), root mean square error (RMSE), sample number (n) and coefficient of determination (R^2) are listed for each regression. The red dashed lines are the 1:1 lines. Pre-treatment data is shown in Figure B.10.

Of most interest, in a practical sense, is the difference between the air temperature measured inside the TMX (T_{ainTMX}), POLY ($T_{ainPOLY}$) and POLY$_P$ ($T_{ainPOLYP}$) low tunnels compared to T_{aouC}. During the pre-treatment period, the agreement for the regression of T_{aouC} vs T_{ainTMX}, $T_{ainPOLY}$ and $T_{ainPOLYP}$ was strong, with slopes of 1.00, 1.01 and 0.99 y-intercepts of 0.03,

111

-0.25 and -0.04 $^{\circ}$C and RMSE values of 0.12, 0.18 and 0.15 $^{\circ}$C, respectively (Figure 3.7). Also, the half-hourly daily $\mu \pm$ SD T_{ainTMX}, T_{ainPOLY}, T_{ainPOLYP} and T_{aouC} were very similar during the pre-treatment period, with values of 16.08 ± 5.10, 15.96 ± 5.16, 15.86 ± 5.06 and 16.00 ± 4.90 $^{\circ}$C (Figure 3.7). The fact that the agreement is so strong provides confidence in the air temperature effects caused by the low tunnel covers during the treatment period.

During the nighttime, T_{ainTMX} had the highest values followed by T_{ainPOLY}, T_{ainPOLYP} then T_{aouC}, with mean nighttime values of 16.7 ± 2.6, 15.8 ± 2.5, 15.3 ± 2.3 and 14.7 ± 2.0 $^{\circ}$C, respectively. Interestingly, the difference between air temperature inside and outside the low tunnels was very similar on cloud-free and cloudy nights. During the daytime the difference between air temperature inside and outside the low tunnels was much larger than during the nighttime, with mean daytime values of 29.1 ± 9.1, 28.0 ± 9.0, 25.0 ± 7.2 and 18.7 ± 3.0 $^{\circ}$C, respectively, which illustrates the large temperature fluctuations that occurred inside the low tunnel, when compared to the outside air. Overall, half-hourly daily (i.e., daytime and nighttime) mean T_{ainTMX}, T_{ainPOLY}, T_{ainPOLYP} exceeded mean T_{aouC} by 7.2, 6.3 and 4.2 $^{\circ}$C. The order of largest to smallest inside to outside tunnel air temperature difference is consistent with the facts that 1) POLY$_{\text{P}}$ has perforations (i.e., $h_{\text{ven}} > 0$) and 2) TMX has a larger α_{L} value than POLY.
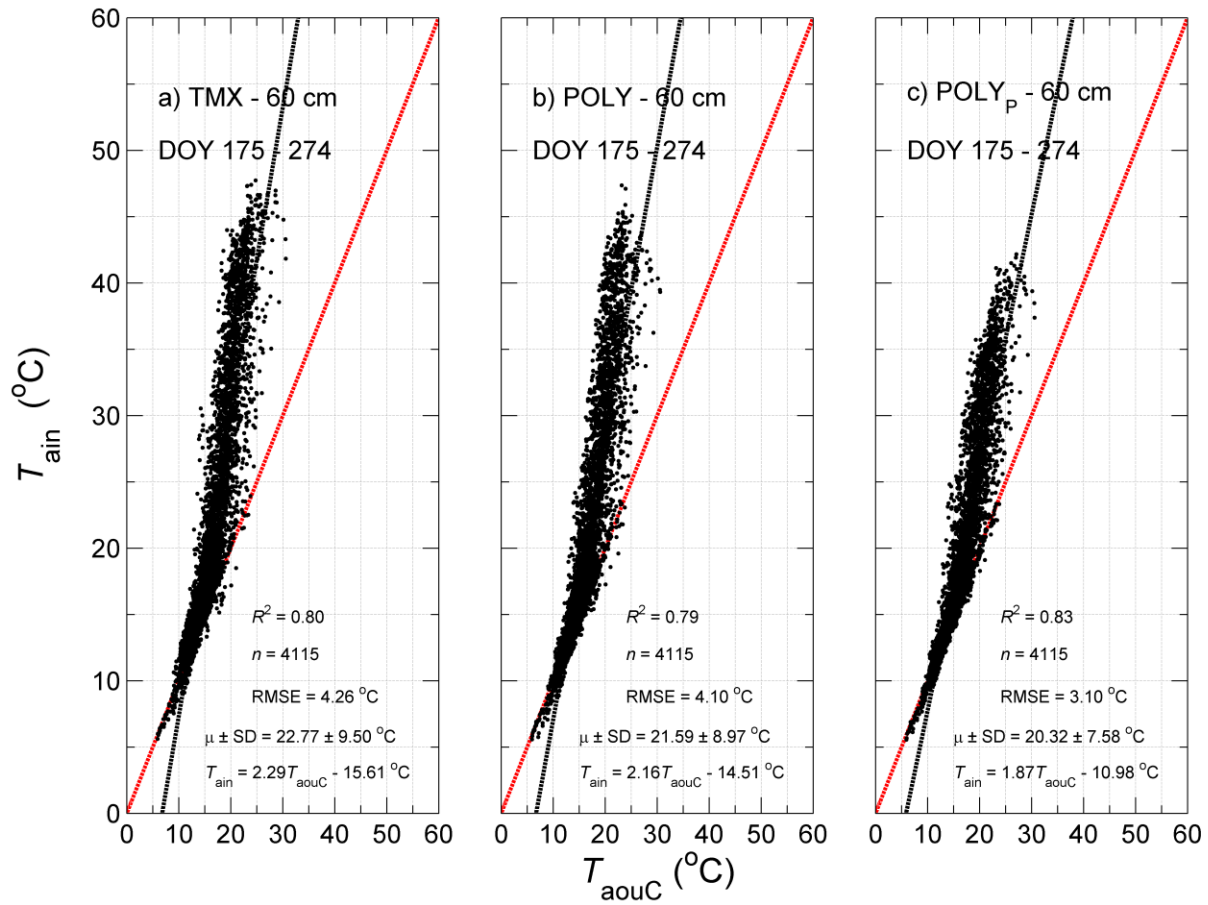
Figure 3.8 Panels a), b) and c) show the regressions for low-tunnel air temperatures T_{ainTMX}, $T_{ainPOLY}$ and $T_{ainPOLYP}$ vs T_{aouC}, respectively, from June 21 (DOY 175) – September 30 (DOY 274). The regression equation ($T_{ain} = aT_{aouC} + b$), $\mu \pm$ SD, root mean square error (RMSE), sample number (n) and coefficient of determination (R^2) are listed for each regression. Pre-treatment data is shown in Figure B.9.

T_{ain} inside all of the low tunnels and above the control reached their minimum value shortly before sunrise. After sunrise, on cloud-free days, the air temperature inside the low tunnels quickly increased in proportion to S_{dou} and reached their maximum values and remained relatively constant 1 – 2 hours after solar noon, despite a 100 to 150 W m^{-2} decrease in S_{dou}

during that time of day. Overall, during the daytime on cloud-free days, the general behavior of T_{ain} was more like S_{dou} than T_{aouC}, even for POLY$_P$, which has perforations. On cloudy days, air temperature inside and outside the low tunnels were more similar, with the low tunnel air temperatures increasing abruptly in response to intermittent increases in S_{dou} (Figure 3.10). During the nighttime, air temperature inside the low tunnels more closely followed changes in L_{dou}, typically associated with changes in cloud cover (Figures 3.9 and 3.10).
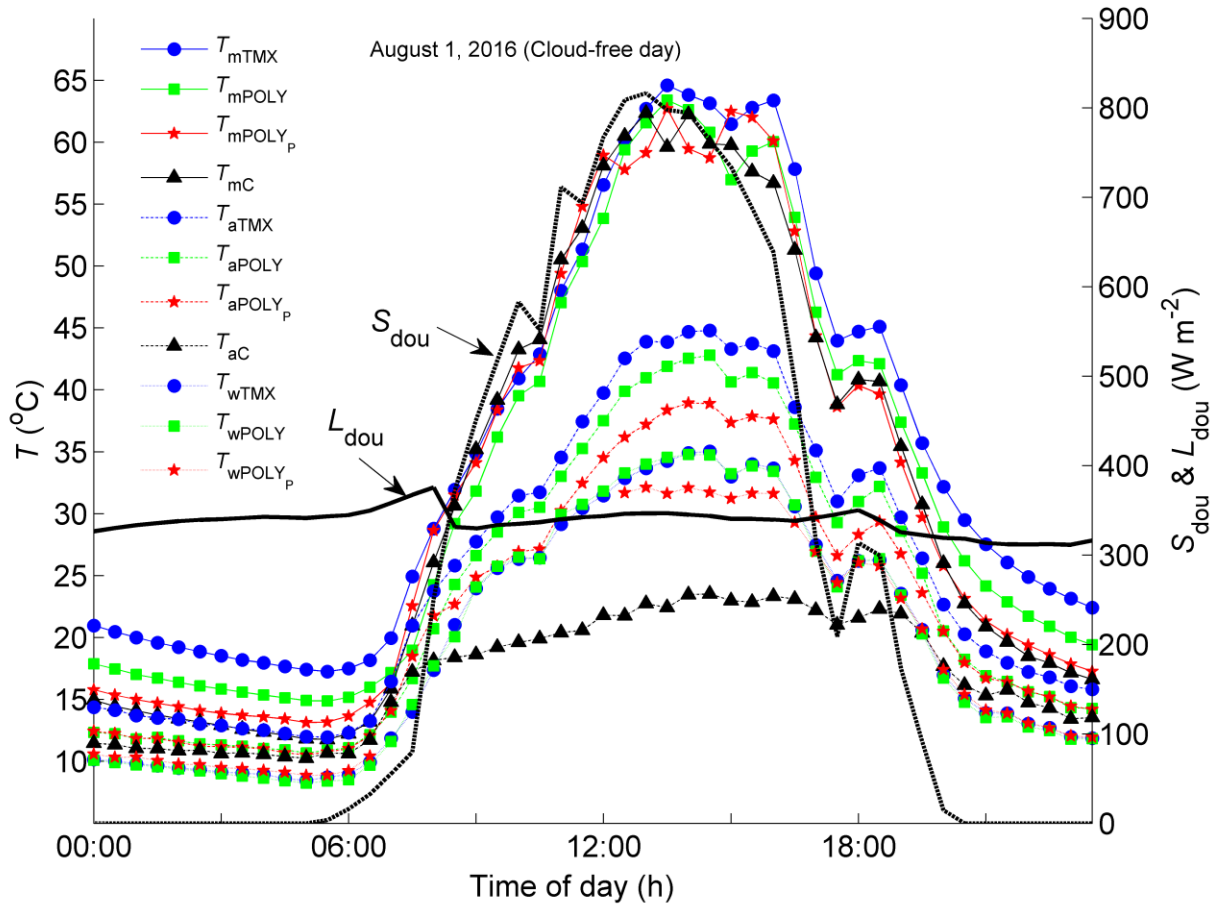
Figure 3.9 Half-hourly mulch surface temperature (T_m) and inside air temperature (T_{ain}) for TMX, POLY, POLY$_P$ and outside the low tunnels above the control (C, T_{aouC}) on a cloud-free day. Cover surface temperatures (T_w) for TMX, POLY and POLY$_P$ are also shown. T_{aouC} was measured using a fine-wire thermocouple positioned 60 cm above the control treatment (C, BE2 black mulch without a low tunnel).
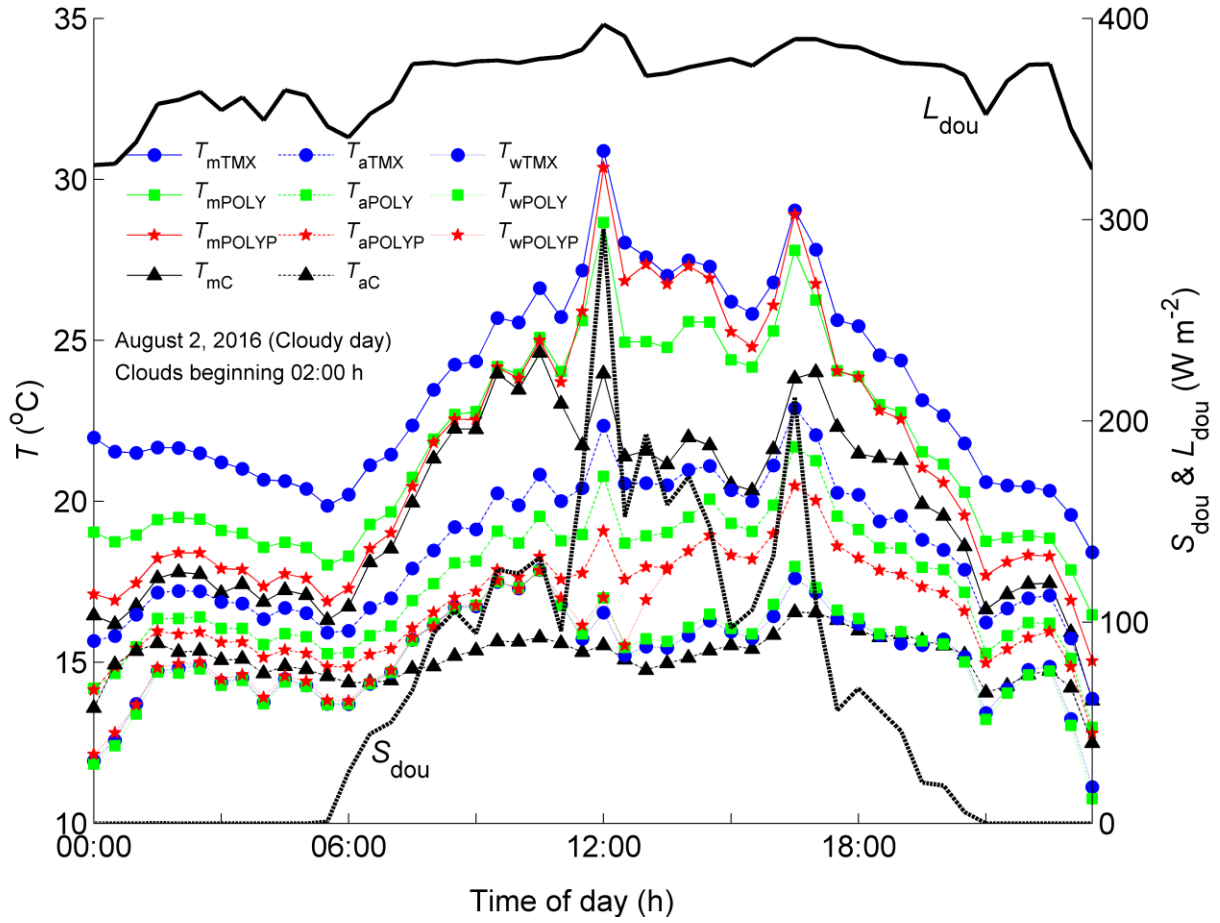
Figure 3.10 Half-hourly mulch surface temperature (T_m) and inside air temperature (T_{ain}) for TMX, POLY, POLY$_P$ and outside the low tunnels above the control (C, T_{aouC}) on a cloudy day. Cover surface temperatures (T_w) for TMX, POLY and POLY$_p$ are also shown. T_{aouC} was measured using a fine-wire thermocouple positioned 60 cm above the control treatment (C, BE2 black mulch without a low tunnel). Measurements of T_{wPOLYP} are missing after 13:00 due to sensor malfunction.

3.4.6   Heat transfer coefficients and air temperature model

3.4.6.1   Heat transfer coefficients

The mulch-to-air heat transfer coefficients (h_m), calculated using Eq. (3), were quite similar for TMX, POLY and POLY$_P$ in this study which indicates that the turbulent transfer within each tunnel was quite similar. The $\mu \pm$ SD half-hourly midday h_{mTMX}, h_{mPOLY}, h_{mPOLYP} and h_{mC} were 22.0 ± 7.3, 17.2 ± 6.8, 16.2 ± 4.1 and 13.9 ± 6.7 W m^{-2} K^{-1} (Figure 3.11). Overall, h_m peaked in mid-morning with values of about 30 W m^{-2} K^{-1} and steadily decreased until becoming negative $1 - 2$ hours after sunset, typically when R_a became most negative. In the morning turbulent mixing inside the tunnels was less than in the afternoon (Figure 3.12). Nevertheless, in the morning, T_{ain} at 0.5 m increased in response to increased T_m and R_{ain} and the difference between the mulch surface temperature and inside air temperature (T_m - T_{ain}) remained small, which indicates that the turbulent mixing within the low tunnels was efficient. As a result, h_m peaked in the morning when H_m was quite large (~ 50% of its maximum value) and T_m - T_{ain} was small due to mixing (Figure 3.12). The gradual decrease in h_m after its peak in the morning is due to the fact that there was increased buoyancy and turbulent mixing inside the tunnels during the afternoon that caused T_m - T_{ain} to decrease. Throughout the afternoon and early evening, T_m - T_{ain} typically declined at a slower rate than H_m, which caused h_m to become even smaller (Figure 3.12).

Interestingly, during a cloud-free day (Sept 28, 2016, Figure 3.12) it is clear than at midday when T_m - T_{ain} is large (20 - 30 ºC) the wind speed at 0.6 m inside the TMX low tunnel (u_{inTMX}) begins to increase in value from 0.01 to 0.35 m s^{-1} which results in increased h_m and a decrease in T_m - T_{ain} near 14:00 h (Figure 3.12). The large decrease in T_m-T_{ain} near 14:00 h PST

inside the TMX tunnel resulted in a decrease in u_{inTMX} after which $T_m - T_{ain}$ increased due to

decreased u_{inTMX} between 14:00 and 15:00 h PST inside the TMX tunnel (Figure 3.12). The

increased turbulence inside the low tunnel is therefore crucial to sensible heat transfer and is

driven by air buoyancy caused by larger temperature differences near the low tunnel plastic film

mulch (Figure 3.12). The fact that u_{inTMX} never reaches values equal to wind speed outside the

low tunnels (i.e., u_{2m}) explains the large reduction in turbulent mixing near the plastic film mulch

surface, caused by the presence of the low tunnel cover.

The heat transfer coefficients for the internal air to the low tunnel wall (h_{win}), calculated

using Eq. (4) were similar in value to h_m which is consistent with our assumption that the

turbulent mixing inside the low tunnels is efficient (Figure 3.11). Nevertheless, h_{win} and h_m did

differ slightly in their diurnal behavior and magnitude. The differences were characterized by

h_{win} peaking 1-2 hours later than h_m with values of 25 W m^{-2} K^{-1} (15 – 30 W m^{-2} K^{-1}) (Figure

3.11), which is slightly lower than peak values for h_m. Since H_m and H_{win} have the same diurnal

behaviour (Figure 3.11) the difference in the behaviour of h_m and h_{win} is due to the fact that the

difference between the low tunnel inside air temperature and cover temperature ($T_{ain} - T_w$) peaked

later in the day than $T_m - T_{ain}$ (Figure 3.12). On Sept 28, 2016 the decrease in $T_m - T_{ain}$ near 14:00

h PST caused $T_{ain} - T_w$ to increase a small amount (0.25 $^{\circ}$C) due to increased T_{ain} (Figure 3.12c).

The low tunnel cover-to-outside air heat transfer coefficient (h_{wou}), calculated using Eq.

(4), had a positive linear relationship with 2-m wind speed outside the low tunnels (u_{ou}) with

slope coefficients of 8.48, 7.29 and 5.35 W m^{-3} K^{-1} s and y-intercepts equal to 20, 15 and 16 W

m^{-2} K^{-1} for TMX, POLY and POLY$_P$, respectively. During the daytime, particularly at midday,

h_{wou} typically ranged in value from 20 – 30 W m^{-2} K^{-1} for all low tunnels with mean midday

values of 32.1, 24.7 and 30.9 W m^{-2} K^{-1} (Figure 3.11). Overall, h_{wou} only maintained stable

values between solar noon and sunset when the difference between the low tunnel cover

temperature and outside air temperature was positive (T_w - T_{aou}) (Figure 3.12). During the

evening and nighttime when cover net radiation was negative and the cover gained sensible heat

from the outside air T_w -T_{aou} was negative (Figures 3.4 and 3.12). The dependence of h_{wou} on u_{2m}

is illustrated on Sept 28, 2016, where h_{wou} decreases near 12:00 h PST in response to a decrease

in u_{2m} from 9:00 to 9:30 h PST after which h_{wou} increased in response to increased u_{2m} near 13:00

to 14:00 h PST (Figure 3.12). The steady decline in h_{wou} between 14:00 to 16:00 h PST is

associated with a steady decline in u_{2m} until $1 - 2$ h before sunset (Figures 3.12 and 3.13). We

used the regression equations shown in Figure 3.13 to calculate h_{wou} because of its strong

dependence on wind speed.
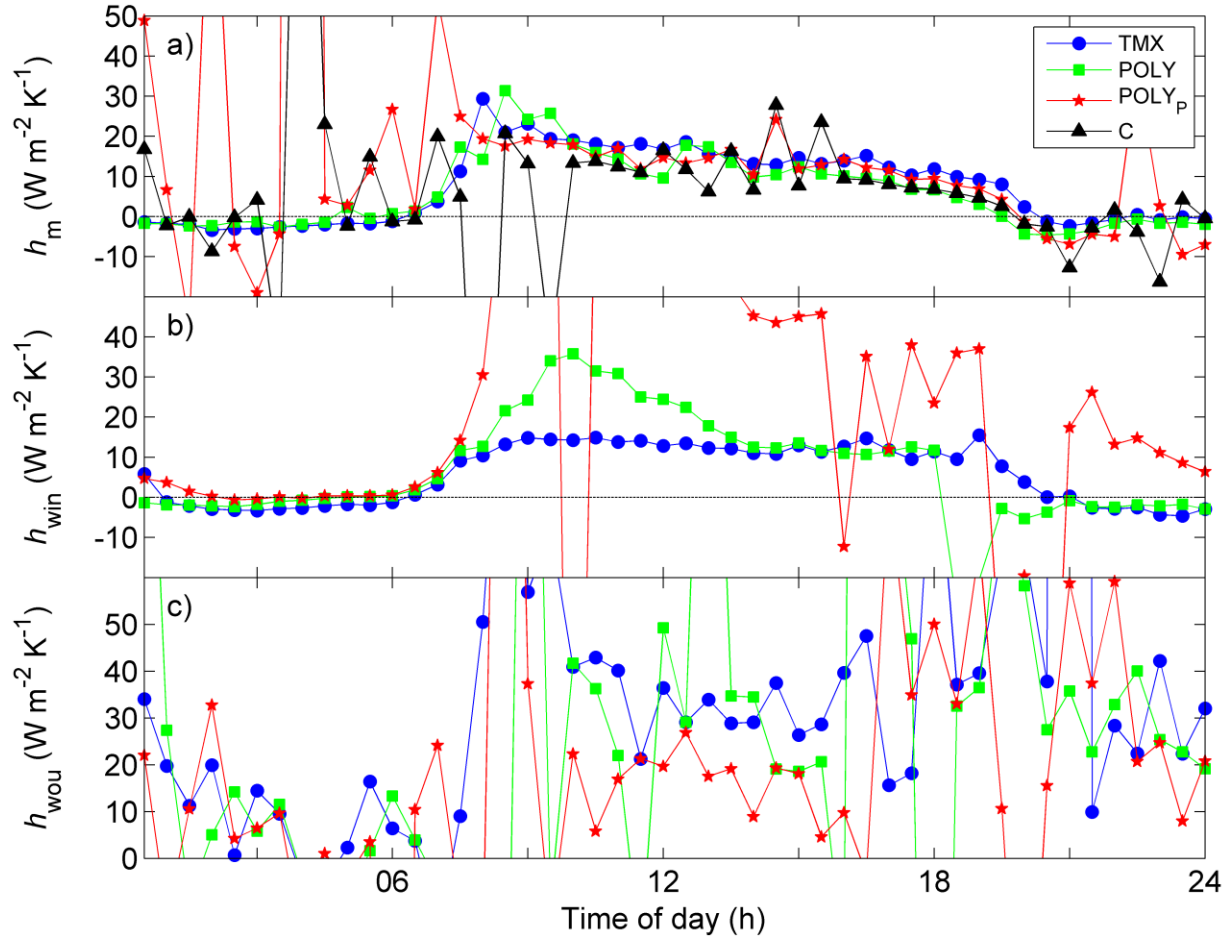
Figure 3.11 Panel a) shows the ensemble mean (only data from June 22 – Sept 1, 2016) heat transfer coefficients for plastic film mulch to air (h_m) inside the low tunnels and for the control. Panels b) and c) show ensemble mean heat transfer coefficients for air inside the low tunnels to the low tunnel covers (h_{win}) and the low tunnel covers to the outside air (h_{wou}), respectively. TMX, POLY, POLY$_P$ and C are represented by blue filled-circles, green filled-squares, red filled-stars and black triangles, respectively. Values of h_{win} for POLY$_P$ between 8:00 and 14:00 PST were greater than 50 W m^{-2} s^{-1} and are considered unreliable (see text).

120
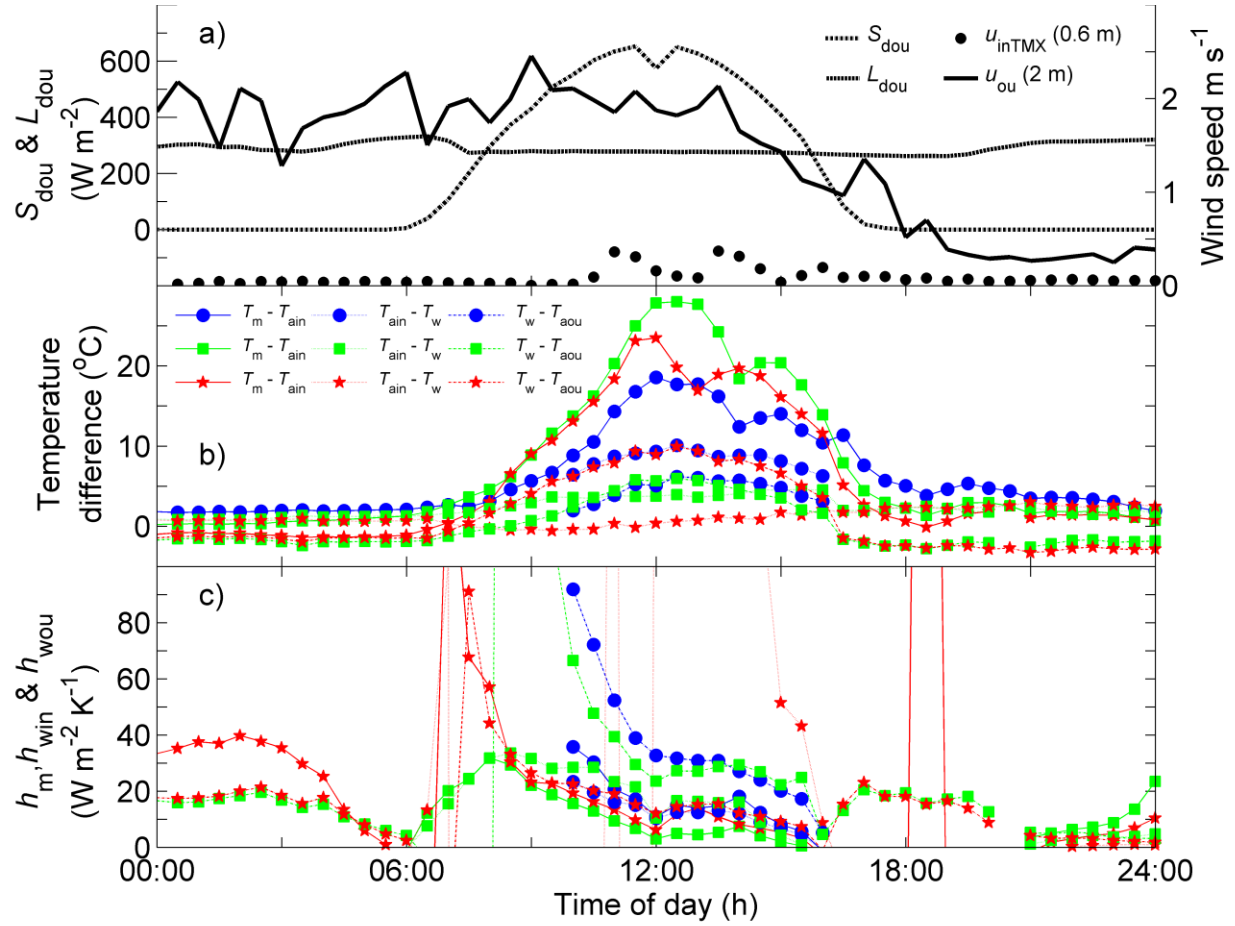
Figure 3.12 Panel a) shows the net radiation outside (R_{nou}, filled-symbols) and inside (R_{nin}, open-symbols), horizontal wind speed 0.6 m above the TMX low tunnel floor (u_{inTMX}) and 2 m above the study site (u_{2m}) on September 28, 2016. Panel b) shows the temperature difference between mulch surface temperature and inside air temperature (T_m - T_{ain}), inside air temperature and cover temperature (T_{ain} - T_w) and cover temperature and outside air temperature (T_w - T_{aou}). TMX, POLY and POLY$_P$ are represented by circles, squares and stars. Panel c) shows heat transfer coefficients for the plastic film mulch and inside air (h_m), inside air and tunnel cover (h_{win}) and tunnel cover and the outside air (h_{wou}). h_m, h_{win} and h_{wou} are represented by solid, dotted and dashed lines, respectively, and TMX, POLY and POLY$_P$ are represented by circles, squares and

stars, respectively. Data for TMX is missing from in the morning (00:00 - 10:00 h PST) and evening (15:00 - 24:00 h PST) due to sensor malfunction.
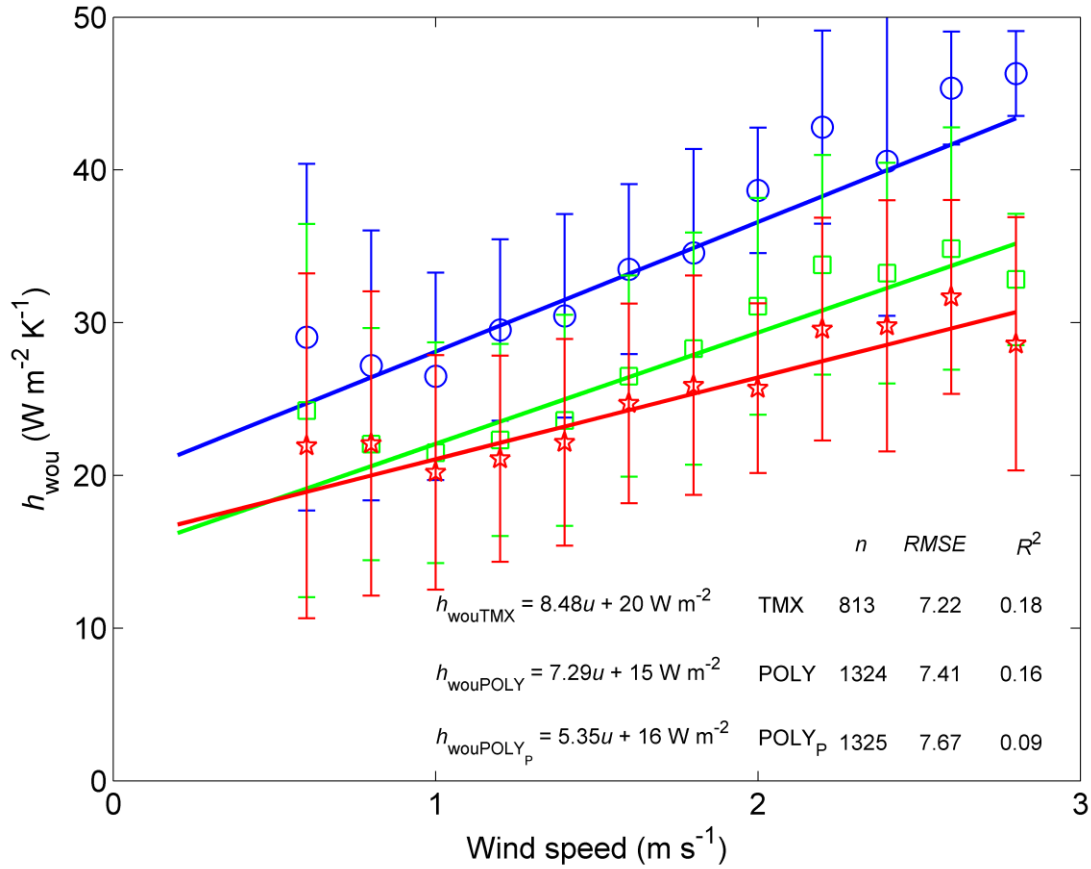
Figure 3.13 Linear regressions for heat transfer coefficient for the low tunnel cover's to the outside air (h_{wou}) vs horizontal wind speed (u_{2m}) (0.2 m s^{-1} bins) for TMX (blue filled-circles), POLY (green filled-squares) and POLY$_P$ (red filled-stars) low tunnels. The bars represent the standard deviation for each bin interval. All available data from the treatment period is shown (June 21 – Sept 30, 2016).

3.4.6.2 Air temperature model

T_{ain} was modelled using Eq (7) with measured R_{nin}, R_{nou} and G_{in}. h_{win} was assumed to be equal to h_m and was set at a constant value of 15 W m^{-2}. H_{wou} was modelled using the empirical equations developed between measured h_{wou} and wind velocity (u_{ou}). There was good agreement between T_{ain} vs. modelled air temperature (T_{ainmod}) inside the TMX, POLY and POLY$_P$ low tunnels (Figure 3.14), with slopes, y-intercepts, R^2 and RMSE values of 0.87, 1.03 and 1.04, 4.25 0.82 and -0.24 ºC, and 0.89, 0.87 and 0.91, and 3.03, 3.36 and 2.16 ºC, respectively. Figure 3.14 illustrates the diurnal agreement between T_{ain} and T_{ainmod}, and shows that the agreement is strongest during the daytime and less so during nighttime and in the early morning. Since POLY$_P$ has perforations it was necessary to account for the ventilation heat transfer coefficient (h_v) and sensible heat flux (H_v), and a fixed h_v of 4 W m^{-2} K^{-1} was found to greatly improve the agreement between $T_{ainPOLYP}$ and $T_{ainPOLYPmod}$ (Figure 3.14). The values of 4 W m^{-2} K^{-1} is reasonable given a typical free-convection heater has a value ranging from 5 – 12 W m^{-2} K^{-1} (Roetzel and Spang 2010). To simplify the air temperature model, a fixed h_m value of 15 W m^{-2}

K^{-1} was used, which provided satisfactory results (Figure 3.14).
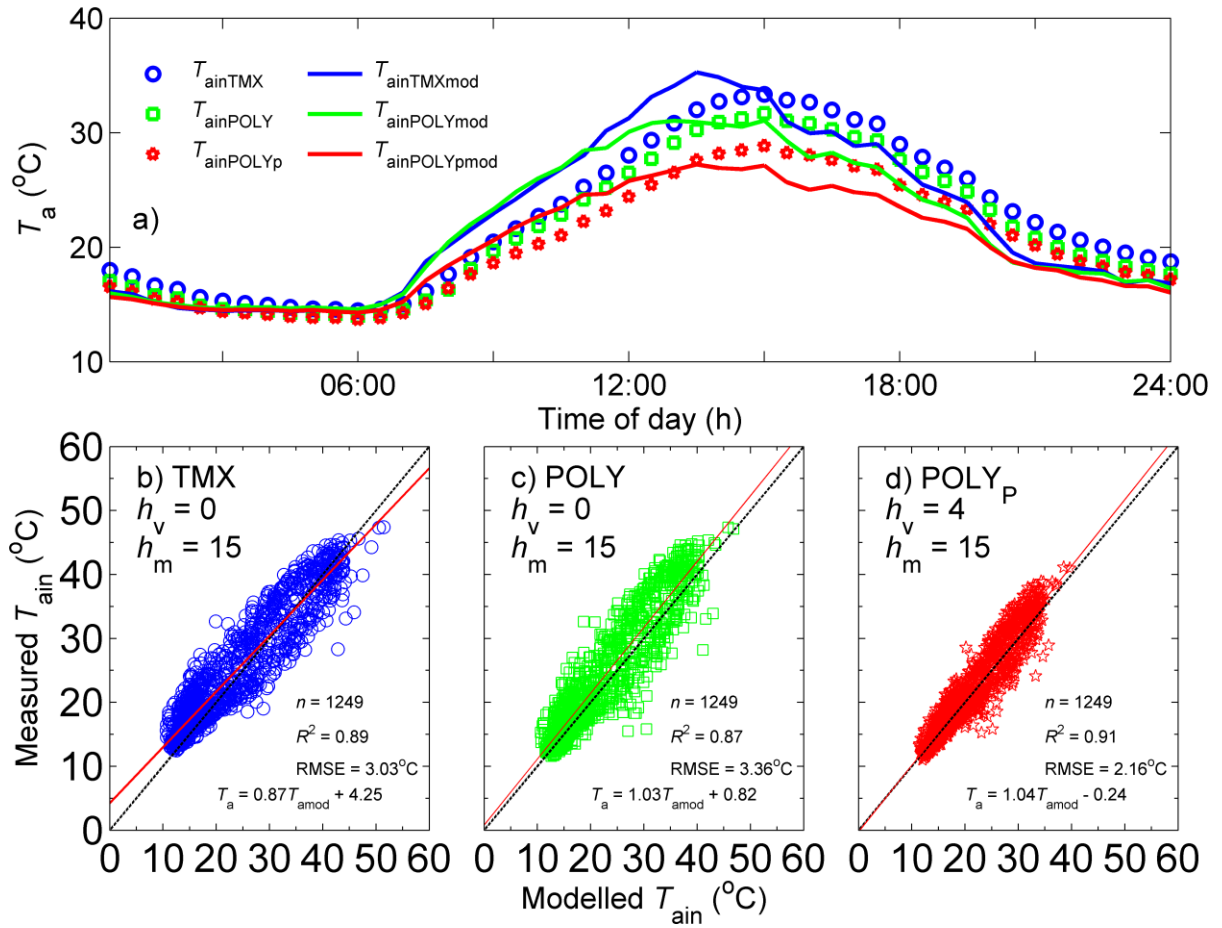
Figure 3.14 Panel a) shows ensemble mean diurnal measured and modelled air temperature inside the TMX, POLY and POLY$_P$ low tunnels (T_{ain}). Panels b), c) and d) show the regression of measured vs. modelled air temperature (T_{ainmod}) inside each low tunnel, using Eq. (8). Also shown are the values of the heat transfer coefficients (h_v and h_m) used in the model. All available data from the treatment period is shown (June 22 – Sept 30, 2016).

3.5 Discussion

3.5.1 Mulch and cover radiative spectral properties

The shortwave radiation transmissivity (τ_s) of a plastic film used to cover a low tunnel is of critical importance to the radiative balance inside the tunnel because downwelling shortwave radiation inside the low tunnel (S_{din}) is the largest terms in the radiation balance during the daytime. During periods when maximum heating and cooling are required, high and low τ_s values are desirable, respectively (Baille et al. 2001). In our study, we used plastic films with τ_s values ranging from 0.77 to 0.86, which is within the range of other enclosure covers studied in the past (0.6 to 0.9) such as glass, polyvinylchloride, high density polyethylene, polycarbonate and ethylenvinylacetate (Baille et al. 2001; Scarascia-Mugnozza et al., 2011). We found that POLY$_P$, which had the highest measured τ_s value in the laboratory (0.86, see Table 3.3), also had the highest daily net shortwave radiation inside the low tunnel (S_{nin}) in the field setting. Even though on a half-hourly basis cover τ_s values in this study fluctuated throughout the daytime, the strong agreement between the daily τ_s values measured in the field and laboratory illustrates the applicability of laboratory spectral measurements in a obtaining a field radiation balance.

In temperate climates, like in our study, and during the shoulder seasons of tropical and arid climates, producers aim to maximize air temperature and as a result seek covers with the highest τ_s values. Although manufacturers typically supply τ_s values for their cover materials, phenomena such as dirt accumulation (i.e., soiling) (Kurata 1990; Geoola et al., 1998), condensation (Geoola et al., 1994; Pieters et al., 1997), cover age (Ngouajio and Ernest 2005), angle of incidence (Jaffrin and Makhlouf 1990) and structure orientation can alter τ_s over time

125

scales of hours, weeks, months and years. In this study, no significant dirt accumulation was observed on the low tunnel covers and condensation was not present inside the tunnels. The impact of dirt accumulation and cover age on τ_s values would likely increase with time and should be accounted for over long time periods. Overall, angle of incidence of downwelling shortwave radiation above the tunnel (S_{dou}) had the largest impact on τ_s values in this study, which caused diurnal variability in the value of τ_s. Interestingly, half-hourly τ_s values fluctuated less on cloudy days, when the fraction of diffuse to direct solar radiation was high, than on cloud-free days for all plastic film covers and had values equal to or greater than the laboratory measured τ_s values. This indicates that, for the plastic films we studied, the transmissivity to diffuse solar radiation was greater than the transmissivity to direct solar radiation. Unfortunately, shortwave transmissivity to diffuse radiation was not measured in this study, but has been studied by many workers (Al-Mahdouri et al. 2013; Baille et al. 2001; Businger 1963; Geoola et al. 1998; Cabrera et al. 2009; Pollet and Pieters 2001) and its impact on crop photosynthesis and heat-stress is well known (Hilker et al. 2008; Li et al. 2014) and should be taken into consideration in crop productivity studies performed inside enclosures.

The longwave radiation transmissivity (τ_L) of plastic film used to cover a low tunnel is important in the radiation balance of the enclosure during both daytime and nighttime (Zhang et al. 1996; Al-Mahdouri et al. 2013; Al-Mahdouri et al. 2014). In this study, downwelling longwave radiation in both TMX (L_{dinTMX}) and POLY ($L_{dinPOLY}$) low tunnels exceeded downwelling longwave outside (L_{dou}) due to their ability to absorb and emit longwave radiation toward the low tunnel floor. In contrast, downwelling longwave in the POLY$_P$ low tunnel ($L_{dinPOLYP}$) was less than that outside due to low cover surface temperature and emissivity of

POLY$_P$ throughout the study. These findings are similar to Al-Mahdouri et al., 2013 who found that a greenhouse covered with silica glass, which has high longwave absorptivity (i.e., emissivity), increased net radiation above that of a greenhouse covered with low density polyethylene (LDPE), which had a low longwave absorptivity. Similarly, Zhang et al., 1996 found that the energy consumption required to maintain constant air temperature inside a greenhouse (T_{ain}) covered with single layer LDPE was 36% higher than that of a greenhouse covered with silica glass (4 mm), whereas LDPE containing thermal additives only required 7% more energy than silica glass to maintain constant T_{ain}. Therefore, for enclosures covered with a single film layer, the ability to increase L_{din} and thereby R_n is fundamental to increasing T_{ain} and the effectiveness of any heating technologies adopted to alter enclosure microclimate.

3.5.2 Radiation balance

During midday hours, S_{din} was the largest input to the radiation balance in the low tunnels and was strongly controlled by the cover spectral properties described above. Interestingly, on a half-hourly basis, the values of S_{din} measured inside the tunnel using the CNR1 pyranometer were greater than the values calculated by multiplying the downwelling shortwave radiation outside the low tunnels (S_{dou}) and the τ_s values measured in the laboratory, by as much as 15 % which is significant in the radiation balance in the low tunnels. The role of multiple reflections is of great importance in the shortwave and longwave regions of the spectrum (Graefe and Sandmann 2015) and can result from reflections from the plant canopy, enclosure walls, enclosure floor or structural features that support the enclosure cover (Kurata 1990). In this study we quantified multiple reflections of shortwave radiation using empirical relationships derived from net radiometer measurements within the low tunnels (see section 2.4.2 and 2.4.3). Since the

longwave radiation reflectivity, ρ_L, values of the plastic films used in this study were all (including the plastic film mulch) less than 0.01 the significance of multiple longwave reflections was small. Nevertheless, in future work multiple reflections should be accounted for to accurately calculate the radiation balance and predict the air temperature inside enclosures.

Perhaps more important to the radiation balance is the shortwave reflectivity (ρ_s) of the low tunnel floor given that it determines the magnitude of S_{nin} and the available radiation to heat the low tunnel air. In this study we used a black plastic film mulch (BE2) with a laboratory measured ρ_s value of 0.05, which is similar to the black plastic film mulch used by Bonachela et al., 2012 in their study of unheated greenhouses with plastic film mulch floors. In this study, field measured ρ_s values were greater than the lab values by as much as 0.03, which is similar to Bonachela et al., 2012 who measured a ρ_s value of 0.08 ± 0.01 in the field for a plastic film with a manufacturer-provided ρ_s value of 0.04. One plausible explanation for the measurement of higher ρ_s values in the field vs in the laboratory is the accumulation of dust (i.e., soiling), which was visible on the mulch floor in this study. Although all plastic films are susceptible to soiling, the relative impact of soiling is higher for plastic films with low ρ_s values because only a small amount of soiling is required to increase ρ_s significantly. The fact that most natural surfaces have ρ_s values near 0.25 (Monteith and Unsworth, 2008) indicates that the accumulation of dust will cause most surfaces to attain a ρ_s value close to 0.25, or the ρ_s value of the local soil. The rate at which this change occurs depends on soil, climatic and other factors.

During midday the surface temperatures of the low tunnel mulches (T_m) were very similar - only ~2 °C greater than C (the control) and as a result the upwelling longwave radiation was

very similar (within 10 W m^{-2}) for all treatments. On the other hand, the net longwave radiation

for the low tunnels differed greatly depending on the longwave absorptivity of their cover. On

clear days, surface temperatures of the low tunnel cover's (T_w) were quite similar for all the

covers, with TMX and POLY reaching T_w values ~12 ^{o}C and 10 ^{o}C greater than outside air

temperature (T_{aouC}), respectively. As a result, the emissivity of each plastic film determined the

magnitude of the downwelling longwave flux towards the tunnel floor and was mainly

responsible for the differences in net longwave radiation measured at the tunnel floor. Hanson

(1963) used a protection index (PI, PI = 100[1 - (R_n with cover / R_n no cover)]) to quantify the

change in nocturnal net radiation caused by the presence of various covers, with glass and

polyethylene having values of 93% and 26%, respectively. In this study, I found PI values of

79%, 69% and 33% on a daily basis for TMX, POLY and POLY$_P$, respectively, which are

comparable to values found by Hansen (1965). Unlike in the daytime, mulch surface

temperatures (T_m) of the tunnel floors during nighttime were not similar to one another. On

cloud-free nights, T_{mPOLYP}, T_{mPOLY} and T_{mTMX} exceeded T_{mC} by as much as 1, 3 and 6 ^{o}C,

respectively. As a result, the upwelling longwave radiation from the plastic film mulch inside the

POLY and TMX tunnels was ~15 and 30 W m^{-2} greater, respectively, than plastic film mulch

outside for the control.

The longwave absorptivity of the covers in this study, and their impact on L_{din}, directly

affected the difference between net radiation outside (R_{nou}) and inside (R_{nin}) the low tunnels (R_{nou}

- R_{nin}), as well as the air temperature rise inside each tunnel. For the POLY$_P$ tunnel, with low

longwave absorptivity, R_{nou} exceeded R_{nin} because the reduction of S_{din} compared to S_{dou}, by

cover shortwave absorption (2%) and reflection (12%), exceeded any increase in L_{din} caused by

129

POLY$_P$, which caused R_{nou} - R_{nin} to be positive. This was also the case for POLY, but the difference was smaller. In an extreme case, to quantify the "wind effect" of enclosure glass house, Businger (1965) calculated the air temperature rise inside an "imaginary" glass house that had τ_s and τ_L values of 1, R_{nou} - R_{nin} = 0. In reality R_{nou} - R_{nin} will only be less than or equal to zero (TMX in Figure 3.2) for low tunnels with high τ_s and τ_L values because no commercially available plastic cover exists that has τ_s and τ_L values equal to 1 (i.e. is similar to thin clean glass).

Unlike POLY$_P$, TMX and POLY have α_L values equal to or greater than 0.5, which allowed them to compensate for the reduction of S_{din} compared to S_{dou}, with increased L_{din} despite the fact that they had lower τ_s values (0.82 and 0.77, respectively) than POLY$_P$ (0.86), respectively. This resulted in TMX and POLY having values of R_{nou} - R_{nin} during the daytime less than or equal to zero for the majority of the study period. This was particularly interesting, and of practical importance, during the nighttime when only TMX caused R_{nou} - R_{nin} to be less than zero (~-10 W m^{-2}) (Figure 3.4). Since T_{ain} - T_{aou} is linearly related to $h_{wou}R_{nin}+h_{win}R_{nou}$ in Eq. (8), increasing R_{nou} by choosing covers with low ρ_s and high α_L values will decrease shortwave loss to the atmosphere above and increase the downward longwave emission from the tunnel cover toward the tunnel floor, respectively, which will increase heating potential. Similarly, increasing R_{nin}, by increasing cover τ_s and L_{din} by increasing the proportional of downwelling longwave from the tunnel cover (i.e., high α_L) rather than the "cold sky" will also increase low tunnel heating potential.

3.5.3 Energy balance

G was very similar for all the low tunnel treatments and control (i.e., no low tunnel) during the pre-treatment and treatment periods. The latter was unexpected given that the reduction in thermal admittance to the atmosphere caused by the presence of the low tunnels was expected to increase thermal admittance to the soil (Tanner 1974), and thereby G inside the low tunnels. A plausible explanation for this is that the resistance to sensible heat flux from the soil surface to the atmosphere in presence of the plastic film mulch is so large that the addition of another layer, i.e., the low tunnel, only caused a marginal increase in resistance to sensible heat flux.

Since the latent heat flux was equal to zero and G was similar for the low tunnel treatments and the control, the magnitude of the sensible heat flux density from the low tunnel floor (H_m) was controlled entirely by R_{nin}. The fact that we used a plastic mulch film with high shortwave absorptivity in this study means near maximum H_m and T_{ain} was achieved which is consistent with the findings of other workers (Bonachela et al. 2012; Boulard and Baille 1987). For example, Bonachela et al., 2012 found that H_m was greater inside an unheated greenhouse floored with black plastic film mulch than a greenhouse floored with transparent much. Although it is well known that the degree of contact between plastic film mulches and the soil (i.e., the contact resistance) will alter the magnitude of G (Ham and Kluitenberg, 1994), and thereby the heat sharing ratio (G/H), black plastic films typically achieve higher T_m values and H_m as a result of their high shortwave absorptivity values. Overall, being selective with regards to the low tunnel cover τ_s and τ_L as well as the plastic film mulch ρ_s will give a crop producer the greatest ability to alter R_{nin} and T_{ain}.

3.5.4 Heat transfer coefficients

In this study the heat transfer coefficient for the plastic film mulch-to-air inside the low tunnel (h_m) peaked in the morning at ~30 W m^{-2} K^{-1} and steadily declined to ~10 W m^{-2} K^{-1} in the late afternoon. Large h_m values occurred in the morning when the sensible heat flux from the mulch was relatively high (~50 - 60 % of the daily maximum) and the temperature difference between the plastic film mulch surface and the inside air (T_m - T_{ain}) was still quite small. The fact that T_m - T_{ain} remained small throughout the morning indicates that there was efficient mixing inside the low tunnels. Despite the fact that the wind speed inside the low tunnels was relatively low the consistently high wind speeds measured outside the tunnels in the morning may have caused the plastic film covers to move and "pump" air throughout the low tunnels. The morning values we found were higher than the values found by other workers, but the afternoon and evening values were comparable (Seginer et al. 1988) and the nighttime relationship we found for h_m vs T_m - T_{in} (data not shown, h_m decreased as T_m-T_{in} increased), was similar to Silva et al., 1988 but greater than Lamrani et al., 2001. Overall, for the air temperature model (discussed in Section 4.5) we found that a mean daily value of 15 W m^{-2} K^{-1} was satisfactory.

Because h_{wou} is difficult to measure directly and is dynamic as a result of changing outdoor wind speed we developed an empirical equation to calculate h_{wou} using wind speed measured at the 2-m height outside the low tunnel (u_{2m}), which agreed well with an existing equation developed using measurements inside a wind tunnel (Iqbal and Khatry 1977). Like Iqbal and Khatry (1977), the equation we developed for calculating h_{wou} produced values which were 2 – 3 times larger than many equations developed in the past (Businger 1963; McAdams 1954; Garzoli and Blackwell 1981; Papadakis 1992). As pointed out by Iqbal and Khatry (1977),

the source of the discrepancy between their equation and previous equations for calculating h_{wou} comes from the fact that previous workers treated the enclosure as a flat surface and did not account for the fact that greenhouses are bluff bodies. Iqbal and Khatry (1977) obtained their equation under wind speeds (4 - 20 m s^{-1}) that were greater than those in our study (0 - 4 m s^{-1}), nevertheless the extrapolation of the equation developed by Iqbal and Khatry (1977) for values between 0 and 4 m s^{-1} agreed very well with the equation developed in this study. Overall, the temperature difference between the tunnel cover and the outside air (T_{w}-T_{aou}) decreased in response to abrupt increases in $u_{2\text{m}}$. One of the potential drawbacks of our equation is that it is linear and only calculates h_{wou} under low wind speed conditions ($u <= 4$ m s^{-1}), unlike Iqbal and Khatry (1977) which calculated h_{wou} under higher wind speeds.

3.5.5   Air temperature model

We developed a model to predict the air temperature inside a vegetation-free low tunnel (T_{ain}) that has an unperforated plastic film mulch floor (i.e., $LE = 0$) and overall the agreement between T_{ain} and T_{ainmod} was strong during both cloudy and cloud-free days. The simplified model requires meteorological drivers which are net radiation inside the low tunnel (R_{nin}), outside the low tunnel (R_{nou}), soil heat flux density inside the low tunnel (G) and wind speed outside ($u_{2\text{m}}$). In addition, model parameters are required and comprise longwave and shortwave spectral properties (reflectivity (ρ), transmissivity (τ), and absorptivity (α)), the heat transfer coefficient for the mulch floor to inside air (h_{m}) and the heat transfer coefficient for the low tunnel cover wall to outside air (h_{wou}). In order to improve the practicality of the model used in our study, so it may be applied to vegetated low tunnels, incorporation of latent heat flux density using existing models (Jones et al., 2017) and wind speed dependent ventilation heat transfer

133

coefficients (Fatnassi et al. 2004) will be crucial to accurately estimate T_{ain}. Nevertheless, the microclimatic conditions within greenhouse-like enclosures can be predicted with relatively few climate variables, which may be of utility to small-scale producers whereas previously it was typically only used by medium- to large-scale commercial crop producers. Empirical relationships that permit the estimation of R_{nin} and R_{nou} from S_{dou} and L_{dou} and G from R_{nin} would remove barriers to using the model and improve the practicality of the model.

3.6   Conclusions

1. Low tunnel plastic film covers with high longwave absorptivity (i.e., high emissivity) increase R_{nin} much more than covers with a low longwave absorptivity or with no cover at all, during both the daytime and nighttime.

2. The difference between net radiation outside (R_{nou}) and inside (R_{nin}) (i.e., R_{nou} - R_{nin}) for low tunnel plastic film covers with high longwave absorptivity (TMX) was negative, whereas R_{nou} - R_{nin} for the plastic film cover with low longwave absorptivity (POLY$_P$) was positive. The ability of any cover to increase R_{nin} above R_{nou} is reliant on its ability to increase L_{din} and compensate for loss of shortwave radiation due to reflection.

3. G was found to be similar for all treatments, with and without low tunnels. This indicates that the impact of applying a single layer of plastic film mulch on G far exceeds the impact of any additional layers.

4. The empirical relationship between the coefficient of heat transfer for the low tunnel wall and the outside air (h_{wou}) vs. wind speed (at the 2-m height) agreed well with previously developed equations, and clearly shows that previous equations that do not account for the bluff body effect of a low tunnel underestimate h_{wou}.

5. Net radiation inside a plastic film covered low tunnel, with a plastic film mulch floor, can be accurately calculated in the field, using the shortwave and longwave spectral properties of the plastic film cover and mulch (absorptivity, transmissivity and reflectivity), measured in a laboratory, in combination with downwelling shortwave and longwave radiation outside the low tunnel, if the mulch surface temperature (T_m) and soil heat flux density (G) are measured or modelled accurately.

6. The temperature rise inside a plastic-film-covered low tunnel, with a plastic film mulch floor, can be estimated using a model that requires external horizontal wind speed (for the external heat transfer coefficient), external downwelling shortwave and longwave radiation, plastic film spectral properties (cover and mulch), measured or modelled G and a fixed internal heat transfer coefficient.

Chapter 4: Effect of plastic film low tunnels on Padrón pepper (*Capsicum annuum*) microclimate, growth and yield in Vancouver, British Columbia

4.1 Summary

Plastic films are widely used as soil mulches and low tunnel covers to alter crop microclimate with the goal of improving crop growth and yield. In temperate regions of the world, hot-houses are generally used to extend the growing season; low tunnels may be a versatile and low-cost alternative strategy that is able to extend the growing season and increase crop yields. We seeded and grew Padrón peppers (*Capsicum annuum*) inside the University of British Columbia (UBC) Horticultural Centre and then transplanted the seedlings into a Podzolic soil at UBC Farm, Vancouver, BC. The experiment comprised three treatments: 1) black embossed #2 plastic film mulch (BE2) with no low tunnel (C_{PP}), 2) BE2 with a low tunnel covered with hardware-store-available polyethylene ($POLY_{PP}$) and 3) BE2 with a low tunnel covered with horticultural anti-drip polyethylene (TMX_{PP}) film. A low tunnel with BE2 and no peppers was also included in the experiment to determine the effect of the peppers on tunnel air temperature. Measurements included radiation components, microclimate, leaf-scale response, plant growth and pepper yield, Results showed that both $POLY_{PP}$ and TMX_{PP} covers decreased shortwave radiation (S) and photosynthetically active radiation (PAR) at the top of the pepper canopy compared to the control, due to the radiative properties of the plastic films (shortwave reflectivity and absorptivity) and condensation. TMX_{PP}, with its anti-drip property, experienced less variability in diurnal S and PAR transmissivities (τ_s and τ_{PAR}, respectively) than $POLY_{PP}$. In general, net photosynthesis (P_N) and stomatal conductance (g_s) were larger for the low tunnel grown peppers, but not significantly. Overall, the low-tunnel-grown peppers had a 10% larger

cumulative yield than the peppers grown in only plastic film mulch, which was primarily due to two harvests at the end of the growing season. Despite the fact that the low tunnels increased the temperature of the air near the top of the pepper canopy by ~2 °C over the whole study period, compared to outside, the low tunnels resulted in declining CO_2 concentrations (i.e., CO_2 depletion due to photosynthetic uptake) and increased water vapour density during the midday in the peak growing season, which highlights the microclimatic trade-offs associated with low tunnels.

4.2   Introduction

Plastic covered low tunnels and plastic film soil mulches are often used together to help crop producers increase growing season length, protect their crops from weather variability and increase the resilience of their cropping systems. The impact of various plastic film mulches on plant growth and yield has been studied extensively for several crops: muskmelon (Taber 1993; Brandenberger and Wiedenfeld 1997; Ibarra et al., 2001), cucumber (Yaghi et al., 2013), lettuce (Semida et al., 2013), echinacea (Burrows and Reese 2007), strawberries (Baumann et al., 1995; Bornt et al., 1998; Meyer et al., 2012), okra (Aniekwe 2013), corn (Kwabiah 2004; Mo et al., 2017; Wang et al., 2016), potato (Wang et al., 2009; Zhang et al., 2017), tomato (Mukherjee et al., 2010; Zheng et al., 2013), pepper (Waterer et al., 2008; Liang et al., 2011; López-López et al., 2015; Ćosić et al., 2017), broccoli (Appendix D), summer squash (Appendix E). Based on the literature, plastic film mulches can significantly increase soil temperature (T_s) (increase growing season length) and decrease soil evaporation (E_s) (decrease irrigation requirements) during critical crop growth periods of the growing season (i.e., early and mid-growing-season). Unlike plastic film mulches, which are used to increase T_s, enclosures covered with high shortwave

137

radiation transmissivity (τ_s) plastic films can be used to increase air temperature near the plant canopy inside enclosures (T_{ain}), which may permit crop growth where (i.e., northern latitudes) and when (i.e., spring and fall) it may not be possible. The two primary mechanisms responsible for the increase in T_{ain} are: 1) enclosures protect the soil and leaf surfaces from the wind thus decreasing sensible heat loss to the air, and 2) they increase net radiation (R_n) at the soil and leaf surfaces by decreasing net longwave loss to the sky (Businger 1963; Lee 1976). For enclosures covered with a single layer, choosing a plastic film that maintains high τ_s, photosynthetically active radiation (PAR) transmissivity (τ_{PAR}), and longwave absorptivity (α_L) values throughout the growth period is crucial to increasing T_{ain} during daytime and nighttime. Although an enclosure's orientation (Jaffrin and Makhlouf 1990) and the age of the cover (Ngouajio and Ernest 2005) can impact τ_s, dynamic changes caused by the environment such as condensation (Geoola et al., 1994; Pieters et al., 1997) and dirt accumulation (i.e., soiling) can have a larger impact on a cover's τ_s value during the growing season (Kurata 1990; Geoola et al., 1998). With regards to condensation, some plastic films are specifically designed with surfactants to distribute water droplets evenly over the plastic cover to maintain higher values of τ_s and τ_{PAR}. Plastic films with high α_L can be purchased but condensation and soiling can also increase α_L, particularly for plastic film covers with low α_L values.

An important consideration for growers who use low tunnels is how they impact stomatal conductance (g_s) and net photosynthesis (P_N), given they are a direct measure of plant stress and carbon dioxide (CO_2) assimilation. Also, it is well known that enclosures can experience low CO_2 (i.e., CO_2 depletion) concentrations ([CO_2]), which can decrease crop photosynthesis (Chandra et al., 2011), and high relative humidity conditions which can increase plant surface

condensation and promote disease and infection (Albajes 1999; Brand et al., 2009; Elad et al., 2014). As a result, when considering that low tunnels may benefit crop growth by increasing T_{ain}, a grower must also consider potential drawbacks associated with low tunnels, such as CO_2 depletion and an increase in relative humidity. Given low tunnels are meant to be low-cost and versatile structures as a potential season extension strategy, simple and cost-effective strategies to keep $[CO_2]$ higher and relative humidity lower (e.g., passive ventilation) within low tunnels should be considered.

There has been considerable research on high plastic film tunnels, some of which may be applicable to low tunnels. Both heated and unheated high tunnels are effective in the early and late growing season. Hunter et al. (2012) showed that early marketable tomato yield increased from 1.2 kg plant^{-1} in an unheated control high tunnel to 1.87 kg plant^{-1} in a soil-and-air-heated high tunnel. Retamal-Salgado et al. (2014) found that cumulative blueberry yield increased 44% when grown in a high tunnel and harvesting began 14 days earlier than blueberries grown outside the high tunnel (i.e., control). Low to medium τ_s enclosures are not only effective during the early and late growing season but can also be an effective management tool during peak growing season to cool crops which would otherwise experience heat stress. In India, Singh et al. 2012 showed that strawberries grown in an environment with a 50% reduction in downwelling shortwave radiation (using a dark green shade-net) had the highest yield due to the heat-stress reduction. In order to improve our understanding of the impacts of low tunnels on crop growth, we designed an experiment that included Padrón pepper (*Capsicum annuum*) during a full growing season. The objectives of this study were to determine the:

1. Impact of low tunnels on Padrón pepper microclimate (i.e., shortwave (S) and photosynthetically active radiation (PAR) above the plant canopy, air temperature, carbon dioxide concentration ($[CO_2]$), and water vapour density (D)).

2. Leaf-scale response of Padrón peppers (i.e., stomatal conductance (g_s) and net photosynthesis (P_N)) to microclimatic changes caused by the low tunnels.

3. Impact of low tunnels on Padrón pepper growth (i.e., basal stem diameter (BSD) and plant height (z)) and yield).

4.3   Methods

4.3.1   Seed establishment and glasshouse growth

Padrón peppers were seeded into 0.1 m x 0.1 m pots with organic soil mix (Sunshine mix #1 LC1, SunGro® Agawam, MA, USA) and grown in the UBC Horticulture Centre glasshouse under controlled climate (Table 4.1 and Figure C.1) from the time they were seeded, April 12 2017, until June 7, 2017 when they were moved to an unheated high tunnel at UBC Farm for 5 days in order to be hardened off. The seedlings were transplanted into the experimental layout (Figure 4.1) on June 12, 2017 (Figure C.3). The transplants were chosen and planted randomly, and the survival rate after transplanting was 100%.

Table 4.1 General climate inside and outside the UBC Horticulture Centre during April, May and June 2017 when Padrón pepper seedlings were prepared. Minimum, maximum and mean outside air temperature (T_{aou}, ^oC), outside wind speed (u_{ou}, m s^{-1}), inside air temperature (T_{ain}, ^oC) and vapour pressure deficit (D_{in}, g m^{-3}), as well as total downwelling shortwave radiation outside the centre (S_{dou}, MJ m^{-2} month^{-1}).

Month		T_{aou}	u_{ou}	T_{ain}	D_{in}	S_{dou}
	Minimum	3.6	-	16.6	0	-
April	Maximum	15.9	-	26.6	18.4	-
	Mean	9.1	1.3	19.1	8.2	-
	Total	-	-	-	-	385
	Minimum	5.1	-	13.8	3.2	-
May	Maximum	27.4	-	32.3	24.7	-
	Mean	13.3	1.0	20.6	8.9	-
	Total	-	-	-	-	592
	Minimum	8.9	-	16.0	3.4	-
June	Maximum	28.5	-	32.6	25.0	-
	Mean	16.0	1.0	21.7	9.2	-
	Total	-	-	-	-	640

141

4.3.2 Site description

Low tunnels were established at the University of British Columbia (UBC) Research Farm (UBC Farm) located on the UBC Vancouver Campus, Vancouver, BC (49°14'56.4"N 123°14'14.0"W, 68 m.a.s.l) from June 10 until November 26, 2017. UBC Farm experiences a mild oceanic climate with humid, mild winters and dry summers with a 25-year (1991-2016) mean annual temperature at the 2-m height (T_{a2m}) and precipitation (P) of 10.6 °C and 1054 mm, respectively, measured at Totem Field (~500 m from the site) (Table 4.2). In June 2017, four treatments (Table 4.3) (three low tunnels and a no-tunnel control, all mulched with black embossed #2 (BE2) plastic film), 10 m x 1 m, were installed on tilled Podzolic soil. The low tunnel treatments used two different polyethylene plastic films: construction polyethylene (0.15 mm thick) (POLY) and Thermax (0.15 mm thick) (TMX). One of the 3 tunnel treatments, also construction polyethylene, did not contain any peppers ($POLY_{EMP}$), and was installed to have a reference microclimate that had a latent heat flux density equal to zero. Site preparation included plowing and disk cultivation to a depth of 10 cm. After cultivation, a drip-irrigation line was installed at the 5-cm depth (near the centre of the treatment area) and feather meal was applied above the dripline at an application rate of 15.7 g m^{-2}. A 0.15 m wide x 0.15 m deep perimeter trench was dug around each 12 m x 1 m treatment area to bury the edges of the BE2 plastic film, after which stones > 0.02 m were removed from the soil surface by hand and the treatment area was levelled again with a ruler (Figure C.3). The BE2 plastic film mulch was installed by 1) securing one edge of the plastic film replacing soil removed during trenching, and 2) minimizing the air gap between the soil surface and the plastic film by pulling the remaining 3 edges of the plastic tight while replacing soil removed during trenching (Figure C.3). Although each plastic

film was installed to minimize the air gap between the soil surface and the plastic film a distribution of air gaps remained present after installation, with a maximum air gap of ~0.01 m. Low tunnels (10 m length x 0.8 m base wide x 0.7 m height) were installed using gable roof shaped steel rod hoops (0.008 m diameter, 0.8 m low tunnel base width, 1.5 m low tunnel perimeter length) (Dubois Agrinovation Inc., Saint Rémi, QC, CA) with ~1.5 m spacing (7 hoops low-tunnel^{-1}). Low-tunnel covers were cut to aforementioned dimensions and secured at the ends using a 0.6 m steel rod stake and cable ties. Finally, each low tunnel cover was secured at each hoop using 1.2 m long bungee cords tied to the tunnel base (Figures C.4, C.5 and C.6).

On June 12, 2017, 80 Padrón peppers (*Capsicum annuum*) were transplanted into 2 rows (40 peppers row^{-1}) in each of the pepper treatments (i.e., POLY$_{PP}$, TMX$_{PP}$ and C$_{PP}$) (Figure 4.1). Each row was planted 0.15 cm from the dripline and both rows were planted with 0.30 m spacing within rows. The two rows within each treatment were staggered 0.15 cm lengthwise to ensure even distribution of leaf area (LA). Each treatment was divided into 4 (2.5 m long) quadrants (i.e., quadrants (Q)) containing ~20 plants Q^{-1} to test the difference in pepper physiological measurements between the treatments.

Table 4.2 Climatic, geographic and soil characteristics for UBC Research Farm.

Treatment period start and end dates	June 10 – Nov 26 (DOY 162 – 331), 2017
Location	49°14'56.4"N 123°14'14.0"W
Elevation (m, above mean sea level)	68
25-year mean annual temperature (^{o}C)	10.6 ± 0.7
25-year mean annual precipitation (mm)	1054 ± 238
Soil order (Canadian System of Soil Classification[a])	Ferro-Humic Podzol
Soil texture	Gravelly sandy loam
Bulk density (Mg m^{-3}) at 0.05 m depth	0.92

[a]Soil Classification Working Group 1998

Table 4.3 List of treatments, mulch names, plastic cover names and plant name for the four treatments in this study.

Treatments	Plastic mulch name	Plastic cover name	Plant name
$POLY_{EMP}$	Black embossed #2 (BE2)	Polyethylene (POLY)	None (i.e., empty)
$POLY_{PP}$	BE2	POLY	Padrón pepper
TMX_{PP}	BE2	Thermax (TMX)	Padrón pepper
C_{pp}	BE2	None	Padrón pepper
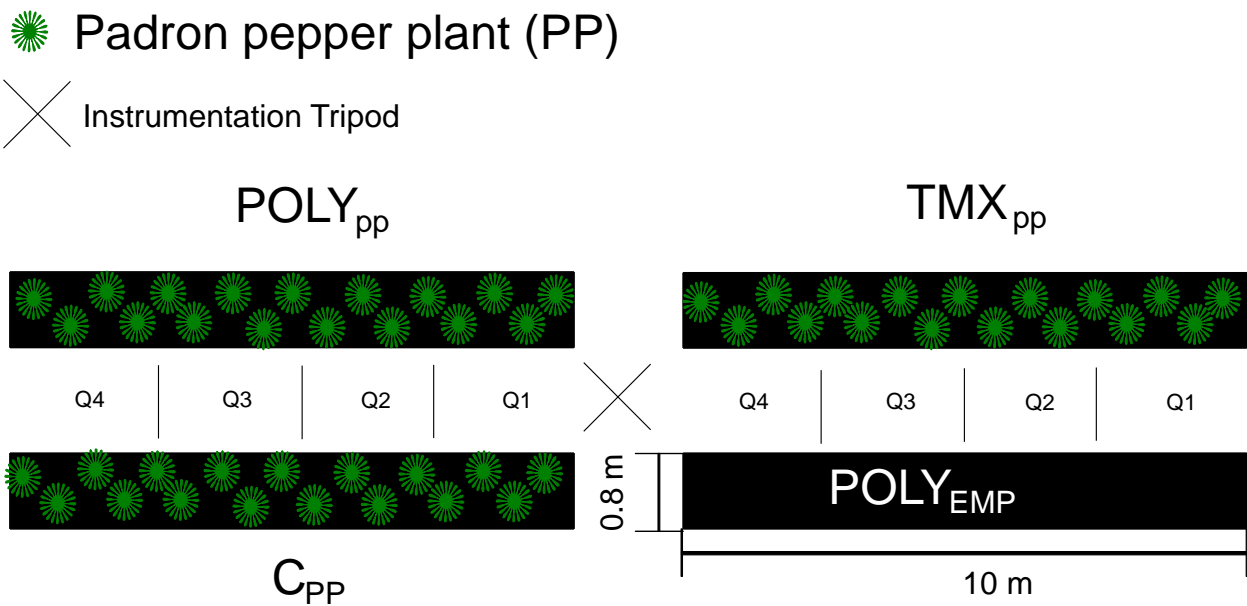
Figure 4.1 Overhead view of the experimental layout for comparing Padrón pepper microclimate and productivity using black plastic mulch and low tunnels. Abbreviations and treatments are listed in Table 4.3. The positions of the four quadrants (Q1, Q2, Q3 and Q4) are labelled.

4.3.3   Irrigation, low tunnel ventilation and management

All treatments were irrigated simultaneously, and the target volumetric water content was 0.3 $m^3 m^{-3}$. No direct measurement of irrigation volume was performed. The low tunnels were passively ventilated during the entire study by keeping the plastic film cover ~ 30 cm above the plastic film surface, secured by the bungee cords, to create an air gap to allow air exchange during the whole study period (day and night). On July 12, 2017 the height of the hoops was increased by 50 cm to accommodate Padrón pepper growth, but the air gap size used for ventilation was unchanged (Figures C.7, C.8, C.9, C.13 and C.15). On August 15, 2017 (15:00 PST) the plastic film cover's in quadrant (Q) Q4 and Q1 of POLY and TMX were removed in order to assess whether the low tunnels provided additional benefit to pepper yield beyond the peak of the growing season (Figures C.10).

4.3.4   Padrón pepper physiological measurements

Pepper harvest measurements were performed on each subplot separately. Pepper harvest consisted of harvesting all peppers which were sufficiently large for sale (~ 10 cm long, ~10 g pepper^{-1}). The number of peppers Q^{-1} and total pepper mass Q^{-1} were recorded bi-weekly (Figures C.11) during the first two months (July and August) of harvest and weekly during the remainder of the harvest (September and early October) as total pepper mass Q^{-1} declined.

Padrón pepper leaf area (LA), height (z) and basal stem diameter (BSD) were measured weekly during the experiment until August 3, 2017 (DOY = 215). BSD and z were estimated one last time at the end of the experiment on November 2 (DOY = 306). LA was calculated using a combination of manual field measurements and regression relationships of LA vs. measured leaf

width (l_w) x leaf length (l_l), developed by Padron et al., (2016) for bell peppers. Initially, manual LA field measurements were performed on 16 randomly chosen pepper plants within each treatment and later reduced to 8 plants treatment^{-1}, and comprised:

1. Separating leaves into small, medium and large size classes

2. Counting the number of leaves within each size class

3. Calculating the mean l_w x length l_l, of each size class

The total LA for each size class was then calculated according to Padron et al., (2016), and LA for all size classes were summed. The measurement of LA was discontinued on August 4, 2017 due to the difficulty of accurately counting the number of leaves (too many leaves) and approximating their dimensions, which resulted in unacceptable variability in the measurements.

Leaf-scale stomatal conductance (g_s) and net photosynthesis (P_N) were measured weekly using a portable photosynthesis system (model LI-6400, LI-COR Biosciences, Lincoln, Nebraska, USA) (Figures C.15). Weekly measurements were performed at midday (12:00 – 2:00 PST) on four randomly chosen leaves (2 sunlit and 2 shaded) from 16 randomly chosen plants treatment^{-1}. Measurements of g_s and P_N continued until August 24, 2017 and then stopped due to malfunctioning of the portable photosynthesis system.

4.3.5   Weather and tunnel microclimate measurements

A weather transmitter (WXT520, Vaisala Oy, Helsinki, Finland) provided half-hourly mean T_{a2m}, P, wind velocity (u_{2m}) and direction and vapour pressure deficit (VPD$_{2m}$) at a height of 2 m. Net radiation (R_n), calculated as the sum downwelling shortwave (S_d) and longwave (L_d)

radiation minus the sum of the upwelling shortwave (S_u) and longwave (L_u) radiation, was measured at various locations using three four-way net radiometers consisting of upward and downward-facing pyranometers and pyrgeometers (two model CNR1, Kipp and Zonen, The Netherlands, and one SN-500, Apogee Instruments Inc. (AI), Logan, UT, USA). One CNR1 was mounted at 1.5 m above soil surface near the tripod tower for the entire experiment (Figures C.14), which measured downwelling shortwave (S_{dou}) and longwave radiation (L_{dou}) and reference-surface measurements (bare soil) of upwelling shortwave and longwave radiation outside the treatments. Another CNR1 was mounted 0.15 m above the C_{PP} (no tunnel w/ peppers) treatment for the entire experiment duration, which provided replicate measurements of S_{dou} and L_{dou} along with measurements of upwelling shortwave (S_{uCPP}) and longwave (L_{uCPP}) radiation for C_{PP} (Figures C.14). The SN-500 was used to measure radiation inside $POLY_{PP}$ and TMX_{PP} (S_{din}, S_{uin}, L_{din}, L_{uin} and R_{nin}) (i.e., between the low tunnel cover and the pepper plants). A net radiometer was not mounted inside $POLY_{EMP}$ at any time during this study because it was decided that alternating the net radiometer between $POLY_{PP}$ and TMX_{PP} was paramount. The shortwave transmissivity for the cover wall for $POLY_{PP}$ and TMX_{PP} was calculated as, $\tau_{sw} = S_{din} / S_{dou}$.

Six quantum sensors (LI-190, LI-COR Inc.) were used in this study. One sensor was mounted upward-facing ~0.15 m above the top of the C_{PP} treatment plant canopy to measure downwelling photosynthetically active radiation (PAR) (Q_{dou}). The second sensor was also mounted ~0.15 m above the C_{pp} plant canopy to measure upwelling PAR from C_{PP} (Q_{uCPP}). The remaining four PAR sensors were positioned on the mulch surface of each treatment (upward-facing) to measure downwelling PAR at the mulch surface (Q_{dbelow}). The bulk PAR

transmissivity of each treatment (i.e., tunnel cover and pepper canopy) was calculated as,

$$\tau_{PARcanopy} = Q_{dbelow} / Q_{dou}.$$

For each treatment, previous to installing the plastic films, four Peltier coolers (HP-127-1.0-1.3-71, TE Technologies Inc., Traverse City, MI, USA) were installed at the 0.03 m depth to measure soil heat flux density (G) (Figure C.2); and two soil temperature (T_s) and volumetric water content (θ_s) profiles were installed comprising sensors (5TM, Decagon Devices Inc., Pullman, WA, USA) (Figure C.2) positioned at the 0.03 m, 0.08 m and 0.15 m depths. The measurements of 3-cm T_s and θ_s (T_{s3cm} and θ_{3cm}) were used to correct the soil heat flux measurements to give G at the soil surface. To account for variability in G, T_{s3cm} and θ_{s3cm} within the treatments, each profile was positioned in pre-determined locations: one profile was located near the irrigation dripline and was shaded, and one profile was located 0.15 m from the irrigation dripline and was sunlit in order to get a representative measure throughout the treatments.

[CO$_2$] and water vapour density (D) were measured using a gas analyzer profile system. The profile system consisted of 4 solenoid valve pairs through which air was circulated into and out of an infrared gas analyzer (IRGA) (model LI-840, LI-COR Inc.). The profile system pump circulated air at a rate of 4 L min^{-1} and subsampled 0.8 L min^{-1} from the main air stream. Four inlet/outlet pairs were installed (one inlet/outlet pair per treatment) at a height of 0.5 m above the mulch surface. The IRGA sampled each inlet/outlet pair in sequence for 45 s at a frequency of 1 Hz, and half-hourly means, and standard deviations of [CO$_2$] and water vapour density were calculated from 1-Hz data.

4.3.6   Statistical analysis

Means between treatments were compared using student t-tests at a 95% probability value (p) of significance ($p < 0.05$) to test the significant differences for stomatal conductance (g_s), net photosynthesis (P_N), plant height (z), leaf area index (LAI) and basal stem diameter (BSD) at each measurement date.

4.3.7   Plastic film spectral properties

The shortwave spectral properties of all plastic films used in this study were measured (Table 4.4) in the laboratory using a shortwave spectroradiometer (350 nm – 2500 nm) which accounts for ~98% of the energy in the solar spectrum (Fieldspec 3, ASD Inc., Longmount CO, USA). The longwave spectral properties were measured for all three plastic films (Table 4.4) using the pyrgeometer of a 4-component net radiometer (model SN-500-SS, Apogee Instruments Inc., Logan, UT), three chromel-constantan thermocouples, and a 0.44 m x 0.82 m x 0.042 m (width x length x thickness) glass sheet (See Chapter 2 for procedure).

Table 4.4 Shortwave and longwave radiative coefficients ($\rho, \tau,$ and α) for all plastic films and the control in this study.

Plastic films abbreviation	Shortwave												Longwave		
	S (350 – 2500 nm)			PAR (400 – 700 nm)			NIR (700 – 1400 nm)			SWIR (1400 – 2500 nm)			L (2500 – 10000 nm)		
	ρ_S	τ_S	α_S	ρ_{PAR}	τ_{PAR}	α_{PAR}	ρ_{NIR}	τ_{NIR}	α_{NIR}	ρ_{SWIR}	τ_{SWIR}	α_{SWIR}	ρ_L	τ_L	α_L
BE2 (Mulch)	0.04	0.00	0.96	0.05	0.00	0.95	0.03	0.00	0.97	0.02	0.00	0.98	0.00	0.06	0.94
POLY	0.10	0.77	0.13	0.13	0.74	0.13	0.07	0.82	0.11	0.04	0.81	0.15	0.01	0.50	0.49
TMX	0.04	0.82	0.14	0.07	0.80	0.13	0.03	0.86	0.11	0.02	0.82	0.16	0.01	0.36	0.63
C (bare soil)	0.07	0	0.93	-	-	-	-	-	-	-	-	-	-	-	-

[1] ρ_{sC} was measured using a 4-component net radiometer at midday (12:00 – 14:00 h PST) on four separate sunny days (see section 2.3.3).
[2] α_{sC} was calculated as a residual 1-ρ_{sC}, assuming τ_{sC} to be equal to 0.

4.4   Results

4.4.1   General climate

The study began close to the sunniest and warmest period of the year with the maximum daily total downwelling shortwave radiation (S_{dou}) and mean daily air temperature (T_{a2m}) of 31.1 MJ m^{-2} day^{-1} and 21.4 °C, respectively, occurring on June 24, 2017, 12 days after the peppers were transplanted. After the maximum, mean daily T_{a2m} remained relatively constant until the end of August 2017 when T_{a2m} began to decline until the minimum mean daily T_{a2m} of -0.1 °C on November 3, 2017. The vapour pressure deficit at the 2-m height (VPD$_{2m}$) was highest during sunny periods in June, July and August, with a half-hourly [mean (μ) ± standard deviation (SD)] value of 0.86 ± 0.4 kPa. During the entire study period the values of daily, daytime and nighttime half-hourly T_a were 14.0 ± 5.5, 16.1 ± 5.1 and 11.7 ± 4.9 °C, respectively (Table 4.5).

From the beginning of the study period until the end of September 2017, the amount of precipitation (P) was low, with a cumulative precipitation of 56.8 mm as of September 30, 2017. The period from October 1 to November 23, 2017 was characterized by cloudy days with large rain events, which contributed 350.8 mm (86%) of the 408 mm total P measured during the study period. Regarding the sensitivity of each treatment to P events, the soil volumetric water content (θ_s) within C$_{PP}$ was far more sensitive to P events than the low tunnel treatments, POLY$_{PP}$ and TMX$_{PP}$, perhaps since rainfall was intercepted by the pepper leaves and channeled into the soil via stem-flow. The shaded 3-cm θ_s (θ_{s3cm}) during the whole study was similar for TMX$_{PP}$, POLY$_{PP}$, POLY$_{EMP}$ and C$_{PP}$, with values of 19.8 ± 2.5, 18.7 ± 3.7, 19.3 ± 2.1 and 17.7 ± 3.3 m^3 m^{-3}, respectively.
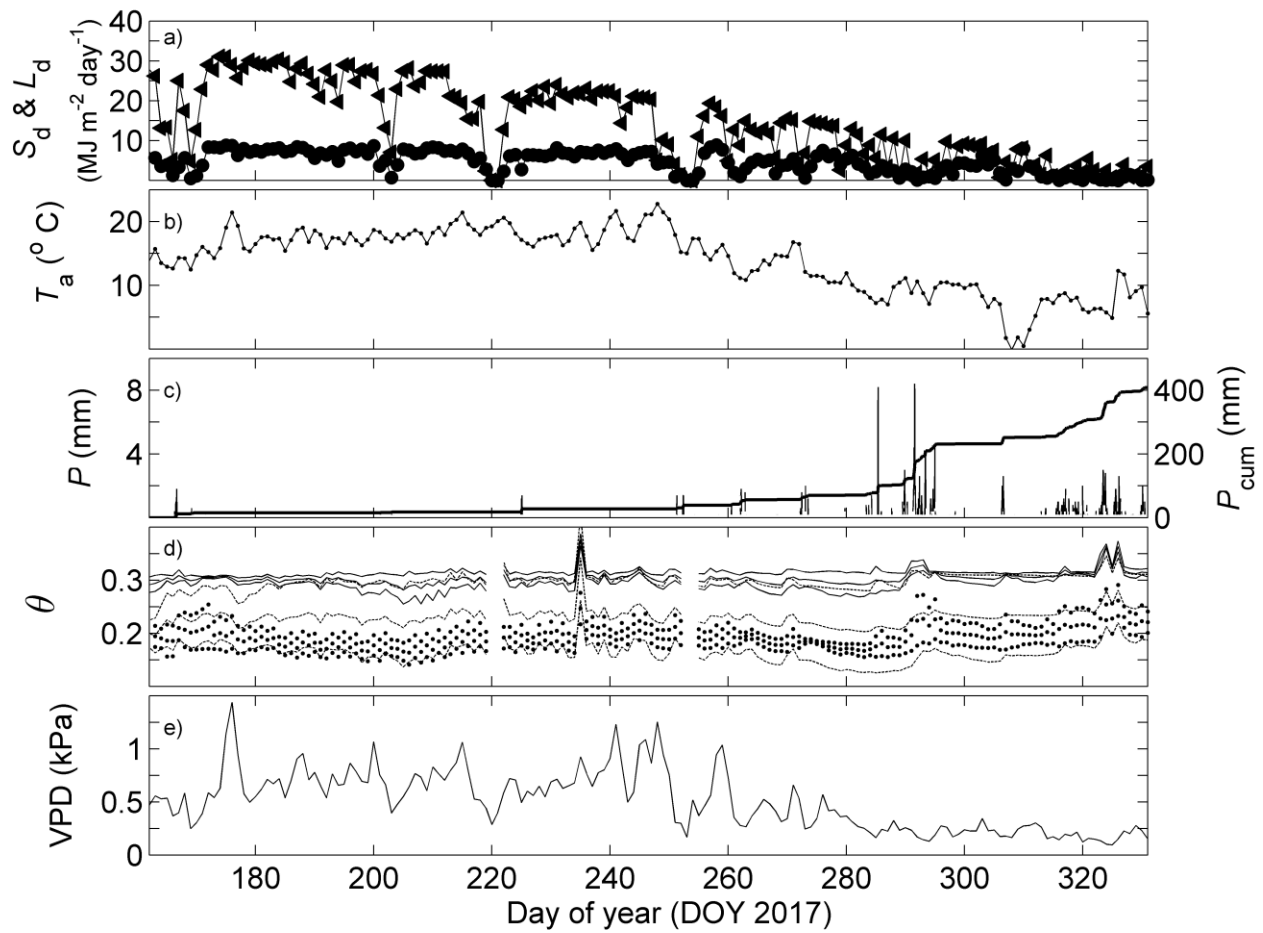
Figure 4.2 Climate data during the whole study period (June 10 – Nov 26, 2017). Panel a) shows

total daily downwelling shortwave (S_{dou}, filled left-facing triangles with line) and longwave

153

radiation (L_{dou}, filled circles with line), panel b) shows mean daily air (T_{a2m}, dotted line) and control soil temperature (T_{s3cm}, stars line), panel c) shows half-hourly precipitation (P, left axis) and cumulative precipitation (P_{cum}), panel d) shows mean (middle line) ± and SD (upper and lower lines) daily volumetric water content at the 3 cm (θ_{3cm}) (dotted line), 8 cm (dashed line) and 15 cm (solid line) depths for all treatments and panel e) shows mean daily vapour pressure deficit (VPD_{2m}).

Table 4.5 Mean ± standard deviation of total daily downwelling shortwave radiation (S_{dou}), total daily downwelling longwave radiation (L_{dou}), half-hourly air temperature (T_{a2m}), half-hourly vapour pressure deficit (VPD_{2m}) and half-hourly 3-cm volumetric water content (θ_{s3cm}) (for C_{PP}) for the whole study period (June 10 – November 26, 2017).

Time of day	S_{dou} (W m^{-2})	L_{dou} (W m^{-2})	T_{a2m} (°C)	VPD_{2m} (kPa)	θ_{s3cm} (m^3 m^{-3})
Daytime	333.32 ± 280.35	±	16.08 ± 5.14	0.67 ± 0.44	17.27 ± 3.07
Nighttime	-	±	11.68 ± 4.88	0.32 ± 0.24	18.26 ± 3.42
Daily (24-h)	173.77 ± 262.09	±	14.02 ± 5.48	0.51 ± 0.4	17.74 ± 3.28

4.4.2 Radiation and microclimate in the low tunnel treatments

In general, the mean ensemble diurnal shortwave transmissivity (τ_s) values measured in the field for TMX and POLY were very similar to the values measured in the laboratory, 0.82 and 0.77, respectively (Figure 4.3a). Interestingly, the variation in diurnal τ_s was greater for POLY than TMX, due to droplet formation observed daily on the underside of POLY (Figure 4.3a). Condensation was present on the underside of TMX as well, but TMX has a directional condensation property which does not allow droplet formation on its downward facing surface. As a result, TMX was able to maintain a less variable τ_s value throughout the daytime which is beneficial for consistent radiation in horticultural production. Both TMX and POLY experienced similarly large variability in τ_s after sunrise and before sunset.

The transmissivity of the canopy to photosynthetically active radiation ($\tau_{PARcanopy}$) was largest at the beginning of the study when LAI was small and declined as LAI increased, for all treatments with peppers (results not shown). The mean τ_{PAR} for the empty low tunnel covered with POLY (POLY$_{EMP}$) exceeded 1, greater than the laboratory measured value of 0.74, which may be due to multiple reflections from the low tunnel cover. For the whole study period, the daytime half-hourly $\mu \pm SD$ of Q_{dbelow} (accounts for both leaves and film) was highest in POLY$_{EMP}$ (501 ± 430 μmol m^{-2} s^{-1}) and lowest in POLY$_{PP}$ (86 ± 106 μmol m^{-2} s^{-1}), and TMX$_{PP}$ and C$_{PP}$ had Q_{dbelow} values of 212 ± 235 μmol m^{-2} s^{-1} and 165 ± 218 μmol m^{-2} s^{-1}, respectively. $\tau_{PARcanopy}$ was lowest for POLY$_{PP}$ due to the presence of droplet condensation, which either

155

absorbed or reflected PAR. Higher $\tau_{PARcanopy}$ for TMX$_{PP}$ than C$_{PP}$ may be due to the ability of the TMX cover to transmit PAR effectively while reflecting some PAR from its sidewalls and increasing PAR lower in the canopy, which would have otherwise transmitted the canopy and been absorbed by the adjacent mulch and soil.

The daytime soil heat flux density (G) within POLY$_{EMP}$ was consistently the highest among all treatments, and the variability in G was lowest, as expected, given that it had an LAI of 0 for the whole study period. G was highest for C$_{PP}$ for the treatments with peppers, which is consistent with the fact that C$_{PP}$ had the smallest LAI of all treatments with peppers. During the nighttime, both C$_{PP}$ and POLY$_{EMP}$ had G values that were more negative than POLY$_{PP}$ or TMX$_{PP}$. The ability of a dense canopy (i.e., high LAI) to increase downwelling longwave radiation likely caused the surface temperature to remain warmer and increase net longwave radiation (less negative) at the plastic film mulch surface. This may also explain why the lowest 3-cm soil temperature (T_{s3cm}) values occurred in the C$_{PP}$ treatment during the nighttime. The $\mu \pm$ SD values of nighttime T_{s3cm} were 16.5 ± 6.1, 16.5 ± 6.2, 17.2 ± 6.9 and $14.1 \pm 5.3\ ^{\circ}$C for TMX$_{PP}$, POLY$_{PP,}$ POLY$_{EMP}$ (highest due to no evaporative cooling) and C$_{PP}$, respectively. Aside from longwave radiation emitted from the pepper vegetation, the plastic films (TMX and POLY) increased longwave emission toward the plastic film mulch surface and plant canopy due to the fact that they both have relatively high longwave absorptivity (α_L) values (i.e., emissivity) of 0.63 and 0.49, respectively (Table 4.4).
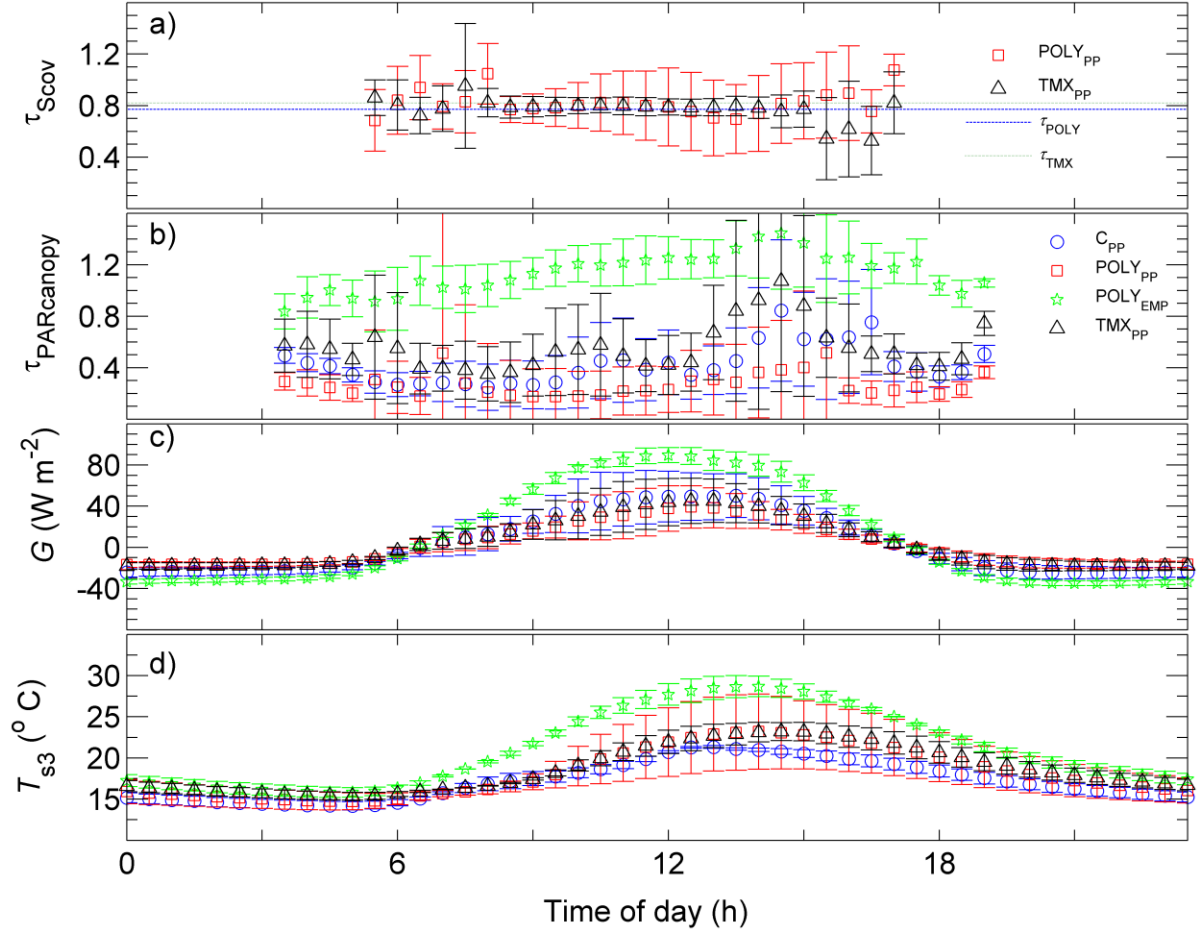
Figure 4.3 Panel a) shows the ensemble mean ± SD (error bars) shortwave cover transmissivity (τ_{sw}) for TMX$_{PP}$ (τ_{sTMXPP}) (only data from Sept 23 15:30 h – Sept 27 15:00 h PST and Oct 3 15:30 h – Nov 23 14:00 h PST) and POLY$_{PP}$ ($\tau_{sPOLYPP}$) (only data from Sept 21 12:00 h – Sept 23 15:30 h PST and Sept 27 15:00 h – Oct 3 15:30 h PST). Dashed and dotted lines are laboratory-measured values. Panel b) shows the ensemble mean ± SD photosynthetically active radiation cover transmissivity (τ_{PARw}) for TMX$_{pp}$ ($\tau_{PARTMXPP}$) (only data from Sept 23 15:30 h – Sept 27 15:00 h PST and Oct 3 15:30 h – Nov 23 14:00 h PST) and POLY$_{PP}$ ($\tau_{PARPOLYPP}$) (only data from Sept 21 12:00 h – Sept 23 15:30 h PST and Sept 27 15:00 h – Oct 3 15:30 h PST). Also shown are τ_{swEMP} and τ_{swC}, the transmissivity for the control canopy (no cover). Panel c)

157

shows the ensemble mean ± SD soil heat flux density (G) (all shaded and sunlit G) for TMX_{PP}, $POLY_{PP}$, $POLY_{EMP}$ and C_{PP}. Panel d) shows the ensemble mean ± SD 3-cm soil temperature (T_{s3cm}) (all shaded and sunlit T_{s3cm}) for TMX_{PP}, $POLY_{PP}$, $POLY_{EMP}$ and C_{PP}.

A primary use of the low tunnels in horticultural production is to elevate the air temperature surrounding the plant canopy (T_{ain}), and in our study the highest T_{ain} values occurred inside the treatments with low tunnels. The empty tunnel covered with POLY ($POLY_{EMP}$) achieved the highest temperature of all the low tunnels because there was no latent heat flux density (LE) (i.e., evaporation) inside $POLY_{EMP}$ and consequently the sensible heat flux density was very high (Figure 4.4b and c). As a result, the $\mu \pm$ SD values of daytime T_{ain} for $POLY_{EMP}$ and C_{PP} were 21.6 ± 9.7 ^{o}C and 16.4 ± 5.6 ^{o}C, respectively. Due to the positive LE inside TMX_{PP} and $POLY_{PP}$, T_{ain} inside each was less than $POLY_{EMP}$ but greater than C_{PP} with values of 18.4 ± 6.6 ^{o}C and 17.9 ± 6.1 ^{o}C, respectively. Although the low tunnels did increase T_{ain} compared to the outside air, they caused large changes in [CO_2] and water vapour density (D) (see Figure 4.4) which could be considered undesirable (discussed below).

For 2 - 4 weeks after the peppers were transplanted, [CO_2] within each treatment (above the canopy) was very similar. Nighttime values fluctuated between 500 and 600 ppm and the daytime values after sunrise were ~420 ppm after which they declined throughout the day to values of 400 ppm at sunset (Figure 4.4d). After the first weeks, [CO_2] inside TMX_{PP} and $POLY_{PP}$ during the daytime declined below the values measured inside $POLY_{EMP}$ and for C_{PP}, by as much as 100 ppm (Figure 4.4e). After the daytime drawdown of [CO_2] began inside TMX_{PP} and $POLY_{PP}$ in mid to late July, it persisted until late August (Figure 4.4f) and even until late September (see Figure 4.6c). For the whole study period, mean diurnal [CO_2] was lowest inside

TMX$_{PP}$ and POLY$_{PP}$ (Figure 4.5b) and the daytime $\mu \pm$ SD half-hourly [CO$_2$] was 392 $\pm$ 48 and 402 $\pm$ 42 ppm, respectively, whereas the daytime $\mu \pm$ SD of half-hourly [CO$_2$] was higher for C$_{PP}$ and POLY$_{EMP}$ with values of 424 $\pm$ 31 and 415 $\pm$ 28 ppm, respectively. The nighttime $\mu \pm$ SD of half-hourly [CO$_2$] values for TMX$_{PP}$, POLY$_{PP}$, POLY$_{EMP}$ and C$_{PP}$ were very similar, with values of 481 $\pm$ 59, 482 $\pm$ 61, 467 $\pm$ 51 and 476 $\pm$ 52 ppm, respectively.

Immediately after transplanting the pepper plants, D inside all treatments was very similar, day and night (Figure 4.4g). As the plants inside the low tunnels grew (e.g., increased LAI and h), D inside the low tunnels with peppers (i.e., TMX$_{PP}$ and POLY$_{PP}$) increased dramatically during the daytime, from values 20 g m^{-3} in C$_{PP}$ to 30 g m^{-3} inside TMX$_{PP}$ (Figure 4.4e). Despite the fact that POLY$_{PP}$ experienced high D values similar to TMX$_{PP}$, POLY$_{PP}$ experienced greater fluctuations in D, perhaps due to the large amount of condensation on its underside. C$_{PP}$ had a slightly larger D when compared to POLY$_{EMP}$ which is expected since there was no evaporation in POLY$_{EMP}$. For the whole study period, the daytime $\mu \pm$ SD of half-hourly D values for TMX$_{PP}$, POLY$_{PP}$, POLY$_{EMP}$ and C$_{PP}$ were 21 $\pm$ 6, 19 $\pm$ 5, 16 $\pm$ 3 and 17 $\pm$ 3 g m^{-3}, respectively, and the nighttime value was 17 $\pm$ 3 g m^{-3} for all treatments (Figure 4.5c). Overall, the use of low tunnels in this study increased T_{ain}, but it also caused [CO$_2$] to decrease and D to increase (Figure 4.5), which illustrates the trade-offs associated using low tunnels, which should be considered by producers.
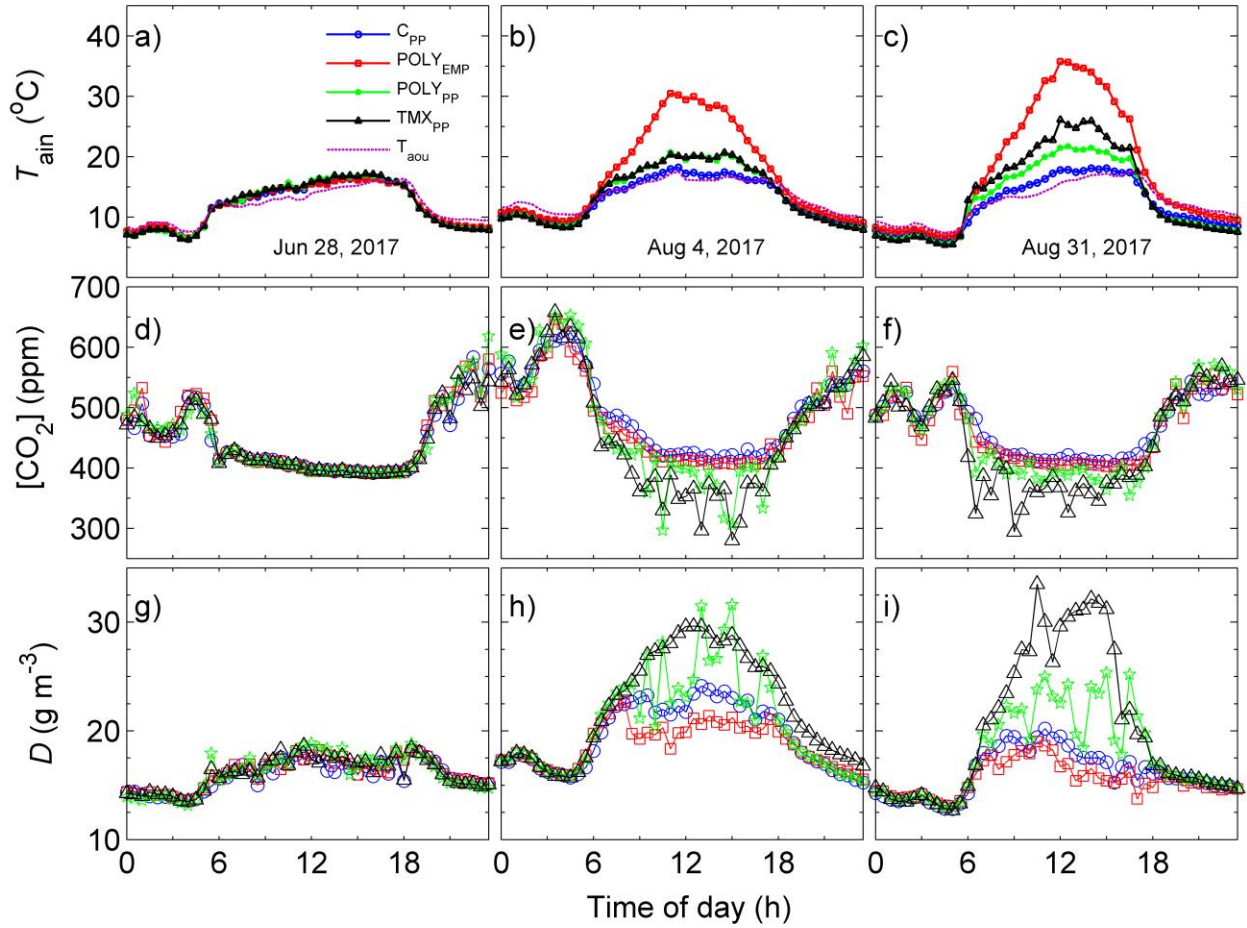
Figure 4.4 The data shown are from three cloud-free days at different stages of Padrón pepper growth development. Panels a), b) and c) show 50-cm air temperature for TMX_{PP} (upward-facing triangle), $POLY_{PP}$ (stars) and C_{PP} (circles), $POLY_{EMP}$ (squares) and 2-m air temperature (T_{a2m}) (dashed line). Panels d), e) and f) show carbon dioxide (CO_2) concentration ($[CO_2]$) for TMX_{PP}, $POLY_{PP}$, $POLY_{EMP}$ and C_{PP}. Panels d), e) and f) show water vapour density (D) for TMX_{PP}, $POLY_{PP}$, $POLY_{EMP}$ and C_{PP}.
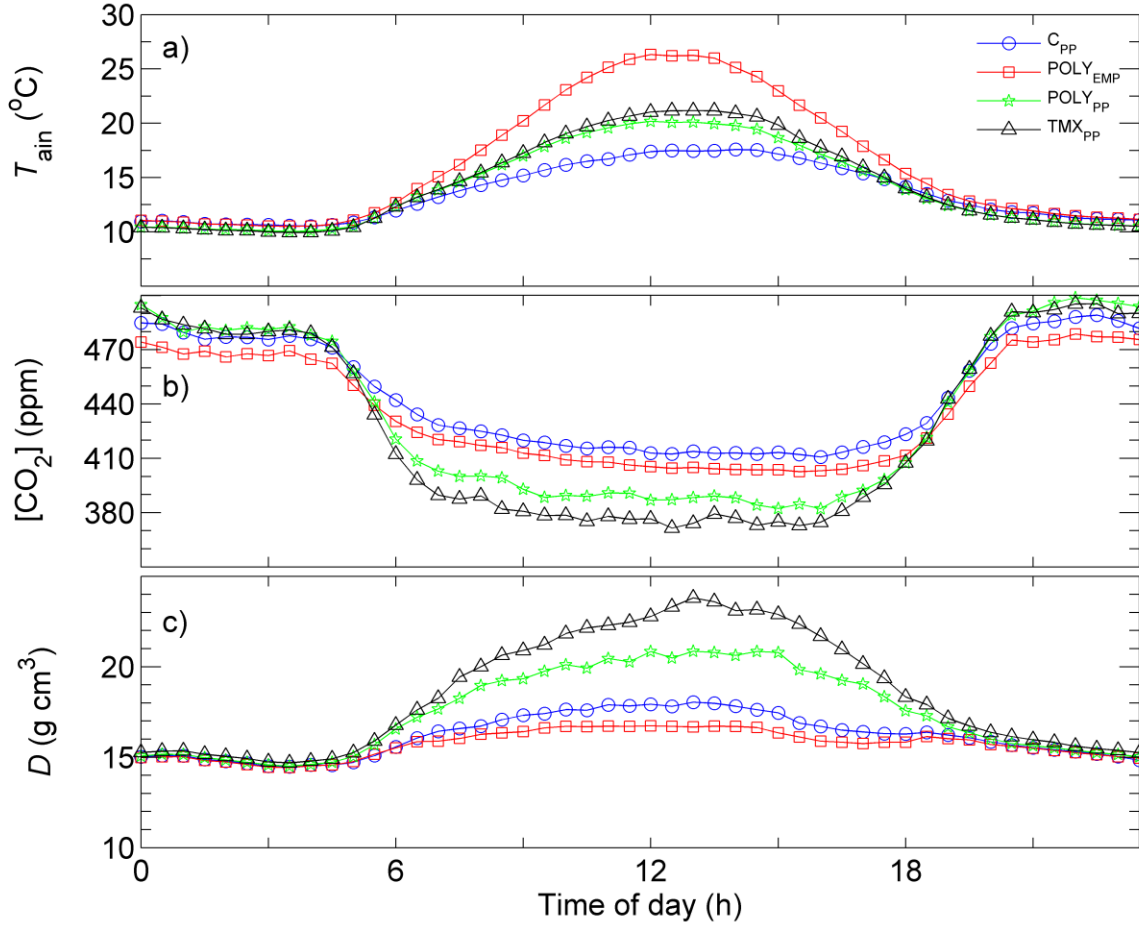
Figure 4.5 Panels a), b) and c) show the ensemble mean air temperature (T_{ain}), carbon dioxide (CO_2) concentration ($[CO_2]$) and water vapour density (D), respectively, for TMX_{PP}, $POLY_{PP}$, $POLY_{EMP}$ and C_{PP} for the whole study period (June 10 – November 26, 2017).

4.4.3   Leaf-scale net photosynthesis and stomatal conductance

Stomatal conductance (g_s) on the first day of measurement (June 22, 2017 (DOY 173)) was ~0.1 mol m^{-2} s^{-1} (i.e., ~2 mm s^{-1}) for both shaded and sunlit leaves (Figure 4.6a), which is expected given that LAI was low and the PAR distribution within the canopy appeared relatively uniform. As the pepper plants grew larger, the sunlit g_s values (~0.2 - 0.6 mol m^{-2} s^{-1} ~5 - 12.5 mm s^{-1}) began to exceed the shaded g_s values (~0.2 mol m^{-2} s^{-1} or ~5 mm s^{-1}) in all treatments

161

(July 6 (DOY 187), 2017 in Figure 4.6a). Mean sunlit g_s peaked for all treatments on July 26

(DOY 207), after which sunlit g_s steadily decreased until August 16 (DOY 228), likely due to the

low PAR setting on the portable photosynthesis system that was match to field measurements of

PAR. The sunlit g_s values were significantly different between $POLY_{PP}$ and C_{PP} on June 22

(DOY 173) (t-test, $p = 0.04$), July 6 (DOY 187) (t-test, $p = 0.0005$), July 13 (DOY 194) (t-test, p

$= 0.0002$), July 19 (DOY 200) (t-test, $p = 0.004$) and August 23 (DOY 235) (t-test, $p = 0.02$).

The sunlit g_s values were significantly different between TMX_{PP} and C_{PP} on July 6 (DOY 187) (t-

test, $p = 0.02$), July 13 (DOY 194) (t-test, $p = 0.04$), July 25 (DOY 206) (t-test, $p = 0.04$) and

August 15 (DOY 235) (t-test, $p = 0.02$). Overall, the shaded g_s values had low variability

throughout the experiment and were only significantly different for $POLY_{PP}$ and C_{PP} (t-test, $p =$

0.01) on August 15 (DOY 227) and TMX_{PP} and C_{PP} on July 25 (DOY 206) (t-test, $p = 0.02$) and

August 15 (DOY 227) (t-test, $p = 0.02$). Shaded g_s values for $POLY_{PP}$ and TMX_{PP} were not

significantly different at any point during the study.

Net photosynthesis (P_N) behaved very similarly to g_s, where both shaded and sunlit

leaves had similar P_N within 2 weeks of transplanting the peppers. Other than for $POLY_{PP}$, P_N

increased for all treatments until July 26 (DOY 207)with mean values of ~22 μmol CO_2 m^{-2} s^{-1}

for all treatments (Figure 4.6b). After July 26 (DOY 207), P_N decreased steadily, which may be

due to the fact that 1) the measurements were taken at relatively low PAR values (~400 μmol

PAR m^{-2} s^{-1}) compared to measurements made before August 8, and/or 2) decreased [CO_2] inside

the low tunnels caused P_N to decline below measured C_{PP} values. P_N for sunlit leaves was not

significantly different between $POLY_{PP}$ and TMX_{PP} at any time in the study. P_N of sunlit leaves

(Figure 4.6b) were significantly different between $POLY_{PP}$ and C_{PP} on June 22 (DOY 173) (t-

test, $p = 0.05$), July 6 (DOY 187) ($p = 0.004$) and July 13 (DOY 194) ($p = 0.005$). P_N of sunlit leaves (Figure 4.6b) were significantly different between TMX_{PP} and C_{PP} on June 22 (DOY 173, t-test, $p = 0.005$), June 27 (DOY 178, t-test, $p = 0.05$), July 6 (DOY 187, $p = 0.001$) and August 15 (DOY 227, $p = 0.004$). P_N for shaded leaves was only significantly different between $POLY_{PP}$ and TMX_{PP} on August 23 (DOY 235).
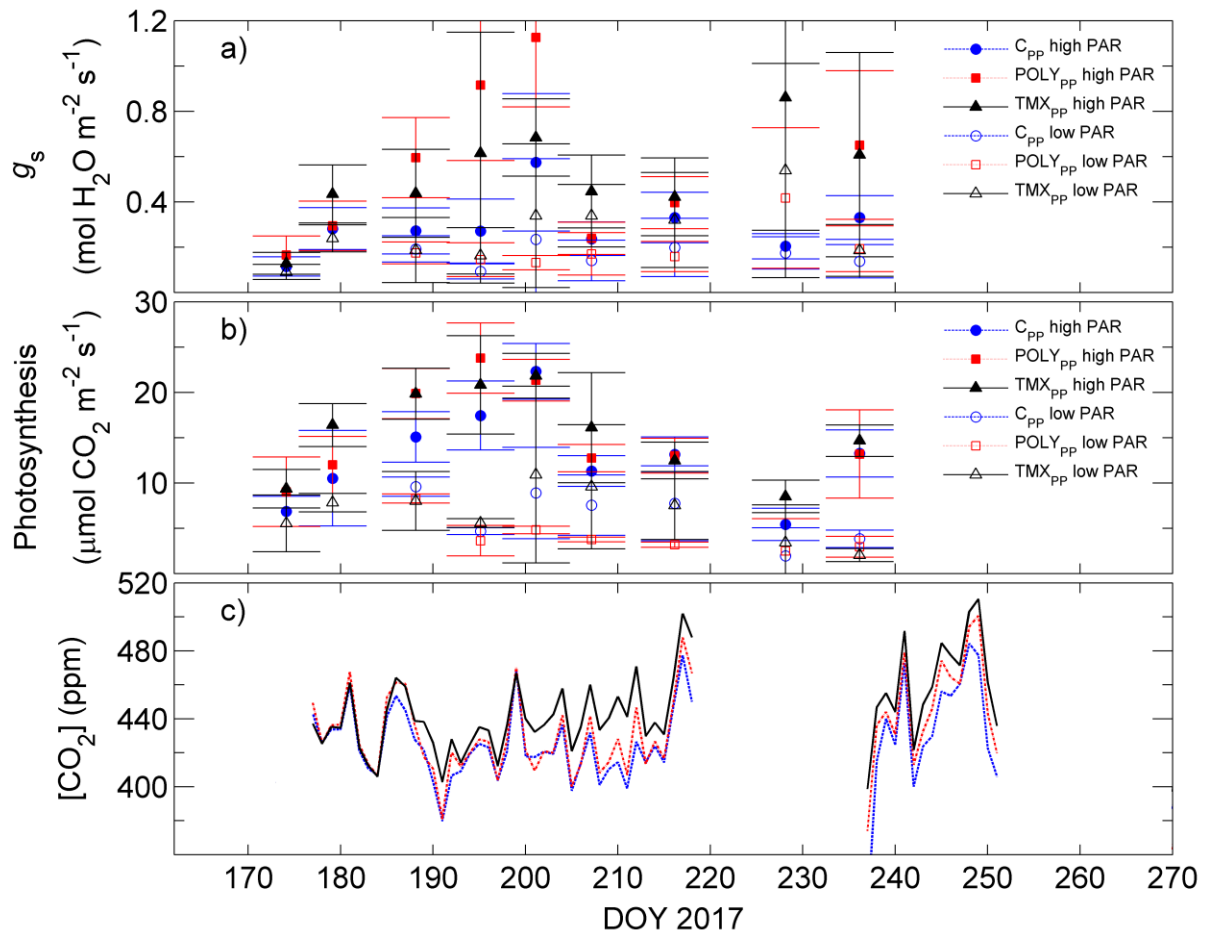
Figure 4.6 Panels a), b) and c) show the mean ± SD (error bars) of stomatal conductance (g_s) and net photosynthesis (P_N) measured near midday (between 12:00 and 15:00 h PST) under low (i.e., shaded) (<400 μmol PAR m^{-2} s^{-1}) and high (i.e., sunlit) (>=400 μmol PAR m^{-2} s^{-1}) PAR

conditions, and mean daily CO_2 concentration ($[CO_2]$), respectively, for TMX_{PP}, $POLY_{PP}$ and C_{PP}.

4.4.4 Padrón pepper growth and yield

Soon after transplanting, on June 19 (DOY 170) and June 27 (DOY 178), pepper plant height (z) for TMX_{PP} was significantly less than for both $POLY_{PP}$ (t-test, $p = 0.017$ and $p = 0.021$) and C_{PP} (t-test, $p = 0.025$ and $p = 0.004$). Also, z was significantly different between $POLY_{PP}$ and both TMX_{PP} and C_{PP} on July 5 (DOY 186) (Figure 4.7a). After July 17 (DOY 198) z for TMX_{PP} and $POLY_{PP}$ were significantly greater than z for C_{PP} (t-test, all p values > 0.02). All the plants in each treatment experienced the greatest rate of increase in z during the period between July 5 (DOY = 186 and July 23 (DOY = 204) during which time, z increased by 41, 35 and 20 cm for TMX_{PP}, $POLY_{PP}$ and C_{PP}, respectively. After July 23, the rate of increase in z decreased quickly and the pepper stems grew very little vertically, and the final estimated z for TMX_{PP}, $POLY_{PP}$ and C_{PP} was 115, 106 and 95 cm, respectively, on Nov 4 (DOY 308).

Regarding LAI, the treatments were only significantly different on August 3, 2017 (DOY 215) between C_{PP} and TMX_{PP} (t-test, $p = 0.04$) and $POLY_{PP}$ (t-test, $p = 0.005$) (Figure 4.7b) However, due to issues of accurately measuring LAI it cannot be definitively stated that there were differences between LAI across treatments. Nevertheless, TMX_{PP} and $POLY_{PP}$ produced a greater number of leaves than C_{PP} from mid-July to late-September (Figure 4.7b). With regard to basal stem diameter (BSD), the treatments were very similar, and the only significant differences were between TMX_{PP} and the other two treatments, $POLY_{PP}$ (t-test, $p = 0.018$) and C_{PP} (t-test, $p = 0.013$), on July 5 (DOY = 186) (Figure 4.7c).
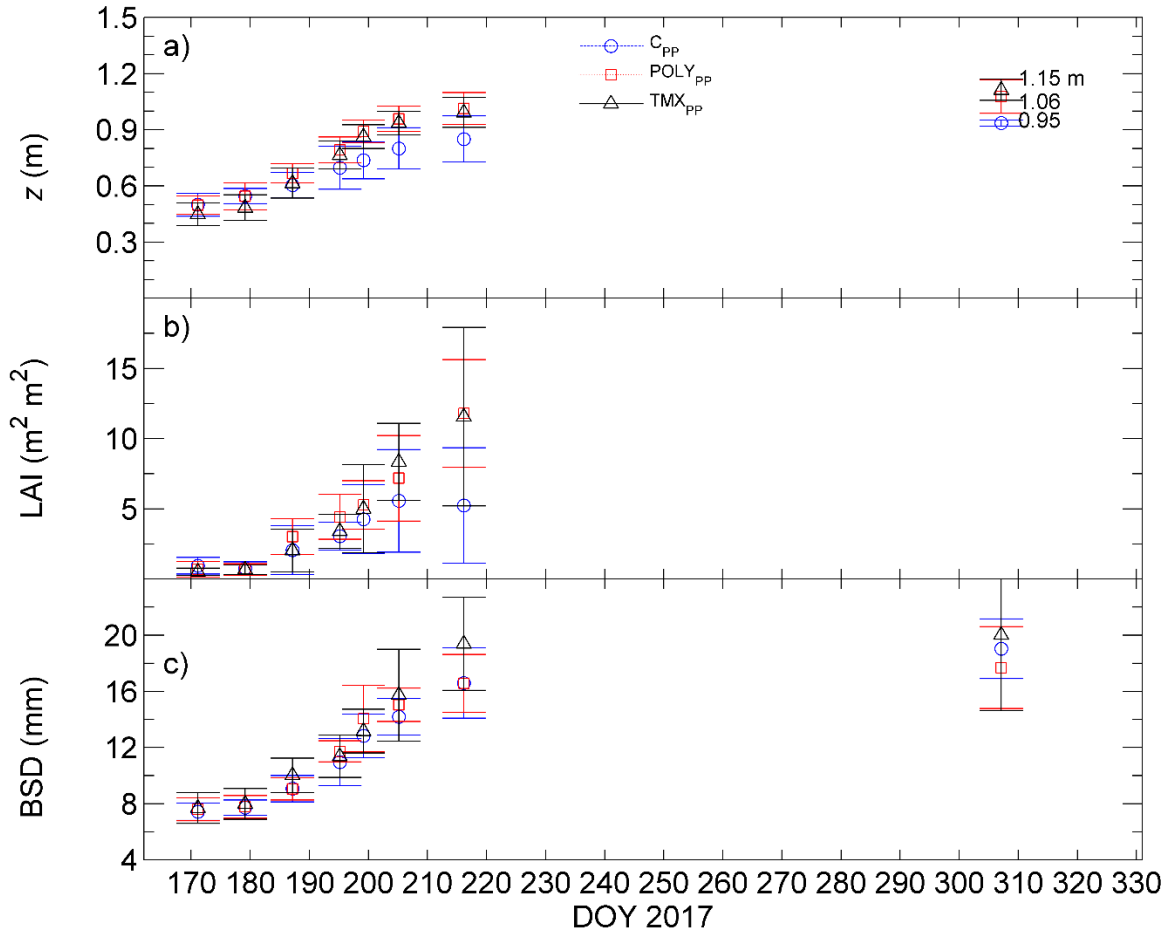
Figure 4.7 Panels a), b) and c) show the mean ± SD (error bars) Padrón pepper plant height (z), leaf area index (LAI) and basal stem diameter (BSD), respectively, for TMX$_{PP}$, POLY$_{PP}$ and C$_{PP}$ (see Figures C.12).

The cumulative yield varied between each quadrant (Q) in each treatment, and the two quadrants at the end of each treatment (Q1 and Q4) had the largest cumulative yield over the whole harvest period season, for all treatments (Figure 4.8). Nevertheless, both Q2 and Q3 in TMX$_{PP}$ and POLY$_{PP}$ had larger cumulative yields than Q2 and Q3 in C$_{PP}$ (Figure 4.8 and Table 4.6). On August 15 (DOY 227), 2017, the low tunnels in Q1 and Q4 were removed in TMX$_{PP}$ and POLY$_{PP}$ treatments in order to assess whether the low tunnels were beneficial beyond the

165

period when z and LAI had reached their maximum. For TMX$_{PP}$, the removal of the low tunnel in Q1 did not appear to impact cumulative yield. On the other hand, the removal of the low tunnel from Q4 in POLY$_{PP}$ coincided with a very large increase in yield, and POLY$_{PP}$ had the largest cumulative yield during that time, with a value of ~9.2 kg (Table 4.6).
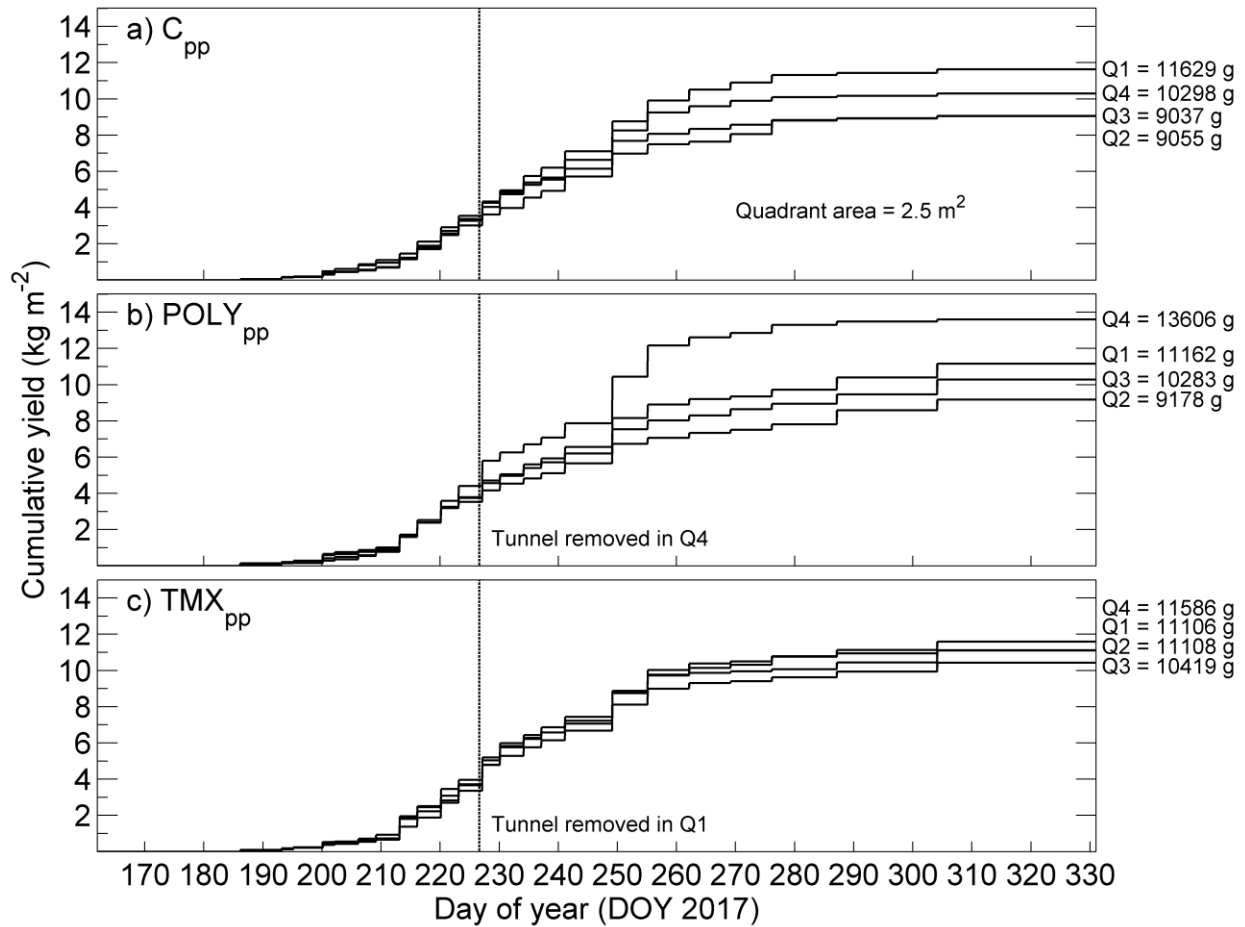
Figure 4.8 Panels a), b) and c) show Padrón pepper cumulative yield each quadrant (area 2.5 m^2) in TMX$_{PP}$, POLY$_{PP}$ and C$_{PP}$. The vertical lines indicate when the low tunnels were removed from Q1 and Q4 for TMX$_{PP}$ and POLY$_{PP}$, respectively.

Table 4.6 Cumulative yield for each quadrant (Q1, Q2, Q3 and Q4) for TMX_{PP}, $POLY_{PP}$ and C_{PP}, for the 1) whole study period, 2) after the low tunnel was removed from Q1 and Q4 for TMX_{PP} and $POLY_{PP}$, respectively, on August 15 (DOY 227), 2017.

Mass (kg)

Quadrant

Treatment	Q1	Q2	Q3	Q4
C_{PP}	11.6, 8.4	9.1, 6.1	9.0, 5.5	10.3, 6.9
$POLY_{PP}$	11.2, 7.4	9.2, 5.7	10.3, 6.5	13.6, 9.2
TMX_{PP}	11.1, 7.2[a]	11.1, 7.5	10.4, 7.1	11.6, 7.9

[a] Values to the right of the comma represent cumulative yield after the low tunnels were removed from Q1 and Q4 for TMX_{PP} and $POLY_{PP}$, respectively, between August 15 (DOY 227) and October 30 (DOY 303), 2017.

As of the final harvest on October 30 (DOY 303), C_{PP} had a cumulative yield of 4.0 kg m^{-2}, and the cumulative yield in both TMX_{PP} and $POLY_{PP}$ was 4.4 kg m^{-2} (including the quadrant that had the low tunnel removed), a 10% increase in pepper productivity (Figure 4.9a). From the first harvest on July 4 (DOY = 185) to the 7th harvest on July 27 (DOY = 208), all pepper treatments had equal cumulative yield, after which the low tunnels began to yield more pepper mass per harvest. Between July 27 (DOY = 208) and August 8 (DOY 220), TMX_{PP} and $POLY_{PP}$ had greater cumulative yield than C_{PP} which was primarily a result of two relatively large harvests on August 17 (DOY = 229) and August 21 (DOY = 233). On September 6 (DOY =

249), all treatments yielded > 0.6 kg m^{-2} which was their largest single harvest of the study. By October 2, the cumulative yield was very similar for all treatments with a value of ~4 kg m^{-2}. Interestingly, the final two harvests on October 13 and 30 were crucial to the 10% increase in cumulative yield in the low tunnels. During the last two harvests TMX$_{PP}$ and POLY$_{PP}$ yields were 0.30 kg m^{-2} and 0.40 kg m^{-2}, respectively, and C$_{PP}$ yield was 0.10 kg m^{-2}. Overall, even though cumulative yield inside the low tunnels consistently exceeded that for C$_{PP}$ throughout the study, the last two harvests of the growing season accounted for nearly all of the cumulative yield difference between peppers grown inside vs outside the low tunnels.

Over the entire study, 16,482 peppers were harvested of which 5,610, 5,756, and 5,116 came from TMX$_{PP}$, POLY$_{PP}$ and C$_{PP}$, respectively (Figure 4.9b). The mean fruit mass in this study started out relatively high with values of ~10 g fruit^{-1} on a wet weight basis for the peppers grown in the low tunnels, but C$_{PP}$ had a value of ~6.5 g fruit^{-1} (Figure 4.9c). The mean fruit mass generally remained above a value 7 g fruit^{-1} until harvest #9 on August 3 (DOY = 215). Beginning at harvest #12 on August 14 (DOY = 226), the mean fruit mass began to decline steadily until harvest # 16 on August 28 (DOY = 201), when the mean fruit mass was ~ 6 g fruit^{-1}. Beginning on harvest #17, the mean fruit mass increased abruptly to values of 10 – 12 g fruit^{-1} until harvest #19, after which it steadily decreased until the end of the study period. As expected,

the length of time between harvests appeared to have a large impact on fruit mass.
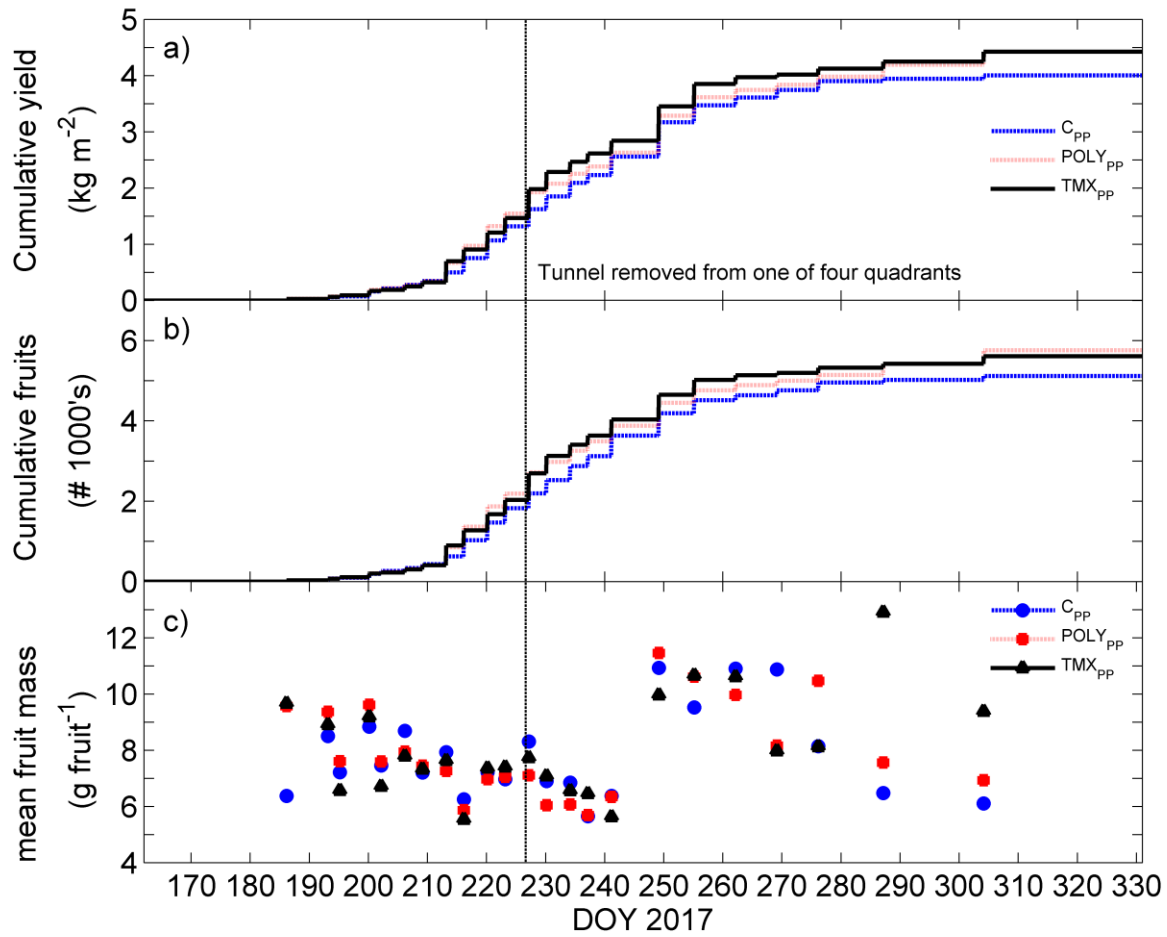
Figure 4.9 Panels a), b) and c) show Padrón pepper cumulative yield (including the quadrant that had the low tunnel removed), cumulative number of fruits and mean mass per fruit, respectively, for TMX_{PP}, $POLY_{PP}$ and C_{PP}. The vertical dashed line indicates when the low tunnels were removed from Q1 and Q4 for TMX_{PP} and $POLY_{PP}$, respectively.

4.5   Discussion

4.5.1   Low tunnel radiation and microclimate

The radiative properties of a plastic film used to cover a low tunnel are fundamental to the internal net radiation (R_{nin}) and air temperature (T_{ain}). With regards to radiative properties, the shortwave transmissivity (τ_s) and longwave absorptivity (α_L) of a plastic film are, arguably, the most determinant of R_{nin}. In northern latitudes, a producer typically desires a plastic film that has a high shortwave radiation transmissivity (τ_s) (e.g., $0.7 - 0.9$) and photosynthetically active radiation (PAR) transmissivity (τ_{PAR}) in order to allow a large fraction of the incoming shortwave radiation and PAR above the enclosure to transmit through the low tunnel cover. In our study we used two plastic films, TMX and POLY, which had laboratory-measured τ_s values of 0.82 and 0.77 and found that the τ_s values fluctuated in a field setting depending on the time of day (i.e., angle of incidence), cloud-cover (i.e., direct vs diffuse shortwave radiation) and condensation. Pieters et al. (1997) showed that cover τ_s was a function of condensation droplet size and produced an empirical model to calculate the impact. We found that the mean diurnal τ_s for each plastic film was quite similar but TMX (with anti-droplet characteristics) experienced less variability in τ_s, which is consistent with findings by Geoola et al. (1998) who showed that films with anti-drip characteristics can experience increases in τ_s ($\sim 2 - 7\%$) in the presence of condensation, whereas films with no anti-droplet characteristics typically experience decreased τ_s values ($\sim$-4%). Geoola et al. (1994) found that newly purchased films experienced decreases in τ_s when wet compared to dry, and that wet plastic films were more susceptible to decreases in τ_s due to soiling as they aged. Based on our findings and of others, the ability to reduce

170

condensation is crucial to maintaining a high τ_s value and reducing soiling due to dust accumulation. On the other hand, Walker (1971) found that the presence of condensation increased α_L of enclosures covered with materials that have low α_L values, like polyethylene (Papadakis et al., 2000), and can improve their thermal performance.

4.5.2   Water vapour density and CO_2 concentration

In this study, mean water vapour density (D) inside the low tunnels was 50% higher than outside the low tunnels, and even higher on sunny days during the peak of the growing season. Excess humidity in greenhouse production is a well know phenomena and has the potential to increase the probability of fungal, pest and disease occurrence (Whipps and Budge 2000). There are many methods and strategies to reduce humidity inside enclosures which include: air-to-air heat exchangers (Han et al., 2015), mechanical refrigeration dehumidifiers (Han et al., 2015), thermal electric dehumidifiers, dessicant dehumidifiers and passive ventilation (Kittas and Bartzanas 2007). Since passive ventilation rates are not always high enough to decrease D within enclosures, other methods such as whitening can be used to decrease canopy transpiration (E_c) and internal D (Baille et al., 2001) during the growing season when E_c is high and large increases in T_{ain} are not necessary. In addition to strategies for dehumidification mentioned above, a producer who uses low tunnels should maintain a mulch area (A_m) to cover-wall area (A_w) ratio that provides sufficient air volume to accommodate the height (z) and leaf area index (LAI) of the crop inside. Even though studies have been done to better understand the impact of enclosures on evapotranspiration (E, $E = E_c + E_s$, where E_s is soil evaporation) (e.g., Qiu et al., 2013 for hot peppers), further work is needed to study E of enclosure-grown crops to validate enclosure temperature models and management in general.

171

Along with increased D and the presence of condensation inside low tunnels, CO_2 depletion is an issue that can negatively impact crop growth and yield, occurring when ventilation rates inside low tunnels are low. CO_2 enrichment has been studied and practiced for hundreds of years and has proven to be a promising technique to increase plant growth and flower production (Mortensen 1987). In this study, CO_2 depletion was observed in the morning and midday hours when pepper photosynthesis was high, and the pepper canopy occupied a large proportion of the low tunnel volume. The minimum half-hourly $[CO_2]$ measured in this study (inside TMX_{PP}) was 216 ppm, whereas $[CO_2]$ outside the low tunnel was 466 ppm at the same time. Therefore, producers who use low tunnels may want to incorporate passive CO_2 enrichment strategies to maintain $[CO_2]$ values that are equal to or above atmospheric levels. Enoch et al. (1976) found that CO_2 enrichment caused strawberry yield to increase by 31% when $[CO_2]$ levels were increased from 300 ppm to 900 ppm and found that cucumber yield increased by 25% for the same level of CO_2 enrichment. Also, for strawberries, Sung and Chen 1991 found that the number of fruit plant^{-1} increased by 47% for plants grown under $[CO_2]$ levels of 1000 ppm when compared to the control plants grown under $[CO_2]$ levels of 340 ppm. In contrast, Fierro et al. (1994) found that both CO_2 enrichment (900 ppm) and supplemental light were required to increase early biomass yield in tomato (*Lycopersicon esculentum* Mill.) and sweet pepper (*Capsicum annuum* L.), and that overall the benefits were not always significant. Tremblay and Gosselin (1997) point to the fact that CO_2 enrichment and light supplementation are often beneficial to early growth in a nursery, but the benefits are often short-lived after the plants are transplanted in the field. Nevertheless, when using low tunnels, it may be advantageous to adopt strategies (passive or active) which will increase $[CO_2]$ levels when they decrease below 300 ppm (Kläring et al., 2007). Jin et al. 2009 incorporated a system into their

172

greenhouse production that captured CO_2 respired from a crop residue and animal manure compost, which significantly increased the yield of celery (*Apium graveolens* L.), leaf lettuce (*Lactuca virosa* L.), stem lettuce (*Lactuca saiva* L.), oily sowthistle (*Sonchus oleraceus* L.), and Chinese cabbage (*Brassica chinensis* L.) by 270%, 257%, 87%, 140%, and 227%, respectively, when compared to the control. Other strategies to increase [CO_2] inside enclosures were summarized by Li et al. (2018) and comprise natural gas, biogas, natural ventilation and liquefied CO_2, but they are typically expensive and infrastructure intensive. Overall, the primary mechanism by which low tunnels benefit the thermal environment for crops is through wind protection, which is also the primary barrier to preventing condensation and high [CO_2] levels for optimal production.

In the interest of simplicity, passive strategies to remove water vapour and increase [CO_2] within low tunnels should be studied further to assist crop producers who seek to benefit from the low-cost and versatile aspects of low tunnels. Interestingly, Al-Kayssi and Mustafa (2016) found that increased [CO_2] improved the thermal performance of un-heated vegetation-free low tunnel by increasing the internal net longwave radiation, which may be a secondary incentive for increasing [CO_2]. Also, studies that focus on understanding the seasonal and annual changes in greenhouse gas balance (e.g., CO_2, methane (CH_4) and nitrous oxide (N_2O)) will be crucial to assessing the environmental costs and benefits of enclosures (Wei-ge et al., 2016).

4.5.3   Low tunnel air temperature

In northern latitudes, the primary incentive for using low tunnels in crop production is the increased daytime and nighttime internal air temperature (T_{ain}) that they achieve by 1) protecting the plant canopy and soil (or mulch) surface from external wind forces, and 2) increasing the

173

internal net radiation (R_{nin}) by using plastic film covers with high α_L values. In this study, the pepper plants grown inside low tunnels were taller, had more leaf area, and yielded more peppers, which could be a result of the increased T_{ain}. Even though T_{ain} inside the TMX covered tunnel was higher than in the POLY covered tunnel, the cumulative harvest was not much different between the treatments, indicating that the higher T_{ain} inside the TMX covered tunnel was not any more beneficial to the peppers. Often low tunnels are used for early season extension to allow producers to sell their product when other producers have yet to harvest their crops, which can increase revenue (Faivor 2014). The present study focused on extending the late growing season and showed that peppers grown in low tunnels can continue to produce peppers ~ 2 weeks longer than pepper plants grown outside low tunnels. Many studies have found that enclosures like low tunnels increase crop yields: strawberry (Lewers et al., 2017; Palonen et al., 2017), spinach (Shiwakoti et al., 2018), pak choi (Shiwakoti et al., 2018),) brussel sprouts (Acharya et al., 2019), tomatoes (Ivanochko 1987), bell peppers (Jolliffe and Gaye 1995; Gerber et al., 1988), broccoli (Appendix D), summer squash (Appendix E). At the Agriculture Canada Research Station, Agassiz, BC, Canada, Jolliffe and Gaye (1995) found that row covers and higher planting density increased and decreased bell pepper yield, respectively, but did not directly attribute the increased yield associated with row covers to changes in T_{ain} or T_{s}. In contrast, Gerber et al. (1988) found that bell peppers experienced increased yield in Urbana, Illinois, USA, when grown under plastic film covered low tunnels, and attributed the increased yield directly to increased T_{ain} and total heat units. In this study, pepper yield was greatest for peppers grown inside low tunnels (+10%), but it is difficult to determine what aspect of the low tunnel microclimate had the greatest impact on pepper yield because, as discussed previously, low tunnels impact all aspects of the growing environment (e.g., [CO_2], water vapour density,

stomatal conductance, net photosynthesis). Therefore, future studies should focus on crop productivity, microclimate, plot-scale gas exchange and nutrient balance so that the dynamics of crop growth, yield and water and carbon balances in low tunnels can be better understood. Future work of this type will be crucial to assessing the limitations and opportunities associated with the use of low tunnels for increasing food security.

4.6 Conclusions

1. The mean diurnal shortwave transmissivity (τ_s) of the low tunnel covers was very similar to the laboratory-measured values, but it varied diurnally mainly in response to condensation and solar angle. The film with anti-drip properties (TMX) maintained a τ_s value with less diurnal variance.

2. Mainly as a result of their transpiration and latent heat flux, peppers reduced mid-day tunnel air temperature (T_{ain}) by up to 10°C in mid growing season, compared to the vegetation-free low tunnel (POLY$_{EMP}$).

3. In general, PAR transmissivity of the canopy and cover ($\tau_{PARcanopy}$) for the low tunnels at mid-day was generally less than or equal to that of the control (C$_{pp}$) canopy.

4. Net photosynthesis (P_N) and stomatal conductance (g_s) of sunlit leave were higher for the plants grown inside the low tunnels than those grown outside, but the differences were generally not statistically significant for shaded leaves.

5. Within one month of transplanting, the plants grown inside the low tunnels were significantly taller than the plants grown outside.

6. The low tunnel treatments yielded 10% more peppers than the control, and this difference was mainly the result of growing season extension in October.

Chapter 5: Conclusions

This dissertation presents studies on the shortwave (S) and longwave (L) radiative properties (reflectivity (ρ), transmissivity (τ) and absorptivity (α)) of a number of plastic films used as mulches and low tunnels and their impact on soil and atmospheric microclimate, and crop productivity. It involved experimental work in the field on three organic farms and in the laboratory as well as testing of a model of low tunnel air temperature. The most important findings of this research are as follows:

(1)   The total daily (24-h) soil heat flux density at the soil surface (G) covered with plastic film mulch strongly correlated with total daily downwelling solar radiation (S_d). On a daily basis, all of the plastic films studied decreased the daily S_d required for daily G to become positive when compared to the control (bare soil) (which required 17.6 MJ m^{-2}), ranging from 9.4 MJ m^{-2} (TMX; τ_s, 0.82; α_L, 0.63) to 16.6 MJ m^{-2} (WB; ρ_s, 0.45; α_L, 0.58). The film with the highest shortwave reflectivity (WB; ρ_s, 0.45; α_L, 0.58) caused G and T_{s2cm} to have values less than the control (i.e., bare soil), but only under cloud-free conditions at midday. Overall, films with high τ_s and α_L values (TMX, S4 and GN) resulted in the greatest increases in G, and films with high α_s and low α_L (BEP, BW and RD) resulted in the next greatest increases in G. Comparison of films with very high α_s values (i.e., black plastics) and different α_L values showed that films with high α_s and low α_L values (BEP and BW) resulted in greater heating than films with high α_s and high α_L values (BE2).

(2)   Low tunnels that are covered with high α_L (i.e., high emissivity) plastic films result in higher R_{nin} in comparison to low tunnels covered with a low-α_L film, during both the daytime and nighttime. Since τ_s of commercial plastic film covers isless than 1, increased R_{nin}

176

due to high α_L helps to compensate for shortwave radiation that is reflected or absorbed by the low tunnel cover.

(3)   Placing a low tunnel over a soil surface already covered by a plastic film mulch did not increase G. This indicates that the effect of a second layer of plastic film (i.e., the low tunnel) has a negligible effect on G and consequently on soil warming.

(4)   The relationship between the heat transfer coefficient obtained for the outer surface of the low tunnel wall (h_{wou}) and 2-m wind speed (u_{2m}) clearly showed that previous equations that do not account for the bluff body effect of a low tunnel underestimate h_{wou}.

(5)   The net radiation in a low tunnel (R_{nin}) with a plastic film mulch floor can be calculated using external radiative forcing variables, plastic film spectral properties (cover and mulch) and surface temperatures of the cover and mulch. Air temperature inside a plastic film low tunnel (T_{ain}), with a plastic film mulch floor, can be estimated using a model that requires knowledge of the values of u_{2m} (for the external heat transfer coefficient), external radiative forcing variables, plastic film spectral properties (cover and mulch), measured or modelled G and a fixed internal transfer coefficient.

(6)   The shortwave transmissivity (τ_s) values of low tunnel covers were very similar to the laboratory-measured values, but they varied in response to condensation and solar angle. Condensation caused large reductions in cover τ_s but a film with anti-drip properties (TMX) maintained a field measured τ_s value that was very close to its laboratory-measured value.

(7)   In comparison to a vegetation-free low tunnel (POLY$_{EMP}$), in which latent heat flux was zero, low tunnels that contained vegetation (e.g, peppers) reduced mid-day tunnel air temperature (T_{ain}) up to 10°C in mid growing season due to evaporative cooling. Net

photosynthesis (P_N) and stomatal conductance (g_s) for sunlit leaves was significantly higher for peppers grown inside vs. outside low tunnels, but P_N and g_s of shaded leaves was not significantly different for peppers grown inside vs outside low tunnels. Pepper plants grown inside low tunnels showed significantly greater height and leaf area index than peppers grown outside. Peppers grown inside low tunnels had 10% more cumulative yield than peppers grown outside, which was due to an extended late growing season (~2 weeks). Despite being more productive inside low tunnels, peppers can deplete CO_2 and increase water vapour density inside low tunnels, which may reduce crop growth.

(8)   A comparison of summer squash grown on black plastic mulch and black plastic with a perforated low tunnel showed that dry mass growth rate, leaf area, and number of fruit harvested were higher by 113%, 20%, and 27%, respectively, in the low tunnel treatment (Appendix E). A comparison of broccoli yield in two consecutive years, 2016 (with no tunnels) and 2017 (with tunnels), showed that broccoli yield nearly doubled in 2017 compared to 2016. The reason for the increased yield is not definitive but was attributed to wind protection in the early growing season, which maintained adequate soil moisture in the low tunnels and increase T_{ain} during a cool summer caused by smoke-filled skies in BC (Appendix D).

This thesis provides novel insights regarding the impact of plastic film radiative properties on soil and atmospheric microclimate when they are used as soil mulch or as low tunnel covers, respectively, as well as their impact on crop growth and productivity. Chapter 2 clearly demonstrates the potential of plastic film mulches to increase growing-season length by increasing G and T_s, even for plastic films meant to cool the soil (i.e., high shortwave reflectivity films), by quantifying the minimum downwelling shortwave radiation required for a plastic

covered soil to achieve positive total daily G, which has not been clearly quantified by previous research. Also, Chapter 2 shows that plastic film mulches with high shortwave transmissivity benefit (i.e., experience increased G and T_s) from having a high longwave absorptivity, which was known, but plastic film mulches with high shortwave absorptivity (i.e., black plastic films) benefit from having a high longwave transmissivity, which was not known.

Chapter 3 shows that adding a low tunnel to a soil that is already covered with a plastic film mulch does not cause any additional increase in G or T_s, which is an unexpected and novel finding. Also, Chapter 3 shows that the air temperature inside a low tunnel, with a plastic film mulch floor, can be accurately predicted with a model that requires the mulch and low tunnel cover spectral properties and external radiative forcing variables (i.e., downwelling shortwave and longwave radiation) to be known. To the best of the authors knowledge, the model validation in Chapter 3 represent the first instance in which the model has been used and validated for low tunnels. Finally, the fact that the empirical relationship found between 2-m wind speed (u_{2m}) vs. h_{wou} in Chapter 3 agrees well with similar relationships found for miniaturized greenhouses inside wind-tunnels (i.e., models), represents a novel linkage between a "controlled scenario" (i.e., wind-tunnels) and "the real world" (i.e., field studies).

With regards to the impact of low tunnels on crop growth and productivity (Chapter 4, Appendix D and Appendix E), this thesis shows that low tunnels can increase crop growth and productivity (e.g., peppers, summer squash and broccoli). On the other hand, Chapter 4 shows that there are drawbacks associated with using low tunnels, CO2 depletion and increased water vapour density (i.e., condensation), that can counteract the potential benefits of low tunnels. If these drawbacks are overcome, hopefully with passive and affordable technologies, the benefits of using low tunnels could increase. Currently, to the best of the authors knowledge, there are no

field studies that examine the impact of low tunnels on pepper growth and productivity in combination with detailed and continuous microclimate monitoring. As a result, Chapter 4 represents a novel approach to studying low tunnel cropping systems and provides new insights and data into the complexity of low tunnel microclimate.

Further experimental and modeling work is required to advance the use of mulches and low tunnels in horticulture. Experiments aimed at quantifying crop growth in the early growing season is required to assess the effectiveness of mulches and low tunnels in extending the growing season. This is an important issue in northern BC. Experiments aimed at careful assessment of the effects of condensation on the underside of the cover on shortwave and longwave radiation properties is urgently needed. This is important in relation to crop temperature (daytime and nighttime) and light for photosynthesis. More work is required to determine the roles of forced and free convection inside the low tunnel - particularly how they affect the heat transfer coefficients inside the tunnel. This will help understand how they vary diurnally and seasonally, and whether floor and wall transfer coefficients can be assumed to be the same. It would be desirable to investigate the most economical and passive way of ventilating the tunnel to prevent excessive heat and humidity build up and depletion of CO_2.

The next important step in developing the low tunnel air temperature model described in Chapter 3 is the inclusion of evaporative cooling resulting from a growing crop. This will require a stomatal conductance sub-model and a growth sub-model to account for changes in stomatal behavior and leaf area index, respectively. The model also requires a ventilation sub-model to better account for the effect of air exchange between the low tunnel and the atmosphere. The model will be valuable in helping growers estimate expected temperature rises as well as in explaining different effects of different films, e.g., why IRT100 results in less soil heat flux than

GN even though their shortwave and longwave properties are quite similar. In the case of plastic film mulches, a model is required to estimate the course of soil temperature over the growing season and particularly early in the growing season. It would have to account for the variable contact resistance between the mulch and the soil in the case of high shortwave radiation absorptivity (e.g., black) films and radiation trapping beneath the mulch in the case of high shortwave transmissivity films (e.g., TMX).

Other issues requiring attention include recovery and storage of low tunnel and mulch films at the end of the growing for future use and modification of hoop structures to permit raising the low tunnel to accommodate increased crop height. Examination of other cover and mulch materials such as polypropylene fabrics which allow for the diffusion of CO_2 and penetration of rainfall is recommended for future research.

References

Acharya, T. P., Welbaum, G. E., and Arancibia, R. A. (2019). Low tunnels reduce irrigation water needs and increase growth, yield, and water-use efficiency in Brussels sprouts production. *Hortscience, 54*(3), 470-475. doi:10.21273/HORTSCI13568-18

Al Khatib, B. M., Sleyman, A. S., Freiwat, M. M., Knio, K. M. and Rubeiz, I.G. 2001. Mulch type effects on strawberries grown in a mild winter climate. *Small Fruits Review*, 1:4, 51-61, DOI: 10.1300/J301v01n04_06

Al-Mahdouri, A., Baneshi, M., Gonome, H., Okajima, J., and Maruyama, S. (2013). Evaluation of optical properties and thermal performances of different greenhouse covering materials. *Solar Energy*, 96, 21-32. doi:10.1016/j.solener.2013.06.029

Al-Mahdouri, A., Gonome, H., Okajima, J., and Maruyama, S. (2014). Theoretical and experimental study of solar thermal performance of different greenhouse cladding materials. *Solar Energy, 107*, 314-327. doi:10.1016/j.solener.2014.05.006

Aniekwe, N.L. (2013). Comparative effects of organic and plastic mulches on the environment, growth and yield of okra in a derived savanna zone of Nigeria. *International Journal of Science and Research*, *4*(1), 1860-1864.

ASHRAE Handbook of Fundamentals. 1972, American Society of Heating, Refrigeration and Air-Conditioning Engineers, New York, NY. pp. 43.

Astrup, T., Fruergaard, T., and Christensen, T. H. (2009). Recycling of plastic: Accounting of greenhouse gases and global warming contributions. *Waste Management and Research, 27*(8), 763-772.

Baille, A., Kittas, C., and Katsoulas, N. (2001). Influence of whitening on greenhouse microclimate and crop energy partitioning. *Agricultural and Forest Meteorology, 107*(4), 293-306. doi:10.1016/S0168-1923(01)00216-7

Bakker, J. C. (1991). Leaf conductance of four glasshouse vegetable crops as affected by air humidity. *Agricultural and Forest Meteorology, 55*(1), 23-36.

Baumann, T. E., Eaton, G. W., and Spaner, D. (1997). Production of short-day strawberries on raised beds in British Columbia. *Journal of Small Fruit and Viticulture, 5*(1), 37-49. doi:10.1300/J065v05n01_03

BC Ministry of Environment 2016. Indicators of Climate Change for British Columbia. 61 pp.

Bonachela, S., Granados, M. R., López, J. C., Hernández, J., Magán, J. J., Baeza, E. J., and Baille, A. (2012). How plastic mulches affect the thermal and radiative microclimate in an unheated low-cost greenhouse. *Agricultural and Forest Meteorology, 152*, 65-72. doi:10.1016/j.agrformet.2011.09.006

Bornt, C. D., Loy, J. B., Lord, W. G., and Wells, O. S. (1998). A revolution in New England: New Hampshire develops an annual strawberry production system. *Hortscience, 33*(2), 203.

Boulard, T., and Baille, A. (1987). Analysis of thermal performance of a greenhouse as a solar collector. *Energy in Agriculture*, *6*(1), 17-26. doi:10.1016/0167-5826(87)90018-0

Boulard, T., Papadakis, G., Kittas, C., and Mermier, M. (1997). Air flow and associated sensible heat exchanges in a naturally ventilated greenhouse. *Agricultural and Forest Meteorology, 88*(1), 111-119.

Boulard, T., Wang, S., and Haxaire, R. (2000). Mean and turbulent air flows and microclimatic patterns in an empty greenhouse tunnel. *Agricultural and Forest Meteorology, 100*(2), 169-181.

Brandenberger, L., and Wiedenfeld, B. (1997). Physical characteristics of mulches and their impact on crop response and profitability in muskmelon production. *Horttechnology, 7*(2), 165.

Brault, D., Stewart, K. A., and Jenni, S. (2002). Optical properties of paper and polyethylene mulches used for weed control in lettuce. *Hortscience, 37*(1), 87-91.

Bristow, K. L., Campbell, G. S., Papendick, R. I., and Elliott, L. F. (1986). Simulation of heat and moisture transfer through a surface residue—soil system. *Agricultural and Forest Meteorology, 36*(3), 193-214.

Burrows, R.L., and Reese, R.N. 2007. Plastic mulch color effects on Echinacea growth, survival, and root phenolic marker compounds. Proceeding of the South Dakota Academy of Science, *86*, 55-58.

Businger J.A. (1963). The glasshouse (greenhouse) climate. W.A. van Wijk (Ed.), Physics of Plant Environment, North Holland Publishing Co., The Netherlands

Cabrera, F. J., Baille, A., López, J. C., González-Real, M. M., and Pérez-Parra, J. (2009). Effects of cover diffusive properties on the components of greenhouse solar radiation. *Biosystems Engineering*, *103*(3), 344-356. doi:10.1016/j.biosystemseng.2009.03.008

Campra, P., Garcia, M., Canton, Y., and Palacios-Orueta, A. (2008). Surface temperature cooling trends and negative radiative forcing due to land use change toward greenhouse farming in Southeastern Spain. *Journal of Geophysical Research - Atmospheres, 113*(D18), D18109. doi:10.1029/2008JD009912

Cantin, D., Tremblay, M. F., Lechowicz, M. J., and Potvin, C. (1997). Effects of CO2 enrichment, elevated temperature, and nitrogen availability on the growth and gas exchange of different families of Jack Pine seedlings. *Canadian Journal of Forest Research, 27*(4), 510-520. doi:10.1139/x96-221

CGU and CSAFM Joint Annual Scientific Meeting, Vancouver, BC, May 28-31.

Chandra, S., Lata, H., Khan, I. A., and Elsohly, M. A. (2008). Photosynthetic response of cannabis sativa L. to variations in photosynthetic photon flux densities, temperature and CO2 conditions. *Physiology and Molecular Biology of Plants, 14*(4), 299-306. doi:10.1007/s12298-008-0027-x

Cohen, O., Riov, J., Katan, J., Gamliel, A., and Kutiel, P. B. (2008). Reducing persistent seed banks of invasive plants by soil solarization—The case of acacia saligna. *Weed Science, 56*(6), 860-865. doi:10.1614/WS-08-073.1

Ćosić, M., Stričević, R., Djurović, N., Moravčević, D., Pavlović, M., and Todorović, M. (2017). Predicting biomass and yield of sweet pepper grown with and without plastic film mulching under different water supply and weather conditions. *Agricultural Water Management, 188*, 91-100. doi:10.1016/j.agwat.2017.04.006

Cózar, A., Echevarría, F., González-Gordillo, J. I., Irigoien, X., Úbeda, B., Hernández-León, S., et al. (2014). Plastic debris in the open ocean. *Proceedings of the National Academy of Sciences of the United States of America, 111*(28), 10239-10244.

Craig, D.S., and Runkle, E.S., 2013. A moderate to high red to far-red light ratio from light-emitting diodes controls flowering of short-day plants. *J. Amer. Soc. Hort. Sci.*, *138*(3), 167-172.

Critten, D., and Bailey, B. (2002). A review of greenhouse engineering developments during the 1990s. *Agricultural and Forest Meteorology, 112*(1), 1-22.

Cuello, J. P., Hwang, H. Y., Gutierrez, J., Kim, S. Y., and Kim, P. J. (2015). Impact of plastic film mulching on increasing greenhouse gas emissions in temperate upland soil during maize cultivation. *Applied Soil Ecology, 91*, 48-57. doi:10.1016/j.apsoil.2015.02.007

Culman, S. W., Duxbury, J. M., Lauren, J. G., and Thies, J. E. (2006). Microbial community response to soil solarization in Nepal's rice–wheat cropping system. *Soil Biology and Biochemistry, 38*(12), 3359-3371. doi:10.1016/j.soilbio.2006.04.053

Darko E., Heydarizadeh P., Schoefs B., and Sabzalian M.R. 2014. Photosynthesis under artificial light: the shift in primary and secondary metabolism. *Phil. Trans. R. Soc. B369*: 20130243. http://dx.doi.org/10.1098/rstb.2013.0243

David K. A. Barnes, Galgani, F., Thompson, R. C., and Barlaz, M. (2009). Accumulation and fragmentation of plastic debris in global environments. *Philosophical Transactions of the Royal Society B: Biological Sciences*, *364* (1526), 1985-1998. doi:10.1098/rstb.2008.0205

Decoteau, D. R., Kasperbauer, M. J., Daniels, D. D., and Hunt, P. G. (1988). Plastic mulch color effects on reflected light and tomato plant growth. *Scientia Horticulturae*, 34(3), 169-175. doi:10.1016/0304-4238(88)90089-1

Diaz, F., Jimenez, C.C., and Tejedor, M. 2005 Influence of the thickness and grain size of tephra mulch on soil water evaporation. *Agricultural Water Management, 74*, 47-55.

Diffey, B. (2015). Solar spectral irradiance and summary outputs using excel. *Photochemistry and Photobiology, 91*(3), 553-557. doi:10.1111/php.12422

Dlamini, P., Ukoh, I. B., van Rensburg, L. D., and Du Preez, C. C. (2017). Reduction of evaporation from bare soil using plastic and gravel mulches and assessment of gravel mulch for partitioning evapotranspiration under irrigated canola. *Soil Research, 55*(3), 222. doi:10.1071/SR16098

Egel, D. S., Martyn, R., and Gunter, C. (2008). Planting method, plastic mulch, and fumigation influence growth, yield, and root structure of watermelon. *Hortscience, 43*(5), 1410-1414.

Emmert, E.M. 1954. University of Kentucky builds a greenhouse covered with polyethylene. Ag N. Letter 22:92-93.

Emmert, E.M. 1955. Low-cost plastic greenhouses. Kentucky Agr. Expt. St. Progress Report 28.

Emmert, E.M. 1956. Plastic row covering. Kentucky Farm and Home Science. Spring 2(2):6-7.

Enoch, H. Z., Rylski, I., and Spigelman, M. (1976). CO_2 enrichment of strawberry and cucumber plants grown in unheated greenhouses in Israel. *Scientia Horticulturae, 5*(1), 33-41. doi:10.1016/0304-4238(76)90020-0

Eriksen, M., Lebreton, L., Carson, H., Thiel, M., Moore, C., Borerro, J., et al. (2014). Plastic pollution in the world's oceans: More than 5 trillion plastic pieces weighing over 250,000 tons afloat at sea. *Plos One, 9*(12), e111913.

Espí, E., Salmerón, A., Fontecha, A., García, Y., and Real, A. I. (2006). PLastic films for agricultural applications. *Journal of Plastic Film and Sheeting, 22*(2), 85-102.

Faivor, R. M. S. (2014). *Low tunnel strategies for microclimate modification and early vegetable production* (Master's thesis).

Fan, X., Chen, H., Xia, X., and Yu, Y. (2015). Increase in surface albedo caused by agricultural plastic film. *Atmospheric Science Letters, 16*(3), 291-296. doi:10.1002/asl2.556

Fan, Y., Ding, R., Kang, S., Hao, X., Du, T., Tong, L., and Li, S. (2017). Plastic mulch decreases available energy and evapotranspiration and improves yield and water use efficiency in an irrigated maize cropland. *Agricultural Water Management, 179*, 122-131. doi:10.1016/j.agwat.2016.08.019

Farzi, R., Gholami, M., Baninasab, B., Gheysari, M., and Varennes, A. (2017). Evaluation of different mulch materials for reducing soil surface evaporation in semi-arid region. *Soil use and Management, 33*(1), 120-128.

Fatnassi, H., Boulard, T., and Lagier, J. (2004). Simple indirect estimation of ventilation and crop transpiration rates in a greenhouse. *Biosystems Engineering, 88*(4), 467-478. doi:10.1016/j.biosystemseng.2004.05.003

Fierro, A., Gosselin, A., and Tremblay, N. (1994). Supplemental carbon dioxide and light improved tomato and pepper seedling growth and yield. *Hortscience, 29*(3), 152-154. doi:10.21273/HORTSCI.29.3.152

Fuchs, M., and Hadas, A. (2011). Mulch resistance to water vapor transport. *Agricultural Water Management, 98*(6), 990-998.

Fuchs, M., Dayan, E., and Presnov, E. (2006). Evaporative cooling of a ventilated greenhouse rose crop. *Agricultural and Forest Meteorology, 138*(1), 203-215.

Fuchs, M., Dayan, E., Shmuel, D., and Zipori, I. (1997). Effects of ventilation on the energy balance of a greenhouse with bare soil. *Agricultural and Forest Meteorology, 86*(3), 273-282.

Garzoli, K. V., and Blackwell, J. (1981). An analysis of the nocturnal heat loss from a single skin plastic greenhouse. *Journal of Agricultural Engineering Research, 26*(3), 203-214. doi:10.1016/0021-8634(81)90105-0

Geoola, F., and Peiper, U. M. (1994). Outdoor testing of the condensation characteristics of plastic film covering materials using a model greenhouse. *Journal of Agricultural Engineering Research, 57*(3), 167-172. doi:10.1006/jaer.1994.1016

Geoola, F., Kashti, Y., and Peiper, U. M. (1998). A model greenhouse for testing the role of condensation, dust and dirt on the solar radiation transmissivity of greenhouse cladding materials. *Journal of Agricultural Engineering Research, 71*(4), 339-346. doi:10.1006/jaer.1998.0333

Gerber, J. M., Mohd-Khir, I., and Splittstoesser, W. E. (1988). Row tunnel effects on growth, yield and fruit quality of bell pepper. *Scientia Horticulturae, 36*(3), 191-197. doi:10.1016/0304-4238(88)90053-2

Ghosal, M. K., and Tiwari, G. N. (2006). Modeling and parametric studies for thermal performance of an earth to air heat exchanger integrated with a greenhouse. *Energy Conversion and Management, 47*(13), 1779-1798.

Ghosal, M. K., Tiwari, G. N., and Srivastava, N. S. L. (2003). Modeling and experimental validation of a greenhouse with evaporative cooling by moving water film over external shade cloth. *Energy and Buildings, 35*(8), 843-850.

Ghosal, M. K., Tiwari, G. N., and Srivastava, N. S. L. (2004). Thermal modeling of a greenhouse with an integrated earth to air heat exchanger: An experimental validation. *Energy and Buildings, 36*(3), 219-227.

Graefe, J., and Sandmann, M. (2015). Shortwave radiation transfer through a plant canopy covered by single and double layers of plastic. *Agricultural and Forest Meteorology, 201*, 196-208. doi:10.1016/j.agrformet.2014.10.011

Groenevelt, P. H., van Straaten, P., Rasiah, V., and Simpson, J. (1989). Modifications in evaporation parameters by rock mulches. *Soil Technology, 2*(3), 279-285.

Gulik D. Van., 1910. Iets over het gebruik van glas in broeikassen. Meded. v. d. R.H.L.T.B., deel III (1910), p. 108-118.

Ham, J. M., and Heilman, J. L. (1991). Aerodynamic and surface resistances affecting energy transport in a sparse crop. *Agricultural and Forest Meteorology, 53*(4), 267-284.

Ham, J. M., and Kluitenberg, G. J. (1994). Modeling the effect of mulch optical properties and mulch-soil contact resistance on soil heating under plastic mulch culture. *Agricultural and Forest Meteorology, 71*(3), 403-424. doi:10.1016/0168-1923(94)90022-1

Ham, J. M., Kluitenberg, G. J., and Lamont, W. J. (1993). Optical properties of plastic mulches affect the field temperature regime. *Journal of the American Society for Horticultural Science, 118*(2), 188.

Han, J. (2015). Comparison of greenhouse dehumidification strategies in cold regions. *Applied Engineering in Agriculture, 31*(1), 133-142. doi:10.13031/aea.31.10723

Hanson, K. J. (1963). The radiative effectiveness of plastic films for greenhouses. *Journal of Applied Meteorology (1962-1982), 2*(6), 793-797. doi:10.1175/1520-0450(1963)002<0793:TREOPF>2.0.CO;2

Hares, M. A., and Novak, M. D. (1992). Simulation of surface energy balance and soil temperature under strip tillage: II. field test. *Soil Science Society of America Journal, 56*(1), 29. doi:10.2136/sssaj1992.03615995005600010004x

Hermida-Carrera, C., Kapralov, M. V., and Galmés, J. (2016). Rubisco catalytic properties and temperature response in crops. *Plant Physiology, 171*(4), 2549.

Hilker, T., Coops, N. C., Schwalm, C. R., Jassal, R. S., Black, T. A., and Krishnan, P. (2008). Effects of mutual shading of tree crowns on prediction of photosynthetic light-use efficiency in a coastal douglas-fir forest. *Tree Physiology, 28*(6), 825-834. doi:10.1093/treephys/28.6.825

Hopfenberg, H. B., SpringerLINK eBooks - English/International Collection (Archive), and SpringerLink (Online service). (1974). *Permeability of plastic films and coatings to gases, vapors, and liquids.* Boston, MA: Springer US. doi:10.1007/978-1-4684-2877-3

Huang, Z., Huang, Y., Chen, L., Fu, B., and Gong, J. (2005). The wheat yields and water-use efficiency in the loess plateau: Straw mulch and irrigation effects. *Agricultural Water Management, 72*(3), 209-222.

Hunter, B., Drost, D., Black, B., and Ward, R. (2012). Improving growth and productivity of early-season high-tunnel tomatoes with targeted temperature additions. *Hortscience, 47*(6), 733-740.

Ibarra, L., Flores, J., and Díaz-Pérez, J. C. (2001). Growth and yield of muskmelon in response to plastic mulch and row covers. *Scientia Horticulturae, 87*(1), 139-145. doi:10.1016/S0304-4238(00)00172-2

Ihara, H., Kato, N., Takahashi, S., and Nagaoka, K. (2014). Effect of soil solarization on subsequent nitrification activity at elevated temperatures. *Soil Science and Plant Nutrition, 60*(6), 824-831. doi:10.1080/00380768.2014.947233

Iqbal, M., and Khatry, A. K. (1977). Wind-induced heat transfer coefficients from glasshouses. *Transactions of the ASAE, 20*(1), 157-160. doi:10.13031/2013.35513

Ivanochko, G. (1987). *Effect of row covers on maturity and yield of field tomatoes* (Master's Thesis).

Jaffrin A; Makhlouf S (1990). Mechanism of light transmission through wet polymer films. *Acta Horticulturae, 281*, 11–24.

Jiang, W., Qu, D., Mu, D., and Wang, L. (2003; 2010). Protected cultivation of horticultural crops in china. *Horticultural reviews* (pp. 115-162) John Wiley and Sons, Inc.

Jin, C., Du, S., Wang, Y., Condon, J., Lin, X., and Zhang, Y. (2009). Carbon dioxide enrichment by composting in greenhouses and its effect on vegetable production. *Journal of Plant Nutrition and Soil Science, 172*(3), 418-424. doi:10.1002/jpln.200700220

Jolliffe, P. A., and Gaye, M. (1995). Dynamics of growth and yield component responses of Bell peppers (*Capsicum annuum* L.) to row covers and population density. *Scientia Horticulturae, 62*(3), 153-164. doi:10.1016/0304-4238(95)00766-M

Jones, H., Black, T., Jassal, R., Nesic, Z., Grant, N., Bhatti, J., et al. (2017). Water balance, surface conductance and water use efficiency of two young hybrid-poplar plantations in canada's aspen parkland. *Agricultural and Forest Meteorology, 246*, 256-271.

Kang, D. H., Gao, H., Shi, X., Islam, S. U., and Déry, S. J. (2016). Impacts of a rapidly declining mountain snowpack on streamflow timing in Canada's Fraser river basin. *Scientific Reports, 6*, 19299-19299. doi:10.1038/srep19299

Katan, J. (2015). Soil solarization: The idea, the research and its development. *Phytoparasitica, 43*(1), 1-4. doi:10.1007/s12600-014-0419-0

Katsoulas, N., Baille, A., and Kittas, C. (2001). Effect of misting on transpiration and conductances of a greenhouse rose canopy. *Agricultural and Forest Meteorology, 106*(3), 233-247.

Kittas, C., and Bartzanas, T. (2007). Greenhouse microclimate and dehumidification effectiveness under different ventilator configurations. *Building and Environment, 42*(10), 3774-3784. doi:10.1016/j.buildenv.2006.06.020

Kittas, C., Bartzanas, T., and Jaffrin, A. (2003). Temperature gradients in a partially shaded large greenhouse equipped with evaporative cooling pads. *Biosystems Engineering, 85*(1), 87-94.

Kläring, H. -., Hauschild, C., Heißner, A., and Bar-Yosef, B. (2007). Model-based control of CO_2 concentration in greenhouses at ambient levels increases cucumber yield. *Agricultural and Forest Meteorology, 143*(3-4), 208-216. doi:10.1016/j.agrformet.2006.12.002

Komariah, Ito, K., Onishi, T., and Senge, M. (2011). Soil properties affected by combinations of soil solarization and organic amendment. *Paddy and Water Environment, 9*(3), 357-366. doi:10.1007/s10333-011-0253-7

Kreith, F. (1965), *Principles of Heat Transfer*, Intern. Textbook Co., Pa.

Kumar, K. S., Tiwari, K. N., and Jha, M. K. (2009). Design and technology for greenhouse cooling in tropical and subtropical regions: A review. *Energy and Buildings, 41*(12), 1269-1275. doi:10.1016/j.enbuild.2009.08.003

Kurata, K. (1990). Role of reflection in light transmissivity of greenhouses. *Agricultural and Forest Meteorology, 52*(3), 319-331. doi:10.1016/0168-1923(90)90089-O

Kwabiah, A. B. (2004). Growth and yield of sweet corn (*Zea mays* L.) cultivars in response to planting date and plastic mulch in a short-season environment. *Scientia Horticulturae, 102*(2), 147-166. doi:10.1016/j.scienta.2004.01.007

Lamont, W. J. (2005). Plastics: Modifying the Microclimate for the Production of Vegetable Crops. *Horticulture Technology, 15(3):* 477-481

Lamrani, M.A., Boulard, T., Roy, J.C., Jaffrin, A. (2001). SE-structures and environment AirFlows and temperature patterns induced in a confined greenhouse. *Journal of Agricultural Engineering Research, 28*(1), 75-88.

Lee, J., Gryze, S., and Six, J. (2011). Effect of climate change on field crop production in California's central valley. *Climatic Change, 109*(1), 335. doi:10.1007/s10584-011-0305-4

Lee, R. (1973). The "Greenhouse" effect. *Journal of Applied Meteorology, 12*(3), 556-557.

Lewers K. S., Fleisher, D. H., Daughtry C. S. T. (2017). Low Tunnels as a Strawberry Breeding Tool and Season-Extending Production System. *International Journal of Fruit Science, 17(3):* 233-258

Li, D., Li, Y., Ding, Y., and Miao, Z. (2018). Automatic carbon dioxide enrichment strategies in the greenhouse: A review. *Biosystems Engineering, 171*, 101-119. doi:10.1016/j.biosystemseng.2018.04.018

Li, F., Guo, A., and Wei, H. (1999). Effects of clear plastic film mulch on yield of spring wheat. *Field Crops Research, 63*(1), 79-86.

Li, N., Tian, F., Hu, H., Lu, H., and Ming, G. (2016). Effects of plastic mulch on soil heat flux and energy balance in a cotton field in northwest China. *Atmosphere, 7*(8), 107. doi:10.3390/atmos7080107

Li, S., Kang, S., Zhang, L., Ortega-Farias, S., Li, F., Du, T., et al. (2013). Measuring and modeling maize evapotranspiration under plastic film-mulching condition. *Journal of Hydrology*, 503, 153-168.

Li, T., Heuvelink, E., Dueck, T. A., Janse, J., Gort, G., and Marcelis, L. F. M. (2014). Enhancement of crop photosynthesis by diffuse light: Quantifying the contributing factors. *Annals of Botany, 114*(1), 145-156. doi:10.1093/aob/mcu071

Liakatas, A., Clark, J. A., and Monteith, J. L. (1986). Measurements of the heat balance under plastic mulches. part I. radiation balance and soil heat flux. *Agricultural and Forest Meteorology, 36*(3), 227-239. doi:10.1016/0168-1923(86)90037-7

Liang, Y., Wu, X., Zhu, J., Zhou, M., and Peng, Q. (2011). Response of hot pepper (*Capsicum annuum* L.) to mulching practices under planted greenhouse condition. *Agricultural Water Management, 99*(1), 111-120. doi:10.1016/j.agwat.2011.07.010

Lightfoot, D. R. (1996). The nature, history, and distribution of lithic mulch agriculture: An ancient technique of dryland agriculture. *The Agricultural History Review, 44*(2), 206-222.

Lightfoot, D. R., and Eddy, F. W. (1995). The construction and configuration of Anasazi pebble-mulch gardens in the Northern Rio Grande. *American Antiquity, 60*(3), 459-470. doi:10.2307/282259

Liu, J., Bu, L., Zhu, L., Luo, S., Chen, X., and Li, S. (2014). Optimizing plant density and plastic film mulch to increase maize productivity and water-use efficiency in semiarid areas. *Agronomy Journal, 106*(4), 1138-1146.

Lopez-Lopez, R., Inzunza-Ibarra, M., Sanchez-Cohen, I., Fierro-Alvarez, A., and Sifuentes-Ibarra, E. (2015). Water use efficiency and productivity of habanero pepper (*Capsicum chinense* Jacq.) based on two transplanting dates. *Water Science and Technology, 71*(6), 885-891. doi:10.2166/wst.2015.040

Mahrer, Y., Avissar, R., Naot, O., and Katan, J. 1987. Intensified soil solarization with closed greenhouses: Numerical and experimental studies. *Agricultural and Forest Meteorology*, *41*, 325-334.

Makowski, D., Asseng, S., Ewert, F., Bassu, S., Durand, J. L., Li, T., et al. (2015). A statistical analysis of three ensembles of crop model responses to temperature and CO2 concentration. *Agricultural and Forest Meteorology, 214-215*, 483-493.

Mariani, L., Cola, G., Bulgari, R., Ferrante, A., and Martinetti, L. (2016). Space and time variability of heating requirements for greenhouse tomato production in the euro-mediterranean area. *Science of the Total Environment, 562*, 834-844.

Markarian, J. (2006). Design trends in colour and effects push plastics forward. *Plastics, Additives and Compounding, 8*(3), 14,16,18,20-14,16,18,21.

Mashonjowa, E., Ronsse, F., Mhizha, T., Milford, J. R., Lemeur, R., and Pieters, J. G. (2010). The effects of whitening and dust accumulation on the microclimate and canopy behaviour of rose plants (*Rosa hybrida*) in a greenhouse in Zimbabwe. *Solar Energy, 84*(1), 10-23. doi:10.1016/j.solener.2009.09.004

McAdams, W. H., and National Research Council (U.S.). Committee on Heat Transmission. (1942). Heat transmission (2d, rev. and enl. ed.). London; New York: McGraw-Hill Book Company, Inc.

McCraw D, Motes JE (1991) Use of plastic mulch and row covers in vegetable production. Cooperative Extension Service. Oklahoma State University. OSU Extension Facts F-6034

Mellouli, H. J., van Wesemael, B., Poesen, J., and Hartmann, R. (2000). Evaporation losses from bare soils as influenced by cultivation techniques in semi-arid regions. *Agricultural Water Management, 42*(3), 355-369.

Mereu, V., Carboni, G., Gallo, A., Cervigni, R., and Spano, D. (2015). Impact of climate change on staple food crop production in Nigeria. *Climatic Change, 132*(2), 321-336. doi:10.1007/s10584-015-1428-9

Meyer, G. E., Paparozzi, E. T., A.Walter-Shea, E., Blankenship, E. E., and Adams, S. A. (2012). An investigation of reflective mulches for use over capillary mat systems for winter-time greenhouse strawberry production. *Applied Engineering in Agriculture, 28*(2), 271-279. doi:10.13031/2013.41345

Miao, L., Zhang, Y., Zhang, H., Zhang, Z., Yang, X., Xiao, J., and Jiang, G. (2016). Colored light-quality selective plastic films affect anthocyanin content, enzyme activities, and the expression of flavonoid genes in strawberry (*Fragaria×ananassa*) fruit. *Food Chemistry, 207*, 93-100. doi:10.1016/j.foodchem.2016.02.077

Modaihsh, A. S., Horton, R., and Kirkham, D. (1985). Soil water evaporation suppression by sand mulches. *Soil Science, 139*(4), 357-361.

Monteith, J. L., and Unsworth, M. H. (2013). Principles of environmental physics, 4th edition. Elsevier, London.

Mortensen, L. M. (1987). Review: CO_2 enrichment in greenhouses. crop responses. *Scientia Horticulturae, 33*(1), 1-25. doi:10.1016/0304-4238(87)90028-8

Mukherjee, A., Kundu, M., and Sarkar, S. (2010). Role of irrigation and mulch on yield, evapotranspiration rate and water use pattern of tomato (*Lycopersicon esculentum* L.). *Agricultural Water Management, 98*(1), 182-189. doi:10.1016/j.agwat.2010.08.018

Muñoz, I., Campra, P., and Fernández-Alba, A. R. (2010). Including CO_2-emission equivalence of changes in land surface albedo in life cycle assessment. methodology and case study on greenhouse agriculture. *The International Journal of Life Cycle Assessment, 15*(7), 672-681. doi:10.1007/s11367-010-0202-5

Murase, J., Shinohara, Y., Yokoe, K., Matsuda, R., Asakawa, S., and Hashimoto, T. (2015). Impact of soil solarization on the ciliate community structure of a greenhouse soil. *Soil Science and Plant Nutrition, 61*(6), 927-933. doi:10.1080/00380768.2015.1079799

NAL Digital Repository.Microclimate modification with plastic mulch. *Microclimate Modification with Plastic Mulch,*

Nan, W., Yue, S., Huang, H., Li, S., and Shen, Y. (2016). Effects of plastic film mulching on soil greenhouse gases (CO_2, CH_4 and N_2O) concentration within soil profiles in maize fields on the loess plateau, China. *Journal of Integrative Agriculture, 15*(2), 451-464. doi:10.1016/S2095-3119(15)61106-6

Ngouajio, M., and Ernest, J. (2004). Light transmission through colored polyethylene mulches affects weed populations. *Hortscience, 39*(6), 1302.

Ngouajio, M., and Ernest, J. (2005). Changes in the physical, optical, and thermal properties of polyethylene mulches during double cropping. *Hortscience, 40*(1), 94.

Nijskens, J., Deltour, J., Coutisse, S., and Nisen, A. (1984). Heat transfer through covering materials of greenhouses. *Agricultural and Forest Meteorology, 33*(2), 193-214. doi:10.1016/0168-1923(84)90070-4

Novak, M. D., Chen, W., and Hares, M. A. (2000). Simulating the radiation distribution within a barley-straw mulch. *Agricultural and Forest Meteorology, 102*(2), 173-186.

Olesen, J. E., Trnka, M., Kersebaum, K. C., Skjelvåg, A. O., Seguin, B., Peltonen-Sainio, P., . . . Micale, F. (2011). Impacts and adaptation of European crop production systems to climate change. *European Journal of Agronomy, 34*(2), 96-112. doi:10.1016/j.eja.2010.11.003

Overbeck, V., Schmitz-Eiberger, M. A., and Blanke, M. M. (2013). Reflective mulch enhances ripening and health compounds in apple fruit. *Journal of the Science of Food and Agriculture, 93*(10), 2575-2579. doi:10.1002/jsfa.6079

Oz, H., Coskan, A., and Atilgan, A. (2017). Determination of effects of various plastic covers and biofumigation on soil temperature and soil nitrogen form in greenhouse solarization: New solarization cover material. *Journal of Polymers and the Environment, 25*(2), 370-377. doi:10.1007/s10924-016-0819-y

Padrón, R. A. R., Lopes, S. J., Swarowsky, A., Cerquera, R. R., Nogueira, C. U., and Maffei, M. (2016). Non-destructive models to estimate leaf area on bell pepper crop. *Ciência Rural, 46*(11), 1938-1944. doi:10.1590/0103-8478cr20151324

Palonen, P., Pinomaa, A., and Tommila, T. (2017). The influence of high tunnel on yield and berry quality in three floricane raspberry cultivars. *Scientia Horticulturae, 214*, 180-186. doi:10.1016/j.scienta.2016.11.049

Papadakis, G., Briassoulis, D., Scarascia Mugnozza, G., Vox, G., Feuilloley, P., and Stoffers, J. A. (2000). Radiometric and thermal properties of, and testing methods for, greenhouse covering materials. *Journal of Agricultural Engineering Research, 77*, 1-38.

Papadakis, G., Frangoudakis, A., and Kyritsis, S. (1992). Mixed, forced and free-convection heat-transfer ar the greenhouse cover. *Journal of Agricultural Engineering Research, 51*(3), 191-205.

Pieters, J. G., Deltour, J. M., and Debruyckere, M. J. (1997). Light transmission through condensation on glass and polyethylene. *Agricultural and Forest Meteorology, 85*(1), 51-62. doi:10.1016/S0168-1923(96)02393-3

PlasticsEurope, Plastics—The Facts 2016: An Analysis of European Plastics Production, Demand and Waste Data.

Pollet, I. V., and Pieters, J. G. (2002). PAR transmittances of dry and condensate covered glass and plastic greenhouse cladding. *Agricultural and Forest Meteorology, 110*(4), 285-298. doi:10.1016/S0168-1923(01)00295-7

Principles of environmental physics: J.L. Monteith and M.H. Unsworth second edition. London: Edward Arnold, 1990. xii + 291 pages. 30.00 (hardback), 14.95 (paperback). ISBN 0-7131-2931-X. (1991). *Plant Growth Regulation, 10*(2), 177-178. doi:10.1007/BF00024969

Privé, J. P., Russell, L., and Leblanc, A. (2008). Use of extenday reflective groundcover in production of 'gala' apples (*Malus domestica*) in New Brunswick, Canada: 1. impact on canopy microclimate and leaf gas exchange. *New Zealand Journal of Crop and Horticultural Science, 36*(4), 221-231. doi:10.1080/01140670809510238

Qiu, R., Song, J., Du, T., Kang, S., Tong, L., Chen, R., and Wu, L. (2013). Response of evapotranspiration and yield to planting density of solar greenhouse grown tomato in Northwest China. *Agricultural Water Management, 130*, 44-51. doi:10.1016/j.agwat.2013.08.013

Rasmussen, S. C., and SpringerLink ebooks - Chemistry and Materials Science. (2012). *How glass changed the world: The history and chemistry of glass from antiquity to the 13th century* (1. Aufl.; 2012 ed.). New York: Springer. doi:10.1007/978-3-642-28183-9

Rayne, S., and Forest, K. (2016). Rapidly changing climatic conditions for wine grape growing in the Okanagan valley region of British Columbia, Canada. *Science of the Total Environment, 556*, 169-178. doi:10.1016/j.scitotenv.2016.02.200

Retamal-Salgado, J., Bastias, R., Wilckens, R., and Paulino, L. (2015). Influence of microclimatic conditions under high tunnels on the physiological and productive responses in blueberry 'O'neal'. *Chilean Journal of Agricultural Research, 75*(3), 291-297. doi:10.4067/S0718-58392015000400004

Roetzel, W.; Spang, B. VDI Heat Atlas, C3 Typical Values of Overall Heat Transfer Coefficients, Springer Materials. Springer-Verlag: Berlin, Germany, 2010.

Scarascia-Mugnozza, G., Sica, C., and Russo, G. (2012). Plastic materials in european agriculture: Actual use and perspectives. *Journal of Agricultural Engineering, 42*(3), 15-28. doi:10.4081/jae.2011.3.15

Schiefer, E., Menounos, B., and Wheate, R. (2007). Recent volume loss of British Columbian glaciers, canada. *Geophysical Research Letters, 34*(16), L16503-n/a. doi:10.1029/2007GL030780

Schonbeck MW (1995) Mulching practices and innovations for warm season vegetables in Virginia and neighboring states. 1. An informal survey of growers. VA Assoc. Biol. Farming, Blacksburg, 24 pp

Seginer, I., Kantz, D., Peiper, U. M., and Levav, N. (1988). Transfer coefficients of several polyethylene greenhouse covers. *Journal of Agricultural Engineering Research, 39*(1), 19-37. doi:10.1016/0021-8634(88)90163-1

Sethi, V. P., and Sharma, S. K. (2007). Greenhouse heating and cooling using aquifer water. *Energy, 32*(8), 1414-1421.

Shiukhy, S., Raeini-Sarjaz, M., and Chalavi, V. (2015). Colored plastic mulch microclimates affect strawberry fruit yield and quality. *International Journal of Biometeorology, 59*(8), 1061-1066. doi:10.1007/s00484-014-0919-0

Singh, A., Syndor, A., Deka, B., Singh, R., and Patel, R. (2012). The effect of microclimate inside low tunnels on off-season production of strawberry (*Fragaria* x *ananassa* duch.). *Scientia Horticulturae, 144*, 36-41. doi:10.1016/j.scienta.2012.06.025

Smith, W. N., Grant, B. B., Desjardins, R. L., Kroebel, R., Li, C., Qian, B., . . . Drury, C. F. (2013). Assessing the effects of climate change on crop production and GHG emissions in Canada. *Agriculture, Ecosystems and Environment, 179*, 139-150. doi:10.1016/j.agee.2013.08.015

Soil Classification Working Group, 1998. The Canadian System of Soil Classification, 3rd

Stanghellini, C., 1987. Transpiration of greenhouse crops: an aid to climate management. Ph.D. dissertation, Agricultural University, Wageningen, 150 pp.

Stapleton, J. J. (2000). Soil solarization in various agricultural production systems. *Crop Protection, 19*(8), 837-841. doi:10.1016/S0261-2194(00)00111-3

Steinmetz, Z., Wollmann, C., Schaefer, M., Buchmann, C., David, J., Tröger, J., et al. (2016). Plastic mulching in agriculture. Trading short-term agronomic benefits for long-term soil degradation? *Science of the Total Environment, 550*, 690-705.

Sung, F. J. M., and Chen, J. J. (1991). Gas exchange rate and yield response of strawberry to carbon dioxide enrichment. *Scientia Horticulturae, 48*(3), 241-251. doi:10.1016/0304-4238(91)90132-I

Taber, H. G. (1993). Early muskmelon production with wavelength-selective and clear plastic mulches. *Horttechnology, 3*(1), 78.

Tanner, C., and Shen, Y. (1990). Water-vapor transport through a flail-chopped corn residue. *Soil Science Society of America Journal, 54*(4), 945-951.

Tanner, C.B. 1974. Microclimatic Modification: Basic Concepts. *Horticultural Science*, *9*(6), 555-560.

Tarara, J. M., and Ham, J. M. (1999). Measuring sensible heat flux in plastic mulch culture with aerodynamic conductance sensors. *Agricultural and Forest Meteorology, 95*(1), 1-13. doi:10.1016/S0168-1923(99)00021-0

Tarara, J.M. 2000. Microclimate Modification with Plastic Mulch. *Horticultural Science*, *35*(2), 169-180.

Teitel, M., and Tanny, J. (1999). Natural ventilation of greenhouses: Experiments and model. *Agricultural and Forest Meteorology, 96*(1), 59-70.

Tetsu, F., Motoo, F., and Masanori, T. (1973). Influence of various surface roughness on the natural convection. *International Journal of Heat and Mass Transfer*, *16* (3), 629-636. doi:10.1016/0017-9310(73)90228-7

Traore, B., Corbeels, M., van Wijk, M. T., Rufino, M. C., and Giller, K. E. (2013). Effects of climate variability and climate change on crop production in southern Mali. *European Journal of Agronomy, 49*, 115-125. doi:10.1016/j.eja.2013.04.004

Trotter, W. R. (1988). The glasshouses at dangstein and their contents. *Garden History, 16*(1), 71-89.

Unger, P., and Parker, J. (1968). Residue placement effects on decomposition evaporation and soil moisture distribution. *Agronomy Journal, 60*(5), 469-469.

Valen, D. (2016). On the horticultural origins of victorian glasshouse culture. *Journal of the Society of Architectural Historians, 75*(4), 403-423.

Valtcho D. Zheljazkov, S. S., and Schlegel, V. (2018). Influence of winter stress and plastic tunnels on yield and quality of spinach, pak choi, radish, and carrot. *Emirates Journal of Food and Agriculture, 30*(5), 357-363. doi:10.9755/ejfa.2018.v30.i5.1687

Walker, J. N. (1971). Effect of condensation on greenhouse heat requirement. *Transactions of the ASAE, 14*(2), 282-284. doi:10.13031/2013.38276

Wang, F., Feng, S., Hou, X., Kang, S., and Han, J. (2009). Potato growth with and without plastic mulch in two typical regions of Northern China. *Field Crops Research, 110*(2), 123-129. doi:10.1016/j.fcr.2008.07.014

Wang, H., Wang, C., Zhao, X., and Wang, F. (2015). Mulching increases water-use efficiency of peach production on the rainfed semiarid loess plateau of china. *Agricultural Water Management, 154*, 20-28.

Wang, S., and Deltour, J. (1999). Studies on thermal performances of a new greenhouse cladding material. *Agronomie, 19*(6), 467-475.

Wang, S., and Deltour, J. (1999). Studies on thermal performances of a new greenhouse cladding material. *Agronomie, 19*(6), 467-475.

Wang, Y. P., Li, F., Li, X. G., Zhu, J., Fan, C. Y., Kong, X. J., . . . Siddique, K. H. M. (2016). Multi-site assessment of the effects of plastic-film mulch on dryland maize productivity in semiarid areas in China. *Agricultural and Forest Meteorology, 220*, 160-169. doi:10.1016/j.agrformet.2016.01.142

Waterer, D., Hrycan, W., and Simms, T. (2008). Potential to double-crop plastic mulch. *Canadian Journal of Plant Science, 88*(1), 187-193. doi:10.4141/CJPS07007

Werner, A. T., Schnorbus, M. A., Shrestha, R. R., and Eckstrand, H. D. (2013). Spatial and temporal change in the hydro-climatology of the Canadian portion of the Columbia river basin under multiple emissions scenarios. *Atmosphere-Ocean, 51*(4), 357-379. doi:10.1080/07055900.2013.821400

Whipps, J. M., and Budge, S. P. (2000). Effect of humidity on development of tomato powdery mildew (*Oidium lycopersici*) in the glasshouse. *European Journal of Plant Pathology, 106*(4), 395-397. doi:10.1023/A:1008745630393

Wood, R. (1909). Note on the theory of the greenhouse. *Philosophical Magazine, 17*(97-102), 319-320.

Yaghi, T., Arslan, A., and Naoum, F. (2013). Cucumber (*cucumis sativus*, L.) water use efficiency (WUE) under plastic mulch and drip irrigation. *Agricultural Water Management, 128*, 149-157. doi:10.1016/j.agwat.2013.06.002

Yang, X., Short, T. H., Fox, R. D., and Bauerle, W. L. (1990). Transpiration, leaf temperature and stomatal resistance of a greenhouse cucumber crop. *Agricultural and Forest Meteorology, 51*(3), 197-209.

Yin, W., Feng, F., Zhao, C., Yu, A., Hu, F., Chai, Q., and Guo, Y. (2016). Integrated double mulching practices optimizes soil temperature and improves soil water utilization in arid environments. *International Journal of Biometeorology, 60*(9), 1423-1437. doi:10.1007/s00484-016-1134-y

Yokoe, K., Maesaka, M., Murase, J., and Asakawa, S. (2015). Solarization makes a great impact on the abundance and composition of microbial communities in soil. *Soil Science and Plant Nutrition, 61*(4), 641-652. doi:10.1080/00380768.2015.1048183

Youssef, B., Dehbi, A. E., Hamou, A., and Saiter, J. M. (2008). Natural ageing of tri-layer polyethylene film: Evolution of properties and lifetime in north africa region. *Materials and Design, 29*(10), 2017-2022.

Zegada-Lizarazu, W., and Berliner, P. R. (2011). Inter-row mulch increase the water use efficiency of Furrow-Irrigated maize in an arid environment. *Journal of Agronomy and Crop Science, 197*(3), 237-248.

Zhang, L., and Lemeur, R. (1992). Effect of aerodynamic resistance on energy balance and penman-monteith estimates of evapotranspiration in greenhouse conditions. *Agricultural and Forest Meteorology, 58*(3), 209-228.

Zhang, X., Zhang, G., and Hu, X. (2013). Runoff and soil erosion as affected by plastic mulch patterns in vegetable field at Dianchi Lake's catchment, China. *Agricultural Water Management, 122*, 20-27. doi:10.1016/j.agwat.2013.02.004

Zhang, Y., Gauthier, L., de Halleux, D., Dansereau, B., and Gosselin, A. (1996). Effect of covering materials on energy consumption and greenhouse microclimate. *Agricultural and Forest Meteorology, 82*(1), 227-244. doi:10.1016/0168-1923(96)02332-5

Zhang, Y., Wang, F., Shock, C., Yang, K., Kang, S., Qin, J., and Li, S. (2017). Influence of different plastic film mulches and wetted soil percentages on potato grown under drip irrigation. *Agricultural Water Management, 180*, 160-171. doi:10.1016/j.agwat.2016.11.018

Zheng, J., Huang, G., Jia, D., Wang, J., Mota, M., Pereira, L., Liu, H. (2013). Responses of drip irrigated tomato (*Solanum lycopersicum* L.) yield, quality and water productivity to various soil matric potential thresholds in an arid region of Northwest China. *Agricultural Water Management, 129*, 181-193. doi:10.1016/j.agwat.2013.08.001

Zhou, L., Li, F., Jin, S., and Song, Y. (2009). How two ridges and the furrow mulched with plastic film affect soil water, soil temperature and yield of maize on the semiarid loess plateau of China. *Field Crops Research, 113*(1), 41-47. doi:10.1016/j.fcr.2009.04.005

Zwiers, F. W., Schnorbus, M.A., Maruszeczka, G.D. 2011. Hydrological Impacts of Climate on BC Water Resources, Summary report for the Campbell, Columbia and Peace River Watersheds. Pacific Climate Impacts Consortium. 24 pp.

Appendix A

This appendix shows photographs and supplementary data regarding the measurement of plastic film 1) shortwave radiative spectral properties in the laboratory on Dec 4, 2015 and June 2, 2018, 2) longwave radiative properties at Totem Field, UBC and 3) the field experiment performed at UBC Farm from July 14 (DOY 194) – September 30 (DOY 273), 2015.

A.1 Shortwave spectral properties: photographs of laboratory measurements
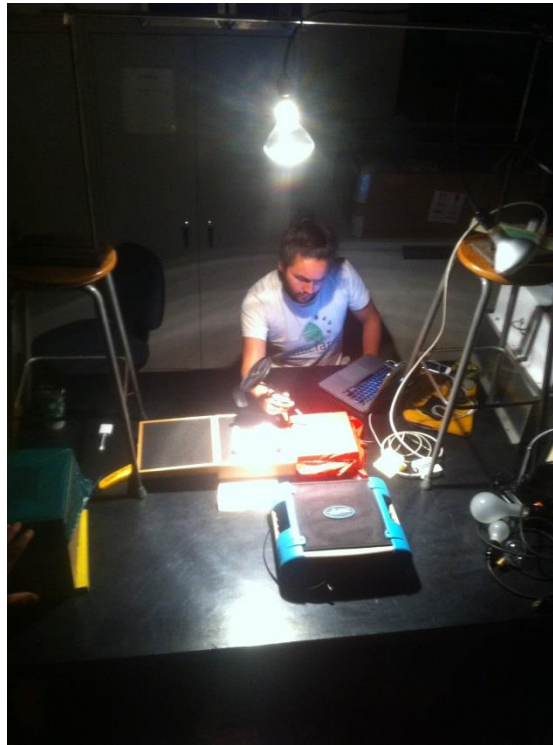
Figure A.1 A photograph (taken Dec 4, 2015) of the author measuring the shortwave spectral reflectivity ($R_{s\lambda}$) of a plastic film (RD in the photo) using the shortwave spectroradiometer (Fieldspec 3, ASD Inc., Longmount CO, USA) and the 0.15 m x 0.15 m reflectance panel (nominal reflectance value = 99%) (model SRT-99-050, Labsphere Inc., North Sutton, NH, USA).
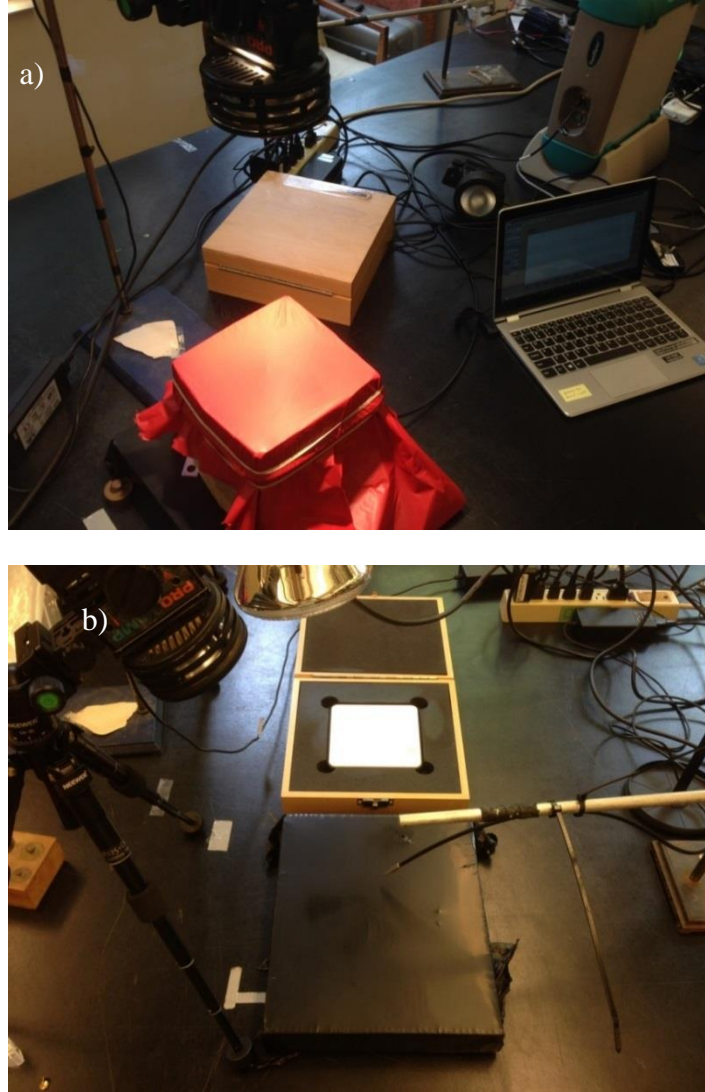
Figure A.2 Panels a) and b) show photographs (Dec 4, 2015 and taken June 2, 2018) of measurements of the shortwave spectral reflectivity ($R_{s\lambda}$) of a plastic film (BE2 in the photo) and spectral transmissivity ($T_{s\lambda}$) of a plastic film (GN in the photo), respectively, using the shortwave spectroradiometer (Fieldspec 3, ASD Inc., Longmount CO, USA) the 0.15 m x 0.15 m reflectance panel (nominal reflectance value = 99%) (model SRT-99-050, Labsphere Inc., North Sutton, NH, USA) and the halogen lamp (Model JC14.5V-50WC, Ushio Inc., Cypress, CA, USA).

Figure A.3 Panels a) shows a photograph (taken August 10, 2018) of the mounting system used

to hold the net radiometer (model SN-500-SS, Apogee Instruments Inc., Logan, UT) and square

foam cutout that held the plastic films. Panel b) shows a photograph (taken August 10, 2018) of

Thomas Andrew Black (left) and Paul Jassal (right) securing a plastic film to the foam cutout in

order to perform four steps (30 s step^{-1}) required to measure longwave radiative properties. The

photograph shows 1) the glass panel, the plastic film and the pyrgeometer of a 4-component net

radiometer.
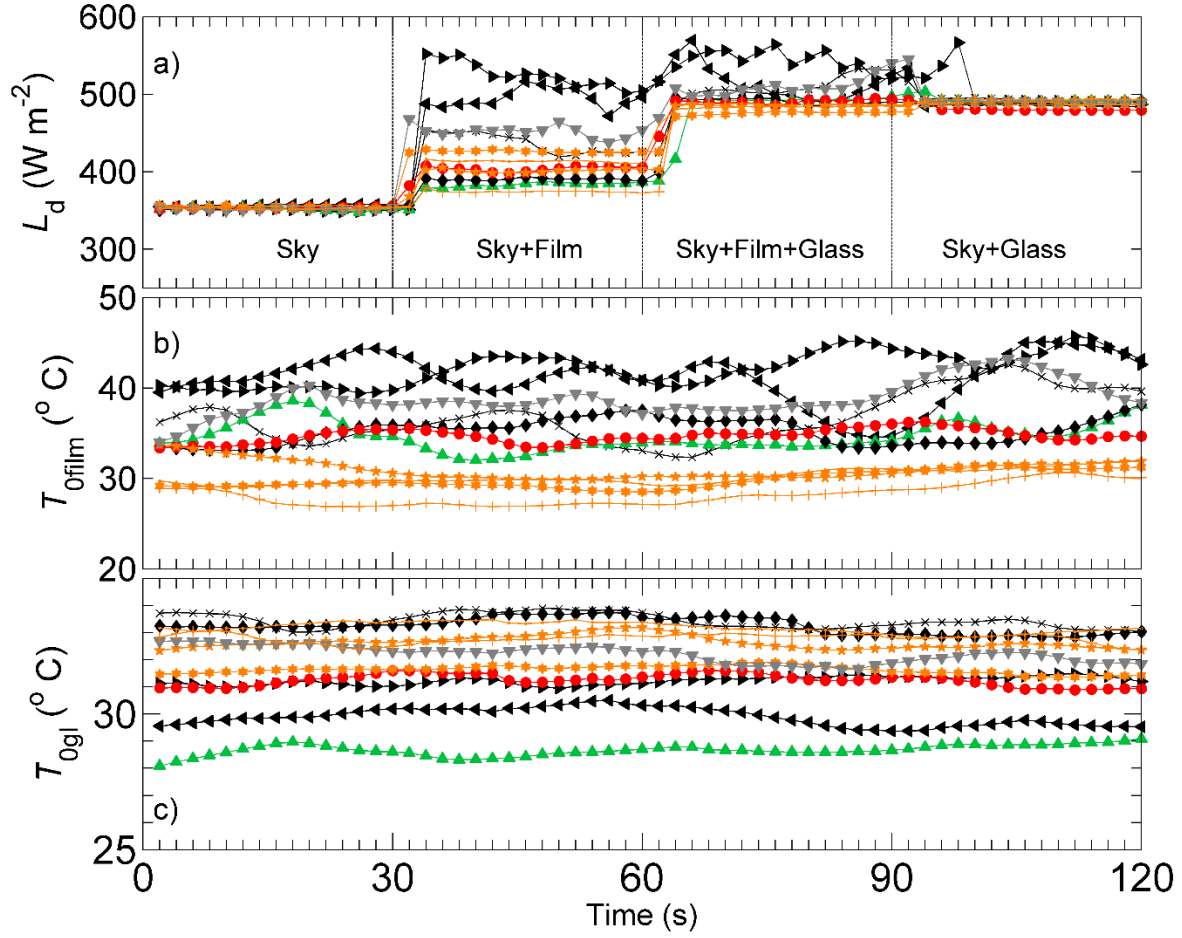
Figure A.4 Panels a), b) and c) show the downwelling longwave radiation (L_d), film surface temperature (T_{0film}), and glass surface temperature (T_{0gl}) during the four steps (30 s step^{-1}) required to measure the plastic film longwave radiative coefficients. Data shown are for BE2 (left-facing triangles), BEP (right-facing triangles), BW (crosses), GN (upward-facing triangles), IRT100 (diamonds), RD (circles), S4 (stars), TMX (pentagrams), WB (downward-facing triangles), POLY$_P$ (plus's) and POLY (dots).

A.3 Field experiment: photographs of experiment setup and design of plastic film mulch experiment at UBC Farm
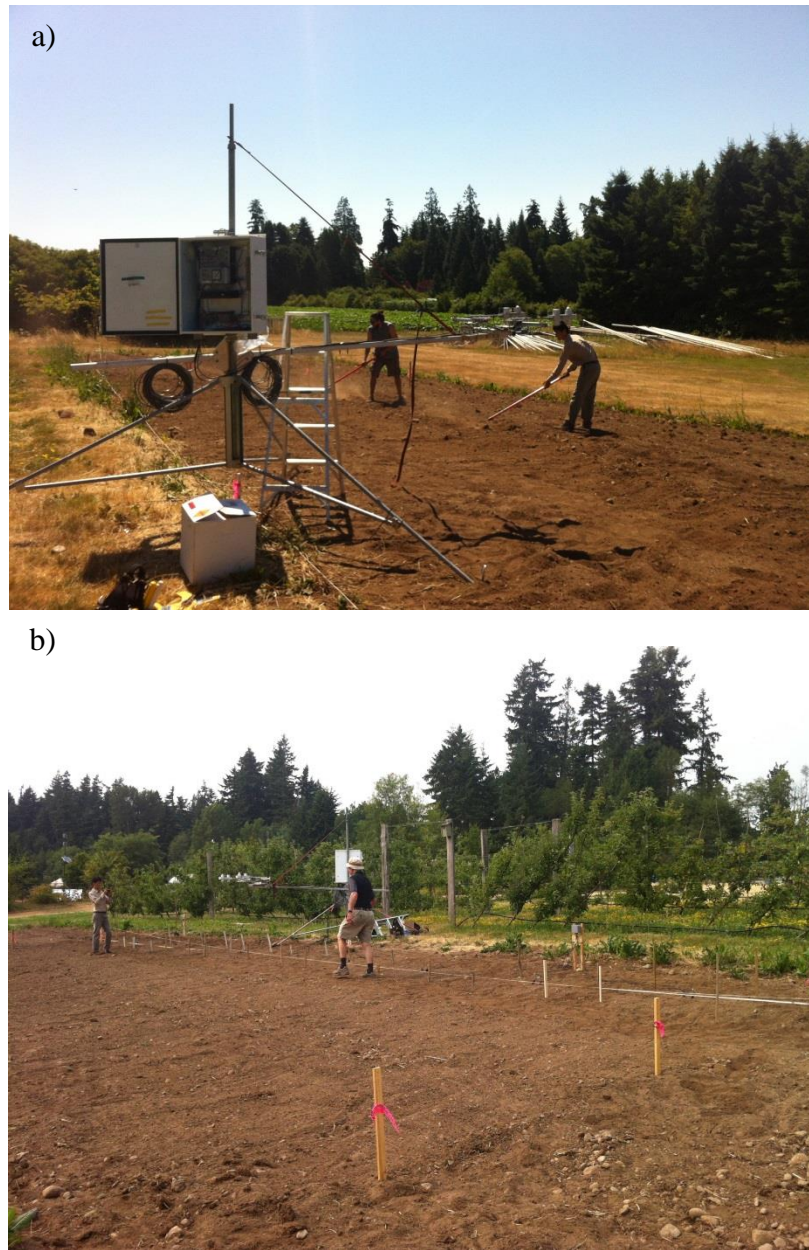
Figure A.5 Panel a) shows a photograph of the author (left) and Ernest (right) preparing the soil surface before the sensor installation. Panel b) shows a photograph (July 6, 2015) of Ernest Wu (left) and Thomas Andrew Black (right) outlining block 1 with twine and wooden stakes.

Figure A.6 Panel a) shows a photograph (July 9, 2015) of Thomas Andrew Black installing a soil temperature (T_s) and volumetric water content sensor (θ_s) sensor (5TM, Decagon Devices Inc., Pullman, WA, USA) 12 cm uphill of the irrigation line (near the center of the wet region). Panel b) shows a photograph (July 15, 2015) of block 1 after the treatments were installed.

Figure A.7 Panel a) and b) show photographs (August 28, 2015), from different angles, of the finished experiment ~ 1 month before the end of the treatment period on Sept 30, 2015 (DOY 273)

| BE2 | BEP | BW | C | GN |

| IRT100 | RD | S4 | TMX | WB |
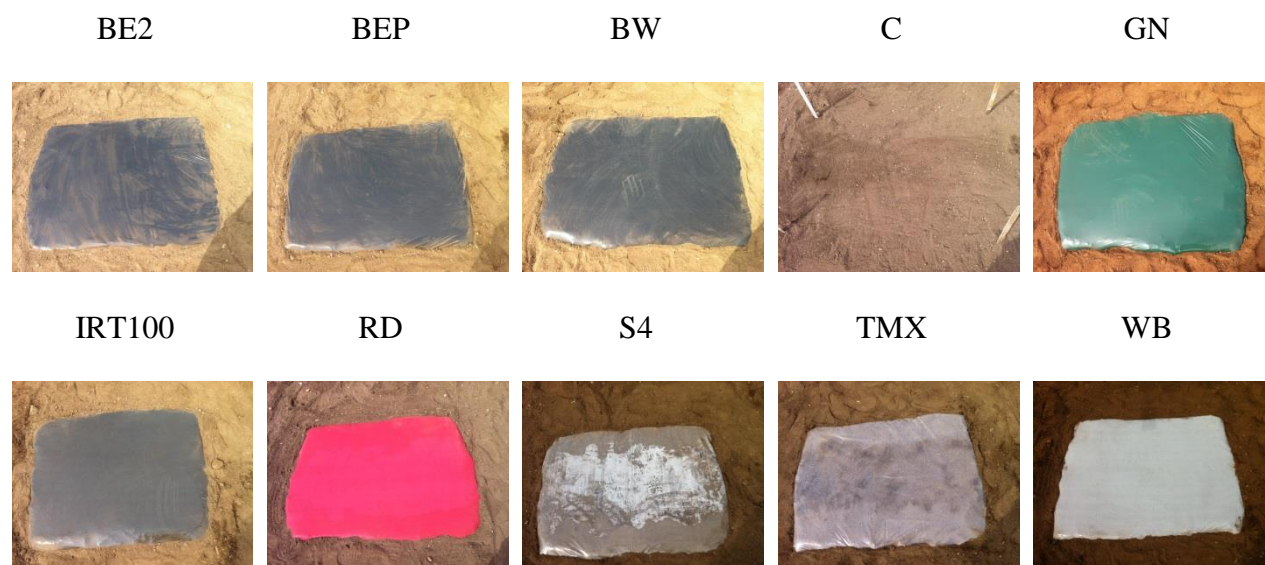
Figure A.8 Photographs (July 15, 2015) of all 10 treatments used in the experiment on the day they were installed.
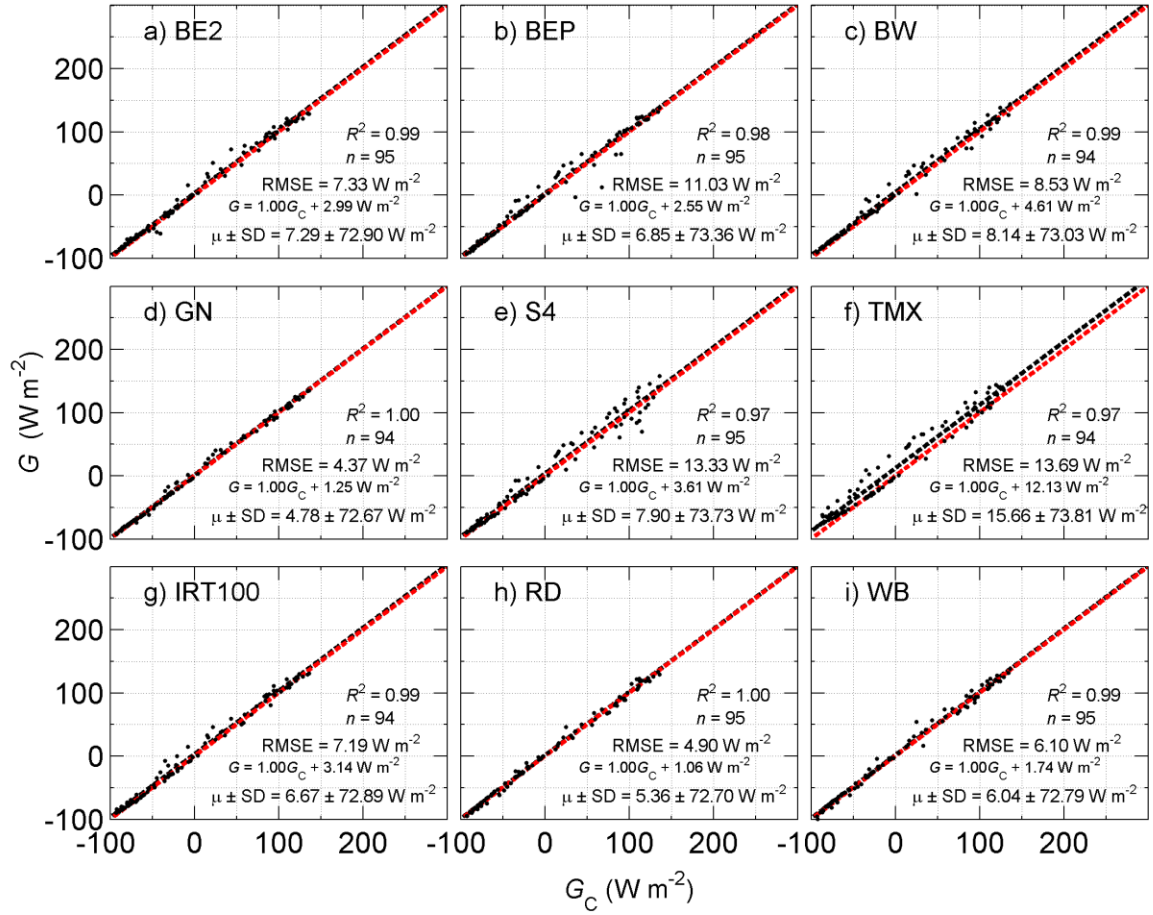
Figure A.9 Panels a), b), c), d), e), f), g), h), and i) show linear regressions for 2-cm soil heat flux density (G) for BE2, BEP, BW, GN, S4, TMX, IRT100, RD and WB vs C, respectively, for data collected during the calibration period (July 12, 2015 and July 14, 2015). For each regression, the coefficient of determination (R^2), sample size (n), root mean square error (RMSE) and linear regression equation are shown.
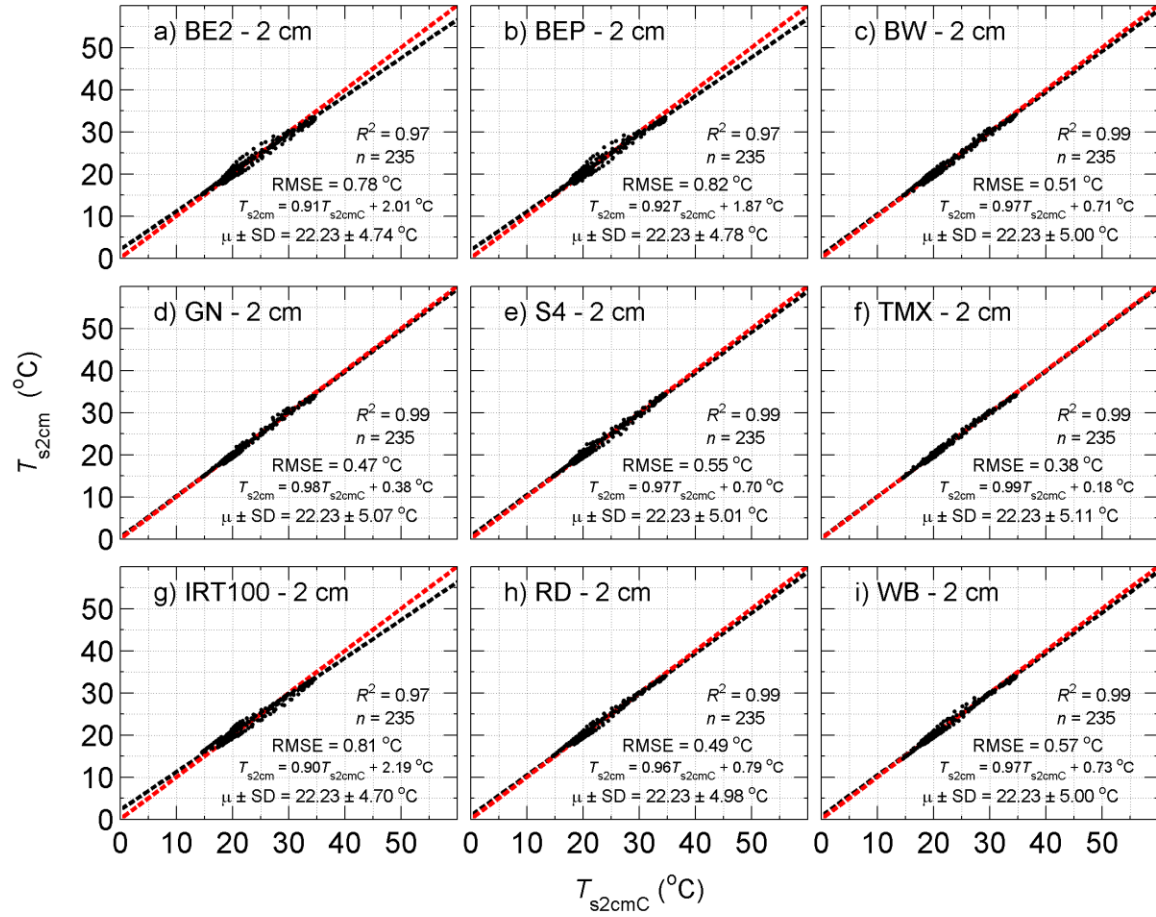
Figure A.10 Panels a), b), c), d), e), f), g), h), and i) show linear regressions for 2-cm soil temperature (T_s) for BE2, BEP, BW, GN, S4, TMX, IRT100, RD and WB vs C, respectively, for data collected during the calibration period (July 12, 2015 and July 14, 2015). For each regression, the coefficient of determination (R^2), sample size (n), root mean square error (RMSE) and linear regression equation are shown.
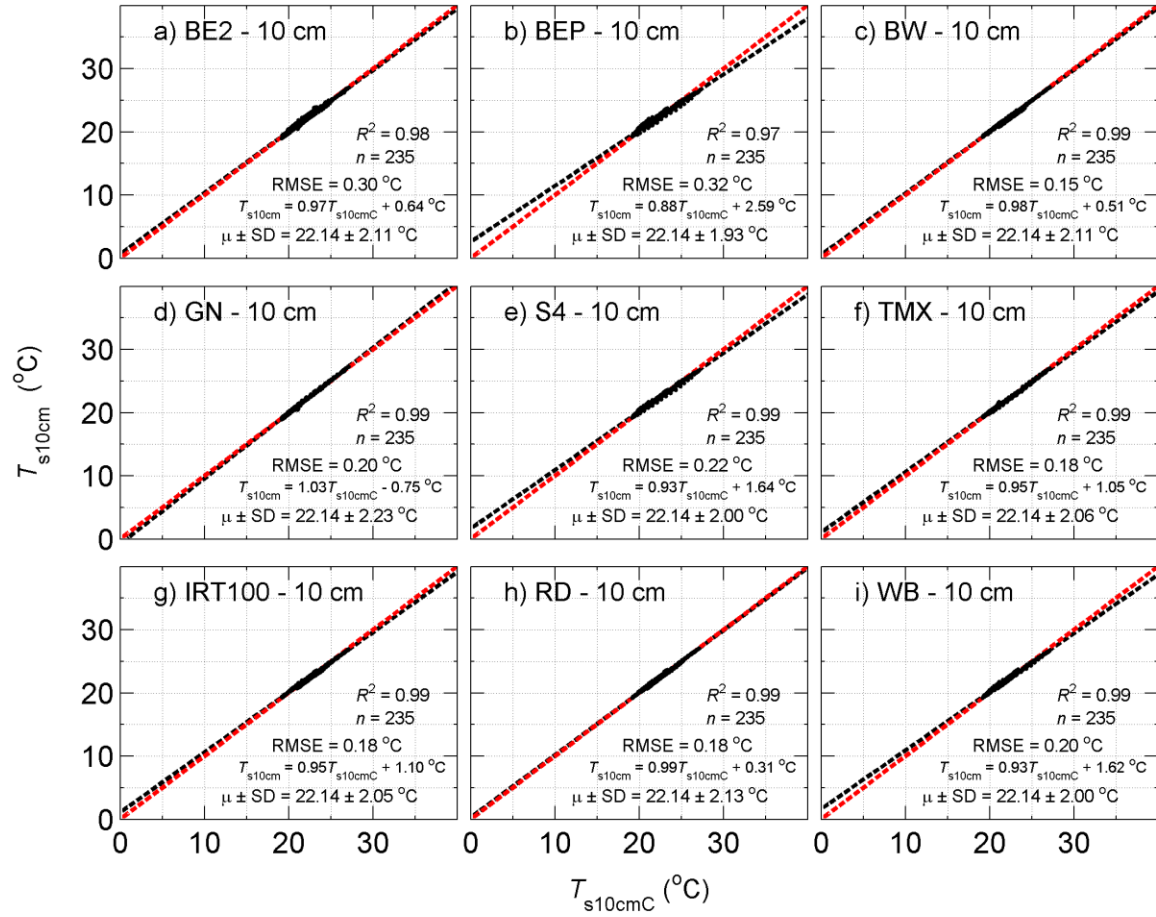
Figure A.11 Panels a), b), c), d), e), f), g), h), and i) show linear regressions for 10-cm soil temperature (T_s) for BE2, BEP, BW, GN, S4, TMX, IRT100, RD and WB vs C, respectively, for data collected during the calibration period (July 12, 2015 and July 14, 2015). For each regression, the coefficient of determination (R^2), sample size (n), root mean square error (RMSE) and linear regression equation are shown.

Appendix B

      This appendix shows photographs and supplementary data regarding the field experiment performed at UBC Farm to study vegetation-free low tunnel microclimate from May 14 (DOY 135) – September 30 (DOY 274), 2016.

B.1   Field experiment: photographs of experiment setup and design of vegetation-free low tunnel experiment at UBC Farm

Figure B.1 A photograph (May 10, 2016) of the instrumentation tripod, data-logging box and power supply used to study vegetation-free low tunnels. In the background, Nicolette Lax is preparing the soil surface before the installation of the soil instruments, black plastic mulch and low tunnels. The low tunnel in the background (right) was not involved in this study.

Figure B.2 Panel a) is a photograph (May 13, 2016) of the trenches that were dug to channel the instrumentation wires and secure the black plastic film mulch. Panel b) is a photograph (May 13, 2016) of Nicolette Lax installing the black plastic film mulch (BE2) after the soil instruments were installed and buried.

Figure B.3 Panel a) and b) are photographs (September 28, 2016) of the TMX and C and POLY$_P$ and POLY treatments, respectively.

Figure B.4 Panel a) is a photograph of the four treatments (POLY$_P$ (right) and POLY (left) in the foreground, C (right) and TMX (left) in the background). Panel a) is a photograph of the POLY$_P$ treatment and one of the tripods used to mount the net radiometer above the treatments (R_{nou}).
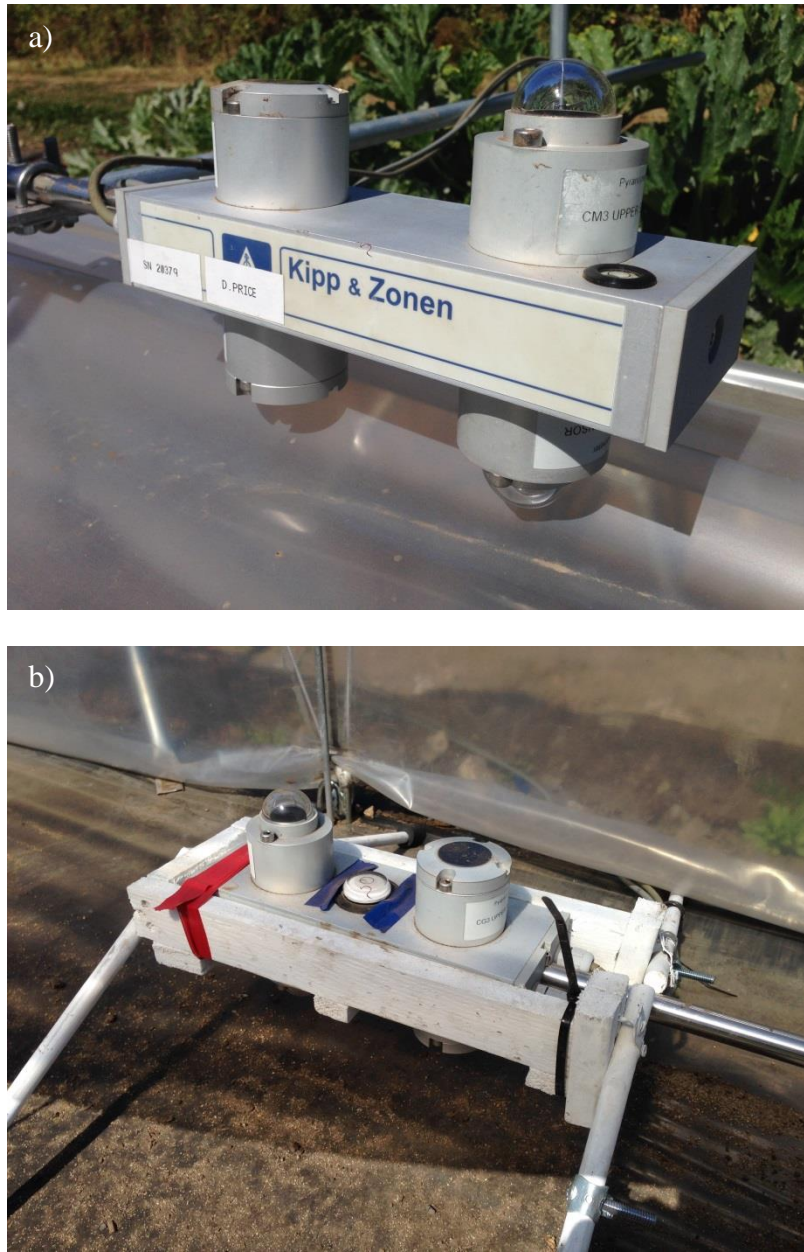
Figure B.5 Panel a) is a photograph (August 25, 2016) of the net radiometer mounted above the low tunnel (TMX in photograph) to measure net radiation above the low tunnel (R_{nou}). Panel b) is a photograph (August 25, 2016) of the net radiometer positioned inside the low tunnel (TMX in photograph) on the plastic film mulch (BE2) to measure net radiation inside the low tunnel (R_{nin}).
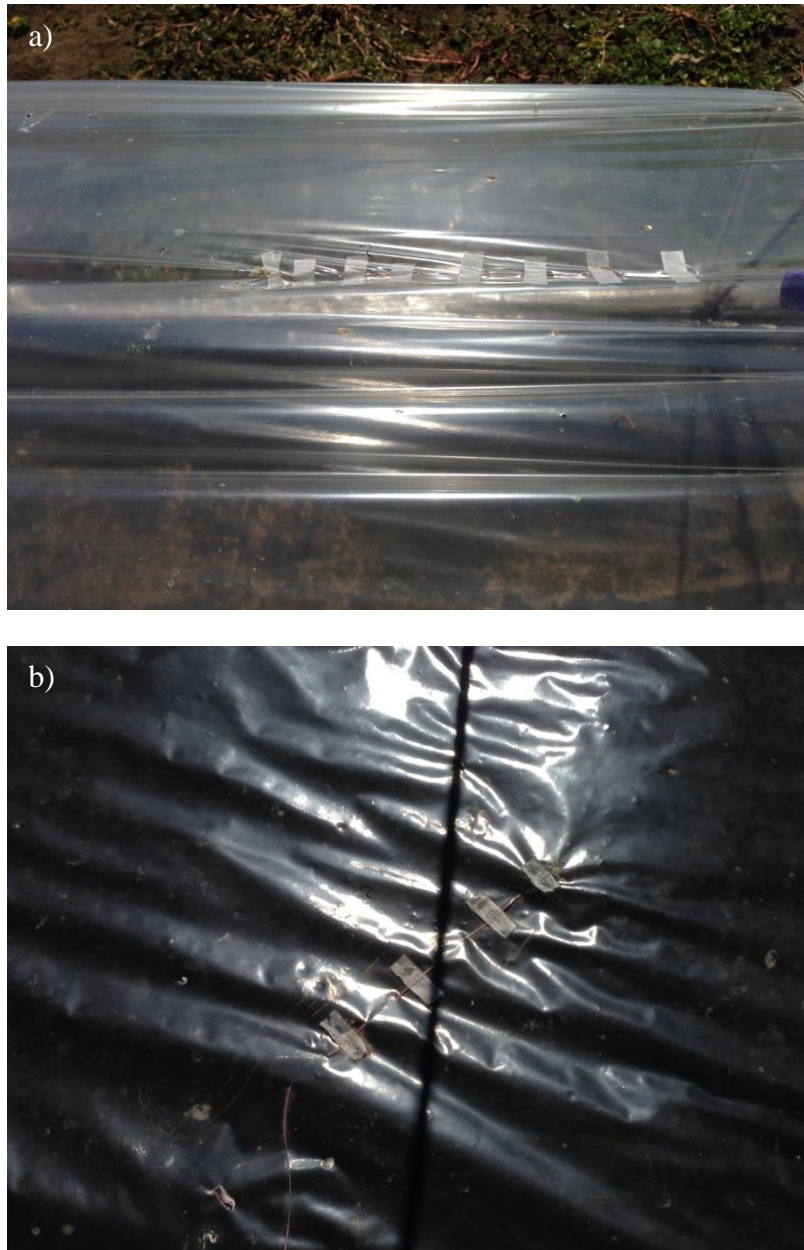
Figure B.6 Panels a) and b) are photographs (August 25, 2016) of the thermocouples (Type-E) woven into and adhered (Omegabond® 101, Omega Engineering Inc., Norwalk, CT, USA) to the low tunnel cover or wall (POLY$_P$ in the photograph), respectively, to measure wall surface temperature (T_w) and mulch surface temperature (T_m).
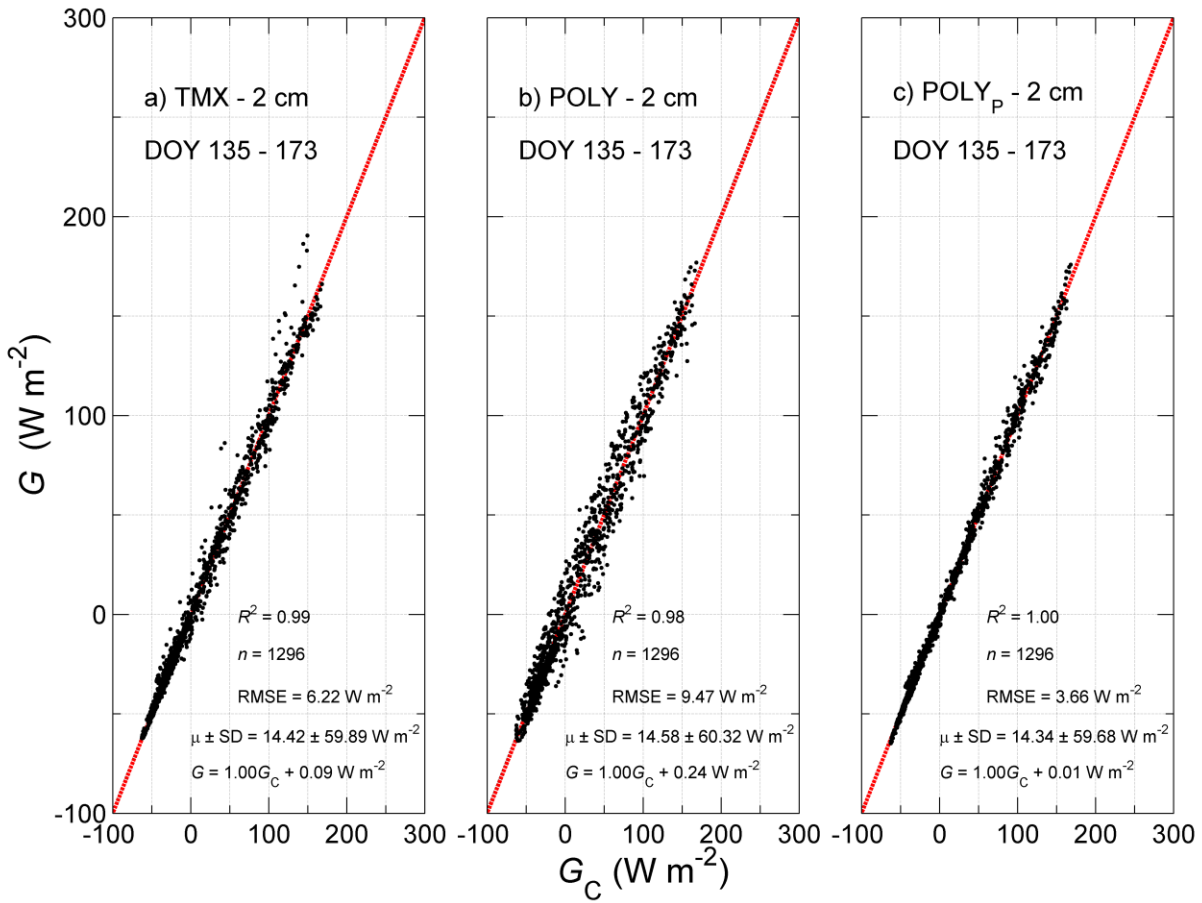
Figure B.7 Panels a), b) and c) show the regressions for low tunnel mulch surface temperatures G_{TMX}, G_{POLY} and G_{POLYp} vs G_{C}, respectively, from June 21 (DOY 173) – June 22 (DOY 174). The regression equation ($T_{\mathrm{m}} = aT_{\mathrm{mC}} + b$), mean ($\mu$) ± standard deviation (SD), root mean square error (RMSE), sample number (n) and coefficient of determination (R^2) are listed for each regression.
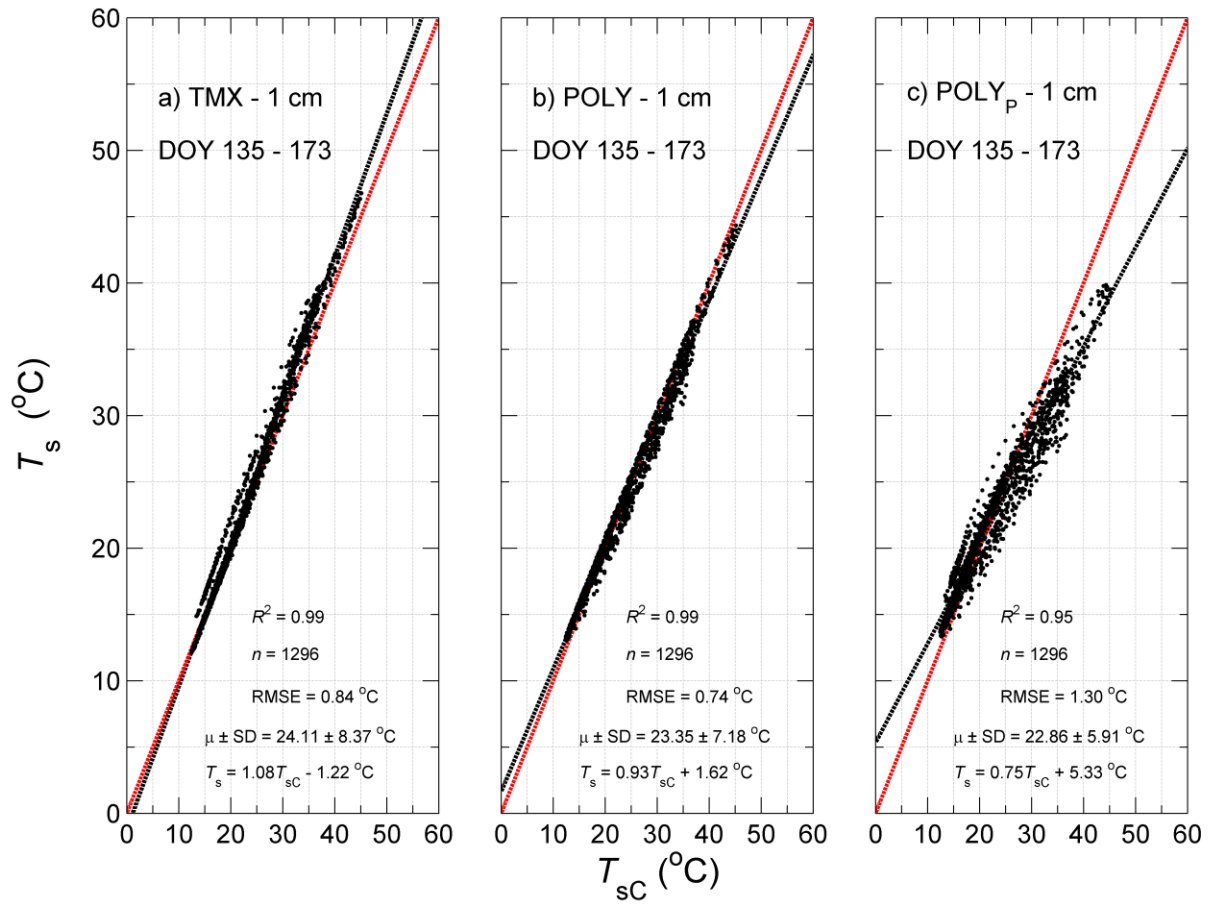
Figure B.8 Panels a), b) and c) show the regressions for low tunnel 1- cm soil temperatures $T_{s1cmTMX}$, $T_{s1cmPOLY}$ and $T_{s1cmPOLYp}$ vs T_{s1cmC}, respectively, from June 21 (DOY 173) – June 22 (DOY 174). The regression equation ($T_{s1cm} = aT_{s1cmC} + b$), mean ($\mu$) ± standard deviation (SD), root mean square error (RMSE), sample number (n) and coefficient of determination (R^2) are listed for each regression.
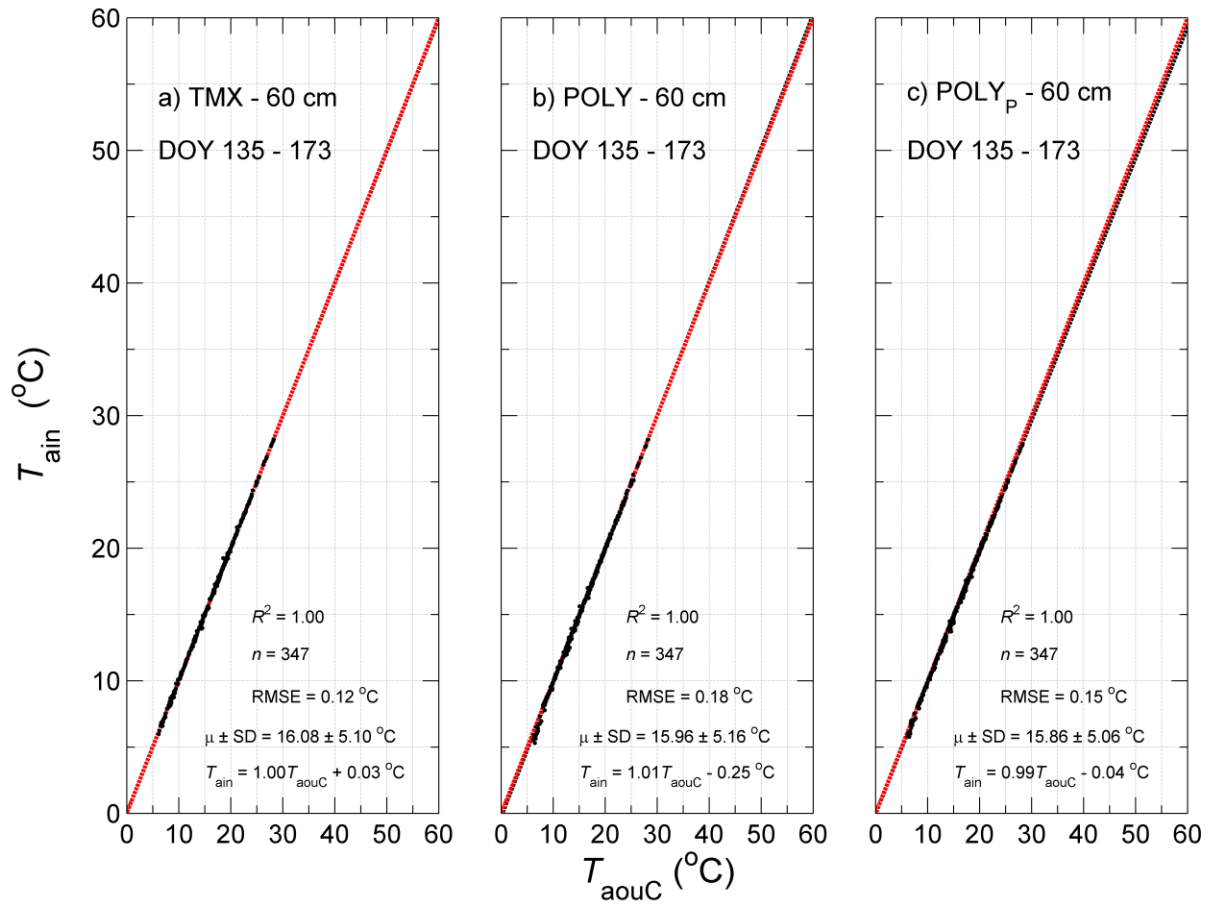
Figure B.9 Panels a), b) and c) show the regressions for low-tunnel air temperatures T_{ainTMX}, $T_{ainPOLY}$ and $T_{ainPOLYp}$ vs T_{aouC}, respectively, from June 21 (DOY 173) – June 21 (DOY 174). The regression equation ($T_{ain} = aT_{aou} + b$), $\mu \pm$ SD, root mean square error (RMSE), sample number (n) and coefficient of determination (R^2) are listed for each regression.
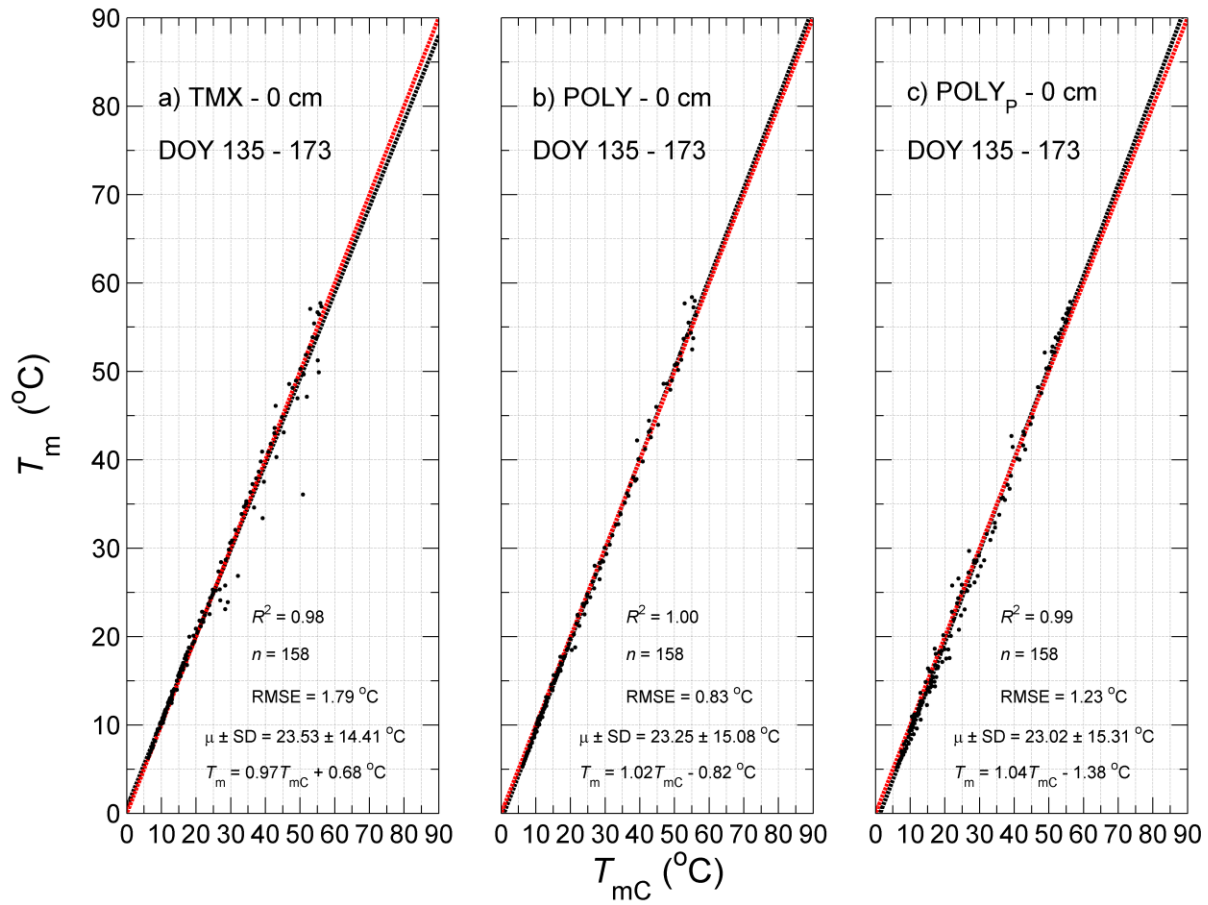
Figure B.10 Panels a), b) and c) show the regressions for low tunnel mulch surface temperatures T_{mTMX}, T_{mPOLY} and T_{mPOLYp} vs T_{mC}, respectively, from June 21 (DOY 173) – June 21 (DOY 174). The regression equation ($T_m = aT_{mC} + b$), mean (μ) ± standard deviation (SD), root mean square error (RMSE), sample number (n) and coefficient of determination (R^2) are listed for each regression.

Figure B.11 Empirical relationships for predicting h_{ou} using wind velocity outside enclosures: h_{ou} = 12.5 + 6.8u (Chapter 2); h_{ou} = 8.3 + 3.8u (ASHRAE); h_{ou} = 5.62 + 3.91u, 0 < u < 5 m s^{-1} and h_{ou} = 7.17$u^{0.78}$, 5 < u < 20 m s^{-1} (McAdams 1954); h_{ou} = 7.2 + 3.8u (Garzoli and Blackwell 1981); h_{ou} = 17.9$u^{0.576}$, u < 20 m s^{-1} (Iqbal and Khatry 1977); h_{ou} = 0.95 + 6.76$u^{0.49}$, $u \leq 6.3$ m s^{-1} (Papadakis et al., 1992); h_{ou} = 3u Businger (1954).

Appendix C Photographs of Padron pepper experiment at UBC Farm

This appendix shows photographs regarding the field experiment performed at UBC Farm to study the impact of low tunnels, with similar shortwave transmissivity and different longwave absorptivity, on Padrón pepper growth and productivity from June 10 (DOY 162) – November 26 (DOY 331), 2017.

Figure C.1 Panel a) is a photograph of the Padrón pepper (June 6, 2017) starts six days before they were transplanted at UBC Farm on July 12, 2017. Panel b) is a photograph of Brian Wang replacing CO_2 canisters in the portable photosynthesis system.
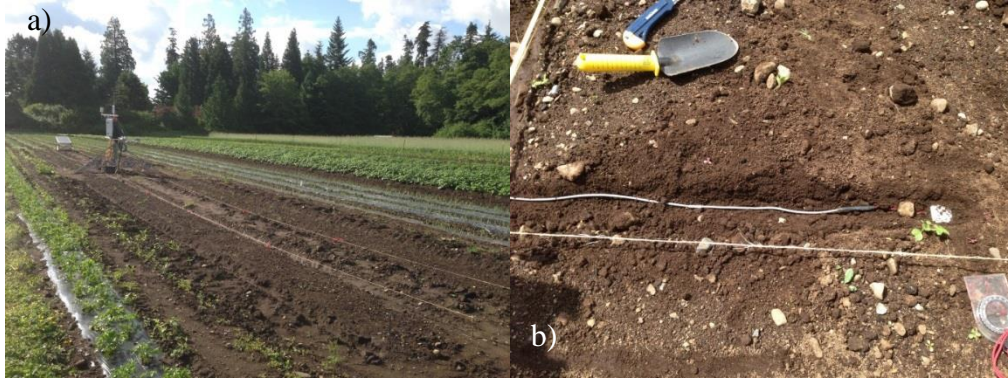
Figure C.2 Panel a), b) and c) are photographs (June 9, 2017) of the site preparation before treatments are installed, a soil heat flux sensor and a soil temperature (T_s) and volumetric water content sensor (θ_s) sensor (5TM, Decagon Devices Inc., Pullman, WA, USA), respectively.
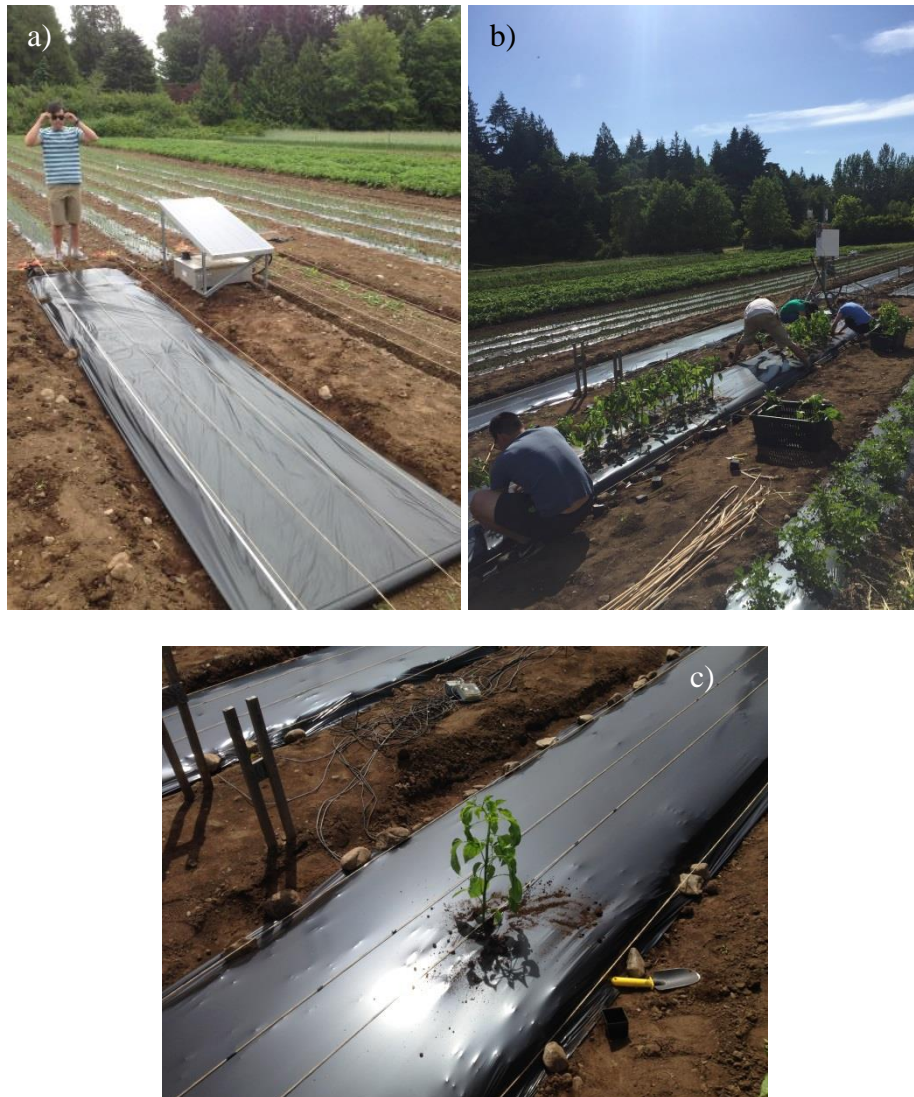
Figure C.3 Panels a), b) and c) are photographs (June 12, 2017) of Brian Wang installing plastic film mulch, the authors colleagues transplanting Padrón pepper and the 1st Padrón pepper transplanted in the experiment, respectively.
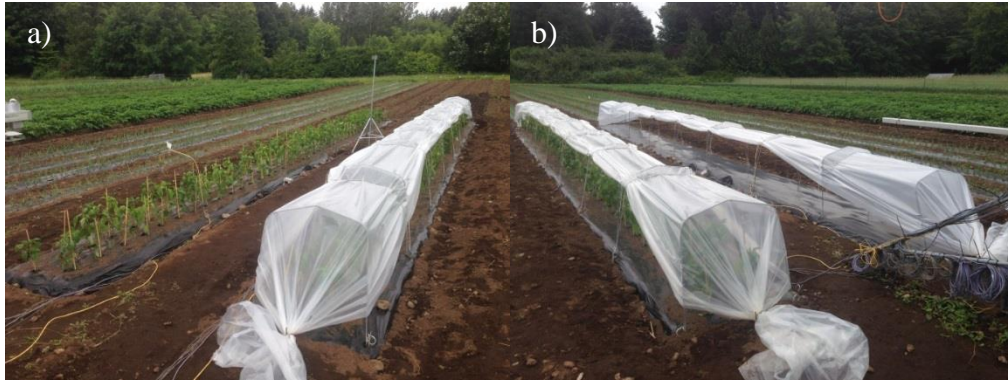
Figure C.4 Panels a), b) and c) are photographs (June 14, 2017) of C (left) and POLY (right), TMX (left) and POLY$_{EMP}$ (right) and all four finished treatments in the experiment 2 days after the pepper plants were transplanted on July 12, 2017, respectively.

Figure C.5 Panel a) and b) are photographs (June 22, 2017) of C (left) and POLY (right), TMX (left) and POLY$_{EMP}$ (right) ten days after the pepper plants were transplanted on July 12, 2017, respectively.

Figure C.6 Panels a), b) and c) are photographs (July 11, 2017) of condensation on POLY, condensation on TMX (with anti-droplet characteristics) and the author, Thomas Andrew Black and Paul Jassal discussing how to increase the height of the low tunnels due to pepper growth.

Figure C.7 Panel a) and b) are photographs (July 17, 2017) of C (left) and POLY (right), TMX (left) and POLY$_{EMP}$ (right) one month after the pepper plants were transplanted on July 12, 2017, respectively.

228

Figure C.8 Panel a) and b) are photographs (July 26, 2017) of C (left) and POLY (right), TMX (left) and POLY$_{EMP}$ (right) one and a half months after the pepper plants were transplanted on July 12, 2017, respectively.

Figure C.9 Panel a) and b) are photographs (July 28, 2017) of C (left) and POLY (right), TMX (left) and POLY$_{EMP}$ (right) one and a half months after the pepper plants were transplanted on July 12, 2017, respectively. Panel c) shows the entire experiment on July 28, 2017.
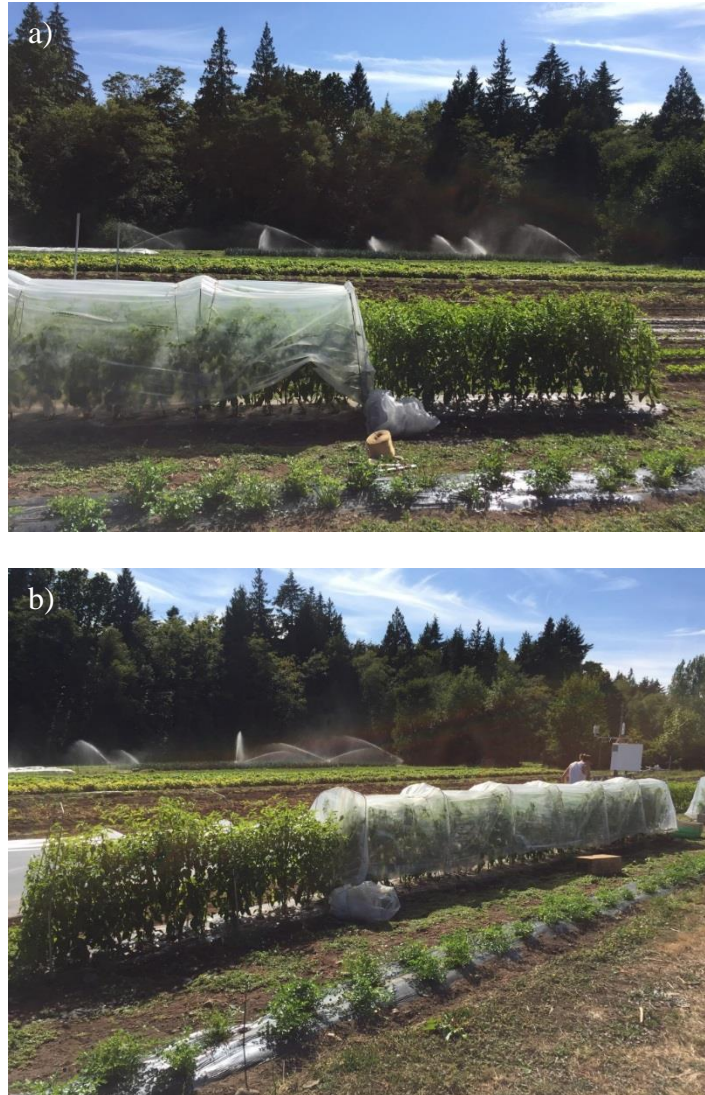
Figure C.10 Panel a) and b) are photographs (August 15, 2017) of POLY$_{PP}$ and TMX$_{PP}$ after the low tunnels were removed from Q4 and Q1, respectively.

Figure C.11 Panel a), b) and c) are photographs of pepper fruit harvest on August 15, 2017, for Q4 from TMX$_{PP}$, POLY$_{PP}$ and C$_{PP}$, respectively.

Figure C.12 Panel a) and b) are photographs (August 23, 2017) of Brian Wang harvesting a pepper plant from C_{PP} and illustrating the height (z) difference between C_{PP} and $POLY_{PP}$, respectively.

Figure C.13 Panel a) and b) are photographs (August 25, 2017) of C (left) and POLY (right), TMX (left) and POLY$_{EMP}$ (right) two and a half months after the pepper plants were transplanted on July 12, 2017, respectively.
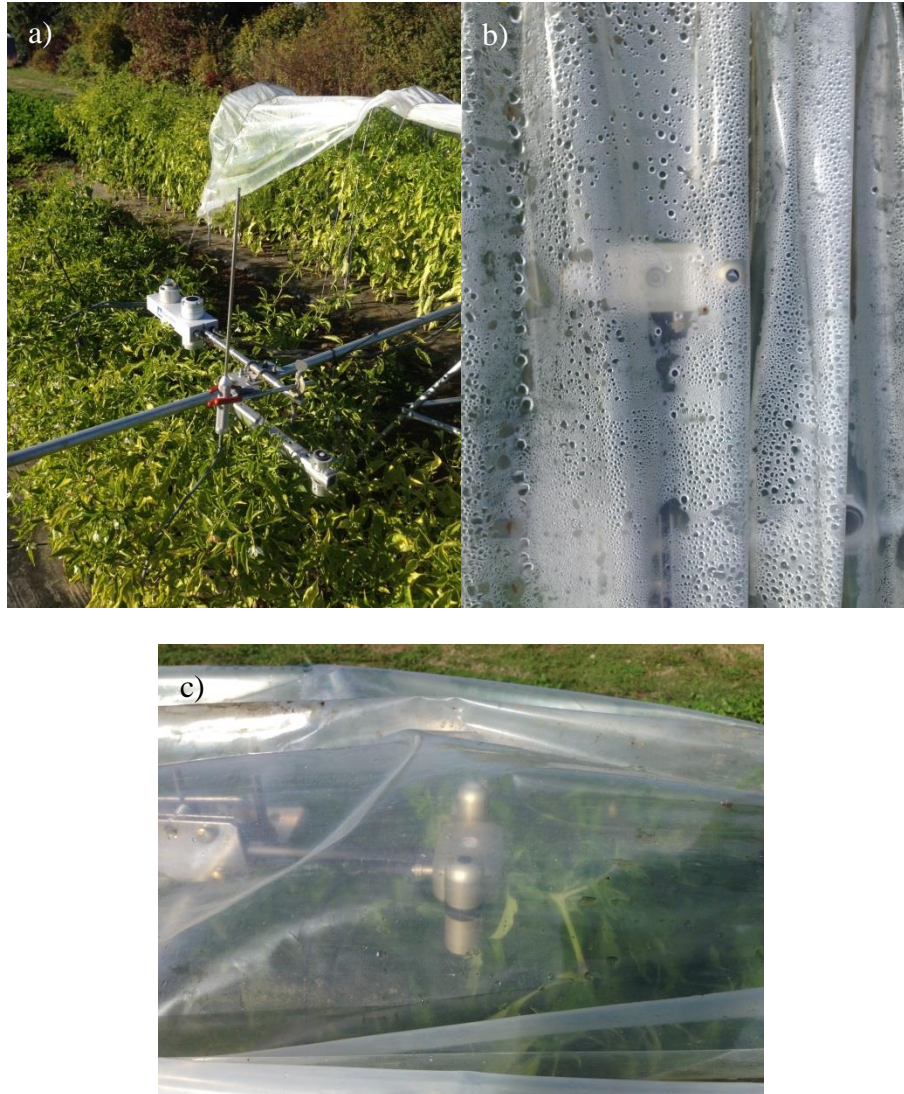
Figure C.14 Panels a), b) and c) are photographs (September 23, 2017) of the net radiometers above C_{PP}, inside $POLY_{PP}$ (note the condensation), inside TMX_{PP} (note the anti-droplet properties), respectively.
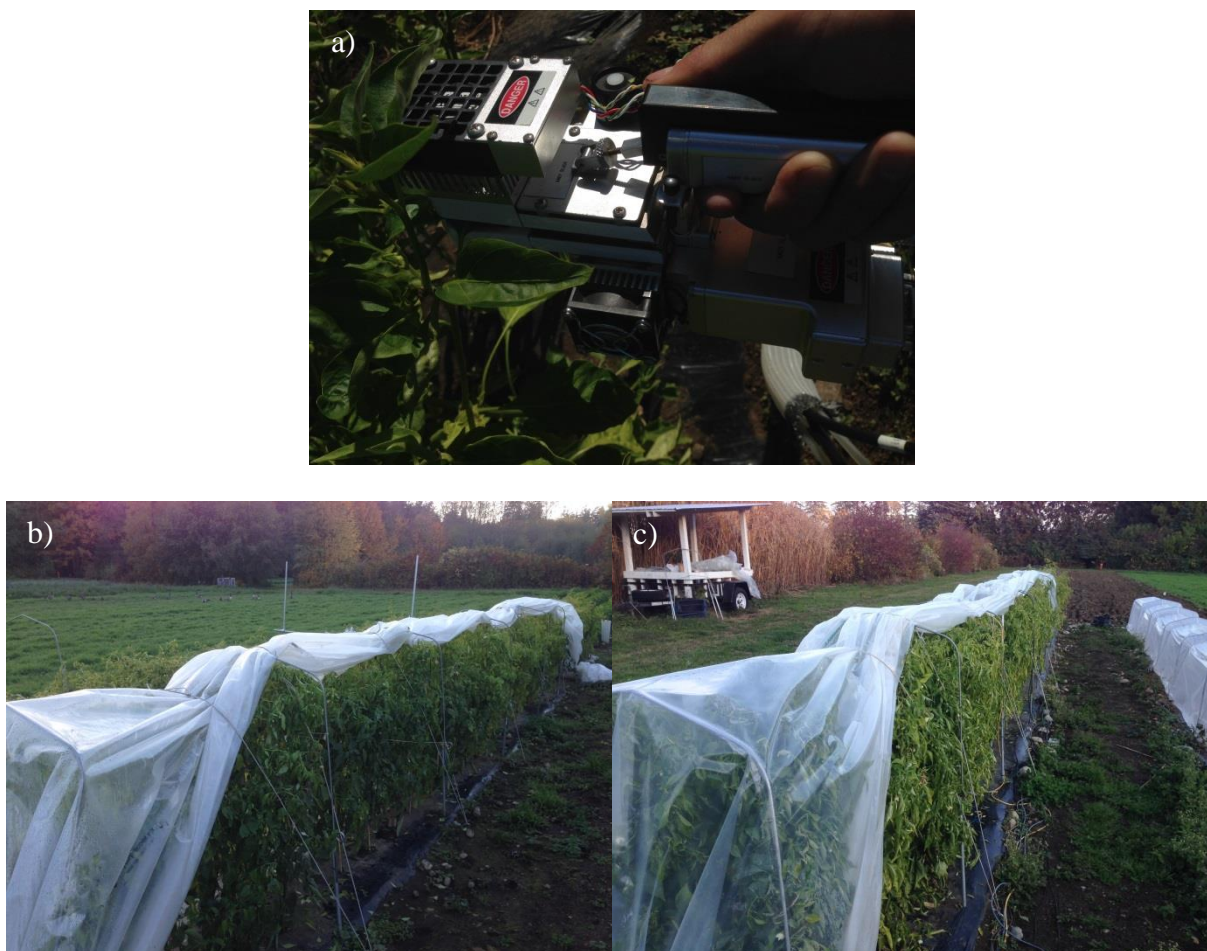
Figure C.15 Panel a), b) and c) are photographs (October 31, 2017) of the portable

photosynthesis system, C (left) and POLY (right), TMX (left) and POLY$_{EMP}$ (right),

respectively.

Appendix D Effect of low tunnels on broccoli yield in central BC

This appendix shows photographs and data regarding two field experiments performed at Mackin Creek Farm, near Soda Creek, BC, CA to study the impact of low tunnels on lettuce spinach mix in 2016 and broccoli in 2016 and 2017. In August 2015, Ernest Wu and the author installed a climate monitoring station at Mackin Creek Farm, BC, to monitor the impact of low tunnels on lettuce/spinach mix in the following year (2016) (Figure E.1.1). In March 2016, Jilmarie Stephens and the author, installed low tunnels treatment (POLY, TMX, S4 and a bare soil control with no low tunnel) (Figure E.1.2) shortly after the snow melted on Mackin Creek Farm in March, and Figure E.1.3 shows the 5 cm soil temperature (T_{s5cm}) for 5 days after the low tunnels were closed. Unfortunately, the lettuce/spinach mix failed due to an unidentified mold.

The low tunnels from the spinach/lettuce mix study were then used in 2016 and 2017, by Rob Borsato and Catherine Allen (owners and operators), to study how broccoli yield was impacted when the crop was grown outside and inside low tunnels, respectively. This data allowed us to compare broccoli yield between 2016 (no tunnels) and 2017 (with tunnels) under different conditions but no direct comparison was done within a single growing season. With regards to the broccoli study Rob Borsato stated "2016 was the earliest and warmest spring I can recall" and harvest began on June 5th, 2016. In 2017 Rob Borsato stated that "in 2017 we encountered frost 40 cm below the soil surface on April 27" and harvest began two week (June 17th) after harvest began in 2016. In 2017, Rob observed that the low tunnels helped to protect

237

the broccoli from high winds in the spring of 2017 and helped reduce moisture loss (via soil evaporation), which he felt benefited the crops later in the growing season. Rob's observations are supported by the climate data we collected (Figure E.1.4). Overall the harvest in 2017 was nearly double the harvest in 2016 (Figure E.1.5 and Figure E.1.6).

A weather transmitter (WXT520, Vaisala Oy, Helsinki, Finland) mounted 2 m above the soil surface measured half-hourly mean air temperature (T_{a2m}), precipitation (P), wind velocity (u_{ou}) and direction and vapour pressure deficit (VPD_{2m}). In addition to P from the weather transmitter, half-hourly P measurements were made using a tipping-bucket (0.1 mm) rain gauge (model TR525 M, Texas Electronics Inc., Dallas, TX, USA). For each low-tunnel treatment and the control, one soil temperature (T_s) and volumetric water content (θ_s) sensors (5TM, Decagon Devices Inc., Pullman, WA, USA) were installed at the 5 cm (T_{s5cm} and θ_{s5cm}). A quantum sensor (LI-190, LI-COR Inc.) was installed at 2 m height. All climate, soil and radiation variables (see following sections) were measured every 5 s using a solid-state multiplexer (model AM25T, Campbell Scientific Inc. (CSI)) and a datalogger (model CR1000, CSI), after which half-hourly averages were calculated and collected daily using a modem (Raven, model XT, Sierra Wireless Inc.).

Figure D.1 panel a), b) and c) are photographs (August 25, 2015) of the uphill view of the experiment site (right of the twine), the downhill view of the experiment site (left of the twine) and the instrumentation box and support post used to monitor the site microclimate, respectively.

Figure D.2 Panels a), b) and c) are photographs (March 10, 2016) of the author installing a rain gauge, testing a rain gauge (out of view) and the experimental site used to study lettuce spinach mix productivity, respectively.
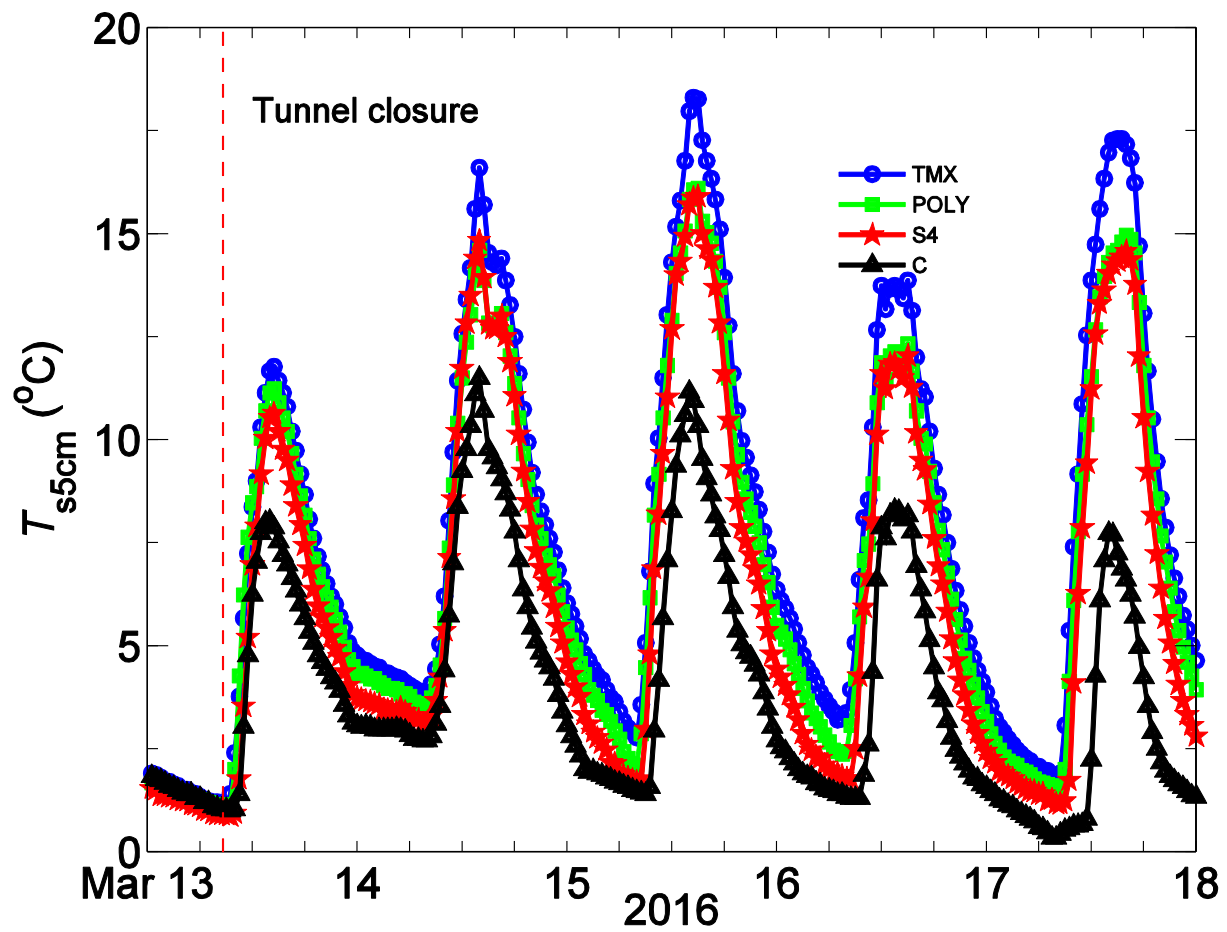
Figure D.3 Five consecutive days of 5-cm soil temperature (T_{s5cm}) inside the four treatments used to study lettuce/spinach mix on Mackin Creek Farm in 2016.
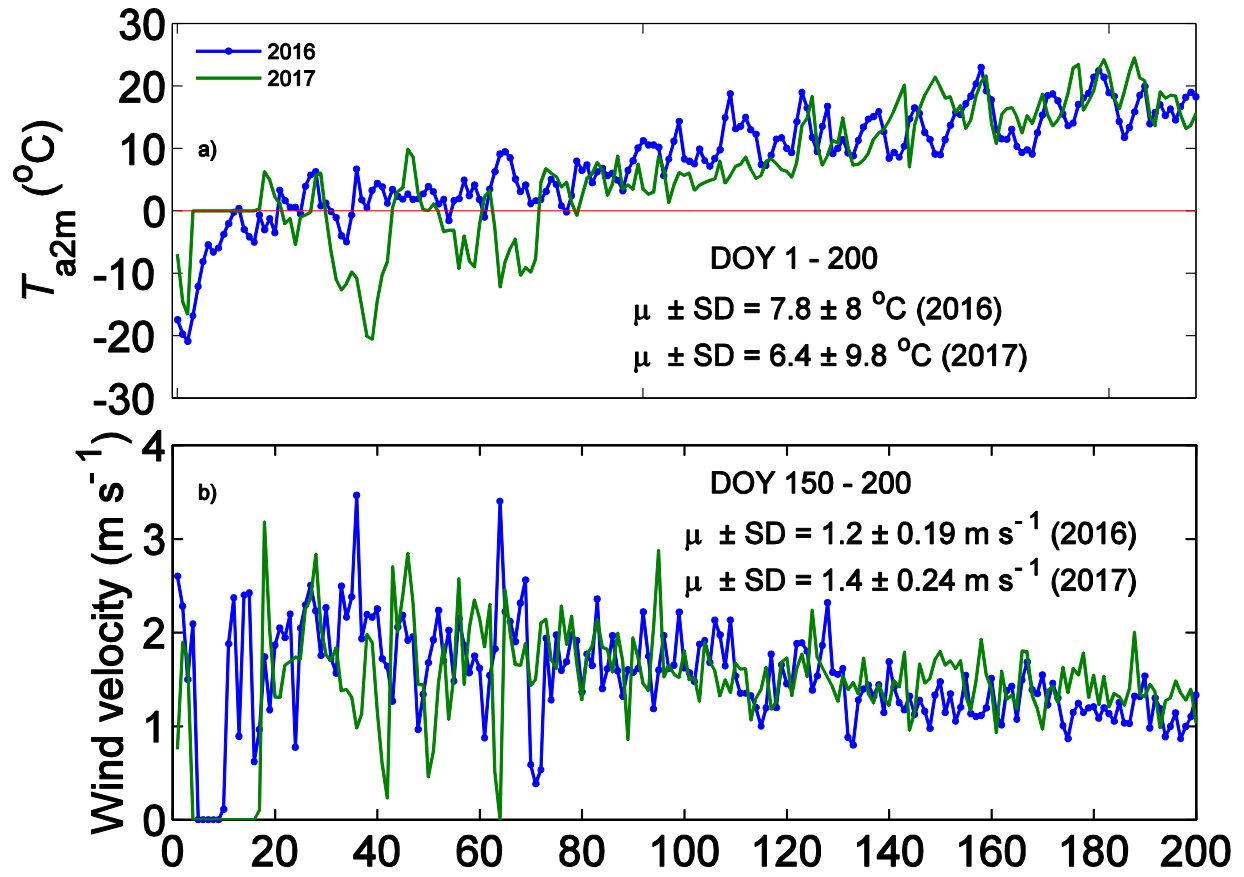
Figure D.4 Panels a) and b) show 2-m air temperature (T_{a2m}) and wind speed (u_{2m}), respectively,

from DOY 1 – 200 of 2016 and 2017.
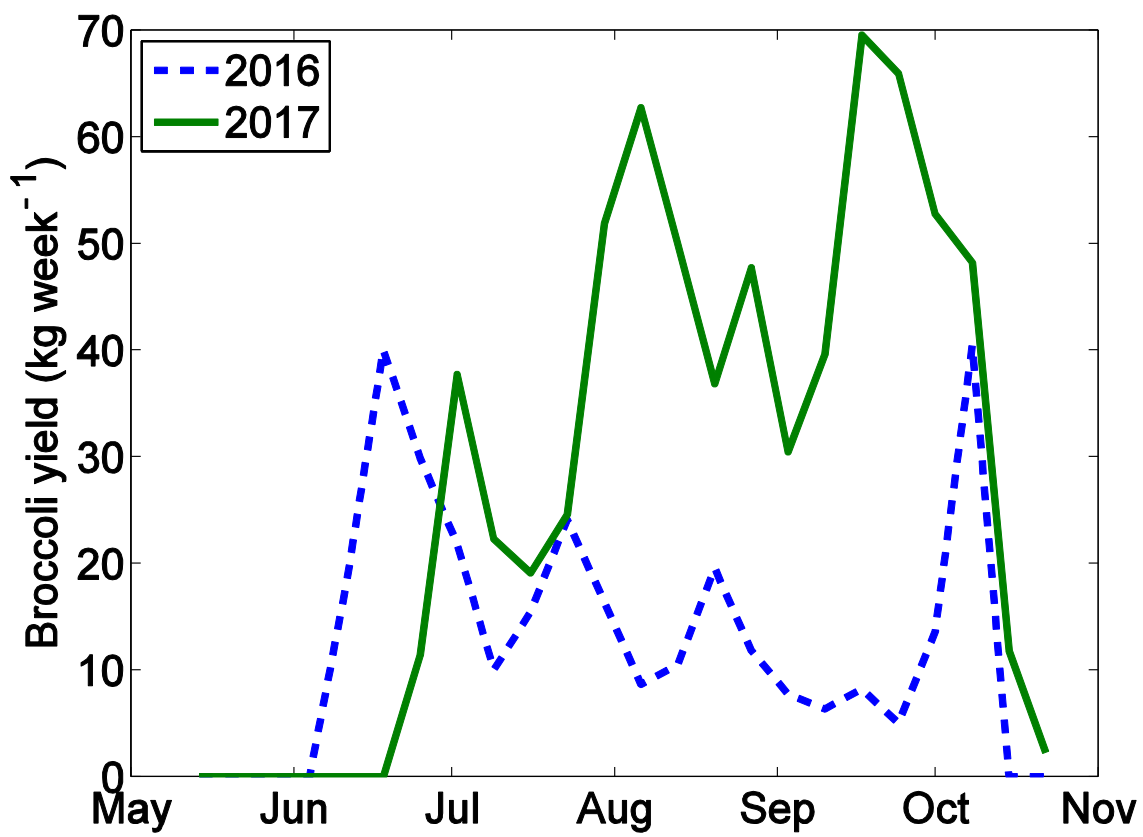
Figure D.5 Broccoli yield during 2016 and 2017.
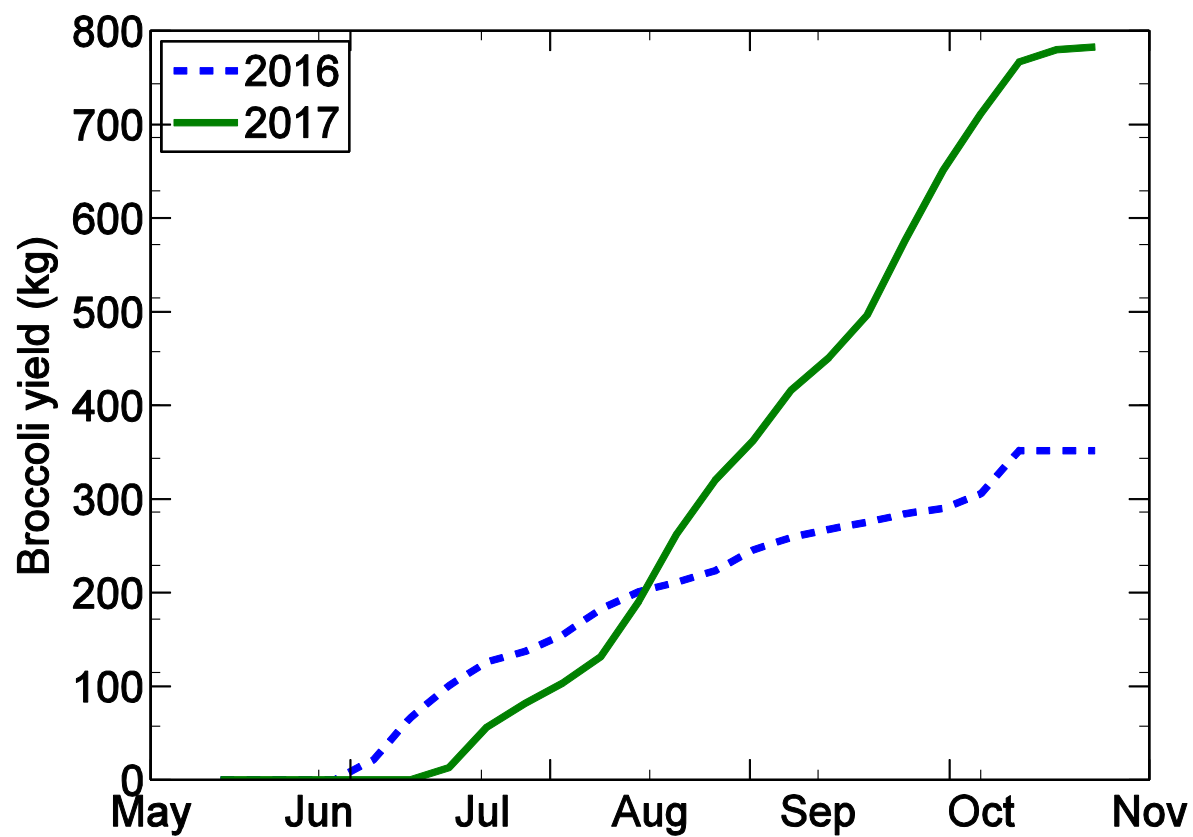
Figure D.6 Cumulative broccoli yield during 2016 and 2017.

Appendix E Effect of plastic film low tunnel cover on leaf area, plant biomass, and fruit yield of summer squash

E.1   Summary

To evaluate the suitability of low tunnels for increased summer squash production in organic agriculture, this study measured the difference in plant biomass and yield of summer squash grown on black plastic mulch (C, control with black plastic mulch) with and without a perforated polyethylene plastic (POLY$_P$, perforated low tunnel with black plastic mulch) low tunnel cover. The changes in summer squash physiology were measured twice a week for two months to quantify plant growth using a non-destructive biomass estimation model. Harvest data were also collected throughout the study period. Leaf area (LA), plant biomass, and fruit yield of summer squash were significantly greater for the summer squash in the POLY$_P$ treatment compared to the black plastic mulch control. Plant dry biomass doubled in the POLY$_P$ treatment compared to C, and significant increases in leaf number, leaf width, plant height, and radial diameter in the low tunnel treatment were seen as well. Overall, dry mass growth rate, LA, and number of fruits harvested were 113%, 20%, and 27%, respectively, higher in the POLY$_P$ treatment.

E.2   Introduction

Plastic film covered low tunnels are increasingly popular in agriculture because they increase air temperature inside the low tunnel (T_{ain}) surrounding the crop (Faivor, 2014), which can increase crop growth and yield (Al-Kayssi and Mustafa, 2016; Appendix E), and protect crops from extreme weather events (e.g., high wind, hail and frost events). Low tunnels increase T_{ain} by 1) increasing net longwave radiation (L_{nin}) inside the low tunnel when low longwave transmissivity plastic films are used and 2) reducing the sensible heat transfer from the crop and mulch surfaces by protecting them from wind (i.e., forced convection). It was shown in Chapter 3 that low tunnels covered with POLY, POLY$_P$ and TMX plastic films significantly increased T_{ain} compared to a black plastic film mulch control with no low tunnel. Given that low tunnels are versatile and low-cost and offer many of the same microclimatic advantages of glasshouses and high-tunnels without significant infrastructure costs (Gordon et. al., 2008), they can help producers increase production and plant growth with minimal time and financial investment (Faivor, 2014). In BC, it is projected that air temperature and wintertime rain will increase, and low tunnels may allow produces to take advantage of changing climate in the future (Zwiers et al., 2011). Therefore, low tunnels represent a promising tool in agriculture that has the potential to increase cropping system resilience and producer adaptability in a changing climate, especially in low-input organic agricultural operations. In general, as global demand for food

continues to increase it is crucial to improve the understanding of management techniques that can be implemented to increase the productivity and resilience of cropping-systems.

Studies have shown improved crop growth and yield in tomatoes (*Solanum lycopersicum*), cucumbers (*Cucumis sativus*), eggplant (*Solanum melongena*), pepper (*Capsicum annuum*), muskmelon (*Cucumis melo*), watermelon (*Citrullus lanatus*), okra (*Abelmoschus esculentus*), potato (*Solanum tuberosum*), sweet corn (*Zea mays*), snap bean (*Phaseolus vulgaris*), pumpkin (*Cucurbita pepo*), and strawberries (*Fragaria* × *ananassa*) grown in low tunnels (Lamont, 2005; Faivor, 2014) (Table E.1). There have been a limited number of studies that have shown increased growth and yield for squash grown inside low tunnels (Gordon et al., 2008; Lopez 1998), but no studies have been performed in BC. Summer squash is an important crop for producers in British Columbia (BC), as a result the potential benefits of using low tunnels to increase summer squash yield and biomass are promising for increasing farm revenue. More specifically, the ability to increase early growing season yields by using low tunnels is very attractive because it may allow producers to sell summer squash during times of the year when summer squash supply is low. Given that summer squash yields the majority of their fruit towards the end of the growing season, the ability to increase yield early in the growing season, when the market demand is high and supply is low, represents a potential advantage for producers who use low tunnels. Although there are many potential benefits to using low tunnels,

studies that explore both the opportunities (i.e., increased yield) and risks (e.g., financial, pathogen persistence) associated with low tunnels are necessary.

Table E.1 A list of studies that compared crop yields between open field and low tunnel crop treatments.

| Study | Treatments yield (kg m^{-2} season^{-1}) | | Percent increase |
	Open field	Low tunnel	
Muskmelon (Ibarra et. al., 2001)	3.08	6.26	103.25
Groundcherries (Abak et. al., 1994)	1.33	2.67	100.75
Summer Squash (Gordon et. al., 2008)	0.97	1.94	100.00
Strawberries (Lewers et. al., 2017)	2.60	4.91	88.85
Spinach (Drost et. al., 2017)	0.02	0.03	50.00
Red Peppers (Maughan et. al., 2014)	2.31	2.96	28.14
Sweet Peppers (Siwek and Libik, 1999)	4.02	5.10	26.87
Asparagus (Maughan et al., 2014)	0.19	0.22	15.79

To evaluate the impact of low tunnels on summer squash growth and yield in south western BC, an experiment was conducted at Cropthorne Farm, in Ladner, BC. This experiment compared summer squash under two treatments: one grown with low tunnel cover on black plastic mulch (POLY$_P$), and an open control grown on black plastic mulch (C). Low tunnels were installed after the summer squash were transplanted into the field and kept for one month prior to data collection. Summer squash plants were evaluated for fruit production and biomass growth over a two-month period. The objective of this study was to evaluate the difference in leaf area (LA), plant biomass, and fruit yield for summer squash grown with black plastic film mulch and black plastic film mulch with a low tunnel.

E.3   Methods

Location and experimental Layout

This study was conducted at Cropthorne Farm, a certified organic farm in Ladner, BC (49°04'56.2"N 123°09'17.1"W), from May to August 2016. Ladner soils are predominantly Humo-ferric Podzols (Lord and Valentine, n.d.). The air temperature and precipitation during the study are shown in Figure E.2. The study comprised two treatments: 36 plants grown in a 1 m tall perforated polyethylene plastic low tunnel with black plastic mulch (BE2, black embossed #2 black plastic film mulch, Dubois Agrinovation Inc. (http://www.duboisag.com/)) (POLY$_P$), and

36 plants grown with BE2 black plastic mulch and no low tunnel as a control (Figure E.1). All

plants were of the Noche variety of zucchini-shaped summer squash (*Cucurbita pepo*).
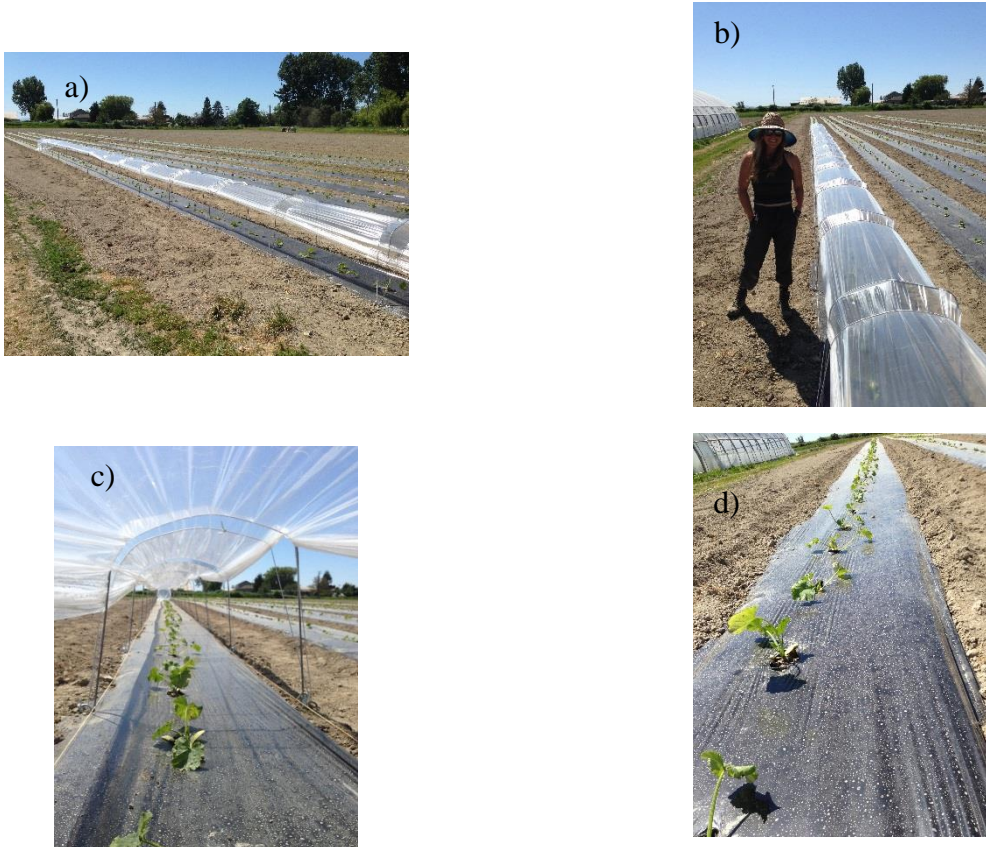
Figure E.1 Panels a) and b) are photographs (May 12, 2016) C (left in first row) and POLY$_P$

(right in first row) and Nicolette Lax posing next to POLY$_P$ on the day the low tunnel was

installed. Panels c) and d) show the low tunnel treatment (POLY$_P$) and black plastic mulch

control (C), respectively.

251

Plants were seeded on April 15th, 2016 and transplanted into a single row on May 9th, 2016 with 0.46 m spacing. Low tunnels were installed on May 12th, 2016 and removed on June 8th, 2016. All plants were irrigated with drip irrigation using 30 cm hole spacing and were watered twice a week for approximately two hours to reach a total of 25 mm of water plant^{-1} week^{-1}. The study row was on the edge row of five cultivated summer squash rows in the field (Figure E.1). Prior to transplanting, the field was plowed, disked, and tilled, and 50 m^3 ha^{-1} of compost was applied (the bulk density of the compost was not measured after application).

To install the low tunnel treatment (POLY$_P$), 1 m tall metal hoops were driven 10 cm into the soil with approximately 2 m spacing along the row and secured with metal stakes. A 2.2 m wide, 0.15 mm thick polyethylene film was then laid over the hoops along the row so that both the edges of the plastic film created full contact with the soil surface. The film was then pulled tightly and secured to additional stakes at the beginning and end of each row. Bungee cords were added to each hoop to secure the polyethylene film and allow the film to be raised during the day

for ventilation (ventilation was performed at the discretion of the Cropthorne Farm manager).
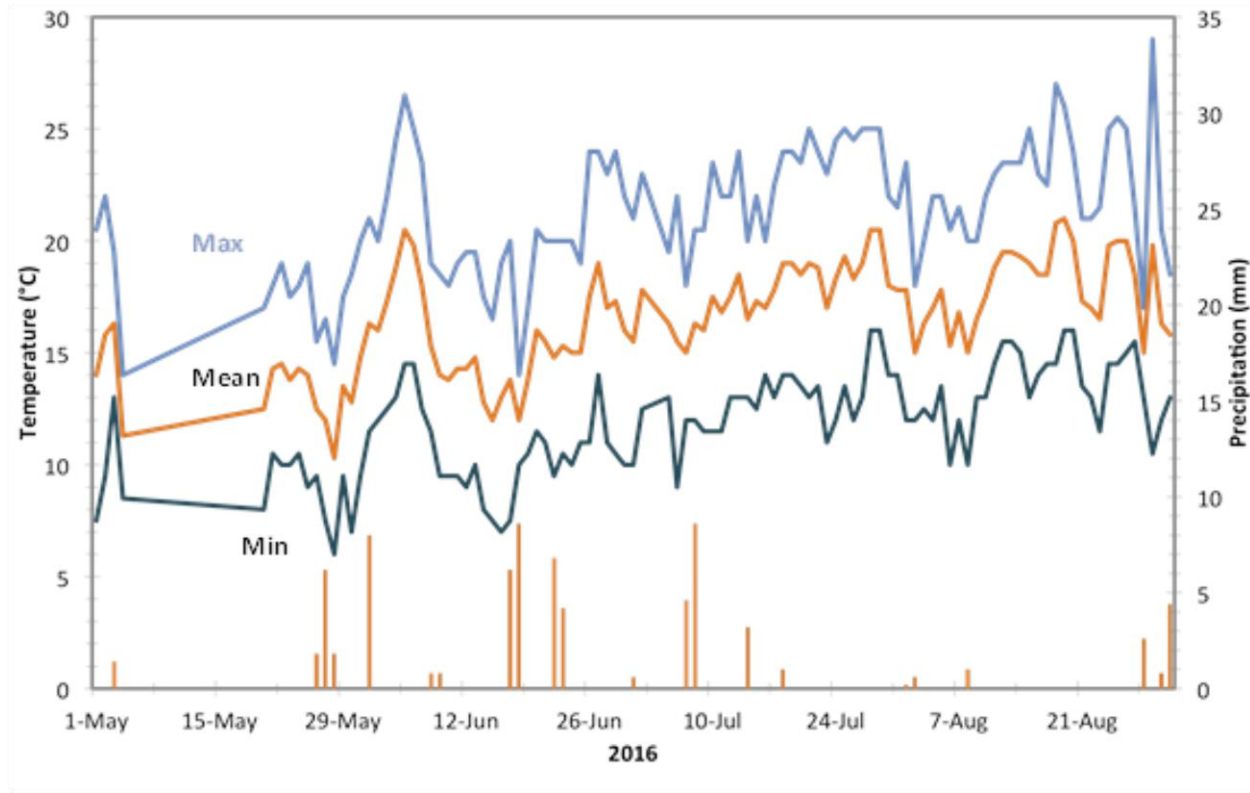
Figure E.2 Maximum (Max), minimum (Min), and mean (Mean) daily temperatures (°C) and precipitation (mm) data from May to August 2016, for the Delta Tsawwassen Beach Weather Station, 12.3 km from Cropthorne Farm.

Data collection

Non-destructive measurements were made twice a week from June 10 to July 20, 2016. On each sample day, leaf number, leaf width, stem length, plant height, stem width, and number

of fruit (Tables E.2-E.4) were measured on half of the plants in each treatment. Leaf number was determined by counting from the first true leaf to the largest healthy leaf. Leaf width was measured by selecting the largest healthy leaf on the plant and measuring its width, while fully flattened, using a 1 m flexible measuring tape (Table E.5). Stem length was measured by selecting the longest stem and measuring its curved width using a 1 m flexible measuring tape. Plant height was measured from the base of the plant to the tip of the highest leaf using a 1 m flexible measuring tape. Stem width was measured using a caliper.

Fruit was harvested on each sample day from all plants in each treatment. Only the fruit that was considered marketable was harvested, which was based on size, shape, color, and damage in accordance to Cropthorne Farm's harvest guidelines. All marketable fruit were counted and weighed immediately after harvest. Destructive samples were taken on August 3 and October 4, 2016. On these sample days, four plants in each treatment were removed from the row and measured for leaf number, leaf width, stem length, plant height, stem width, and number of fruits using the same methods as the non-destructive sampling procedures. Leaves were then separated from the plant stem and weighed to determine leaf wet mass (Table E.6). Stems were also weighed to determine stem wet mass (Table E.7). Two leaf samples from each plant were measured for leaf width and run through a LI-COR Inc. LI-3000C leaf area meter to determine the leaf area to width ratio (Table E.8). This ratio was used to approximate leaf area over the

study period. Two stem samples and two leaf samples from each plant were dried at 60°C for 24 hours and re-weighed to determine an average wet/dry mass ratio for the leaves and stems. These wet/dry ratios were then used to approximate the dry mass for the entire plant. A plant volume estimation model was created using physiological plant measurements and were correlated with wet and dry mass to approximate plant dry weight over the study period. Significant differences between treatments was determined using student *t*-tests at a 95% probability value (*p*) of significance ($p < 0.05$). The *t*-tests and the calculation of means and standard deviations were performed in Excel.

Estimation of leaf area

On the destructive sampling days, the area of two leaves per plant was measured using a LI-COR Inc. LI-3000C leaf area meter. The leaves were also measured in width to determine a leaf width / leaf area ratio of 18.2 cm^{-1}. This ratio was then applied to all leaf width data collected throughout the study to determine changes in leaf area over time and between the two treatments.

Estimation of plant biomass

In many studies that evaluate plant biomass (Bumgarner et. al., 2011; Ibarra et. al., 2001; Ernst, 2012), destructive sampling is used (in which plants are removed from the field/production) to determine biomass. Given that this study was conducted on a working farm,

destructive sampling was not possible during the mid-growing-season since Cropthorne

management did not want the squash plants to be taken out of production. In order to estimate

biomass, a non-destructive sampling procedure was used to quantify plant physiological changes

without destroying squash that was in production. The procedure involved measuring leaf

number, leaf width, stem length, plant height, and stem width to quantify physical changes and

estimate plant volume. At the end of the growing season, plant growth had slowed down, and the

farm management allowed some individual plants to be removed. The biomass data from these

plants was correlated with the plant volume model to determine changes in biomass between the

two treatments over the study period.

To estimate plant volume, a volumetric model was established to fit the shape of the

Noche Zucchini summer squash using the measurements of leaf number (n), leaf width (l_w), stem

length (l_{stem}), plant height (z), basal stem diameter (BSD). Leaf area was estimated using the area

equation for an equilateral triangle and leaf width data (Eq. (1)). Leaf volume was estimated

using the volume equation for a triangular prism and leaf width and an estimated leaf thickness

of 0.1cm (Eq. (2)). Stem volume was estimated by assuming that the stems were cylinders, using

BSD and l_{stem} as equation inputs (Eq. (3)). Full plant volume combined stem and leaf volumes

multiplied by the number of plant leaves (Eq. (4)). Because stem and leaf size vary throughout

the plant based on the different ages of the shoots, half of the stem and leaf volumes were

estimated as full volume, and the other half estimated at half volume. This allowed the size

distribution of shoots on the plant to be represented, and plant volume to be estimated.

Leaf area $$\qquad\qquad\qquad\qquad \mathrm{LA} = \frac{\sqrt{3}}{4} l_\mathrm{w}{}^2 \qquad\qquad\qquad\qquad (1)$$

Leaf volume $$\qquad\qquad\qquad V_L = 0.5t l_\mathrm{w}{}^2, \text{ where } t = 0.1 \text{ cm} \qquad\qquad\qquad (2)$$

Stem volume $$\qquad\qquad\qquad\qquad V_S = \pi l \mathrm{BSD}^2/4 \qquad\qquad\qquad\qquad (3)$$

Plant volume $$\qquad\qquad\qquad\qquad V_P = 0.75n(V_L + V_S) \qquad\qquad\qquad\qquad (4)$$

Destructive samples were taken at the end of the growing season to determine the

relationship between wet and dry biomass with plant volume (see Data Collection). The wet/dry

mass ratio was determined to be 0.16 for stems, and 0.22 for leaves. Leaf wet mass and stem wet

mass were divided by their respective ratios and combined to estimate total plant dry mass.

Dry mass was correlated with estimated plant volume to establish a dry mass/volume

ratio that could be applied to the non-destructive samples. The dry mass/volume ratio was

determined to be $5.72 \times 10^{-5} \text{ cm}^3 \text{ kg}^{-1}$. Estimated average plant volumes from the non-destructive

sampling dates were divided by this ratio to determine plant biomass.

E.4   Results and discussion

Leaf area

Leaf area (LA) was significantly higher in summer squash grown in the low tunnel treatment ($POLY_P$) compared to in the control (C) ($p < 0.05$). On average, LA was 20% greater for $POLY_P$ than C. Both treatments showed similar growth rates of LA over time (Figure E.3). By the last sampling day, plants grown in the $POLY_P$ treatment had a LA of 923 cm^2 compared to a leaf area of 756 cm^2 in C. This increase of leaf area under low tunnel cover is consistent with similar studies conducted on various other crops (Siwek and Libik, 1998; Chapter 4).

Figure E.3 Estimated leaf area of summer squash grown in low tunnels (POLY$_P$) compared to control (C), both with plastic mulch. Vertical bars show 95% confidence intervals.

Plant Biomass

Significant differences in plant physical characteristics were observed in leaf number, leaf width, plant height, and radial diameter between the two treatments ($p < 0.05$). On average, leaf number was 25% higher, leaf width and plant height were 19% higher, and radial diameter was 40% higher in summer squash grown in the POLY$_P$ treatment than C. These results are consistent with other studies conducted on summer squash grown under low tunnel cover.

Gordon et. al. (2008) found significant increases in plant height and stem diameter in summer squash grown in low tunnels compared to the no low tunnel control. Lopez (1998) also found significant increases in leaf number and stem length in summer squash grown in low tunnels compared to the no low tunnel control, and found a 43% increase in radial diameter.

Plant dry biomass was significantly higher in the low tunnel treatment than the open control ($p < 0.05$), with average plant dry mass of the low tunnel treatment being twice the mass of the black plastic control (Figure E.4). Over the sampling period, summer squash plants grown in the low tunnel treatment had a dry mass growth rate of 17 g day^{-1} compared to the control growth rate of 8 g day^{-1}.

The biomass estimation model used in this study allowed the use of non-destructive sampling to quantify plant growth at different stages of plant development. This model could be adapted to fit various crops and could be used by a producer without causing inconvenience for the producer. This allows crop biomass to be studied by producers, and could be used to evaluate the impact of low tunnels, or any other treatment of interest, on crop development. With regards to leaf area index, Padron et al. (2016) developed a relationship between leaf width x leaf length vs. LA in order to estimate leaf area index without having to destructuvely sample. Non-destructive leaf area and biomass models of this type represent a useful tool for on-farm demonstration research and management practice evaluation.
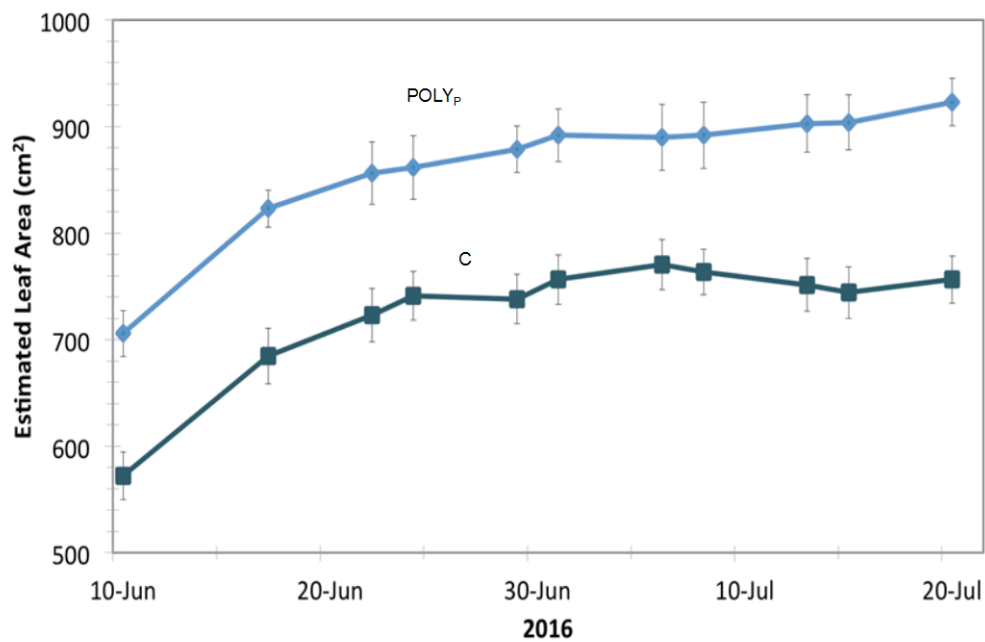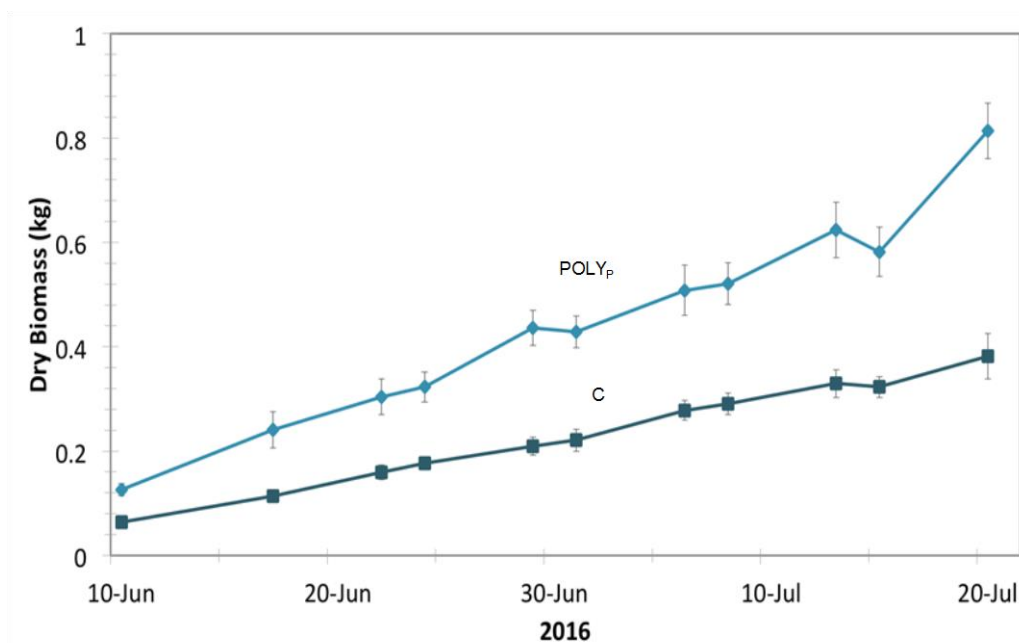
Figure E.4 Estimated plant dry biomass of summer squash grown in low tunnels (POLY$_P$) compared to control (C), both with plastic mulch. Vertical bars show 95% confidence intervals.

Yield

Marketable fruit yield was significantly higher in the low tunnel treatment compared to in the open control. Cumulative yield in the low tunnel treatment was 27% higher in number of fruit harvested and 22% higher in wet mass. Also, summer squash grown in the POLY$_P$ treatment had a greater early season yield, with over double the yield on the earliest sampling days (Figures E.5 and E.6) than the control. These results are consistent with earlier studies conducted on summer squash grown under low tunnel cover. In Alabama, USA, Gordon et al. (2008) found that summer squash yield increased from 26.0 kg plot^{-1} when grown in black

261

plastic film mulch to 37.3 kg plot[-1] when grown with black plastic film mulch and polyethylene covered low tunnel. Similarly, In Oman, Lopez (1998) found that summer squash yield plant[-1] increased from 311.11 g plant[-1] for summer squash grown without low tunnels to 1085.59 g plant[-1] for sumer squash grown inside low tunnels for 30 days. In contrast, Dickerson et al. (2003) found no increase in yield when they compared summer squash grown with black plastic film mulch (5843 kg ha^{-1}) vs. summer squash grown with black plastic film mulch and low tunnels (5814 kg ha^{-1}).
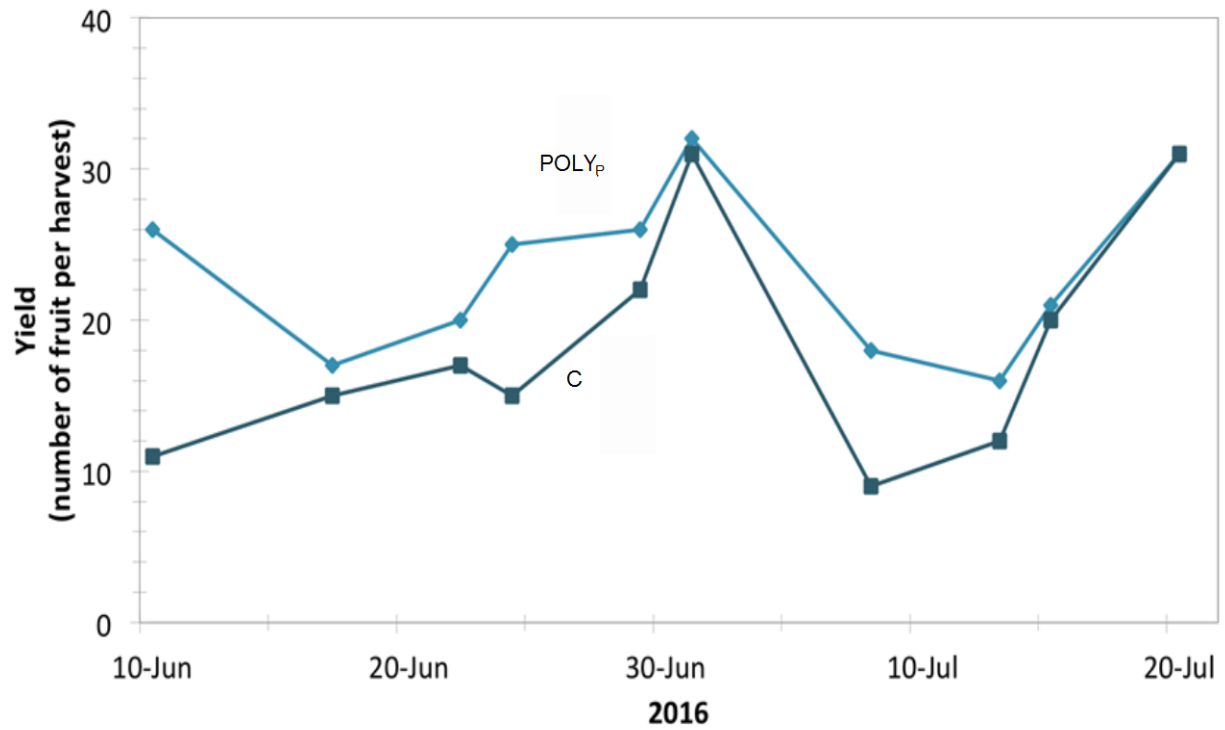
Figure E.5 Marketable fruit yield per harvest of summer squash grown in low tunnels (POLY$_P$) compared to control (C), both with black plastic mulch.
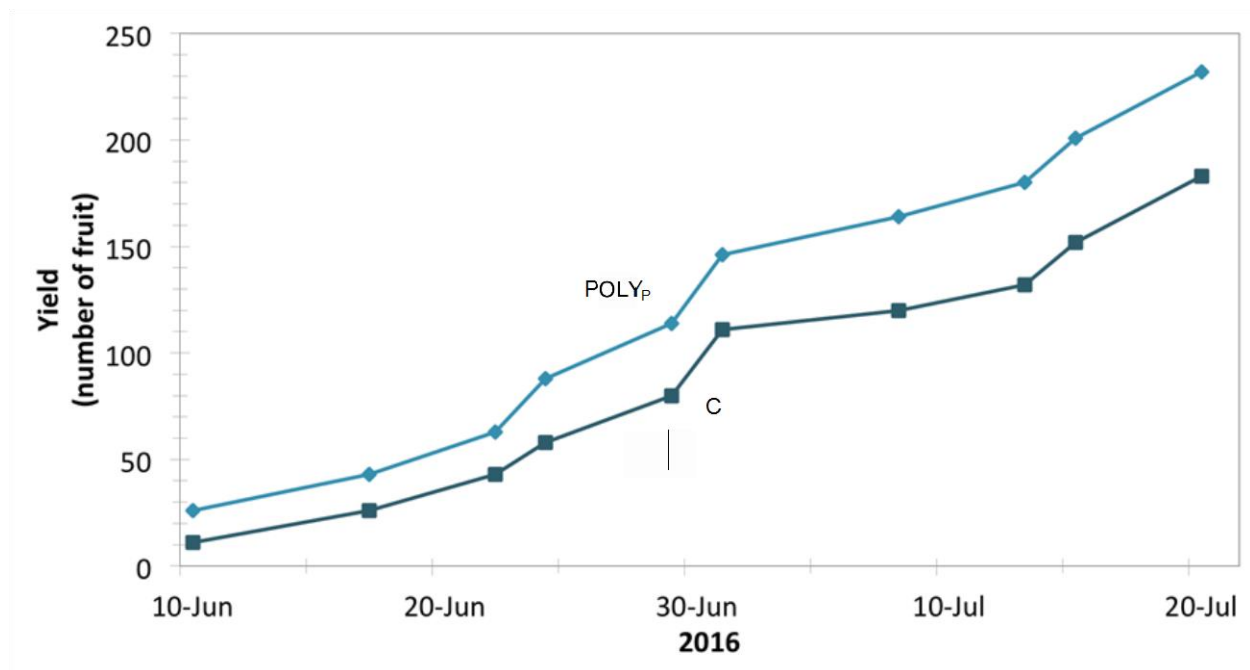
Figure E.6 Cumulative marketable fruit yield of summer squash grown in low tunnels (POLY$_P$) compared to control (C), both with black plastic mulch.

Table E.2 Average leaf number, leaf width (cm), shoot length (cm), plant height (cm), and number of fruits over the sampling period (June and July 2016) for the POLY$_P$ and C treatments.

sample date	Polyethylene Plastic Low Tunnel with Black Plastic Mulch						Black Plastic Mulch Control					
	avg. leaf number	avg. leaf width (cm)	avg. shoot length (cm)	avg. shoot width (cm)	avg. plant height (cm)	avg. number of fruit	avg. leaf number	avg. leaf width (cm)	avg. shoot length (cm)	avg. shoot width (cm)	avg. plant height (cm)	avg. number of fruit
10-Jun	16.1	38.8	32.3	2.1	35.7	2.2	14.0	31.4	23.6	1.7	26.8	1.4
17-Jun	17.0	45.2	40.7	2.7	45.8	2.2	13.3	37.6	32.8	2.2	37.1	1.5
22-Jun	19.8	47.1	44.3	2.7	57.2	2.6	15.7	39.7	37.7	2.3	43.9	1.5
24-Jun	20.7	47.3	45.8	2.7	59.3	2.3	16.7	40.7	39.0	2.3	46.8	1.4
29-Jun	24.2	48.3	47.7	2.9	64.2	2.5	17.8	40.6	42.7	2.4	53.2	2.0
1-Jul	25.0	49.0	48.8	2.7	62.9	2.9	19.6	41.6	41.3	2.3	56.2	3.0
6-Jul	28.3	48.9	49.9	2.8	67.3	no data	23.1	42.3	44.9	2.3	61.2	no data
8-Jul	28.9	49.0	50.2	2.8	66.3	1.9	24.0	41.9	44.4	2.4	60.8	1.3
13-Jul	33.0	49.6	49.4	2.9	70.6	1.9	27.2	41.3	44.2	2.4	64.4	1.4
15-Jul	32.6	49.7	49.4	2.7	75.0	2.3	27.0	40.9	41.2	2.5	64.9	2.3
20-Jul	38.8	50.7	49.4	3.0	74.3	3.2	30.8	41.6	41.1	2.5	63.2	2.9

265

Table E.3 Total number and weight of marketable fruit per treatment harvested over the sampling period (June and July 2016) for POLY$_P$ and C.

	Polyethylene Plastic Low Tunnel with Black Plastic Mulch		Black Plastic Mulch Control	
sample date	number of fruit	weight of fruit (kg)	number of fruit	weight of fruit (kg)
10-Jun	26	3.6	11	1.76
17-Jun	17	3.8	15	3.8
22-Jun	20	9.41	17	6.18
24-Jun	25	7.34	15	5.15
29-Jun	26	9.27	22	7.09
1-Jul	32	10.33	31	10.8
8-Jul	18	5.56	9	2.45
13-Jul	16	4.71	12	2.97
15-Jul	21	8.14	20	8.43
20-Jul	31	10.38	31	10.85
total:	232	72.54	183	59.48

Table E.4 Leaf and stem wet mass and dry mass data for August 3, 2016 destructive samples, used to determine the wet/dry leaf ratio.

sample	wet leaf mass (g)	dry leaf mass (g)	wet stem mass (g)	dry stem mass (g)
LT_11_1	60.39	9.66	41.37	9.07
LT_11_2	59.35	14.80	35.09	13.13
LT_21_1	54.40	12.97	40.87	5.72
LT_21_2	50.92	15.49	35.17	3.79
LT_31_1	29.77	6.46	34.28	5.88
LT_31_2	50.14	12.04	33.00	8.10
LT_41_1	45.16	11.24	25.29	5.10
LT_41_2	23.11	4.63	38.28	1.92
BP_3_1	36.91	8.10	21.89	2.11
BP_3_2	35.26	6.45	31.37	3.50
BP_13_1	41.00	8.92	28.00	3.60
BP_13_2	25.88	4.43	27.91	2.94
BP_23_1	38.89	6.51	31.46	4.36
BP_23_2	22.41	4.65	34.17	4.29
BP_33_1	26.72	5.36	35.36	6.36
BP_33_2	32.47	6.92	40.33	5.27
average	**39.55**	**8.66**	**33.37**	**5.32**

wet/dry
leaf ratio: 39.55/8.66=x/y
y=8.66x/39.55
0.219

wet/dry
stem ratio: 33.37/5.32=x/y
y=5.32x / 33.37
0.159

Table E.5 Leaf area and width data for August 3, 2016 destructive samples, used to determine

the leaf width/area ratio.

sample	leaf area (cm^2)	leaf width (cm)	width/area ratio (cm/cm^2)
LT_11_1	861.71	46.00	5.34
LT_11_2	916.70	43.00	4.69
LT_21_1	888.85	44.00	4.95
LT_21_2	589.85	40.00	6.78
LT_31_1	519.94	32.00	6.15
LT_31_2	813.26	39.00	4.80
LT_41_1	756.77	33.00	4.36
LT_41_2	537.02	33.00	6.15
BP_3_1	768.79	38.00	4.94
BP_3_2	555.63	33.00	5.94
BP_13_1	693.88	35.00	5.04
BP_13_2	456.74	30.00	6.57
BP_23_1	643.04	36.00	5.60
BP_23_2	398.47	28.00	7.03
BP_33_1	460.85	30.00	6.51
BP_33_2	584.94	34.00	5.81
		average	5.67

Table E.6 Plant wet mass and estimated dry mass for August 3, 2016 destructive samples.

sample	full plant wet mass (kg)	stem wet mass (kg)	estimated all leaf dry mass (kg)*	estimated stem dry mass (kg)**	plant dry mass (kg)
LT_11	5.47	4.00	0.32	0.64	0.96
LT_21	7.40	5.37	0.44	0.86	1.30
LT_31	7.47	5.46	0.44	0.87	1.31
LT_41	6.37	4.55	0.40	0.73	1.12
BP_3	4.92	3.39	0.34	0.54	0.88
BP_13	4.83	3.26	0.34	0.52	0.86
BP_23	4.89	3.09	0.39	0.49	0.89
BP_33	5.73	4.25	0.32	0.68	1.00
LT_avg	**6.68**	4.85	0.39	0.77	**1.16**
BP_avg	**5.09**	3.50	0.34	0.55	**0.90**

*using wet/dry leaf ratio as equation: y=8.66x/39.55

**using wet/dry stem ratio as equation: y=5.32x/33.36

Table E.7 Plant wet mass and estimated dry mass for October 4, 2016 destructive samples.

sample	full plant wet mass (kg)	stem wet mass (kg)	estimated all leaf dry mass (kg)*	estimated stem dry mass (kg)**	estimated full plant dry mass (kg)
LT_9	4.74	2.63	0.46	0.42	0.88
LT_17	5.25	3.00	0.49	0.48	0.97
LT_27	5.35	2.76	0.57	0.44	1.01
LT_37	6.04	2.90	0.69	0.46	1.15
BP_1	6.97	3.75	0.71	0.60	1.30
BP_7	4.34	2.22	0.46	0.35	0.82
BP_17	4.25	2.56	0.37	0.41	0.78
BP_27	4.95	2.69	0.50	0.43	0.92
LT_avg	5.35	2.82	0.55	0.45	1.00
BP_avg	5.13	2.80	0.51	0.45	0.96

*using wet/dry leaf ratio as equation: $y = 8.66x/39.55$
**using wet/dry stem ratio as equation: $y = 5.32x/33.36$

Table E.8 Measurements of plant physical characteristics, estimated volume, and full plant dry mass for October 4, 2016 destructive samples, used to determine the dry mass/volume ratio.

sample	leaf number	leaf width (cm)	shoot length (cm)	shoot width (cm)	plant height (cm)	estimated volume (cm^3)	full plant dry mass (kg)	
LT_9	82	41.00	67.00	2.68	84.00	28395.65	0.88	*outlier
LT_17	55	45.00	52.00	2.88	73.00	18120.87	0.97	
LT_27	49	48.00	54.00	2.69	75.00	15545.52	1.01	
LT_37	55	51.00	45.00	3.38	82.00	22049.72	1.15	
BP_1	57	40.00	48.00	2.07	76.00	10345.73	1.30	*outlier
BP_7	53	44.00	43.00	2.64	64.00	13168.68	0.82	
BP_17	50	42.00	46.00	2.78	65.00	13793.10	0.78	
BP_27	49	38.00	43.00	2.38	66.00	9701.32	0.92	*outlier

average (excluding outliers): 16535.58   0.95

Dry mass / volume: $y = 5.72 \times 10^{-5}$ kg cm^{-3} * x

E.5 Conclusions

Low tunnels are commonly used in agriculture because they increase air temperature, which can increase crop quality, crop resilience, leaf area, plant biomass, and the potential for multiple cropping's. Perhaps most importantly, low tunnels can increase crop yields and can extend the growing season. In this study, leaf area, plant biomass, and fruit yield of summer squash increased significantly when they were grown inside a perforated polyethylene plastic low tunnel with black plastic mulch ($POLY_P$) compared to the black plastic mulch control (C). Plant dry biomass doubled in the $POLY_P$ treatment compared to C, and significant increases in leaf number, leaf width, plant height, and radial diameter were also observed. Estimated increases in dry mass growth rate, leaf area, and number of fruits harvested in the low tunnel treatment were 113%, 20%, and 27% higher than in the control, respectively. These findings are consistent with previous research on the impact of low tunnels on crop growth and productivity, but more research is needed to better understand how low tunnels impact crop microclimate.

E.6   References

Al-Kayssi, A. W., Mustafa, S. H. (2016). Impact of elevated carbon dioxide on soil heat storage and heat flux under unheated low-tunnels conditions. *Journal of Environmental Management, 182,* 176-186.

Brown, J. E., Yates, R. P., West, M. S., Stevens, C. (1993). Effects of planting methods and row cover on summer squash production. *Proc. Natl. Agr. Plast. Congr. 24:* 270-273.

Bumgarner, N., Bennet, M., Ling, P., Mullen, R., Kleinhenz, M. (2011). Canopy Cover and Root-Zone Heating Effects on Fall and Spring Grown Leaf Lettuce Yield in Ohio. *Horticulture Technology, 21,* 737 – 744.

Dickerson, G., S. Guldan, L.M. English, and P. Torres. 2003. Effects of woven, black plastic mulch and row cover on winter squash and pepper production. Proc. Natl. Agr. Plast. Congr. 31:63–67.

Drost, D., Ernst, T., Black, B. (2017). Soil Heating and Secondary Plant Covers Influence Growth and Yield of Winter High Tunnel Spinach. *Horticultural Science, 52(9):* 1251-1258.

Ernst, T. (2012). Optimizing winter spinach production in high tunnels. *Utah State University,* 52 – 54.

Faivor, R. M. S. (2014). Low Tunnel Strategies for Microclimate Modification and Early Vegetable Production. *University of Michigan.*

Gordon, G. G., Foshee, W. G., Reed, S. T., Brown, J. E., Vinson, E., Woods, F. M. (2008). Plastic Mulches and Row Covers on Growth and Production of Summer Squash. *International Journal of Vegetable Science, 14(4):* 322-338.

Ibarra, L., Flores, J., Diaz-Perez, J.C. (2001). Growth and yield of muskmelon in response to plastic mulch and row covers. *Scientia Horticulturae, 87:* 139-145.

CGU and CSAFM Joint Annual Scientific Meeting, Vancouver, BC, May 28-31.

Lamont, W. J. (2005). Plastics: Modifying the Microclimate for the Production of Vegetable Crops. *Horticulture Technology, 15(3):* 477-481.

Lewers K. S., Fleisher, D. H., Daughtry C. S. T. (2017). Low Tunnels as a Strawberry Breeding Tool and Season-Extending Production System. *International Journal of Fruit Science, 17(3):* 233-258.

Lord, T. M., Valentine, K. W. G. (no date). The Soil Map of British Columbia. *British Columbia Ministry of Environment, Retrieved from: http://www.env.gov.bc.ca/soils/landscape/3.2soilmap.html*

Lopez, M. V (1998). Growth, Yield and Leaf NPK Concentrations in Crop-Covered Squash. *Journal of Sustainable Agriculture, 12(4):* 25-38.

Maughan, T., Black, B., Drost, D. (2014). Low tunnels: a low-cost protected cultivation option. *Utah State University Horticulture Extension.*

Singh, A., Syndor, A., Deka, B. C., Singh, R. K., Patel, R. K. (2012). The effect of microclimate inside low tunnels on off-season production of strawberry. *Scientia Horticulturae, 144,* 36-41.

Siwek, P., Libik, A. (1994). Changes in soil temperature affected by the application of plastic covers in field production of lettuce and watermelon. *Acta Horticulturae, 371:* 269 - 274

Siwek, P., Libik, A. (1999). The impact of tunnel cover type on growth and yield of sweet pepper. *International Agrophysics, 12:* 119 – 124.

Tilman, D., Balzer, C., Hill, J., & Befort, B. L. (2011). Global food demand and the sustainable intensification of agriculture. *Proceedings of the National Academy of Sciences of the United States of America*, *108*(50), 20260-20264. doi:10.1073/pnas.1116437108.